Evoluzione spettrale nelle Galassie

Materiale didattico per gli studenti

A.A. 2008/09 – Laurea Specialistica in Astrofisica e Cosmologia

Prof. Alberto Buzzoni

MORPHOLOGY

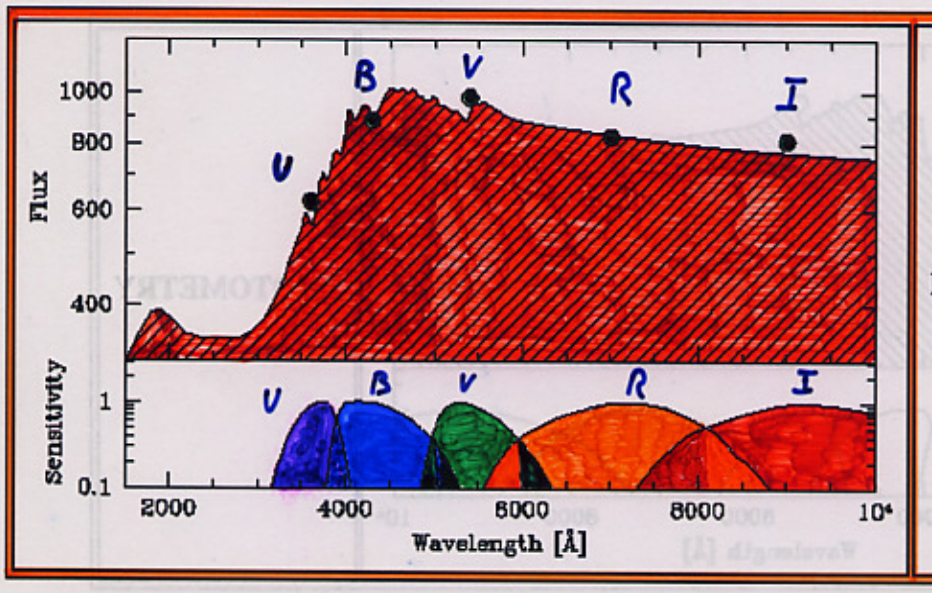

PHOTOMETRY

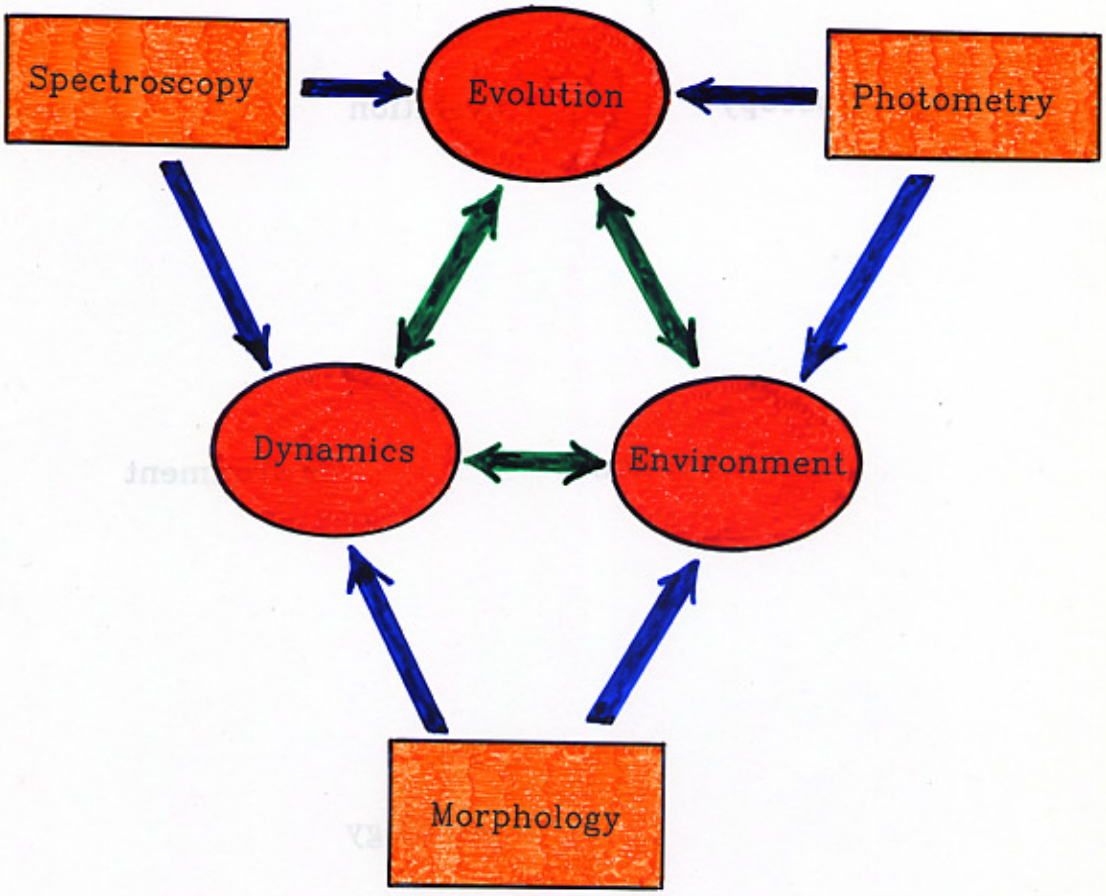
Spectroscopy
Evolution
Photometry
Dynamics
Environment
Morphology

SPECTROSCOPY

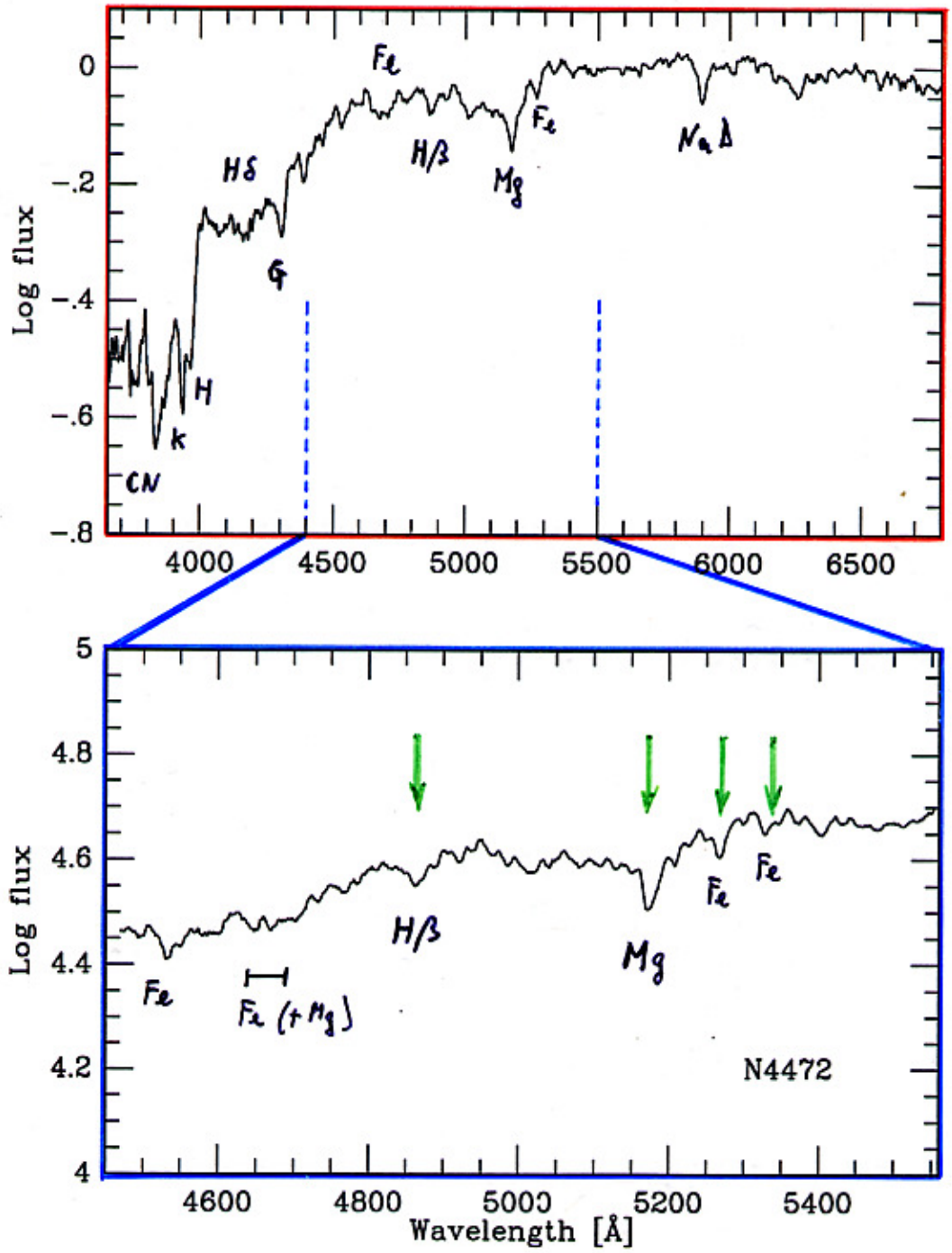

HUMASON et al. (1956)

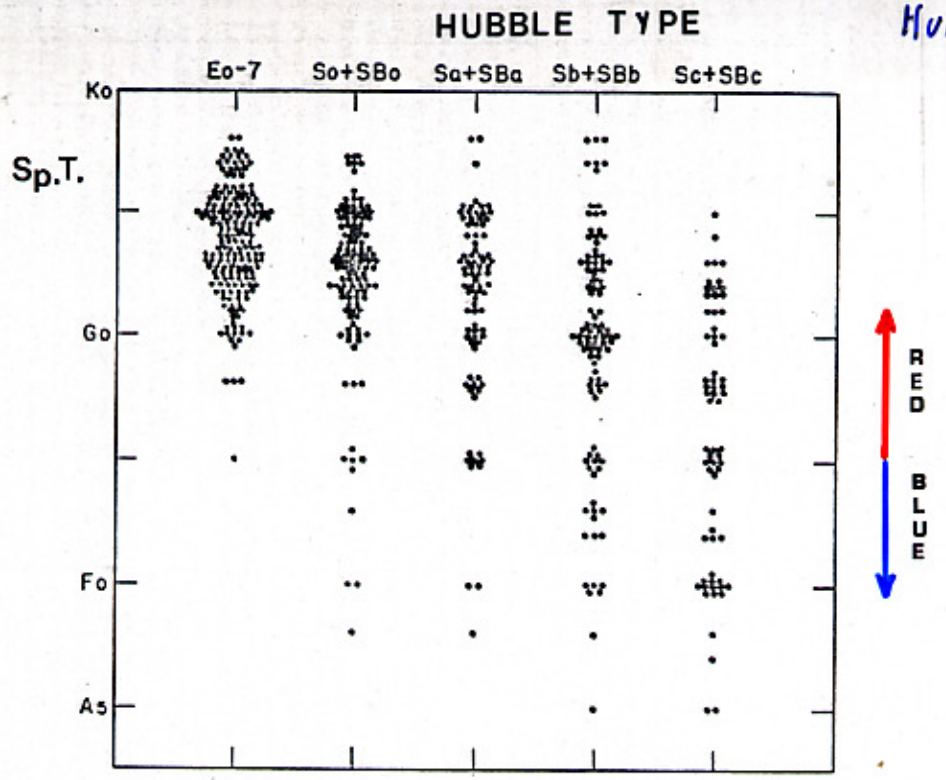

Figure 2. The distribution of spectral type as a function of nebular type for 546 nebulae from Tables I and II.

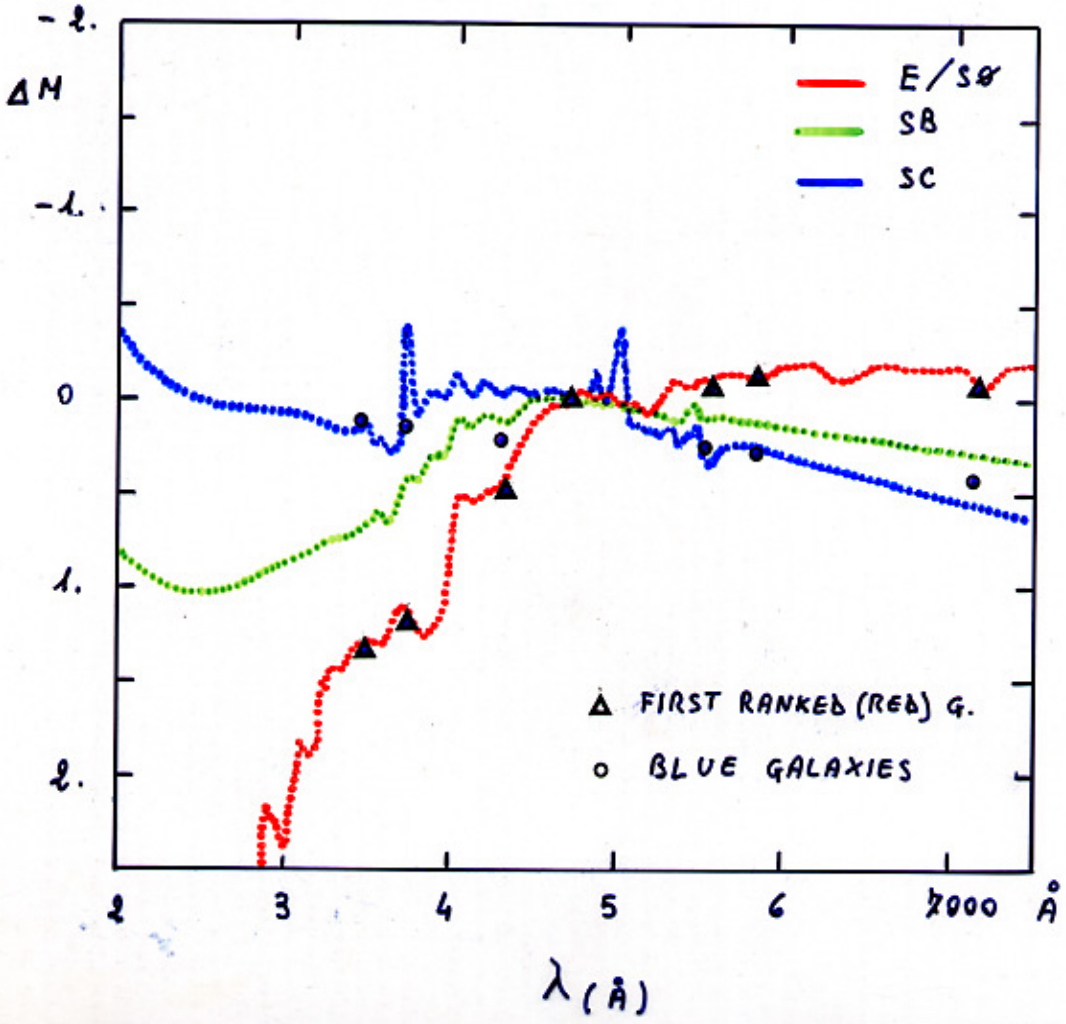

STELLAR EVOLUTION

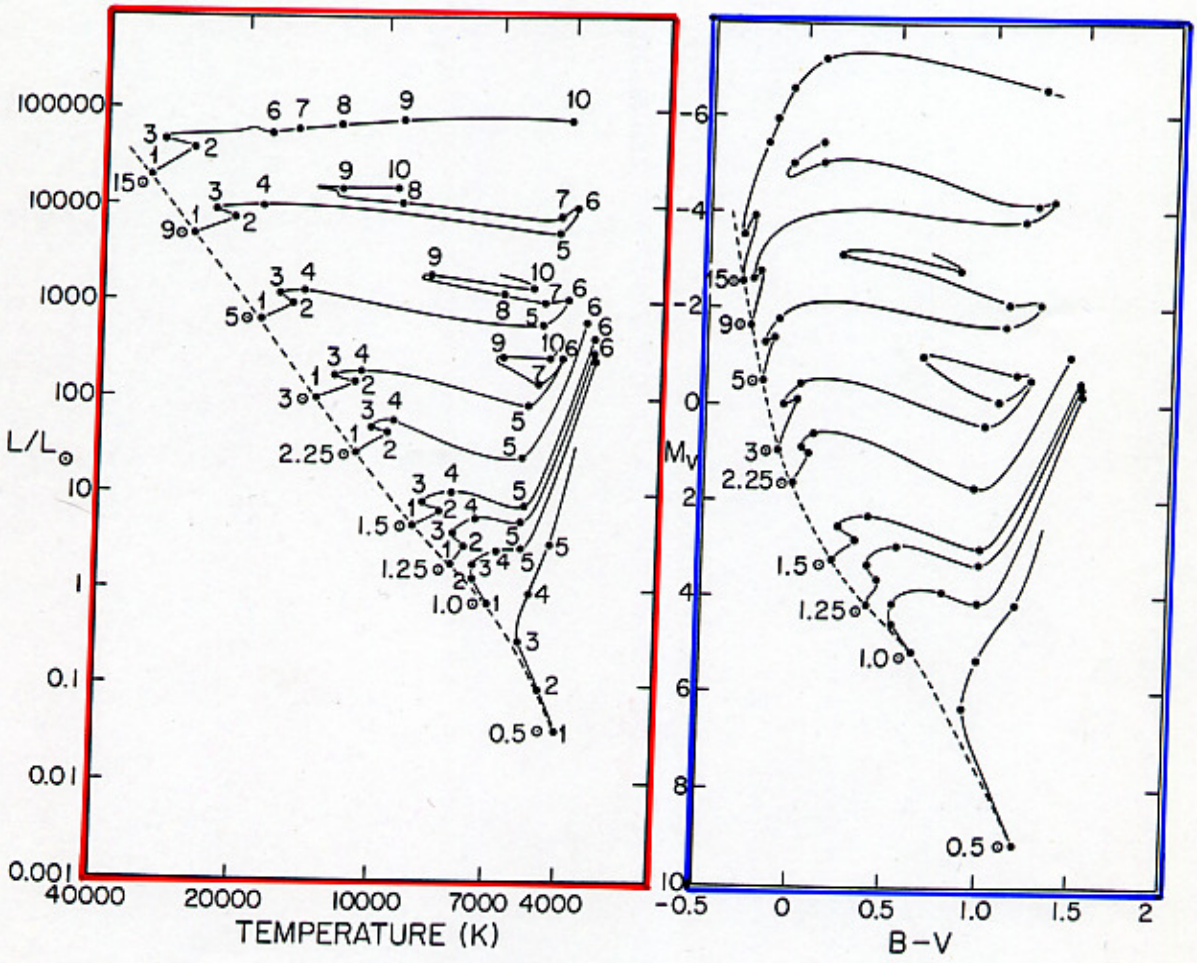

IBEN (1962)

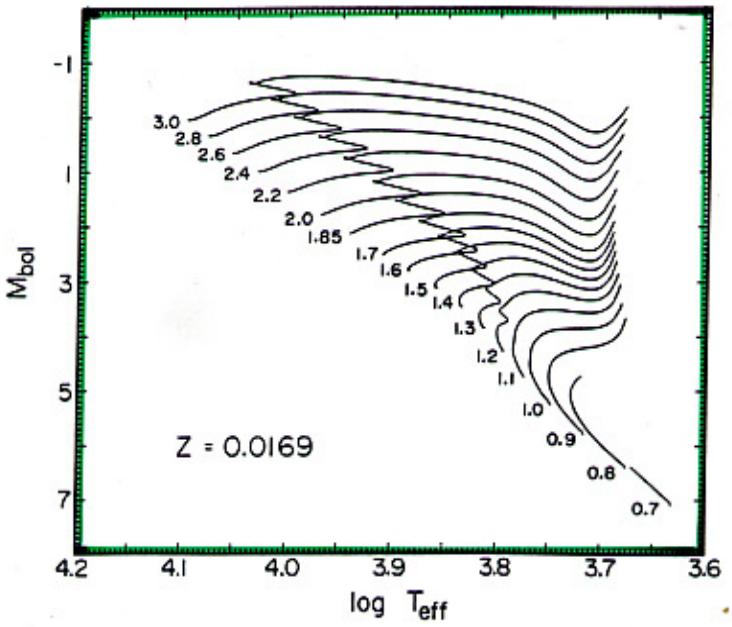

-Evolutionary sequences for $Z = 0.0169$, assuming $Y = 0.25$ and $\alpha = 1.6$. Each track is labeled adjacent to the ZAMS location by its mass in

VANDENBERG (1983)

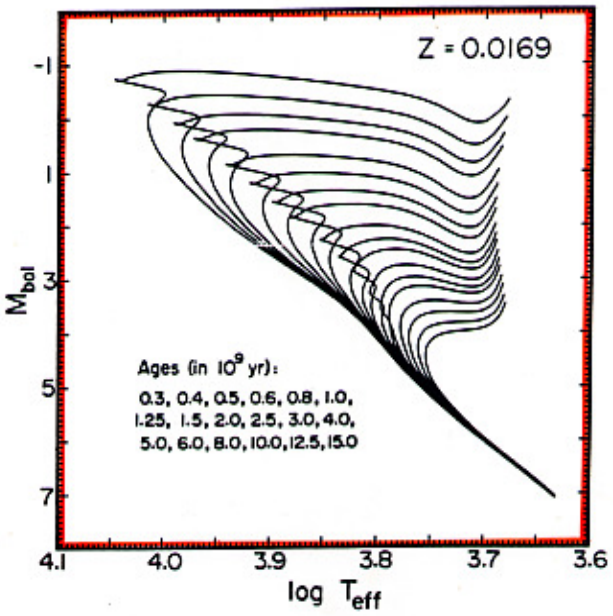

FIG. 4.—The isochrones which have been calculated from the evolutionary tracks illustrated in Fig. 1. The indicated ages apply to the isochrones in the order of decreasing turnoff luminosity.

M 3 (11,000 *)

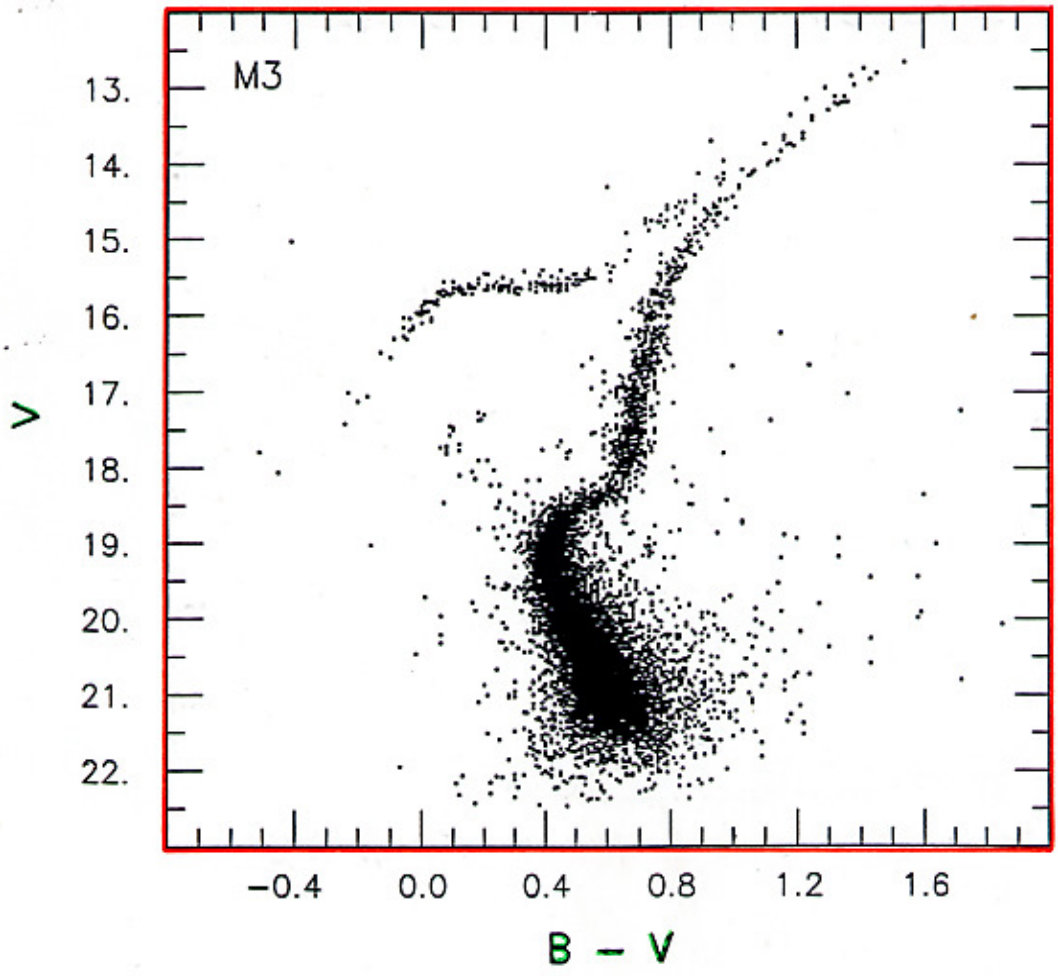

Buonanno et al.
(1994)

SWEIGART, GREGGIO & RENZINI (1989)

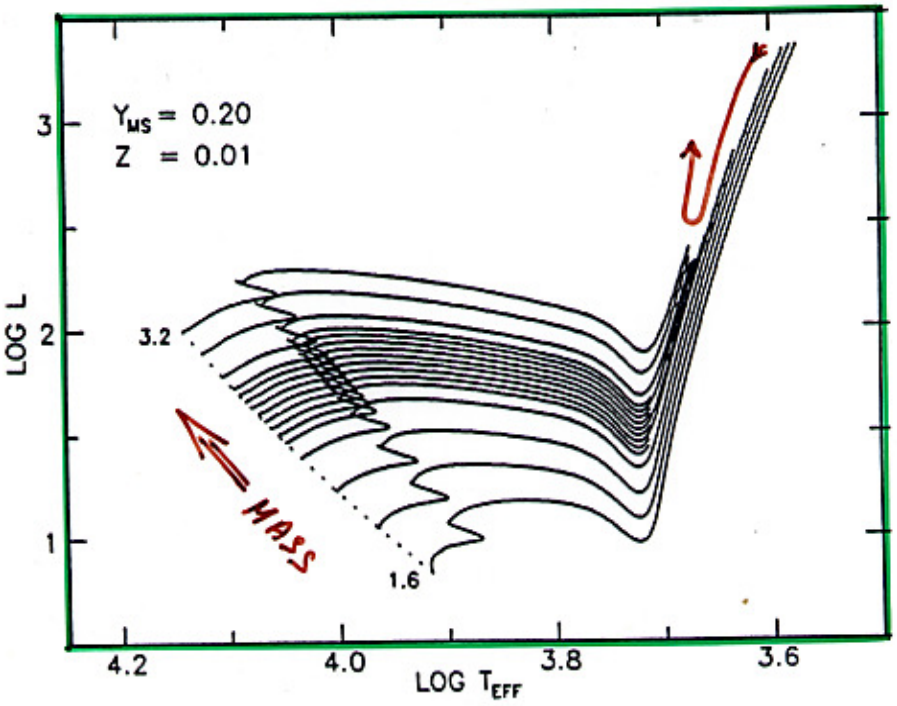

RENZINI & BUZZONI (1986)

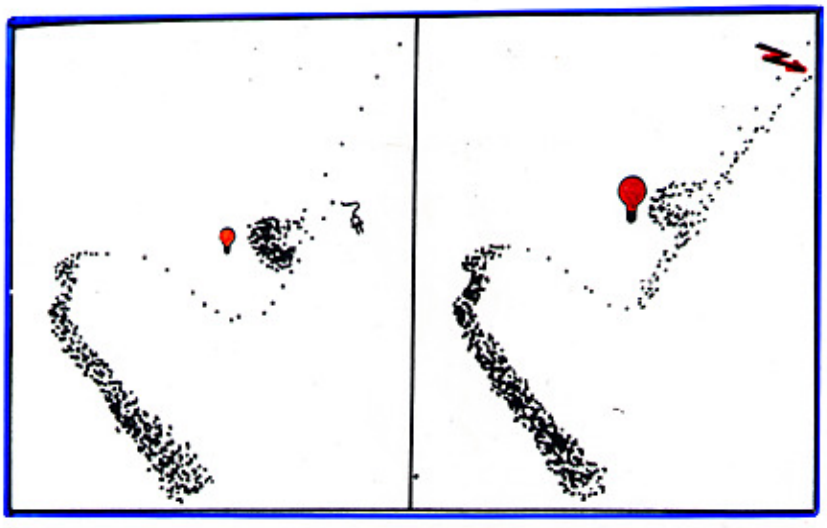

Figure 14. An artist view of the RGB phase transition. On the left panel the HR diagram of a cluster slightly younger than $t(M_{HeF})$. On the right panel the same cluster when slightly older than $t(M_{HeF})$. Note the virtual identity of the main sequences, and, by contrast, the development of the RGB. The plug indicates the point when helium ignites (non degenerately). The jagged arrow indicates the helium flash location. The growing light bulb emphasizes the brightening of the clump giants across the RGB phase transition. The AGB stays nearly the same across the transition.

Figure 2.5. Course of the color–magnitude array for a number of well-known open clusters of different ages. From top to bottom: NGC 6231, κ Crucis (NGC 4755), h, χ Persei (NGC 864, 886), Pleiades, Hyades, NGC 752, Messier 67 (NGC 2682), and NGC 188.

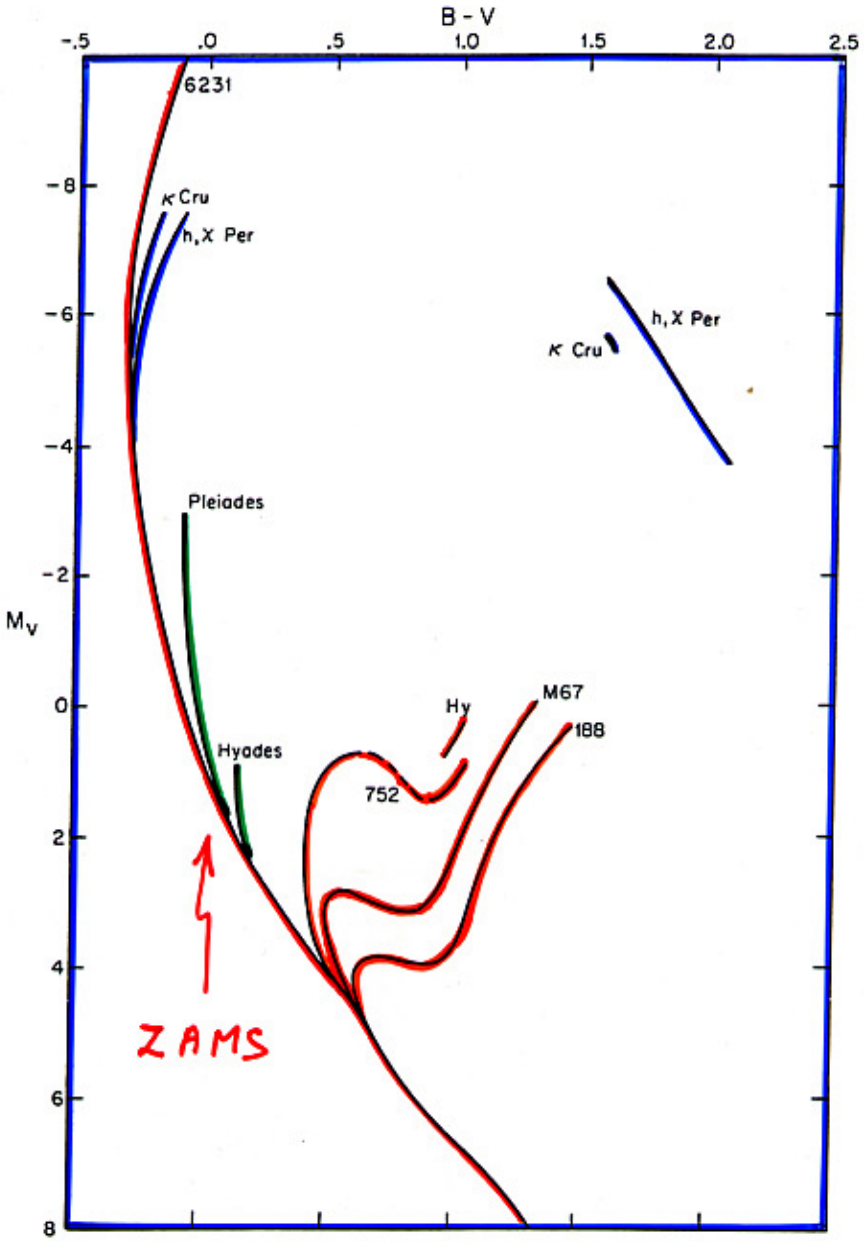

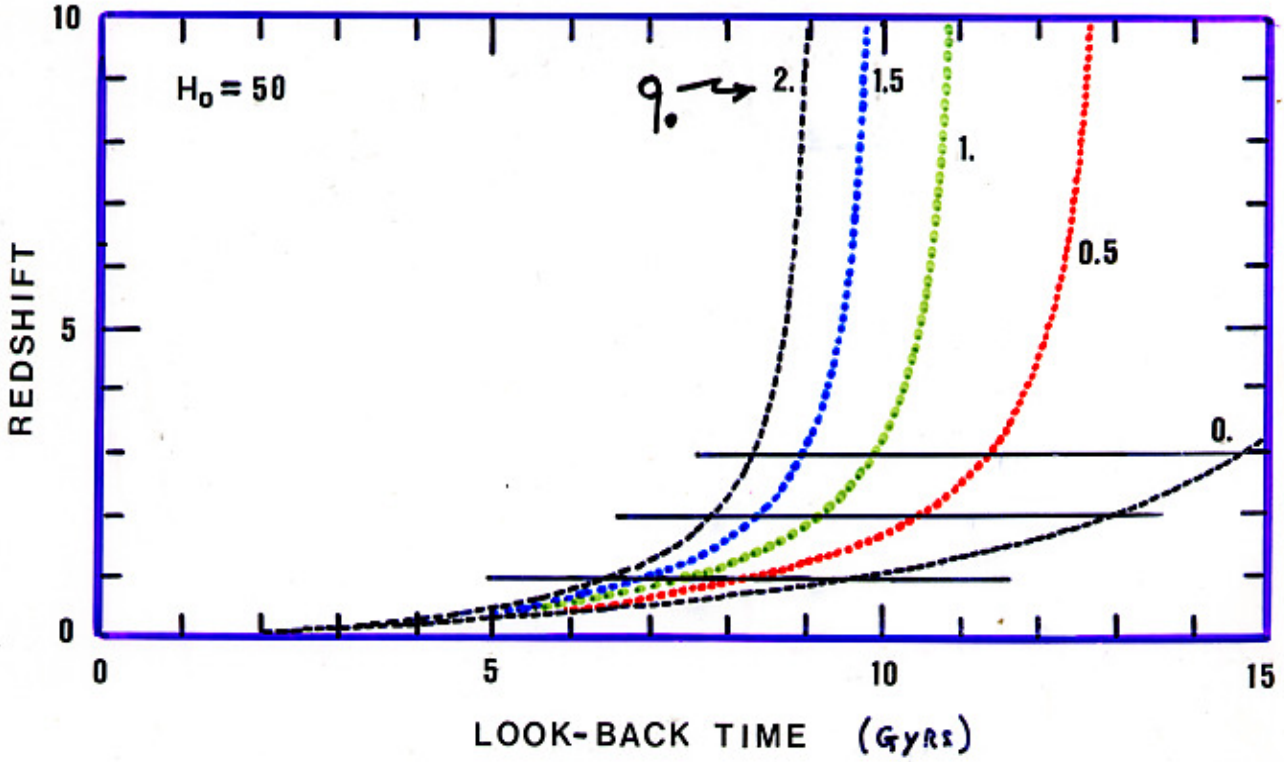
REDSHIFT
LOOK-BACK TIME (GyRs)
$H_o = 50$
$q_o \rightarrow$
2.
1.5
1.
0.5
0.
0
5
10
15

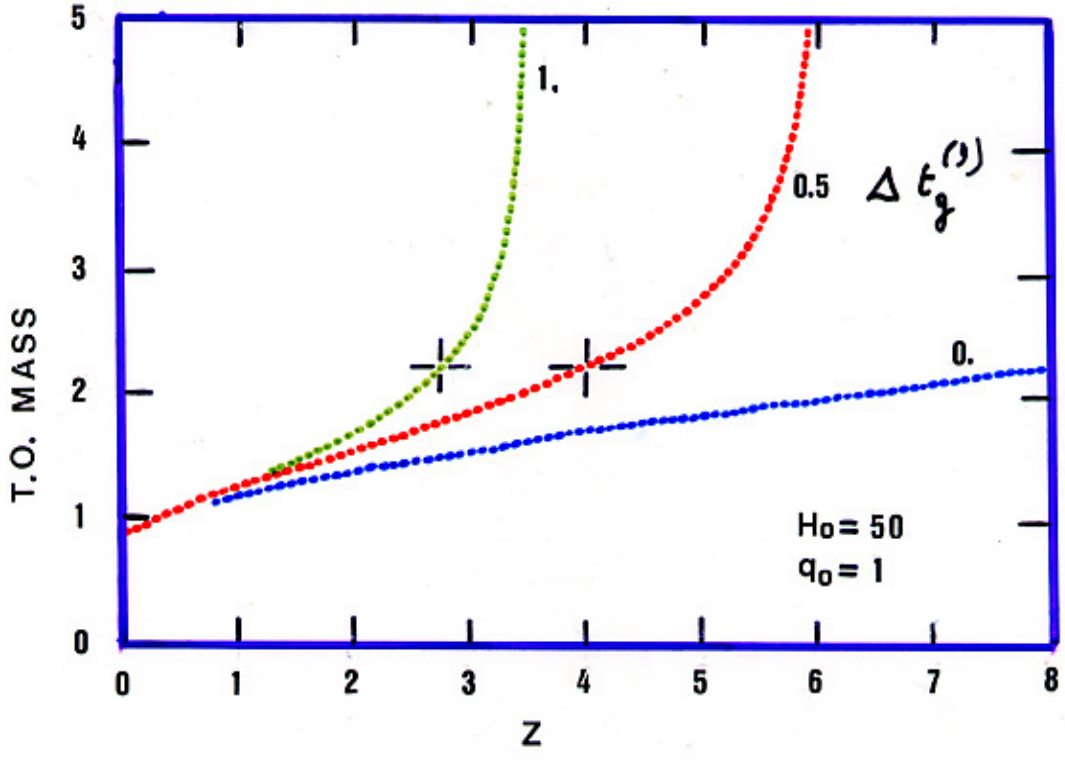
T.O. MASS
Z
1.
0.5
0.
$\Delta t_g^{(1)}$
$H_o = 50$
$q_o = 1$
0
1
2
3
4
5
6
7
8

DISTINCTIVE PARAMETERS IN A STELLAR POPULATION

1) AGE $\Rightarrow$ t

2) CHEMICAL COMPOSITION $\Rightarrow$ Z, $[Fe/H]$

3) STAR MASS DISTRIBUTION $\Rightarrow$ IMF

4) STAR FORMATION HISTORY $\Rightarrow$ SFR

CANONICAL ASSUMPTIONS

1) IMF $N_{(M)} \propto M_*^{-s}$ $(s = 1.35)$

2) SFR
- $\delta(0)$ → SSP
- $f(t)$ → CSP

STELLAR MASSES

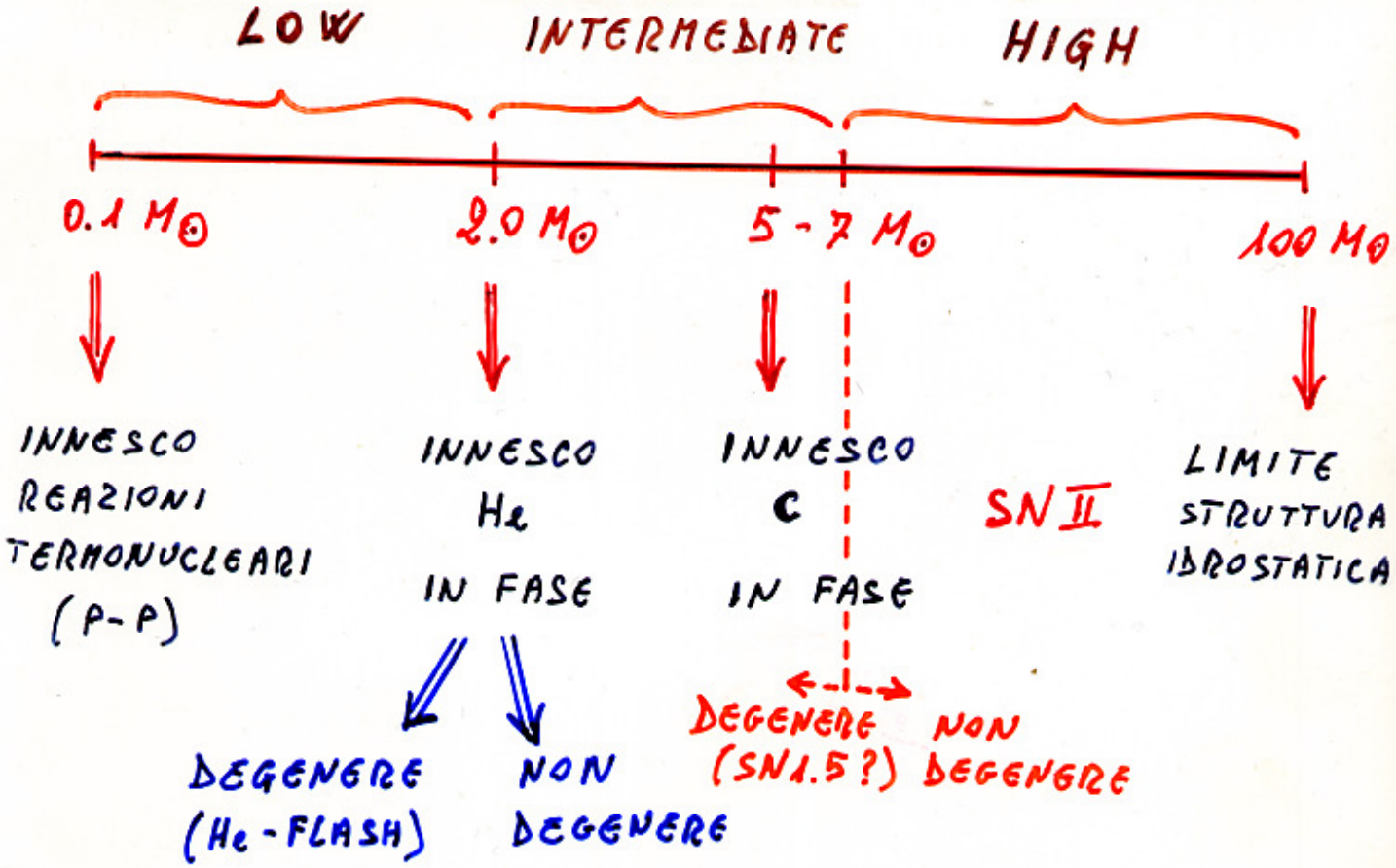

FASE	LOW-MASS	HIGH-MASS
CORE H-BURNING	MS	MS
SHELL H-BURNING	SGB RGB	1-ST GB
CORE He-BURNING	HB	1-ST BLUE LOOP
DOUBLE (MULTIPLE) SHELL BURNING	AGB	2-ND, 3-RD etc. GBs

$$
\begin{cases}
1) \quad \nabla P = -\rho g \Rightarrow \dfrac{P}{R} \propto \rho \dfrac{M}{R^2} \Rightarrow P \propto \rho \dfrac{M}{R} \\
2) \quad \nabla M = 4\pi R^2 \rho \\
3) \quad \nabla L = 4\pi R^2 \varepsilon \\
4) \quad \nabla T = -\dfrac{3\rho k L}{16\pi a c T^3 R^2} \Rightarrow \dfrac{T}{R} \propto \dfrac{\rho L}{T^3 R^2} \Rightarrow T^4 \propto \dfrac{\rho L}{R} \\
5) \quad P = \dfrac{\rho k T}{\mu H} \Rightarrow P \propto \rho T
\end{cases}
$$

$$
\rho T \propto \rho \frac{M}{R}
$$

$$
\Downarrow
$$

$$
\begin{cases}
T \propto \dfrac{M}{R} \\
T^4 \propto \dfrac{\rho L}{R} \Rightarrow \dfrac{M^4}{R^4} \propto \dfrac{M}{R^4} L \Rightarrow \boxed{L \propto M^3}
\end{cases}
$$

$$
L\, t \propto M
$$

$$
\Downarrow
$$

$$
\begin{cases}
t \propto \dfrac{M}{L} \\
L \propto M^3
\end{cases}
\Rightarrow
\boxed{
\begin{aligned}
t &\propto M^{-2} \\
t &\propto L_{T.O.}^{-2/3}
\end{aligned}
}
$$

The Clock

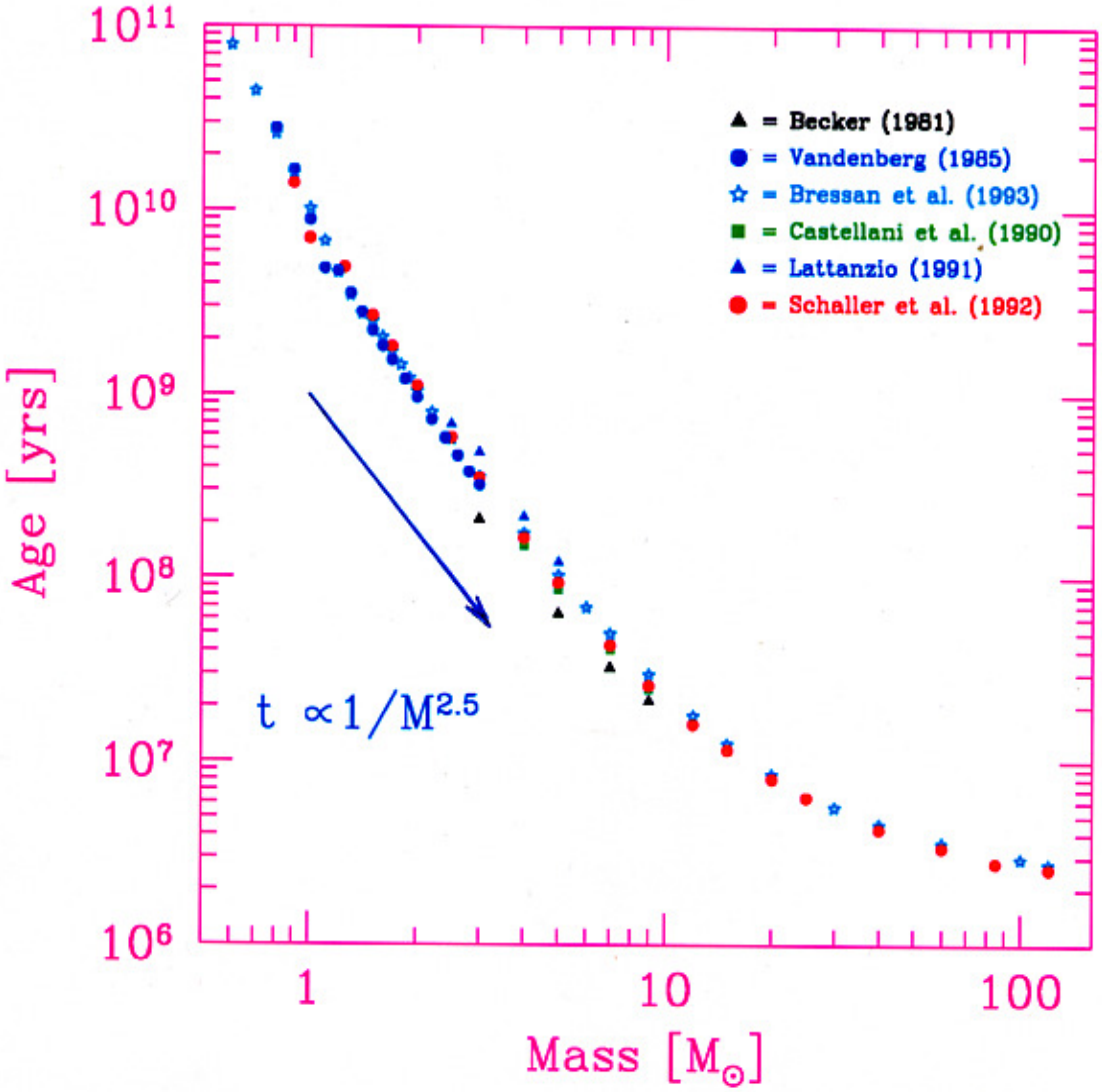
Age [yrs]
10^{11}
10^{10}
10^{9}
10^{8}
10^{7}
10^{6}
1
10
100
Mass [$M_\odot$]
▲ = Becker (1981)
● = Vandenberg (1985)
☆ = Bressan et al. (1993)
■ = Castellani et al. (1990)
▲ = Lattanzio (1991)
● = Schaller et al. (1992)
$t \propto 1/M^{2.5}$

THERMOMETERS & CLOCKS

GLOBAL PROPERTIES OF STELLAR POPULATIONS

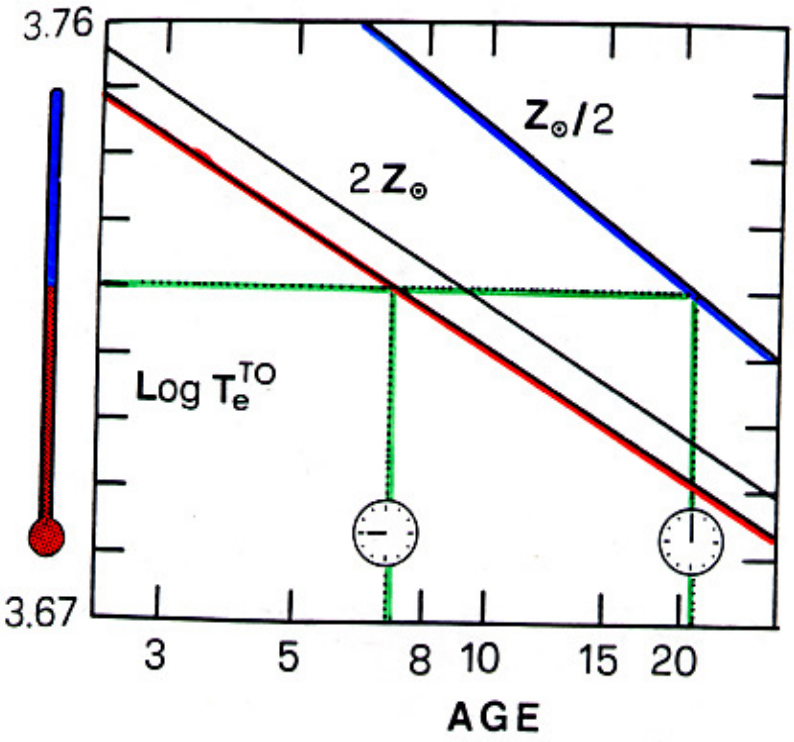

- MASSA -

III LEGGE DI KEPLERO :

$$P = \sqrt{\frac{4\pi}{G}} \left(\frac{R^3}{M_1 + M_2} \right)^{1/2}$$

$$365 \times 86400 = \sqrt{\frac{4\pi}{6.6\,10^{-8}}} \frac{(150\,10^{11})^{3/2}}{\sqrt{M_\odot}}$$

$$M_\odot = 2\,10^{33}\ gr \qquad (\sim 3\,10^5\ M_\oplus)$$

NOME		$M/M_\odot$	$L/L_\odot$
SOLE		1	1
SIRIO	A	2.14	25
	B	1.05	0.003 *
PROCIONE	A	1.78	7
	B	0.65	0.08
KRÜGER 60	A	0.25	0.01
	B	0.16	0.004
ζ AUR	A	8.30	4400
	B	5.60	1100

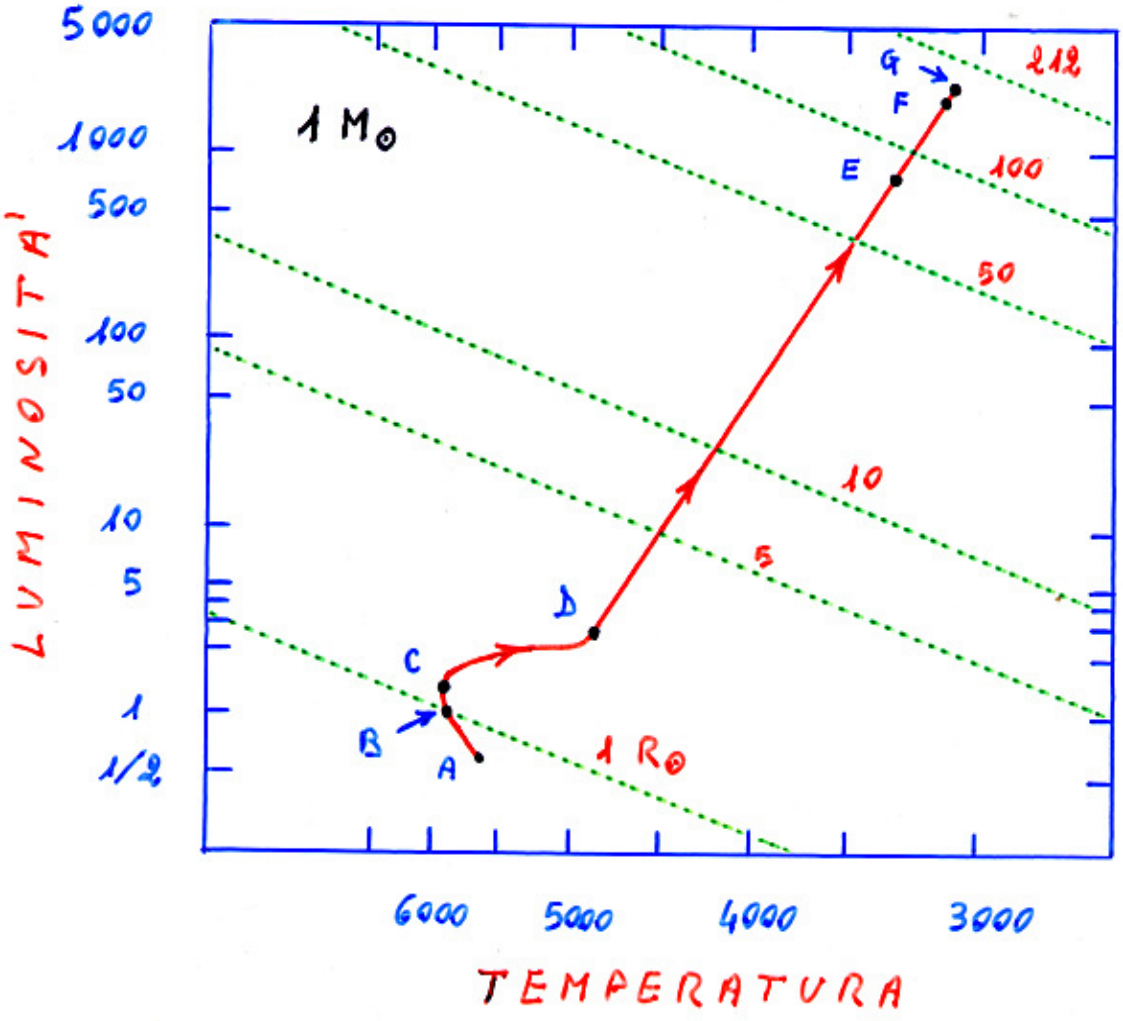

	ETA' (Gyr)	$L/L_\odot$	T	$R/R_\odot$	
A	0	0.6	5600	0.83	
B	6.5	1	5780	1	
C	8.9	1.2	5850	1.07	MAX TEMP.
D	13.5	3.5	4800	2.7	
E	13.990	270	3500	82	ORB. MERCURIO
F	13.997	2000	3100	153	ORB. VENERE
G	14.0	2300	3100	170	MAX RAGGIO

$\Delta R \sim 5$ Km/ANNO

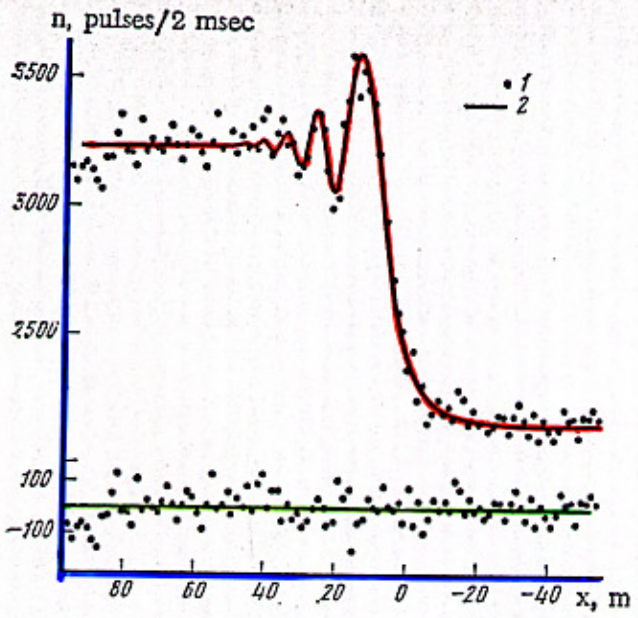

61 δ^1 TAU
(1984)

$d = 0''.0028$

5 ℓ
1473 km

FIG. 1. Diffraction pattern of a lunar occultation of the star 61 δ^1 Tau. 1) Observational data (readings every 2 msec); 2) theoretical behavior of the intensity as a function of the x coordinate (in meters; see text) corresponding to the optimum model with an angular diameter d = 0".0028 for $\mu = 0.6$. The deviations of the observed points from the model curve are shown in the lower part of the figure.

α ORI
BETELGEUSE
(1979)

$d = 0''.025$

$R = 800\ R_\odot$

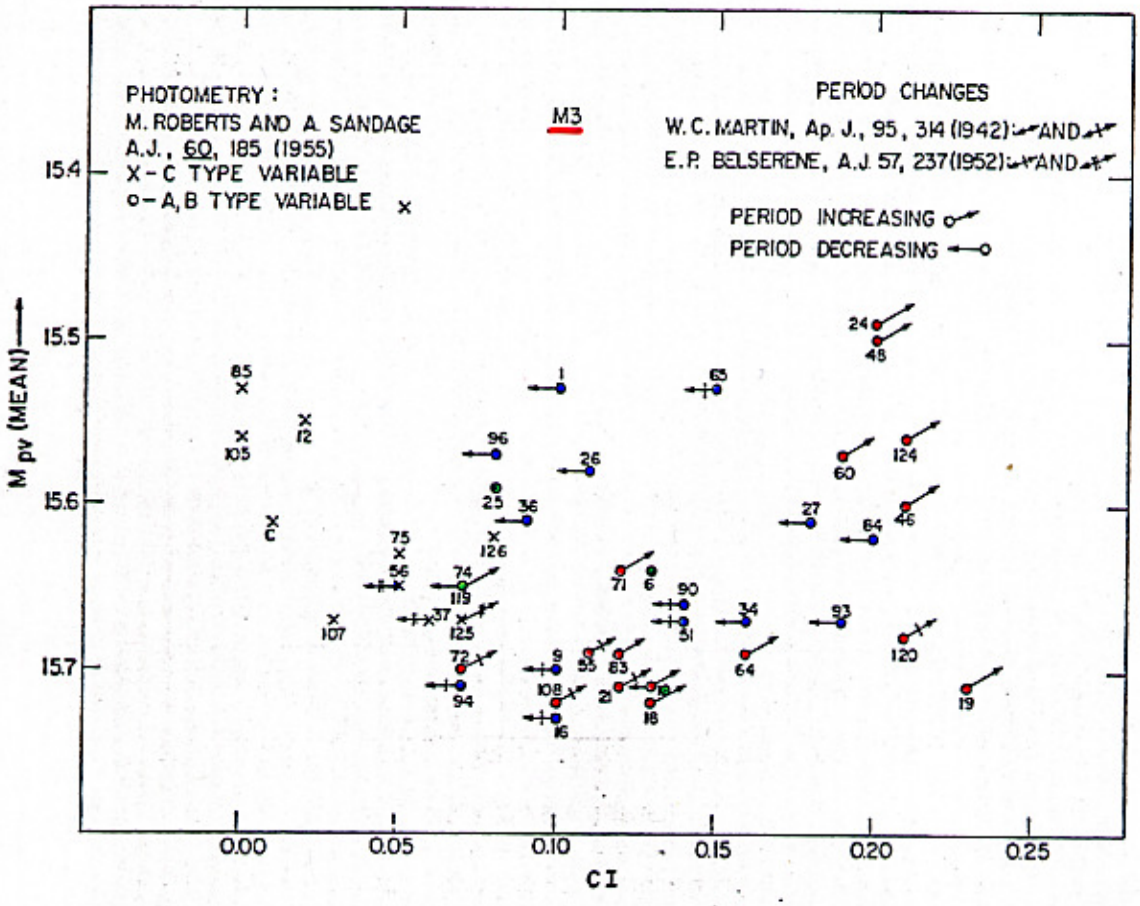

FIG. 10.—Distribution of rates of period change in the C-M diagram. Arrows pointing upward and to the right mean $dP/dt > 0$. Arrows pointing to the left mean $dP/dt < 0$.

$$P \propto \frac{1}{\sqrt{\bar{\rho}}} \propto \frac{R^{1.5}}{\sqrt{M}}$$

$$\frac{dP}{dt} = \frac{3}{2}\,\frac{P}{\bar{R}}\,\frac{d\bar{R}}{dt} \qquad R = \frac{1}{\sqrt{4\pi\sigma}}\,\frac{L^{1/2}}{T^{2}}$$

$$\log P = -0.3\, M_{BOL} - 3 \log T - 0.5 \log M + \text{cost.}$$

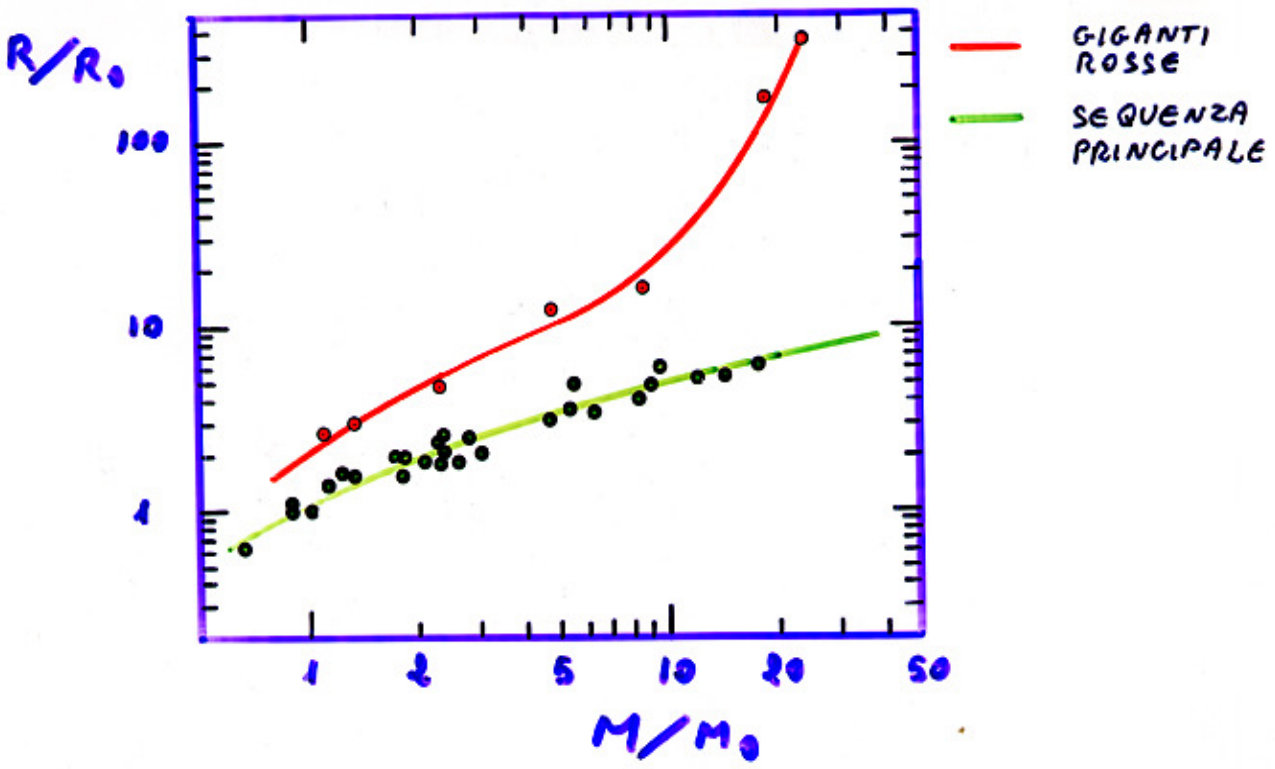

- DENSITA' -

$$\bar{\rho} = \frac{M}{\frac{4}{3}\pi R^3}$$

$$\bar{\rho}_\odot = \frac{2\,10^{33}}{\frac{4}{3}\pi (7\,10^{10})^3} = 1.4 \ g/cm^3$$

NANE BIANCHE

$M \sim 1\ M_\odot$

$R \sim 10.000$ Km

$\rho \simeq 5\,10^5 \ g/cm^3$

BUCO NERO

$M \sim 5\ M_\odot$

$R \sim 15$ Km

$\rho \simeq \frac{2\,10^{16}}{M^2} \sim 8\,10^{14} \ g/cm^3$

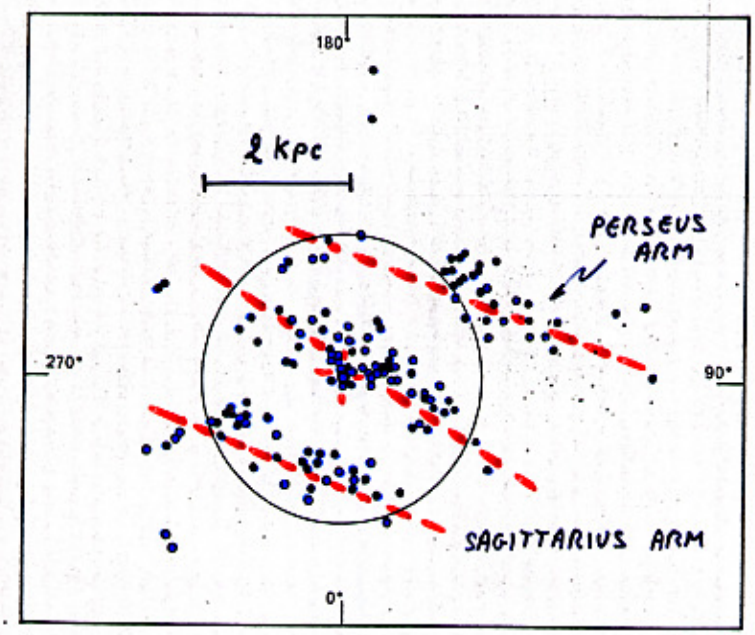

O-B ASSOCIATIONS

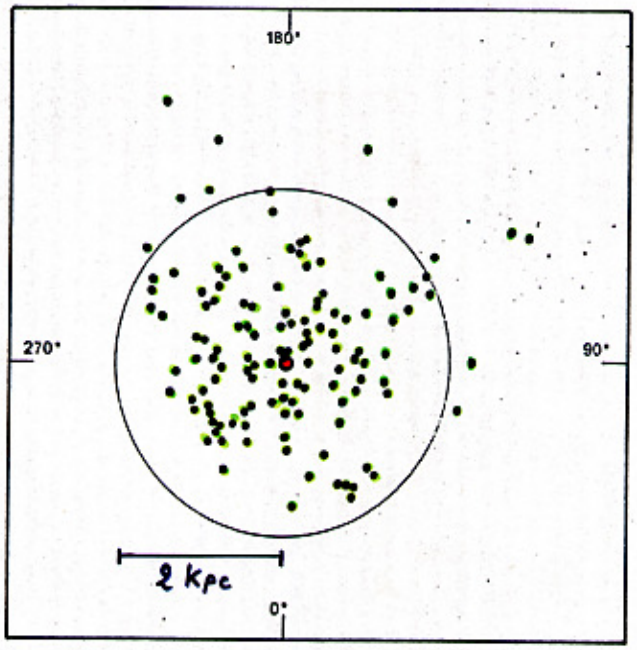

OPEN CLUSTERS

Figure 11.5. Distribution of open clusters of different ages, projected on the galactic plane. The sun is situated at the central cross; the arrow points in the direction of the galactic center. Intervals of one kiloparsec are marked off. The approximate ages are as follows: top left, 10^6 to 5×10^6 years; top right, 5×10^6 to 10^7 years; bottom left, 10^7 to 10^8 years; bottom right over 10^8 years.

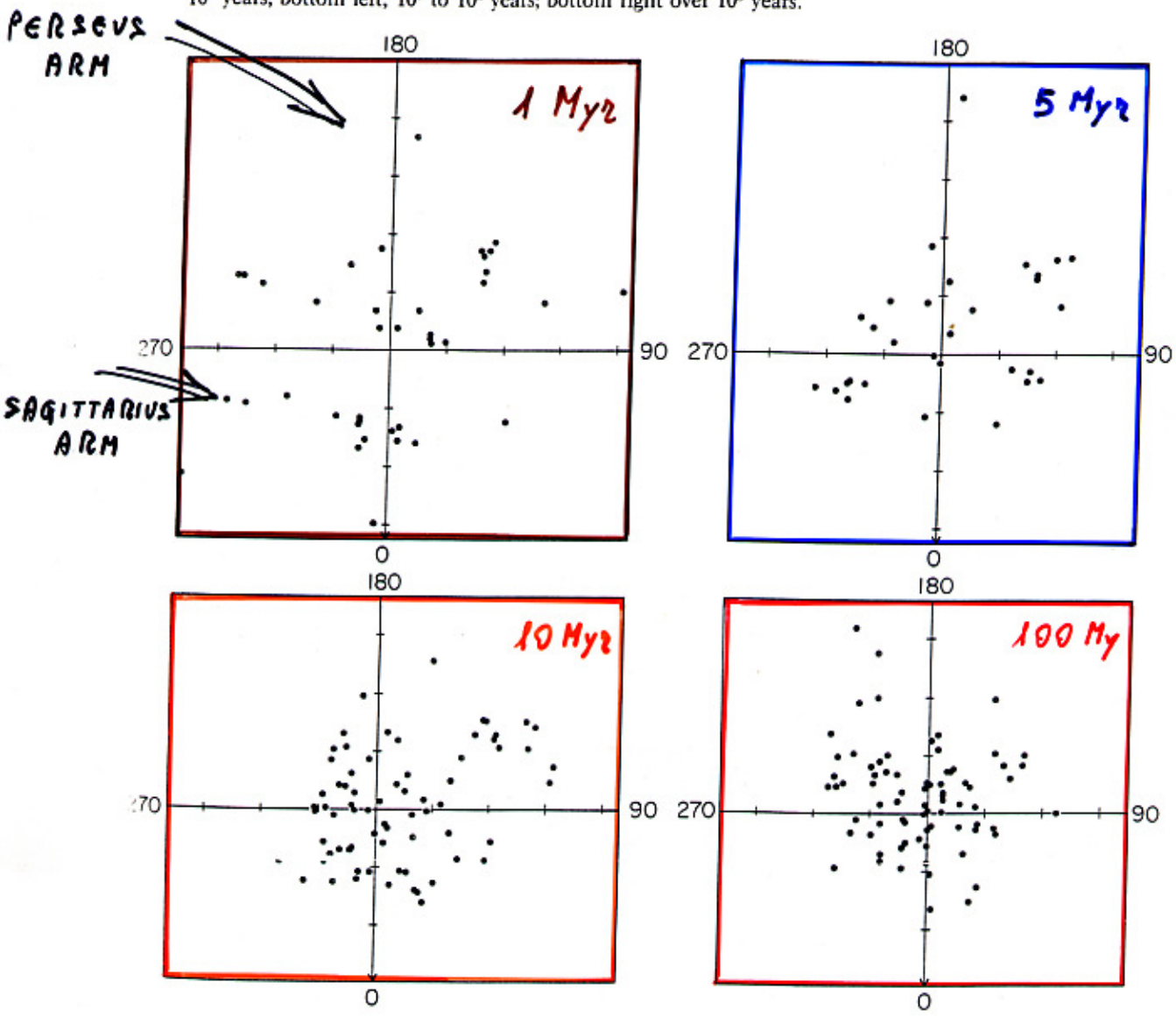

Figure 12.1. Apparent distribution of the open clusters (top) and globular clusters (bottom). They are marked on an equal-area projection of the sky that shows the galactic center in the middle of the diagram, marked by a cross; the central horizontal line marks the galactic plane. The sharp contrast in distribution shows that the open clusters are strongly concentrated to the plane; even those that are far from it in latitude are actually very close in distance, such as the nearby Coma Berenices, which appears at the top of the ellipse. The globular clusters, on the other hand, concentrate toward the galactic center.

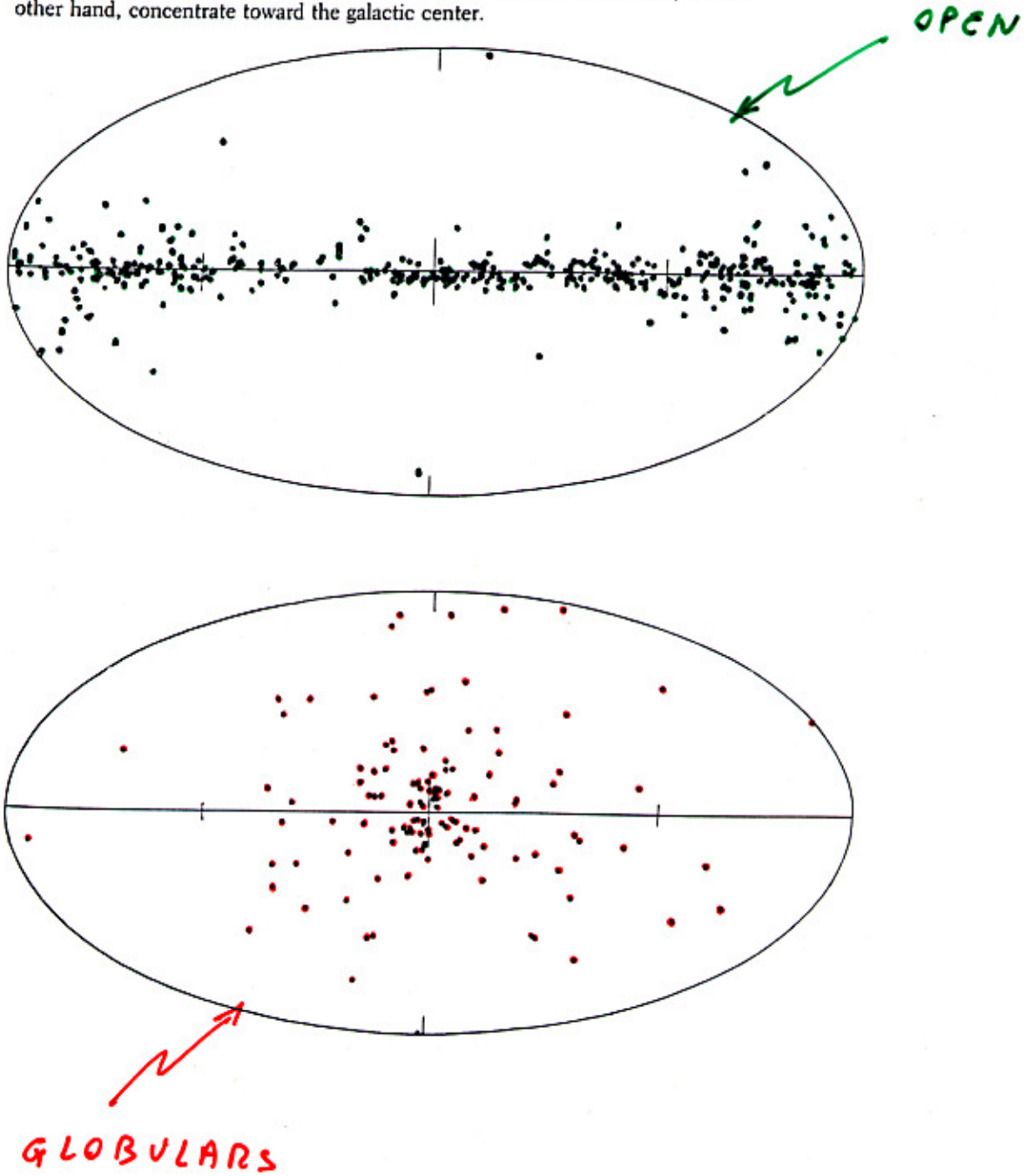

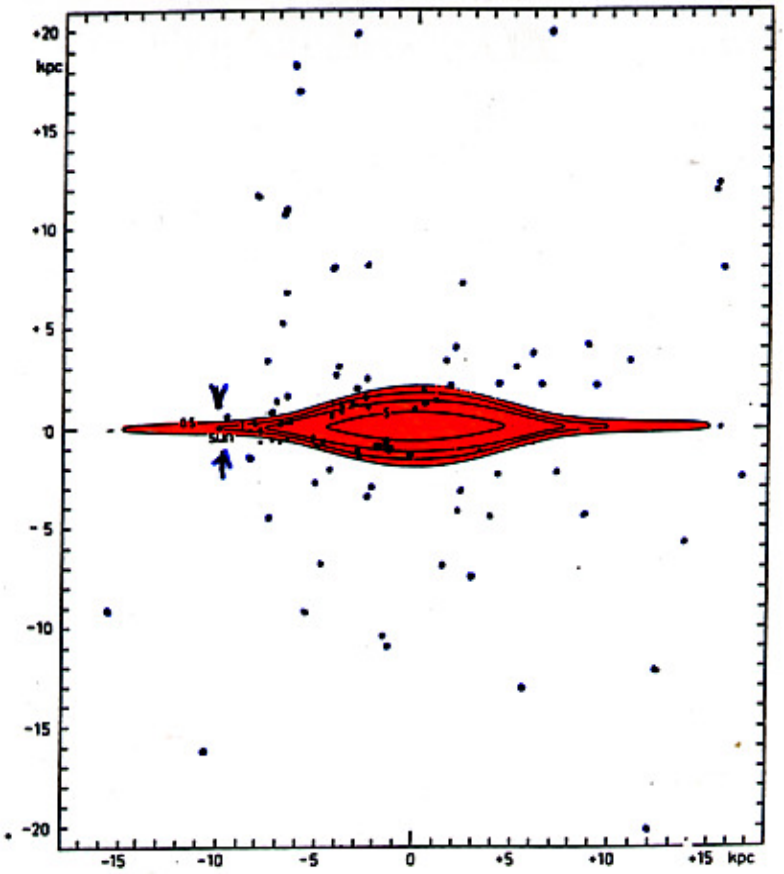

Fig. 23.6: Il *sistema galattico*: distribuzione spaziale degli ammassi globulari, proiettata su di un piano passante per il sole e perpendicolare al piano galattico, ed aree di uguale densità (riferite alle vicinanze del sole). Nel piano galattico è rappresentato, punteggiato, il sottile strato di materia interstellare con popolazione I estrema (braccio della spirale) (secondo J. H. Oort).

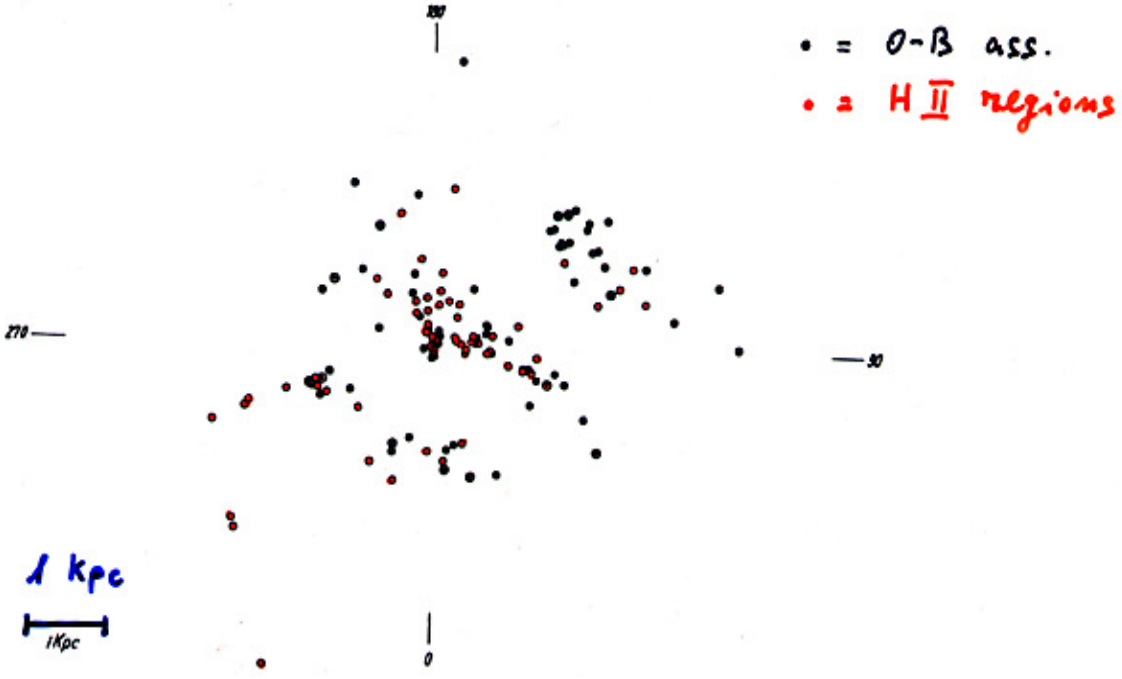

Fig. 23.7: Distribuzione degli *ammassi galattici giovani* • (comprendente anche stelle O-B2), delle regioni H II o e degli ammassi con regioni H II $_{o}$, nel piano galattico, secondo W. Becker. La longitudine galattica $^{II} = 0$ (verso il basso) indica il centro galattico. Il sole si trova nel centro del diagramma cartesiano. Tutti gli oggetti rappresentati sono disposti lungo i bracci della spirale ed appartengono alla popolazione I estrema.

DIAGRAMMA DI BOTTLINGER

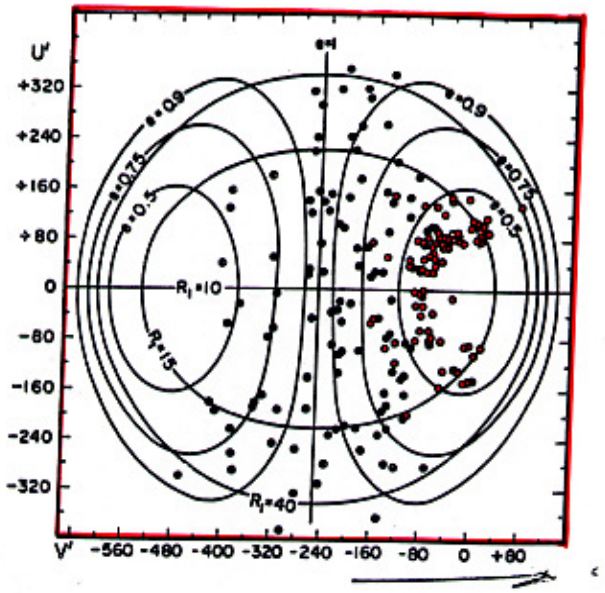

Fig. 23.10: *Diagramma di Bottlinger*. Sono riportate le componenti delle velocità galattiche U' (verso l'anticentro) e V' (nel senso della rotazione) relative ai dintorni del sole. Gli assi ortogonali rappresentano le U e V assolute. Per ogni curva è data l'eccentricità orbitale e e la distanza apogalattica R_I in kpc. Nel capitolo 27 diremo sulle stelle (segnate con •) aventi un eccesso nell'ultravioletto $\delta\,(U-B) > +0^m.16$, cioè le stelle povere di metalli della popolazione II di « halo ». Queste sono, incidentalmente, stelle veloci con grande velocità spaziale. Con o sono segnate le stelle con $\delta\,(U-B) < +0^m.16$, le quali costituiscono una transizione dalla popolazione II di halo alla popolazione del disco galattico, con orbite meno eccentriche (secondo O. J. EGGEN).

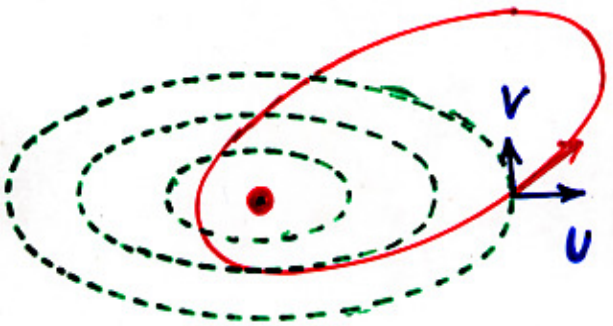

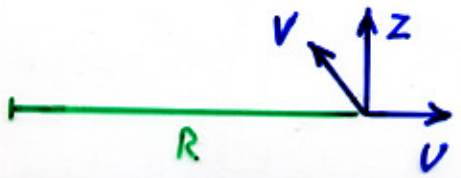

SANDAGE (1982)

SANDAGE & FOUTS (1987)

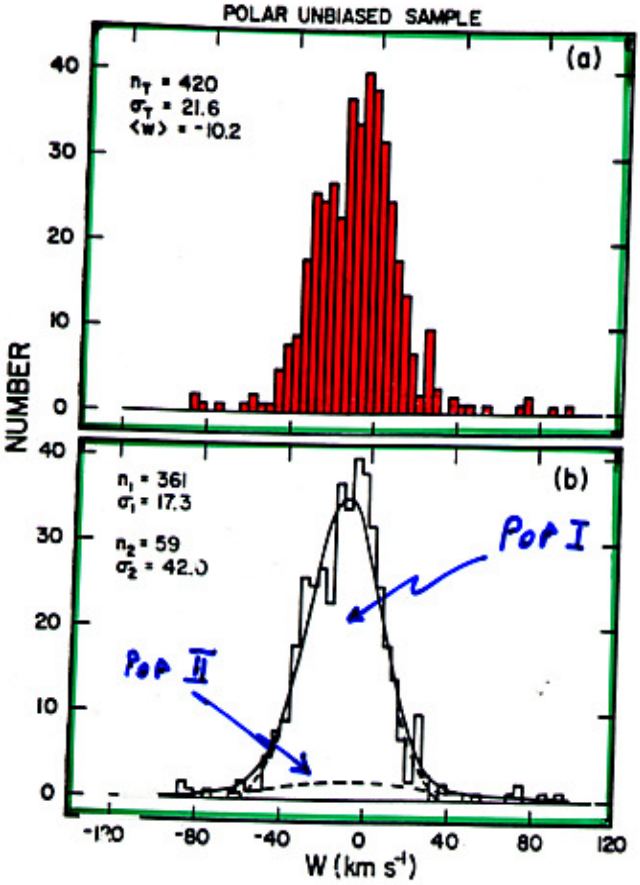

FIG. 2. (Top) Distribution of W velocities from Table VI for the 420-star sample, binned in 4 km s^{-1} intervals. (Bottom) Two-Gaussian fit to the observed distribution. The $\langle W \rangle_2$ and σ_2 values for the high-velocity component have been assumed.

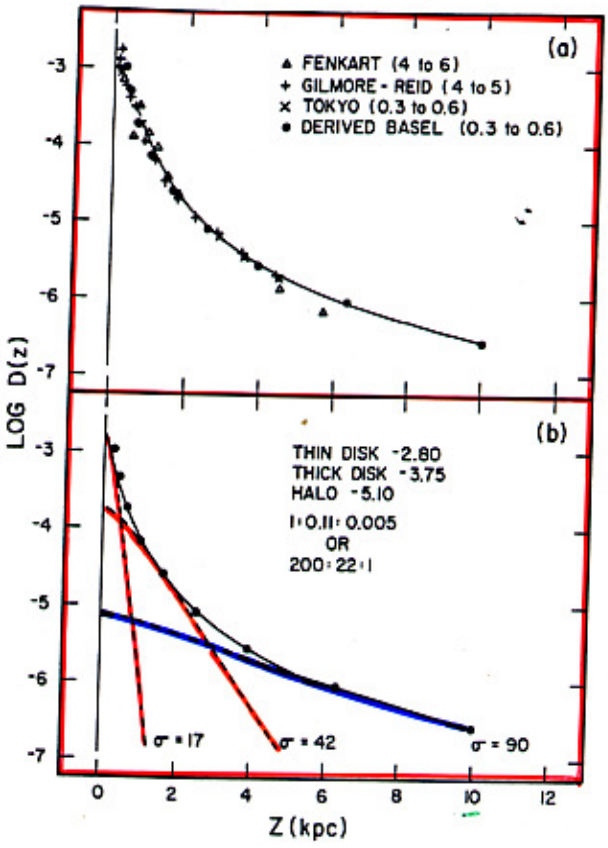

FIG. 2. (Top) The density $D(Z)$ perpendicular to the galactic plane for the four data sets listed in Table II, III, and V. (Bottom) Decomposition of the observed log $D(Z)$ function into three components using the calculated densities shown in Fig. 1.

HALO 1

THICK DISK 22

THIN DISK 200

ρ/ρ_{HALO}

Figure 5.1. Observed numbers of stars of different spectral classes and absolute magnitudes in volume 1 of the *Michigan Spectral Catalogue*, which includes stars south of declination −53° (normal stars with good quality spectra). Because of the wide range in luminosity, this diagram does not show the actual numbers of stars of each kind. The catalogue has a roughly uniform limit of apparent magnitude, so we must take into account the volume of space that is included for each luminosity in order to deduce the true numbers. The result of such a calculation (the Hess diagram) is shown in figure 5.2 (which is not, however, based on the same sample of stars). (From an unpublished paper by Nancy Houk and Richard Fesen.)

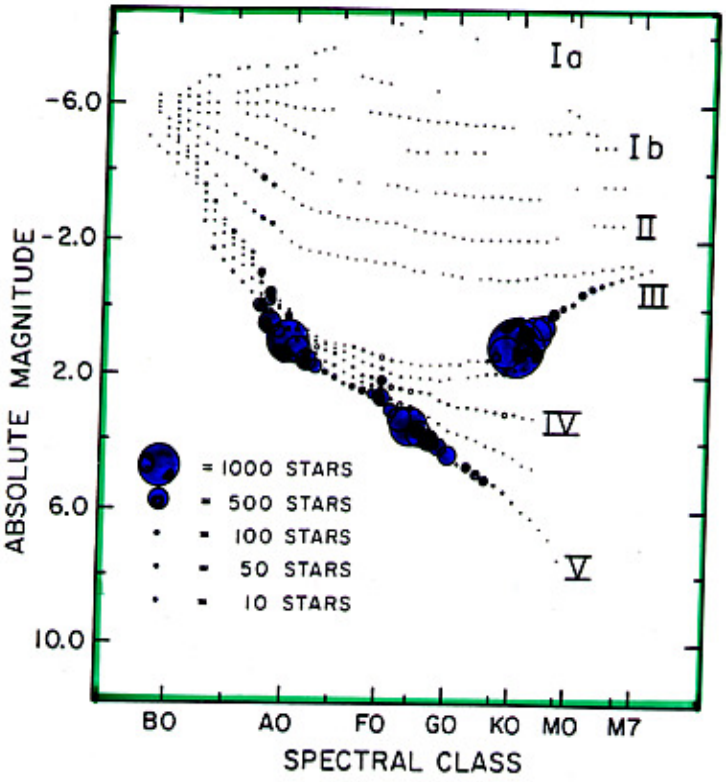

App. Mag. limited

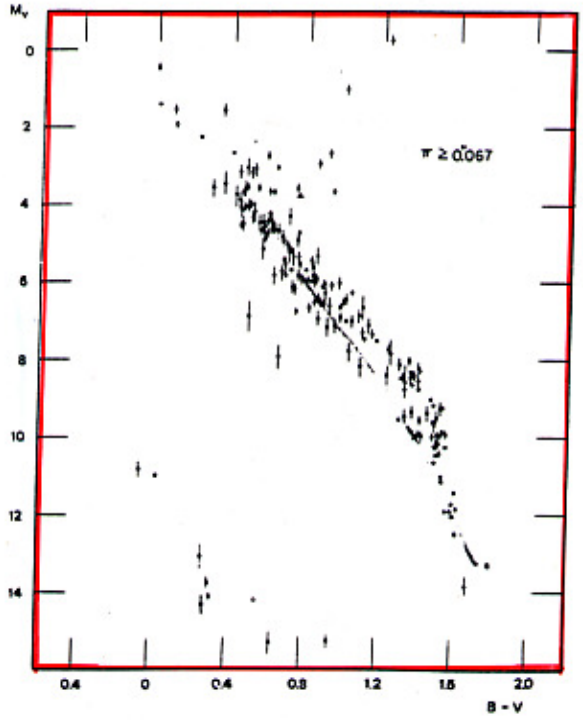

Distance limited

Fig. 9. Diagramma di Hertzsprung-Russell nella forma colore-magnitudine assoluta visuale per le stelle più vicine di 15 pc (da A. Sandage). Le linee verticali rappresentano gli errori delle magnitudini assolute.

Figure 5.2. Schematic Hess diagram for stars in our neighborhood. Numbers of stars per cubic parsec are shown by contours which refer to 20, 200, 2000, and 20,000 stars. The main sequence runs along the ridge. Probably the peak is reached at about the bottom right corner of the diagram, with about 40,000 stars per cubic parsec. Statistics for fainter stars do not permit us to say how fast the slope falls off from there. The contours for white dwarfs are not shown; these stars populate a moderately high ridge, roughly parallel to the main ridge and separated from it by a deep valley.

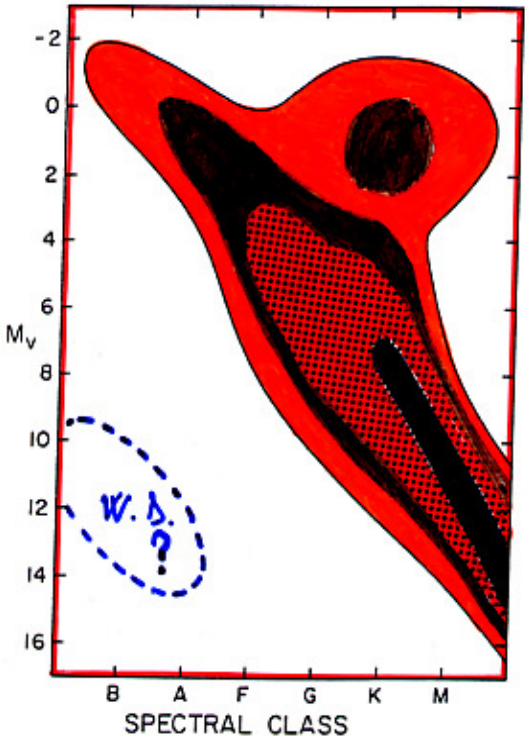

DIAGRAMMA DI HESS

20
200
2000
20,000

$*/Pc^3$

Statistica stellare. Funzione di luminosità

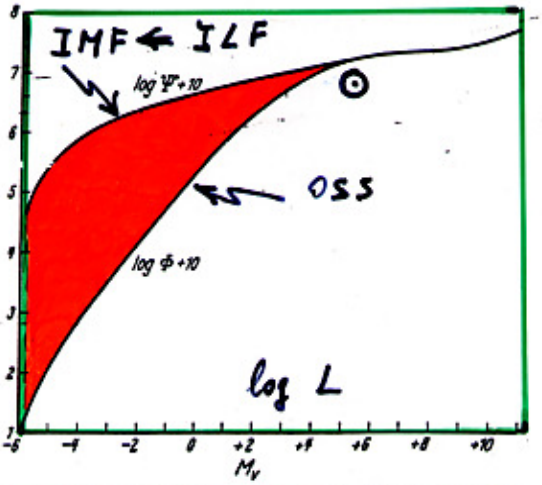

log N

KAPTEYN & VAN RHIJN '20

SALPETER (1953)

Fig. 26.8: Funzione di luminosità $\Phi(M_v)$ e funzione iniziale di luminosità $\Psi(M_v)$, per stelle della sequenza principale nei dintorni del sole. La Φ e la Ψ dànno rispettivamente il numero osservato di stelle per pc³ comprese fra $M_v - 1/4$ ed $M_v + 1/4$, e di quelle formatesi a partire dalla formazione della Galassia.

PARDI & FERRINI (1994)

SCALO (1987)

RANA (1991)

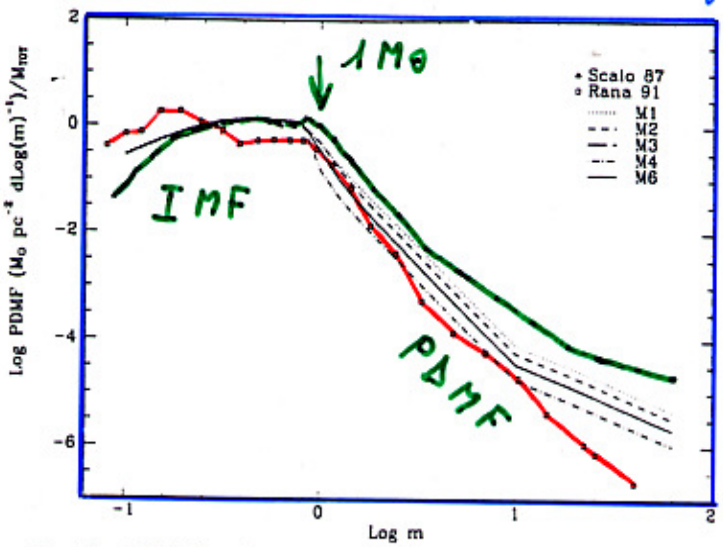

log N

[*/d log M/Pc²]

FIG. 12.—PDMFs predicted by the model in cases M1–M4 and M6 superposed on data of Scalo (1987 [*triangles*]) and Rana (1991 [*squares*]).

A) $\psi_{(M)} \propto M^{-1.3}$

B) $\psi_{(M)} \propto M^{-2.2}$

C) $\psi_{(M)} \propto M^{-2.7}$

A B C

0.5 1.0 $M_\odot$

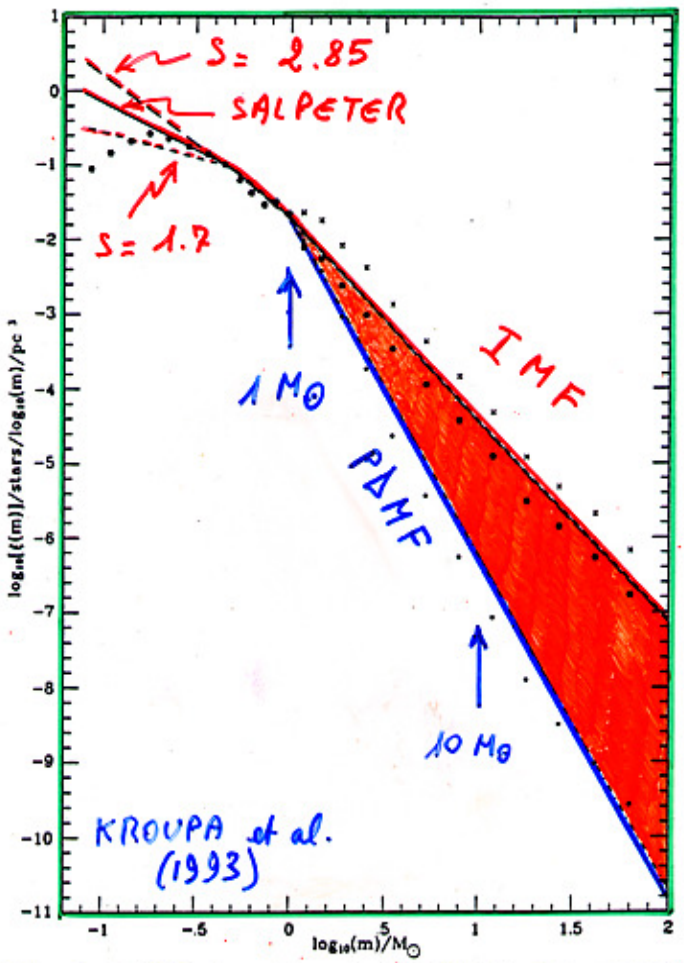

log $\psi_{(M)}$

[*/d log M/Pc³]

Figure 22. The stellar initial mass function (IMF) and present-day mass function (PDMF). The solid line represents the IMF given by equation (13), and the long- and short-dashed lines are for the cases $\alpha_1 = 1.85$ and 0.70, respectively. The PDMF ($\alpha_3 = 4.5$, Section 2) is indicated by the dot-dashed line. At masses below about 1 $M_\odot$ the PDMF equals the IMF. As a comparison, we show the PDMF derived by Scalo (1986) by solid dots. He corrects for stellar evolution; for a Galactic disc age of $T_0 = 9$ Gyr the IMF is indicated by stars, and for $T_0 = 12$ Gyr by crosses.

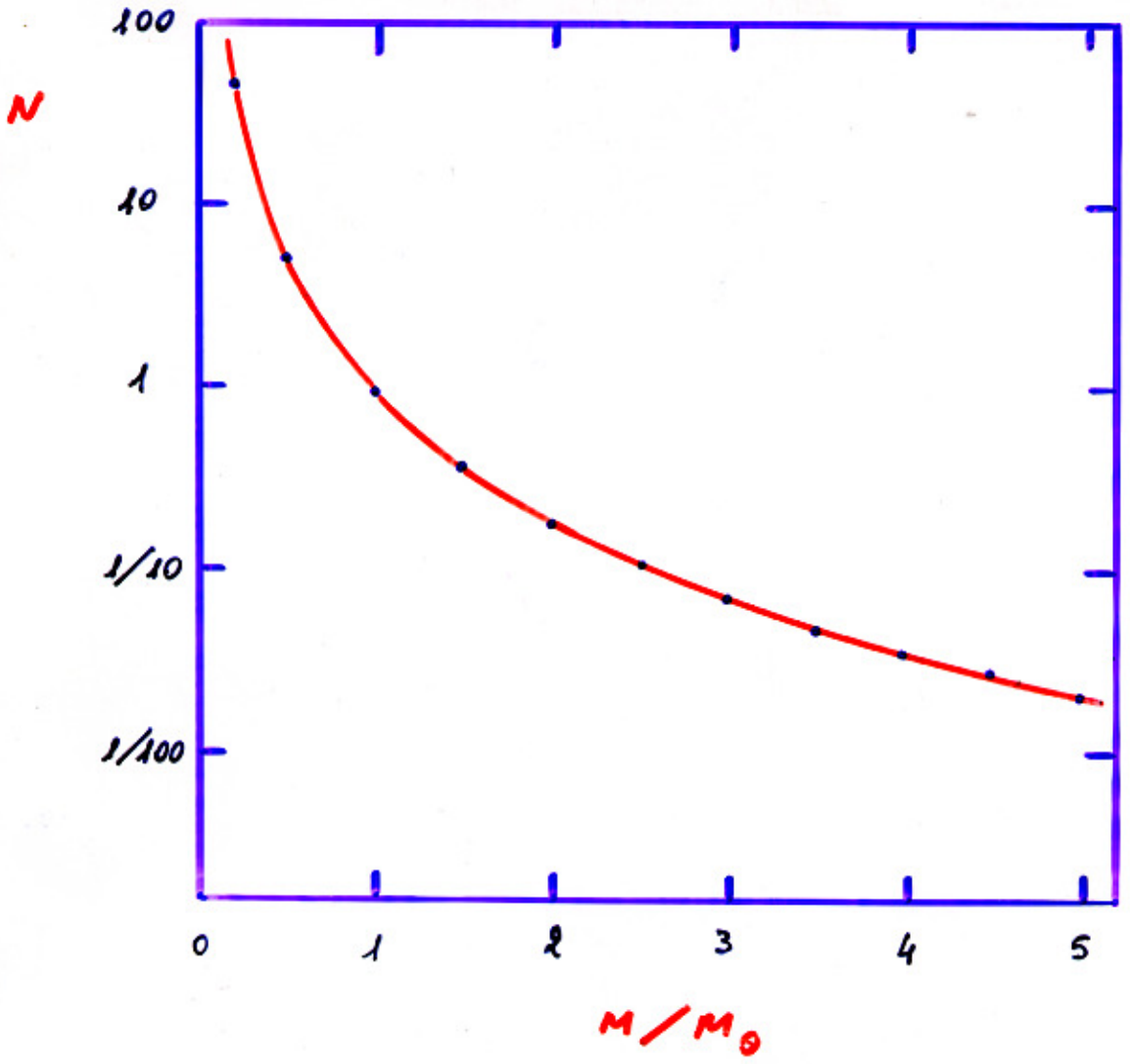

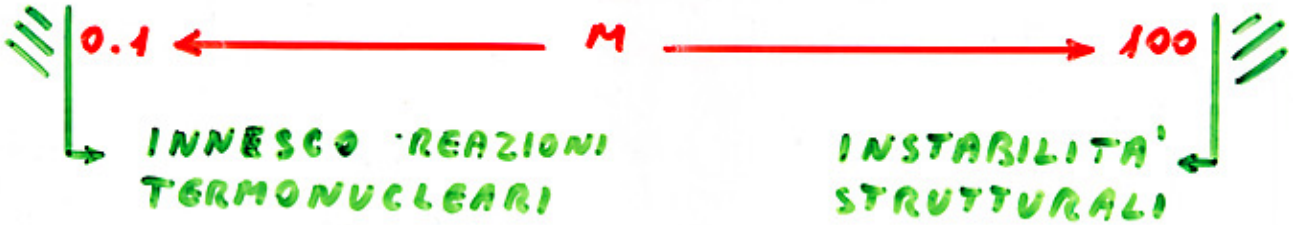

M	L	N
0.1	0.0001	220
0.5	0.06	5
1	1	1
2	16	1/5
5	625	1/40
10	10.000	1/220
50	$6\,10^6$	1/10.000

THEORY OF SSPs

Definition of SSP:

1) A generation of COEVAL stars ($SFR = \delta_0$)
(so that we can define an AGE of the population)

2) Fixed metallicity (unique Z)

Star partition:

MS: $\boxed{N_{(M)} = A\, M^{-s}}$ (IMF)

Post-MS:

$$\Delta M = M_{DYING} - M_{TO} \simeq - \left.\frac{dM}{dt}\right|_{TO} \tau_{PMS} \simeq M_{TO} \frac{\tau_{PMS}}{T}$$

$$\boxed{N_{PMS} = A\, M_{TO}^{-s}\, \Delta M = A\, M_{TO}^{-s}\, \dot{M}_{TO}\, \tau_{PMS}}$$

$$N_{PMS} = \underbrace{A\, M_{TO}^{-s}\, \dot{M}}\; \tau_{PMS}$$

$$\ell = B\, L_{TOT}$$

$$N_{PMS} = B\, L_{TOT}\, \tau_{PMS} = 1.7\, 10^{-11} \left(\frac{L}{L_\odot}\right)\left(\frac{\tau}{yr}\right)$$

$\Downarrow$

specific Evolutionary Flux

LUMINOSITY

$$L_{MS} = A \int_0^{TO} \ell_* M^{-s} dM \qquad \begin{cases} \ell_* \propto M^3 \\ t_* \propto M^{-2} \end{cases}$$

$$L_{MS} \simeq \frac{A}{4-s} M_{TO}^{4-s} \qquad (s < 4)$$

$$L_{MS} \propto t^{-\frac{4-s}{2}} \sim t^{-0.85}$$

$$L_{PMS} = \int_{PMS} \ell_* dN = A\, M_{TO}^{-s}\, \dot{M}_{TO} \underbrace{\int_{PMS} \ell_* d\tau}$$

fuel ~ const.

$$L_{PMS} \propto t^{-\frac{3-s}{2}} \sim t^{-0.35}$$

$$\frac{L_{PMS}}{L_{MS}} \propto \frac{t^{-\frac{3-s}{2}}}{t^{-\frac{4-s}{2}}} \propto \sqrt{t}$$

Conclusion: MS always dominates with decreasing time

Corollary: Total SSP luminosity is a DECREASING function of time

Model evolutionary rate at different bands

$$L_{BOL} \propto t^{-0.75}$$

$$L_B \propto t^{-0.95}$$

$$L_V \propto t^{-0.86}$$

$$L_I \propto t^{-0.75}$$

$$L_K \propto t^{-0.71}$$

$Z = Z_\odot$

$s = 2.35$

(BUZZONI 1996)

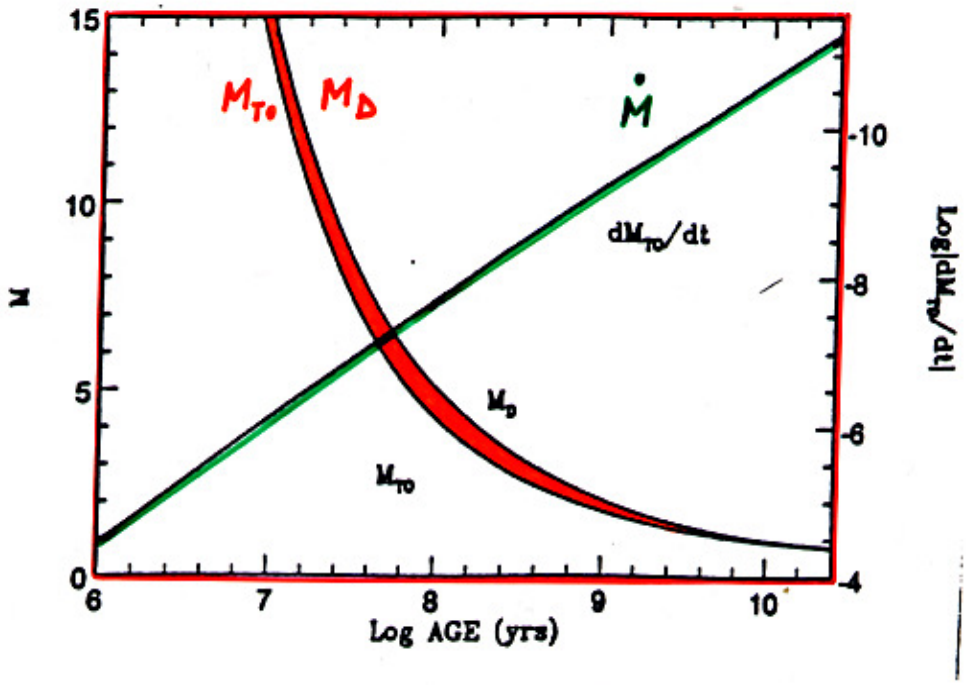

Renzini & Buzzoni (1986)

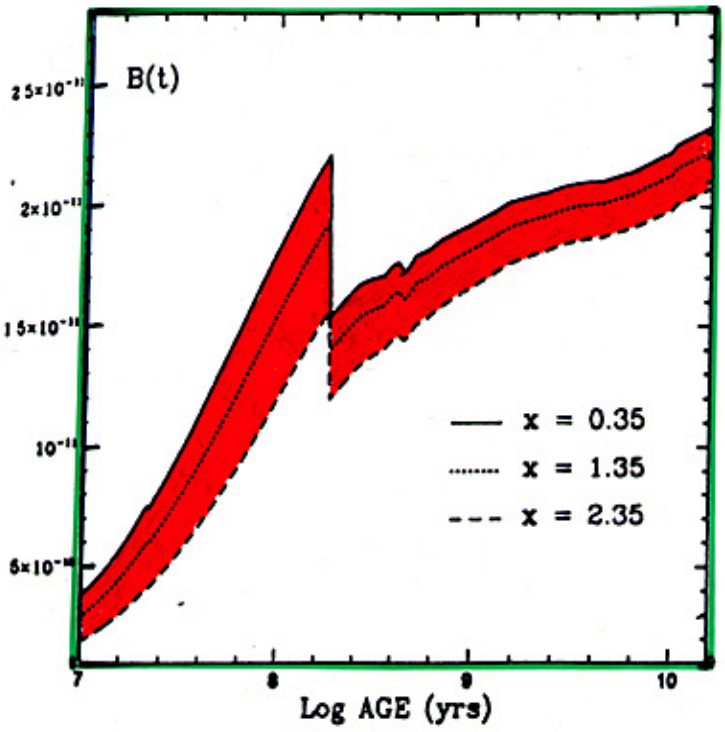

Fig. 1.3: The specific evolutionary flux $B(t)$ as a function of age for three IMF slopes $(1 + x)$.

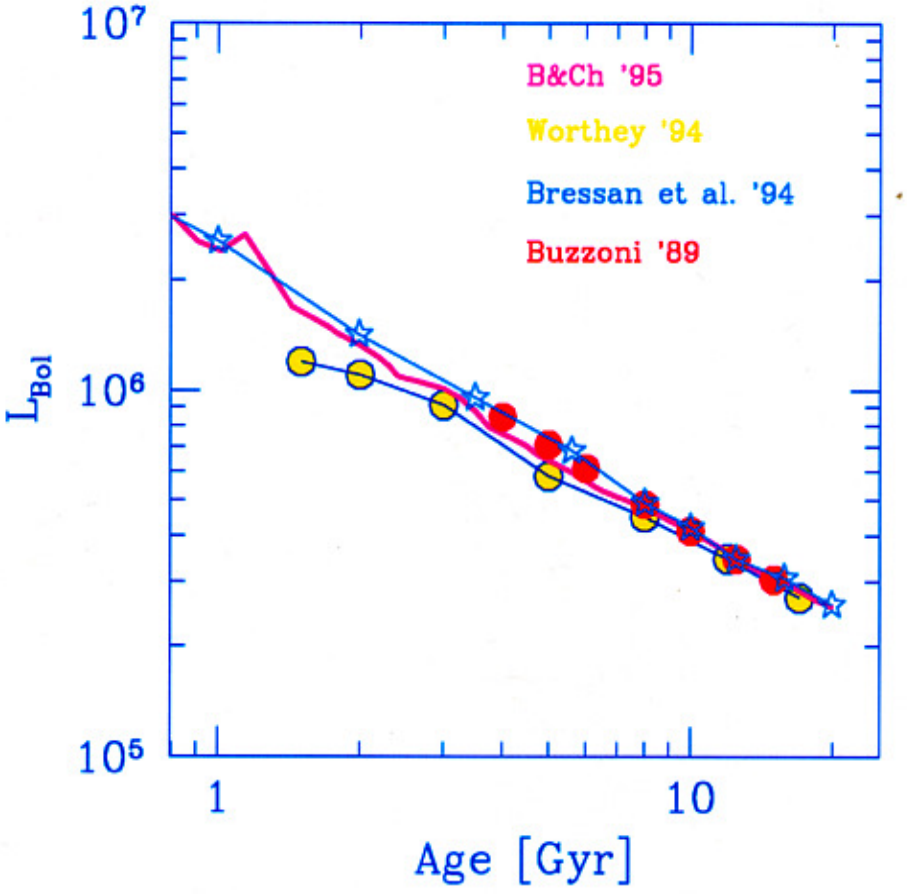
10^7
10^6
10^5
L_{Bol}
B&Ch '95
Worthey '94
Bressan et al. '94
Buzzoni '89
1
10
Age [Gyr]

"PERTURBED" GALAXIES

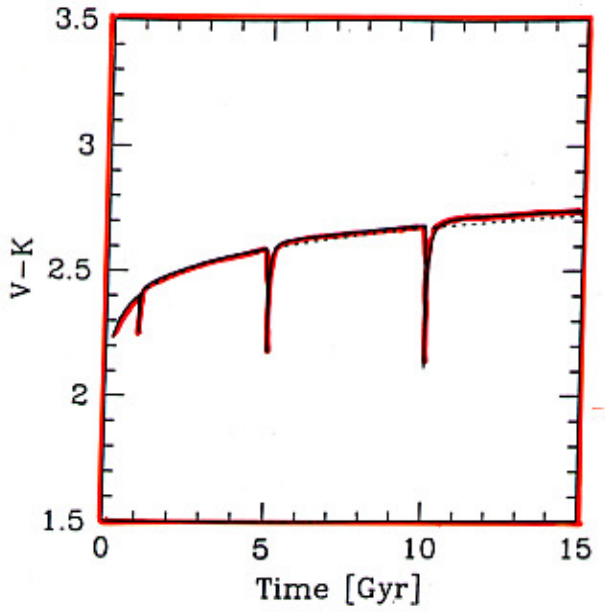

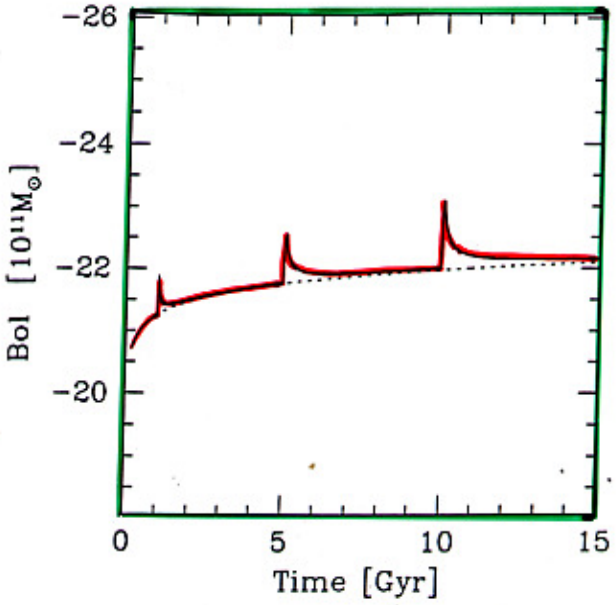

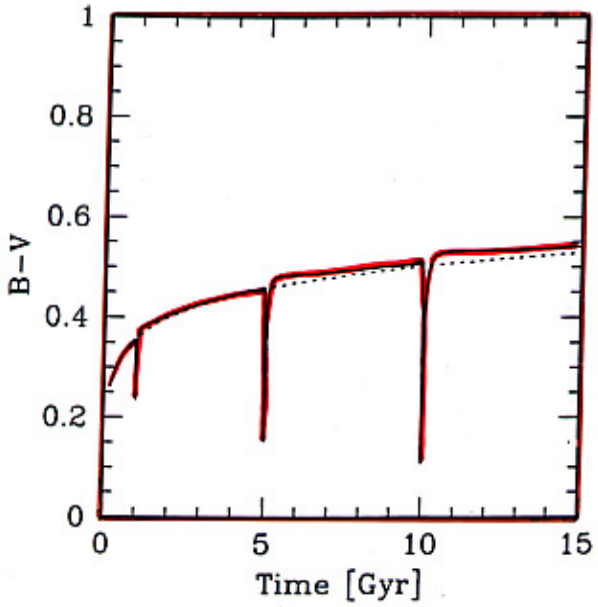

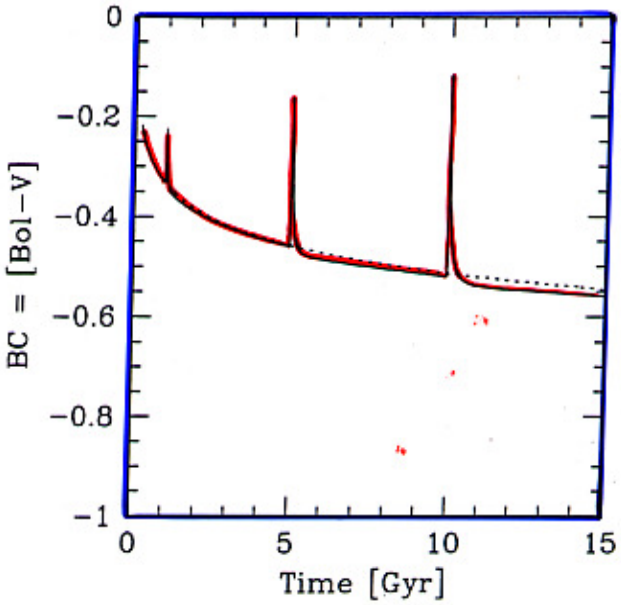

$M_{gal} = 10^{11} M_\odot$ $\quad SFR_0 =$ cnst.

Burst : 10% M_{gal}

$\tau_B = 10^7$ yrs

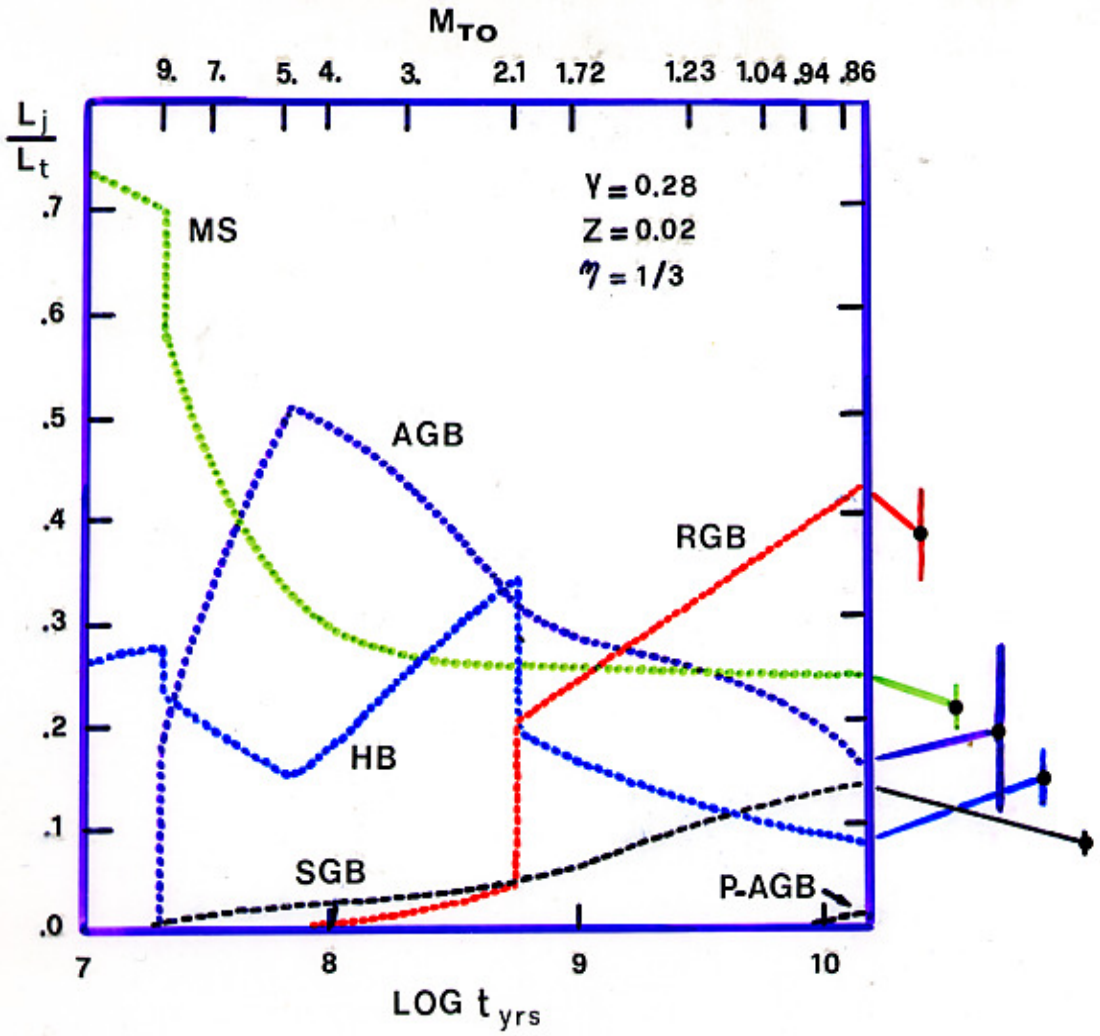
M_{TO}
9. 7. 5. 4. 3. 2.1 1.72 1.23 1.04 .94 .86
$\frac{L_j}{L_t}$
.7
.6
.5
.4
.3
.2
.1
.0
MS
AGB
RGB
HB
SGB
P-AGB
Y = 0.28
Z = 0.02
η = 1/3
7
8
9
10
LOG t_{yrs}

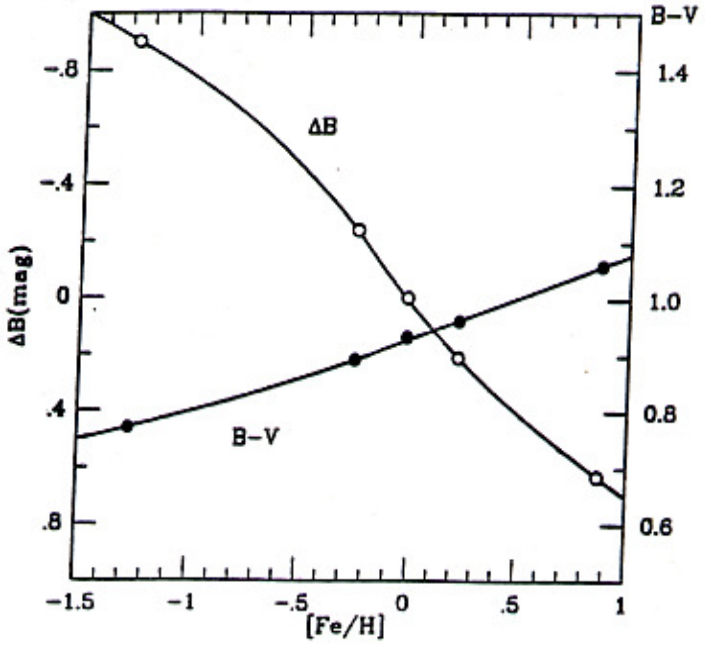

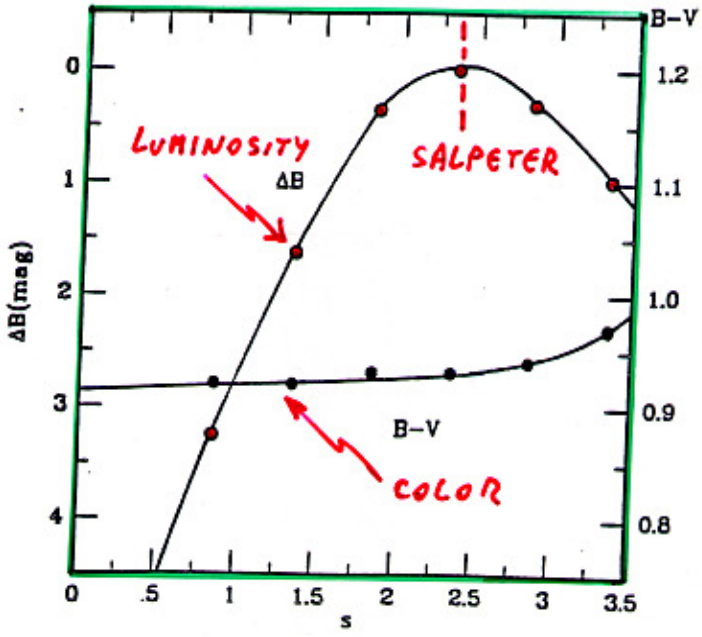

BUZZONI (1995)

$$M_{TOT} = A \int M\, M^{-s} = \frac{A}{2-s}\left[M_u^{2-s} - M_l^{2-s} \right]$$

$s > 2$ DWARF - DOMINATED SSP

$s < 2$ GIANT - DOMINATED SSP

Bower, Lucey & Ellis '92

● = 16 galx VIRGO

● = 43 galx COMA

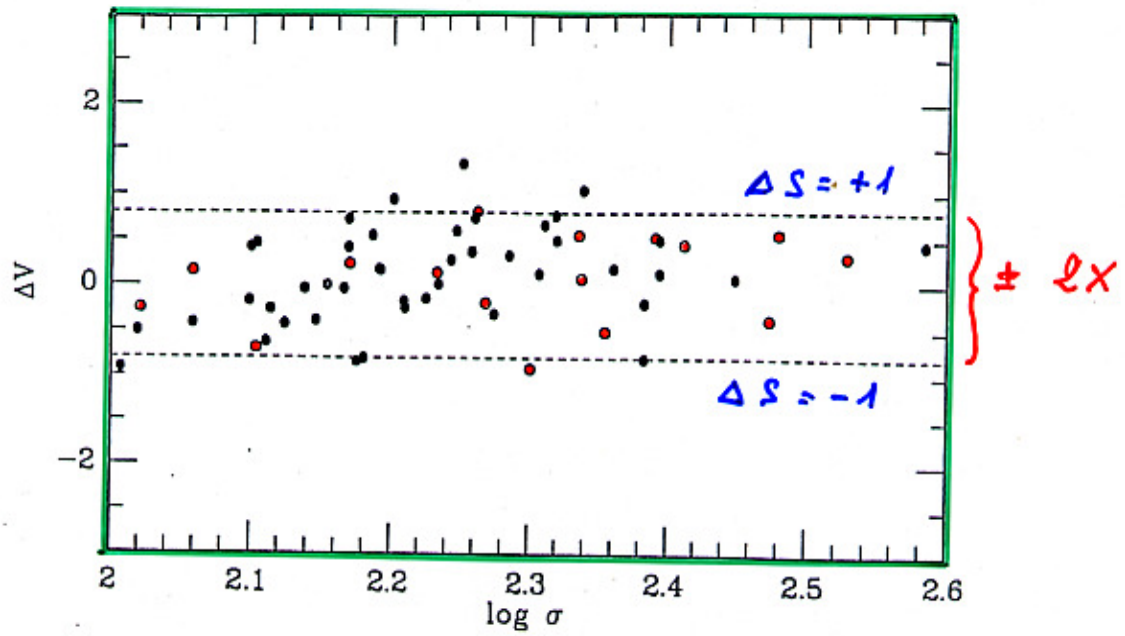

same σ ⇒ same Mass ⇒ same $[Fe/H]$

IF (AGE = CONST)

THEN ⇒ $\Delta V_{mag} \Leftrightarrow \Delta S$

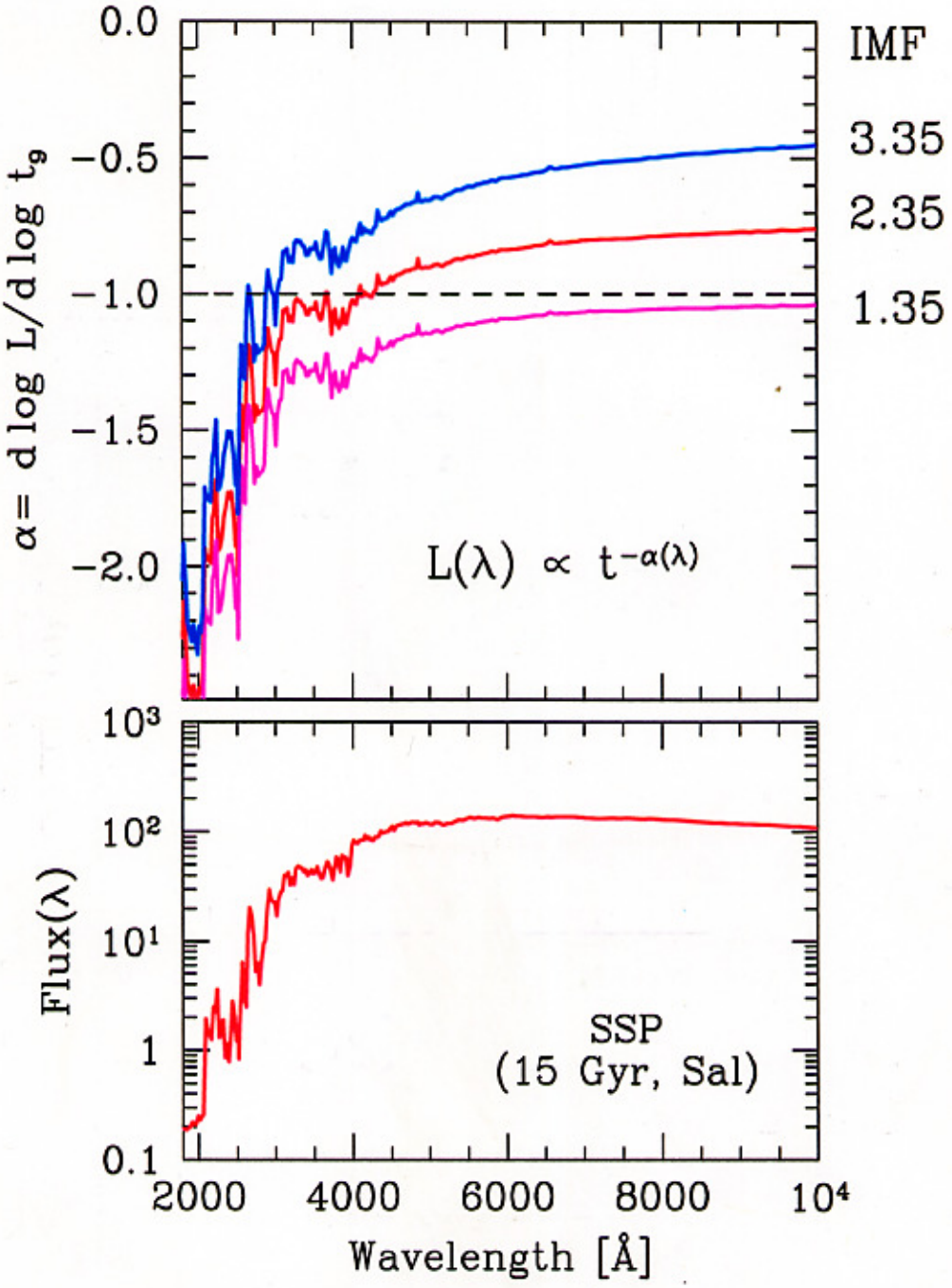
0.0
−0.5
−1.0
−1.5
−2.0
α= d log L/d log t9
IMF
3.35
2.35
1.35
L(λ) ∝ t−α(λ)
10³
10²
10¹
1
0.1
Flux(λ)
SSP
(15 Gyr, Sal)
2000
4000
6000
8000
10⁴
Wavelength [Å]

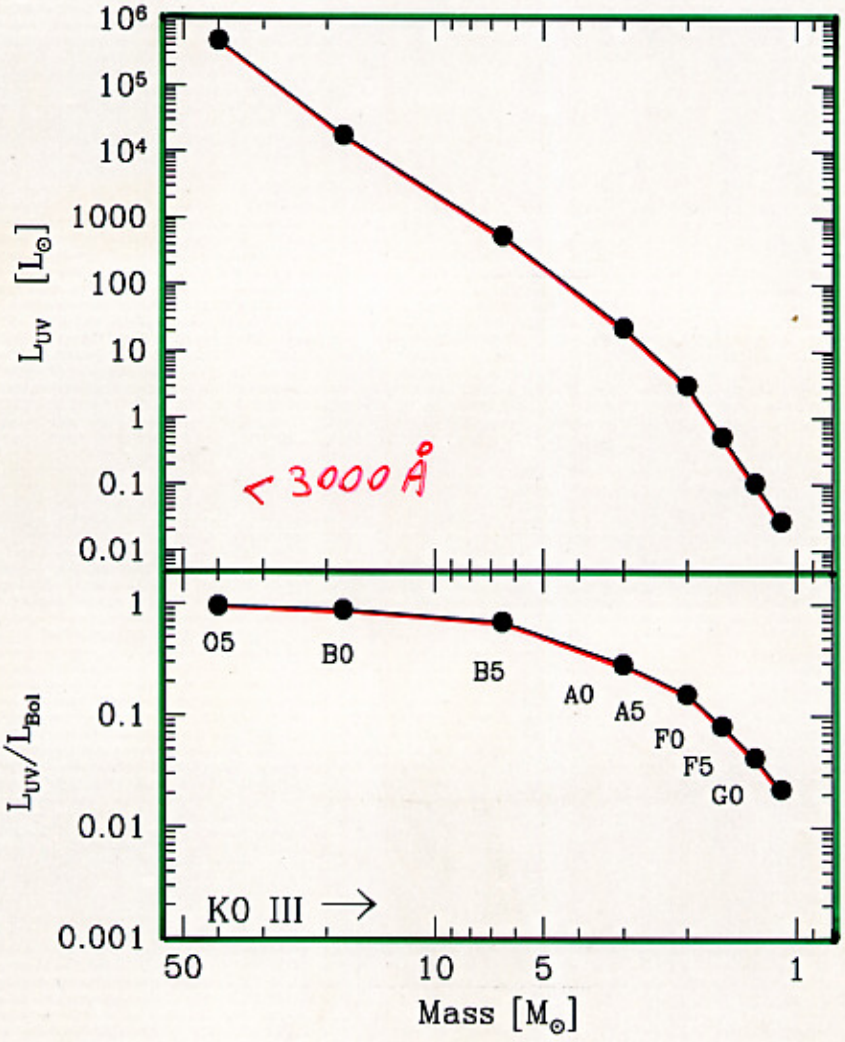
10^6
10^5
10^4
1000
100
10
1
0.1
0.01
L_{UV} [$L_\odot$]
< 3000 Å
1
0.1
0.01
0.001
L_{UV}/L_{Bol}
O5
B0
B5
A0
A5
F0
F5
G0
K0 III →
50
10
5
1
Mass [$M_\odot$]

$L_{UV} \rightarrow SFR$

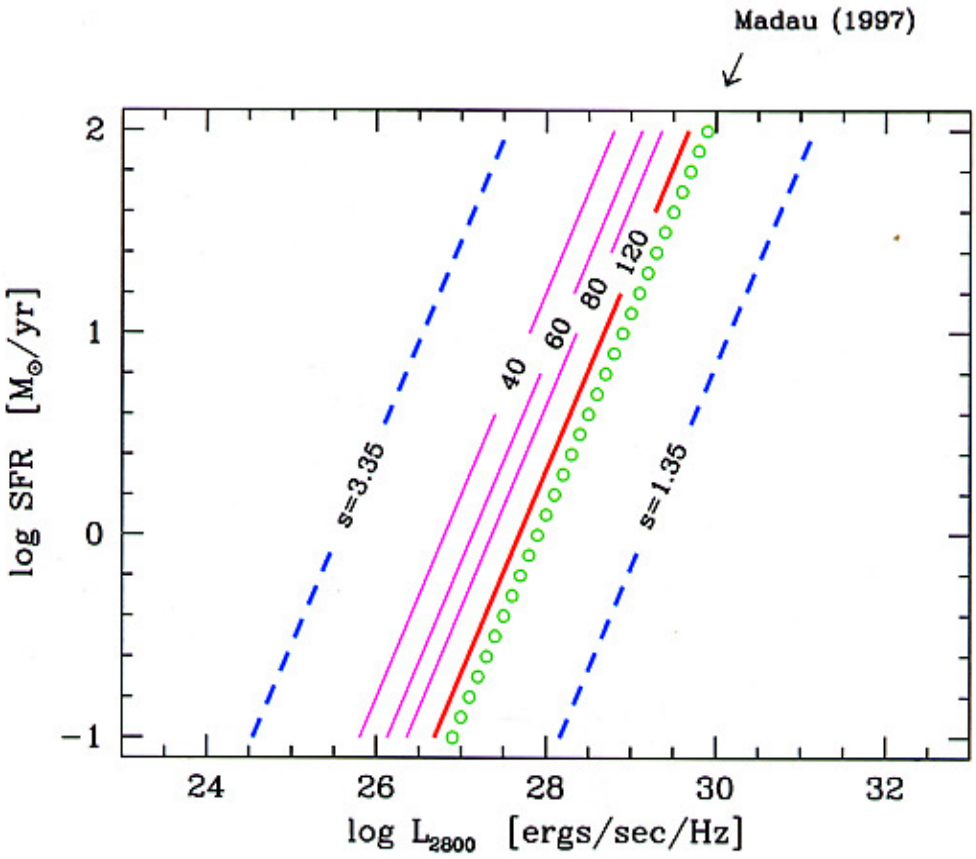

(Buzzoni 2002)

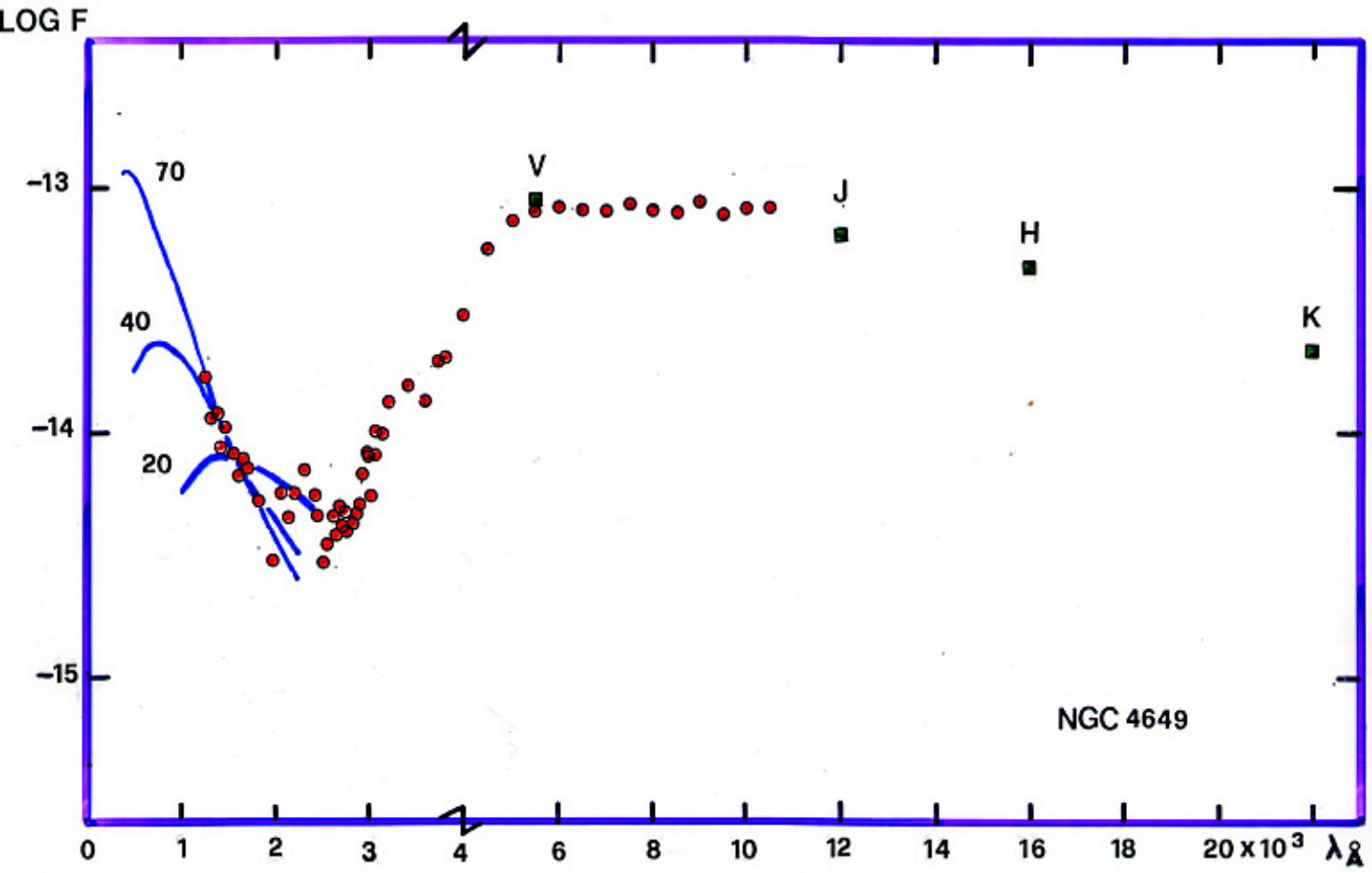

T_{BB}	L_U / L_{TOT}
$2\ 10^4$	0.014
$4\ 10^4$	0.021
$7\ 10^4$	0.057

CASTELLANI et al. (1991)

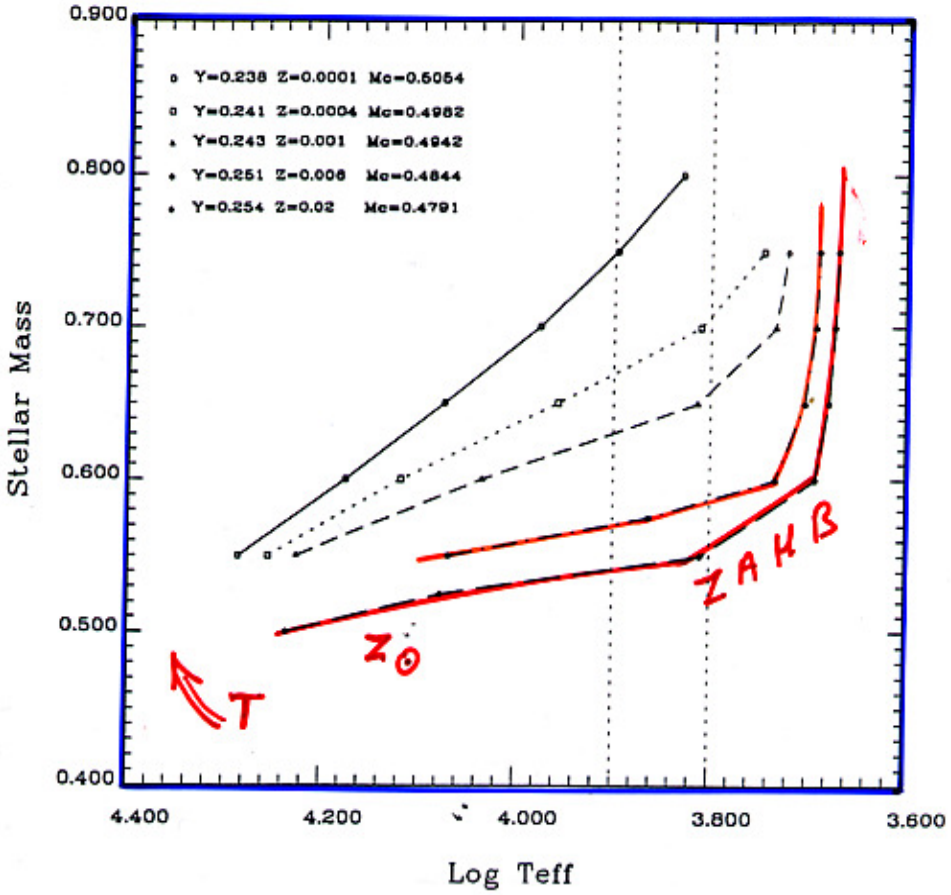

FIG. 6.—The distribution of stellar masses vs. effective temperatures for ZAHB models of the various labeled metallicities. Symbols on the right vertical axis show the masses of the corresponding red giants for a cluster age $t = 15 \times 10^9$ yr. The dotted lines indicate the range of temperatures approximately covered by RR Lyrae pulsators.

M. CASTELLANI et al. (1994)

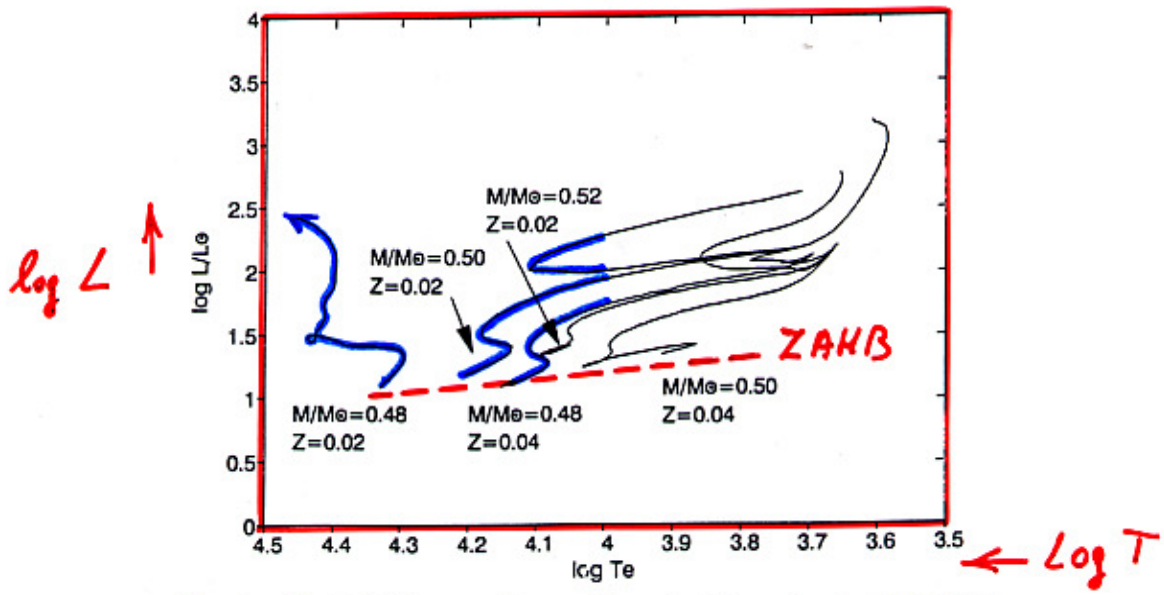

FIG. 1.—The H-R diagram of the models evolved at constant mass covering the central He-burning phase and (in some models) the initial He shell–burning phases.

V. CASTELLANI & TORNAMBÉ (1992)

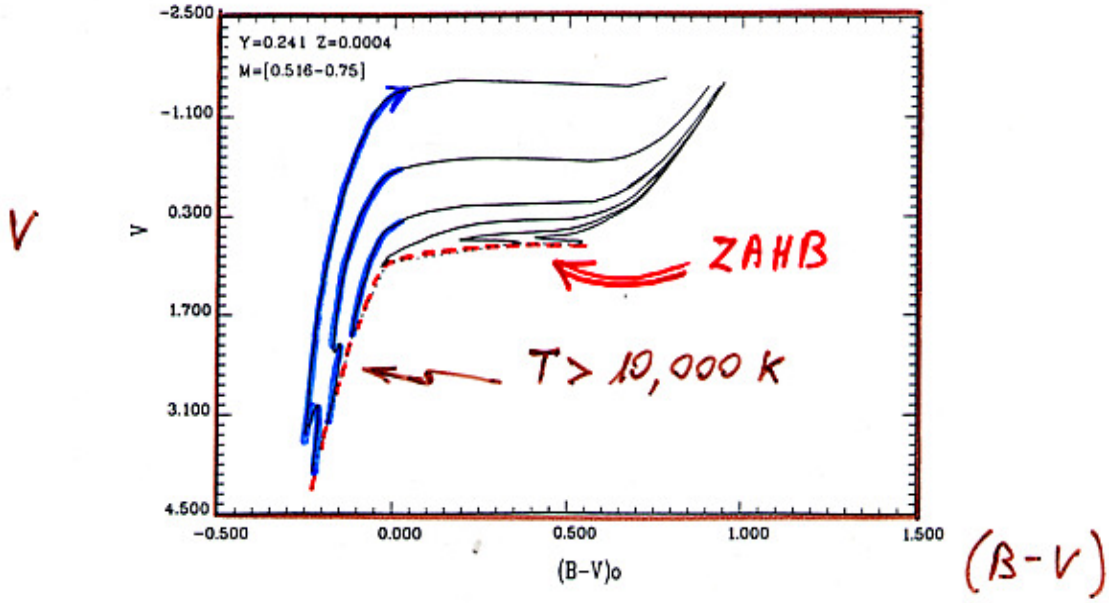

Fig. 5. The evolutionary paths in the V, $B-V$ plane of HB models with $Z = 0.0004$ and for selected values of the stellar mass in the labeled range of masses

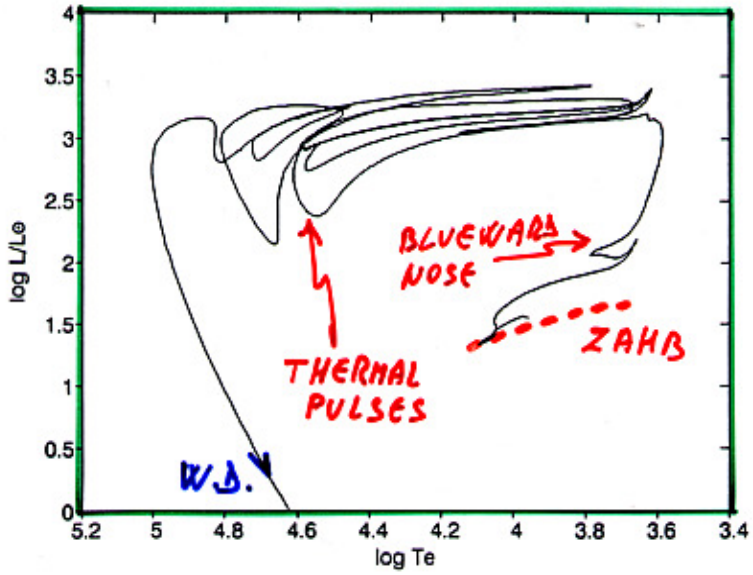

FIG. 4.—The H-R diagram of the 0.52 $M_\odot$, $Z = Z_\odot$ model including the fast loops determined by the thermal pulses.

CASTELLANI et al. (1994)

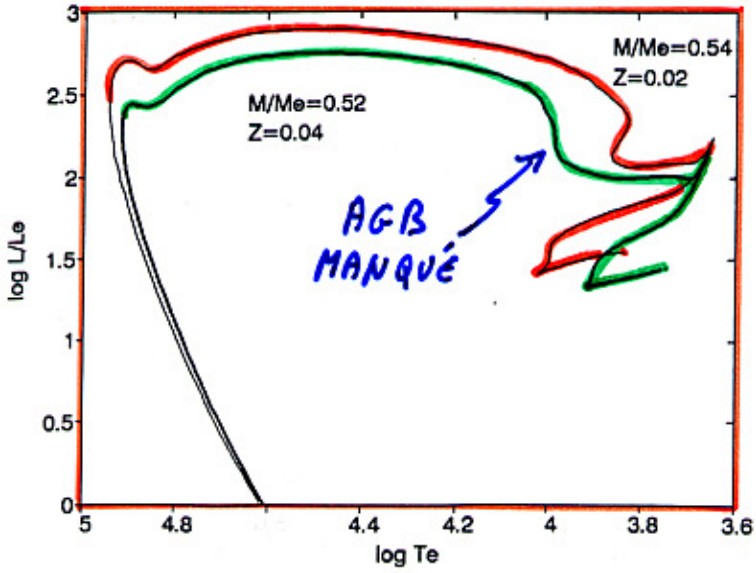

FIG. 9.—The H-R diagram of the two models evolved including mass loss as discussed in the text. The solid line refers to the 0.54 $M_\odot$, $Z = Z_\odot$ model, while the heavy solid line refers to the 0.52 $M_\odot$, $Z = 2Z_\odot$ model.

HB EVOLUTION

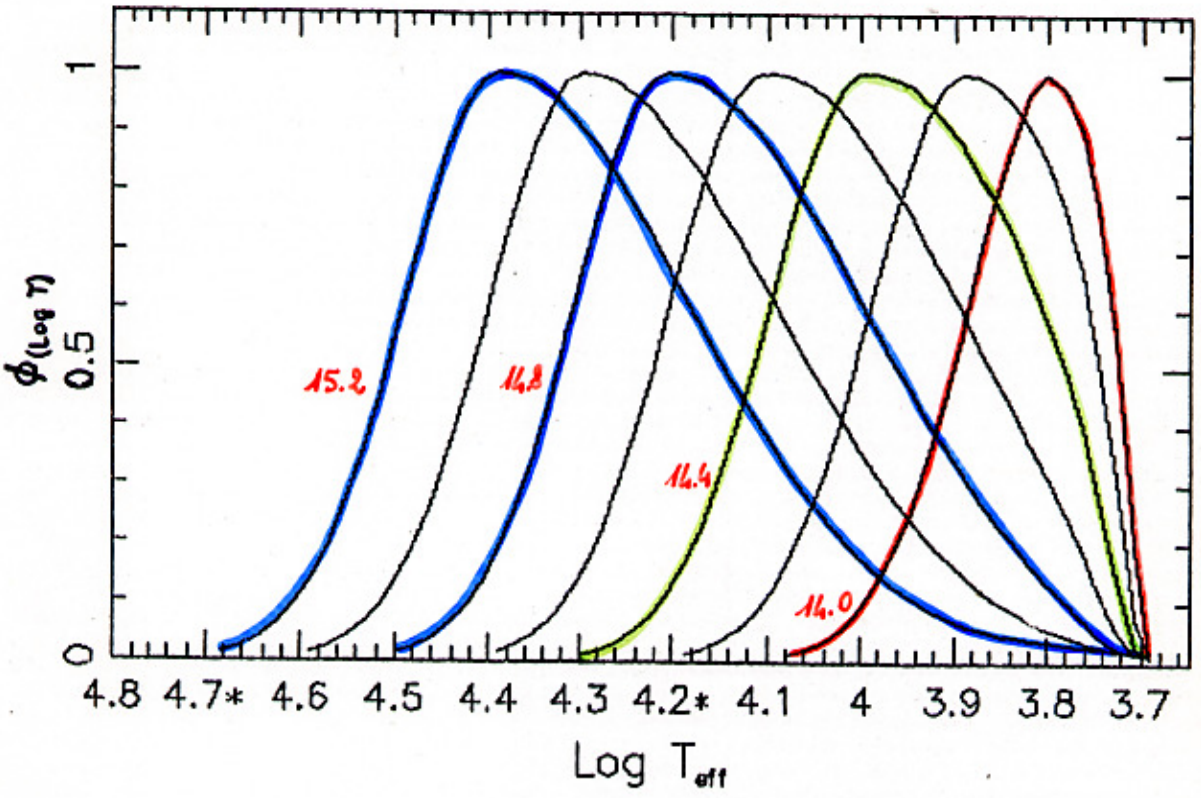

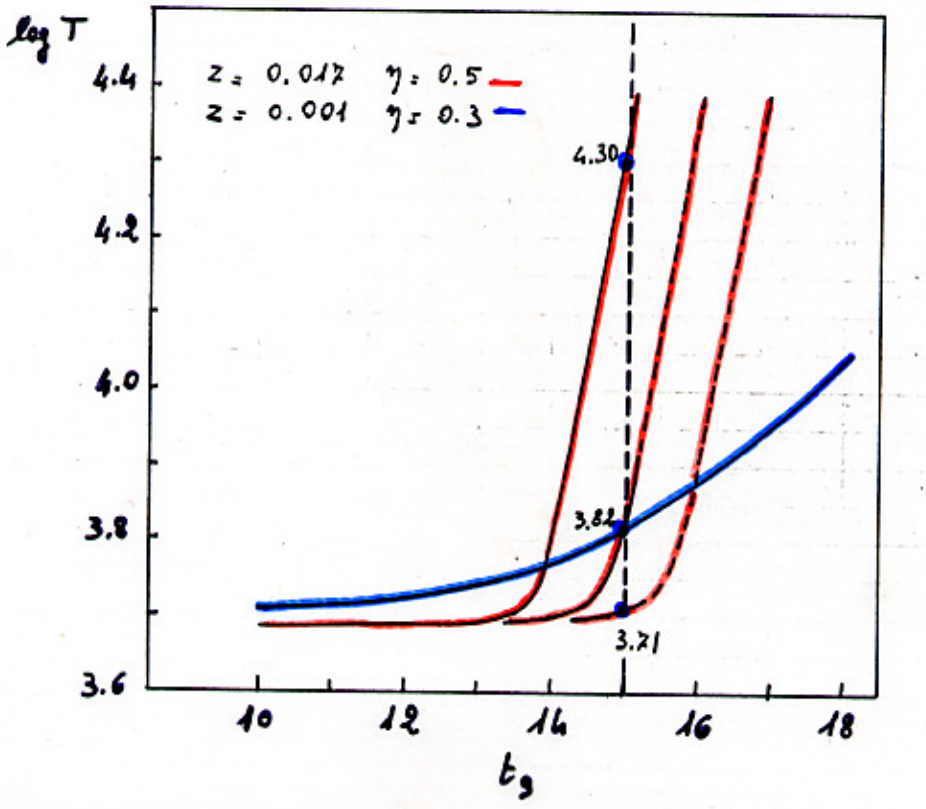

HB EVOLUTION

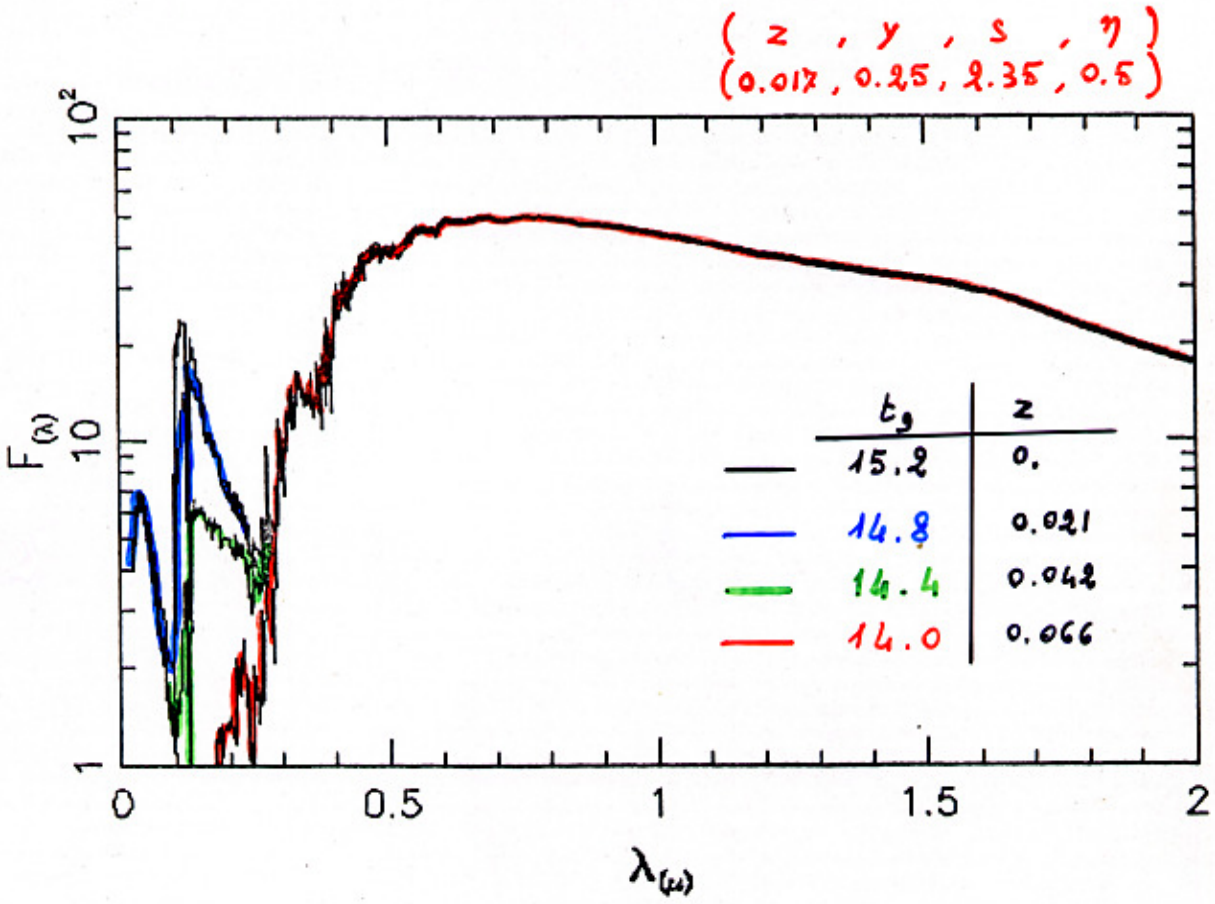

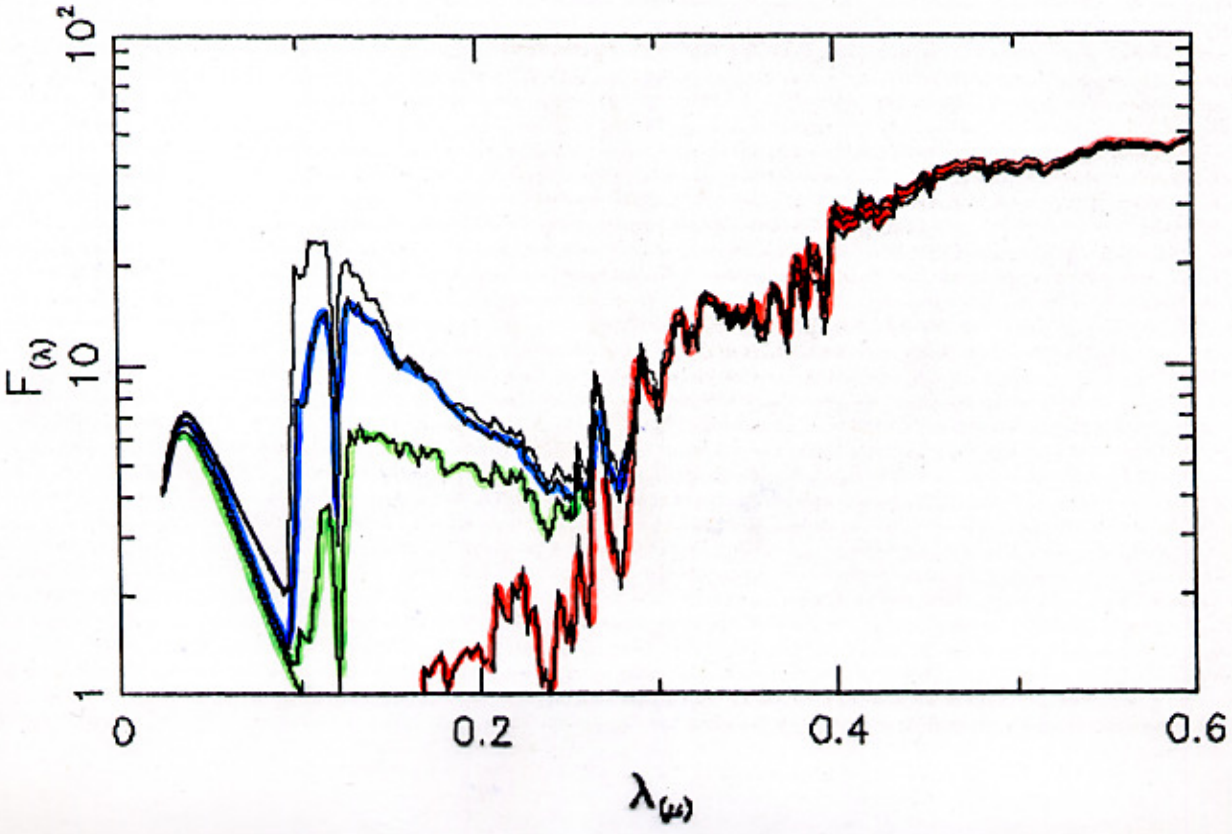

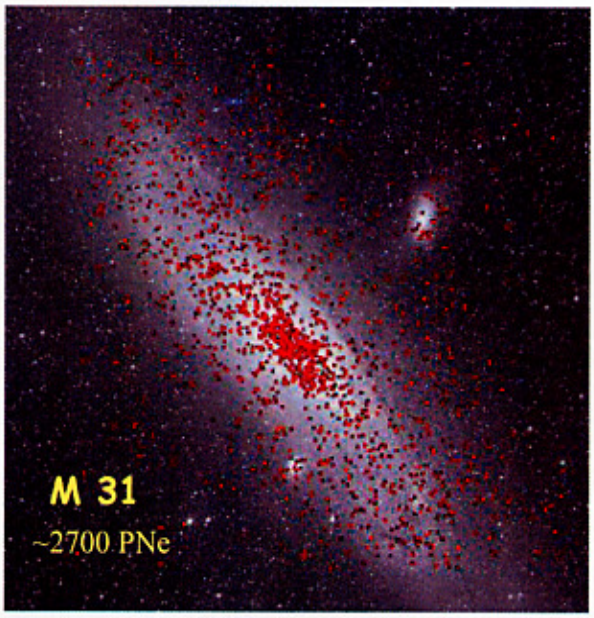

[OIII]-g *vs.* Ha-r color-color diagrams

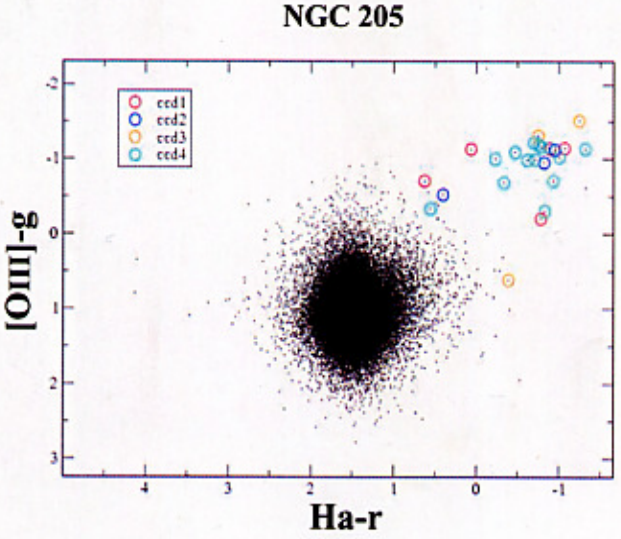

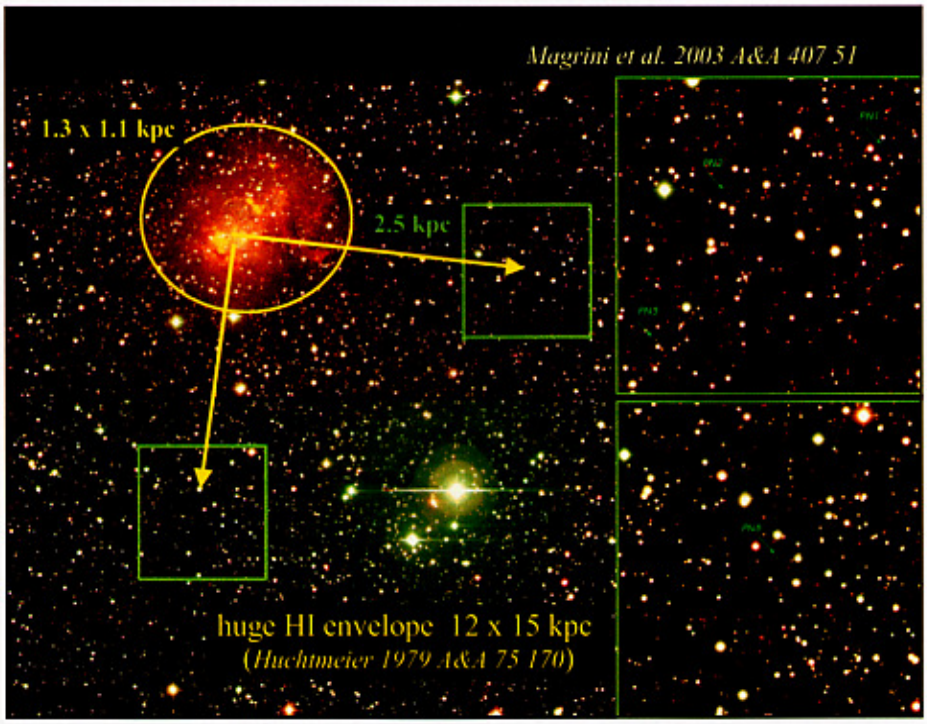

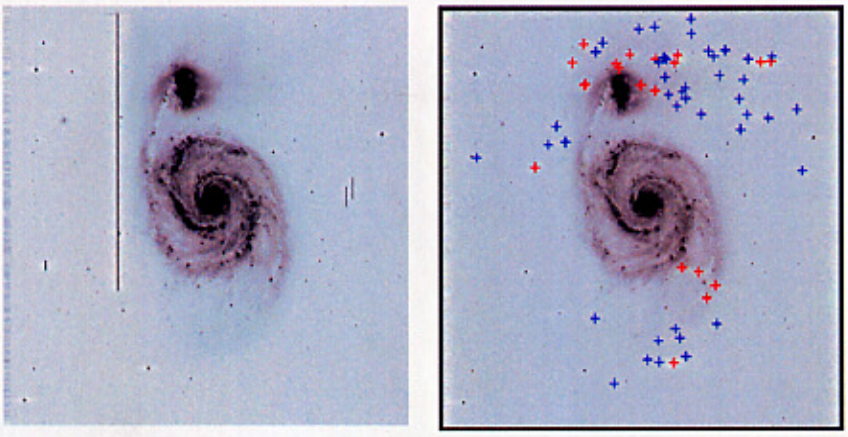

Feldmeier, Ciardullo & Jacoby (1997)

Planetary Nebulae follow Luminosity not surface brightness!

Stars can exist at great distances from luminous galaxies

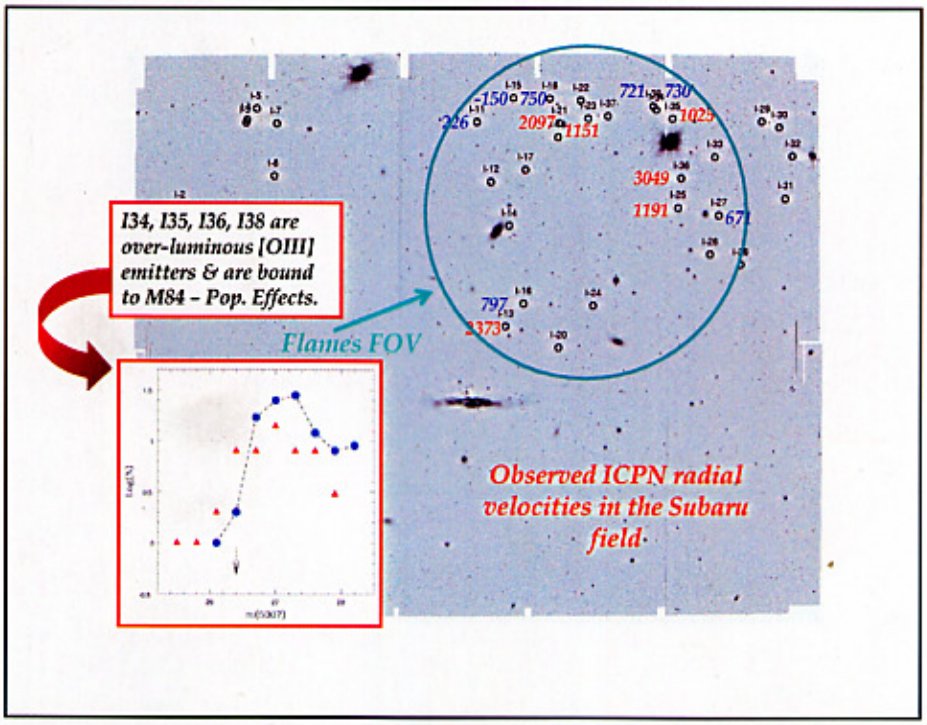

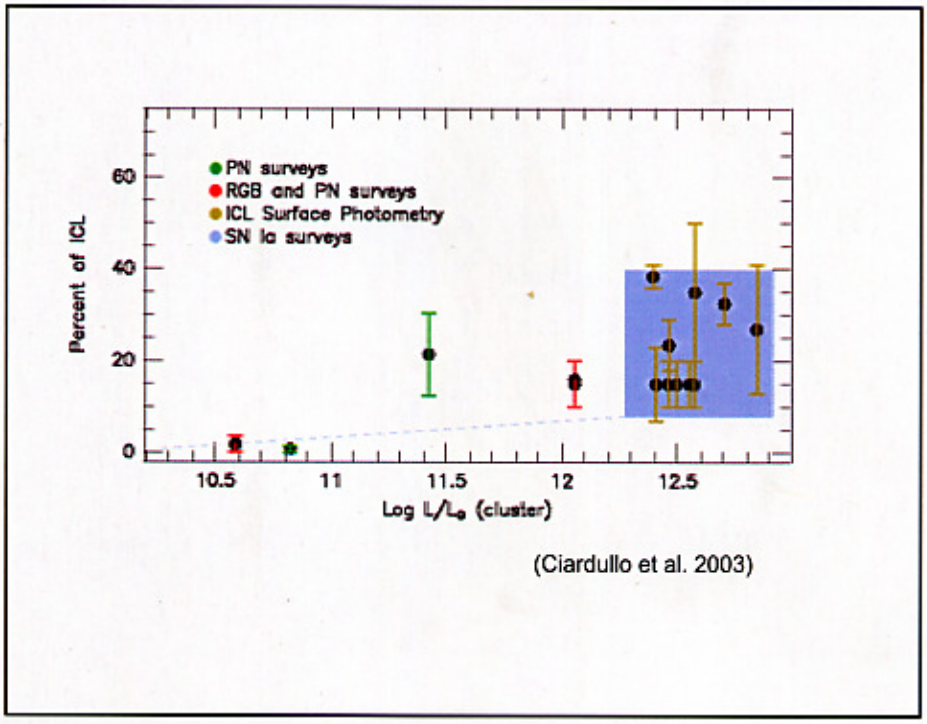

(Ciardullo et al. 2003)

The puzzling problem of Planetary Nebulae

Buzzoni, Arnaboldi & Corradi (2006)

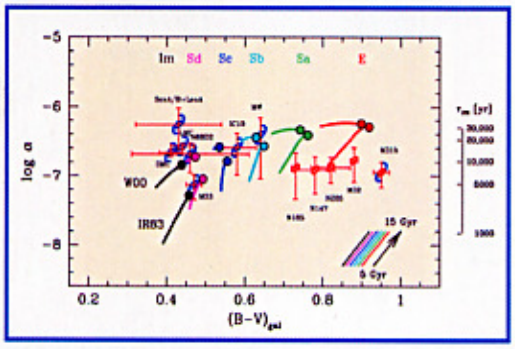

$$\alpha = N_{PN} / L_{gal}$$

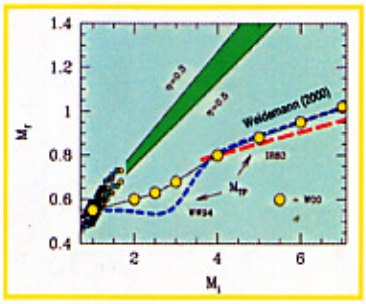

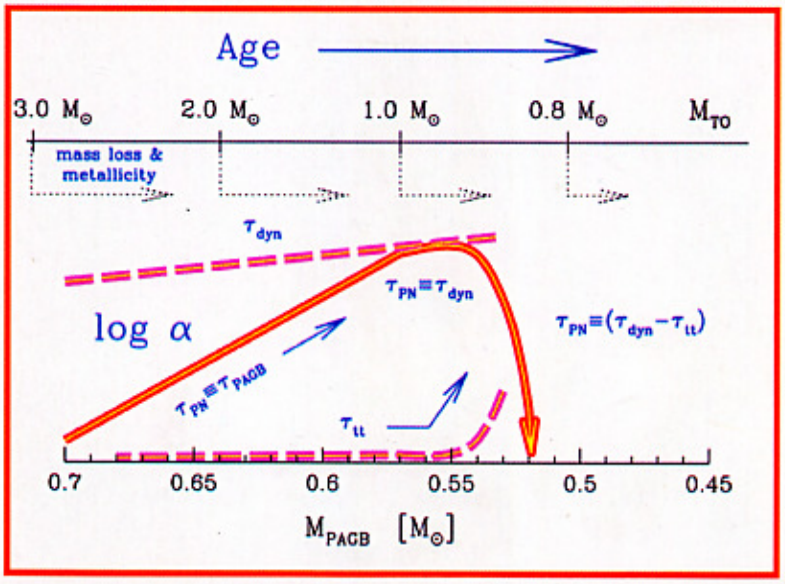

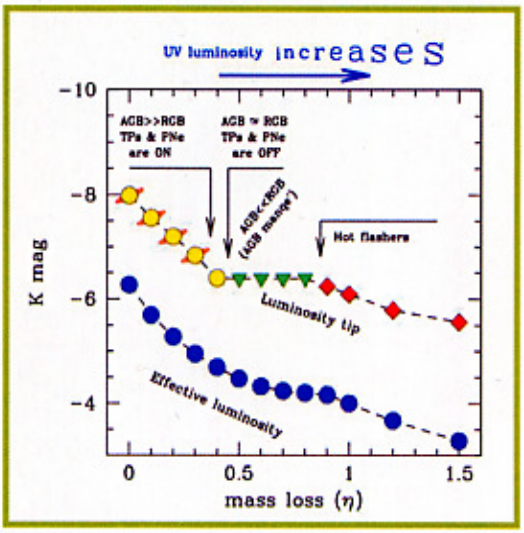

Reimers's law →

$$\dot{M} = \eta \frac{LR}{GM}$$

$$\alpha = N_{PN} / L_{gal}$$

PNe and galaxy environment

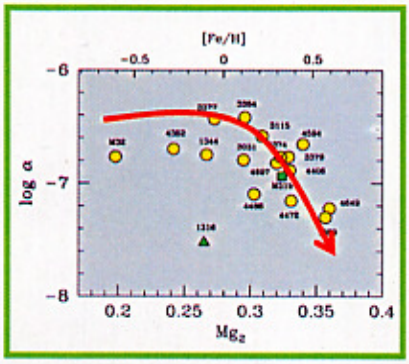

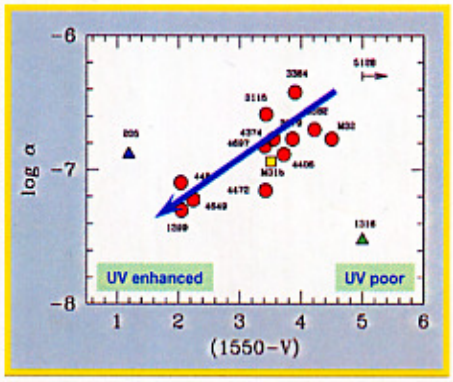

What a Photometric Entropy theory is for?

Entropy is a measure of the intrinsic "variance" of a stellar aggregate along the different spectral range of observation.

- Surface-brightness Fluctuations
- Crowding
- Diagnostics from Narrow-band Spectroscopy

Some Fundamentals

$$p(x) = \frac{e^{-\lambda}\,\lambda^{x}}{x!} \quad \text{for } \lambda > 0 \text{ and } x = 0, 1, 2\ldots$$

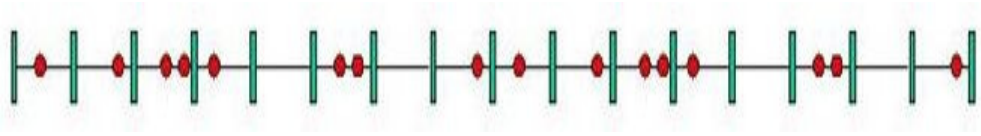

1, 2, 3, ... N_{tot}

→ N= 1± 1 for each cell $L_{tot} = \Sigma\, \ell_* = N_{tot}\, \ell_*$

$\sigma(N_{tot}) = \sqrt{\Sigma 1} = \sqrt{N_{tot}}$ $\sigma(L_{tot}) = \sqrt{\Sigma \ell_*^2} = \ell_*\, \sqrt{N_{tot}}$

$$\sigma(L_{tot})/L_{tot} = 1/\sqrt{N_{tot}}$$

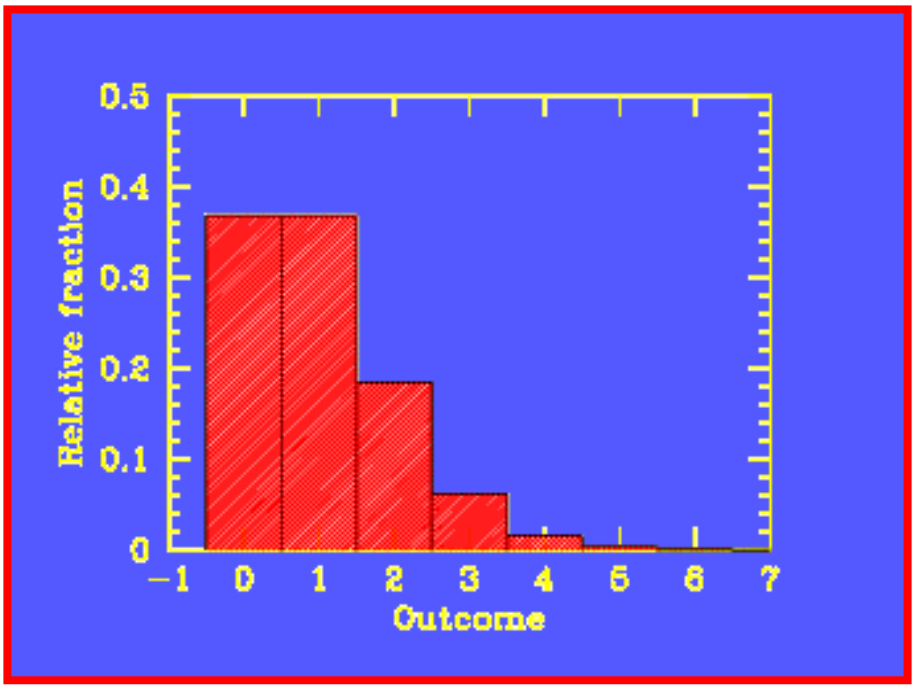

More generally, if ℓ_* is NOT a constant, we can still define

$$\sigma(L_{tot})/L_{tot} = 1/\sqrt{N_{eff}}$$

where, always,

$$N_{eff} \leq N_{tot}$$

N_{eff} will depend on λ as ℓ_* depends on λ

$$S = \text{Log}\,(N_{eff}/N_{tot})$$

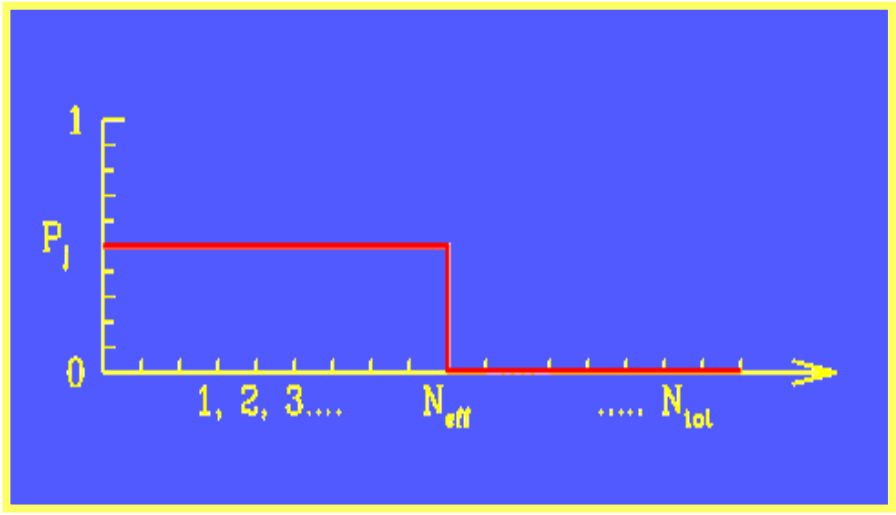

Quite importantly,

$$S = S(\lambda)$$

In order to fix N_{eff} (and Entropy) we need a photometric argument

$$\sigma^2(L_{tot}) \,/\, L_{tot} = \Sigma \ell_*^{\,2} \,/\, \Sigma \ell_* = \ell_{eff}$$

At every λ, it must be:

$$N_{eff} \times \ell_{eff} = L_{tot}$$

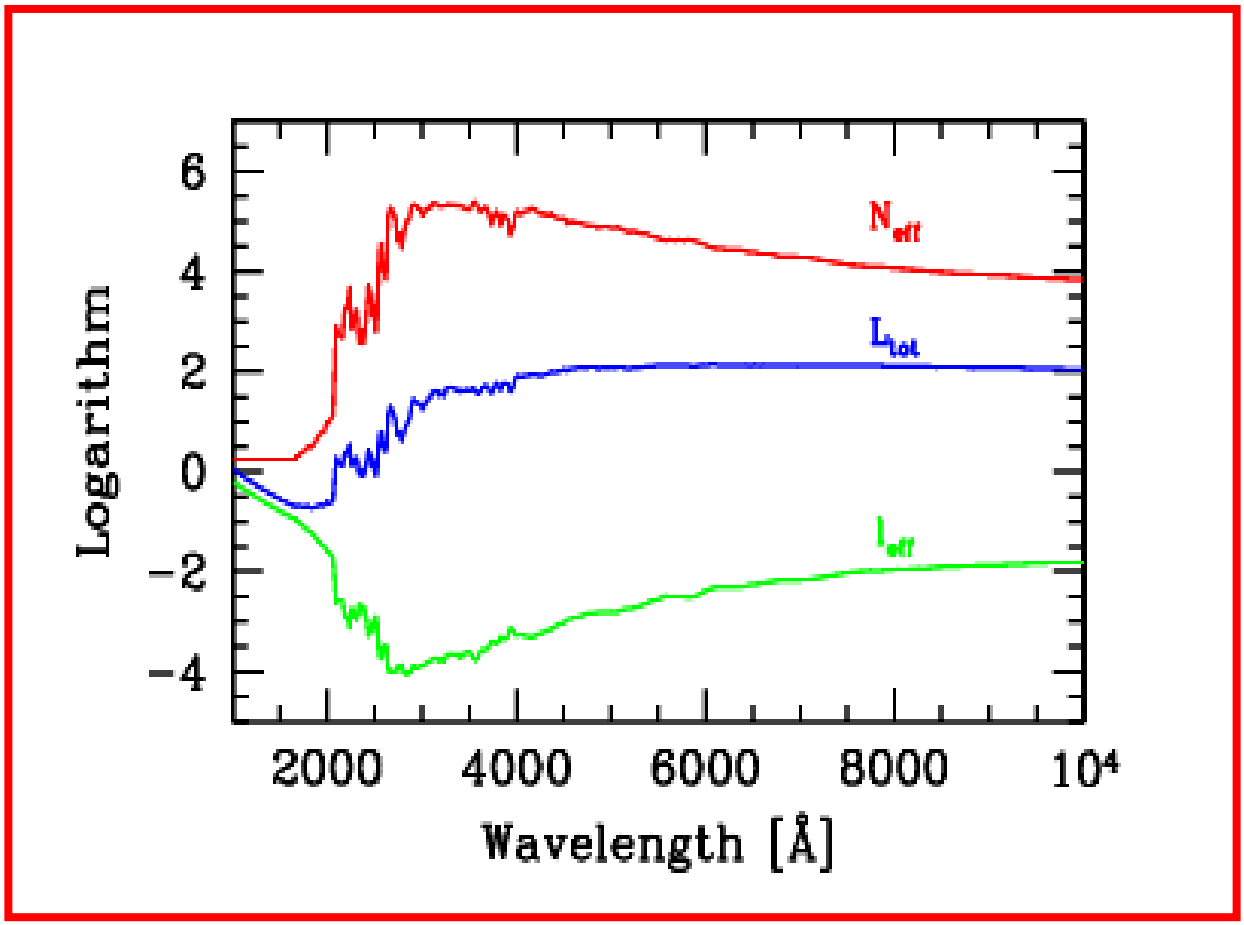

Buzzoni (1993), A&Ap, 275, 433

Cerviño et al. (2002), A&Ap, 381, 51

Surface-Brightness Fluctuations: an alternative approach for the case of M53

First application of the theory to galx's: Tonry & Schneider (1988) and Tonry (1991)

$$\sigma^2(L_{tot}) / L_{tot} = \Sigma \ell_*^2 / \Sigma \ell_* = \ell_{eff}$$

Observations

Theory: Population synthesis models → ℓ_{eff}

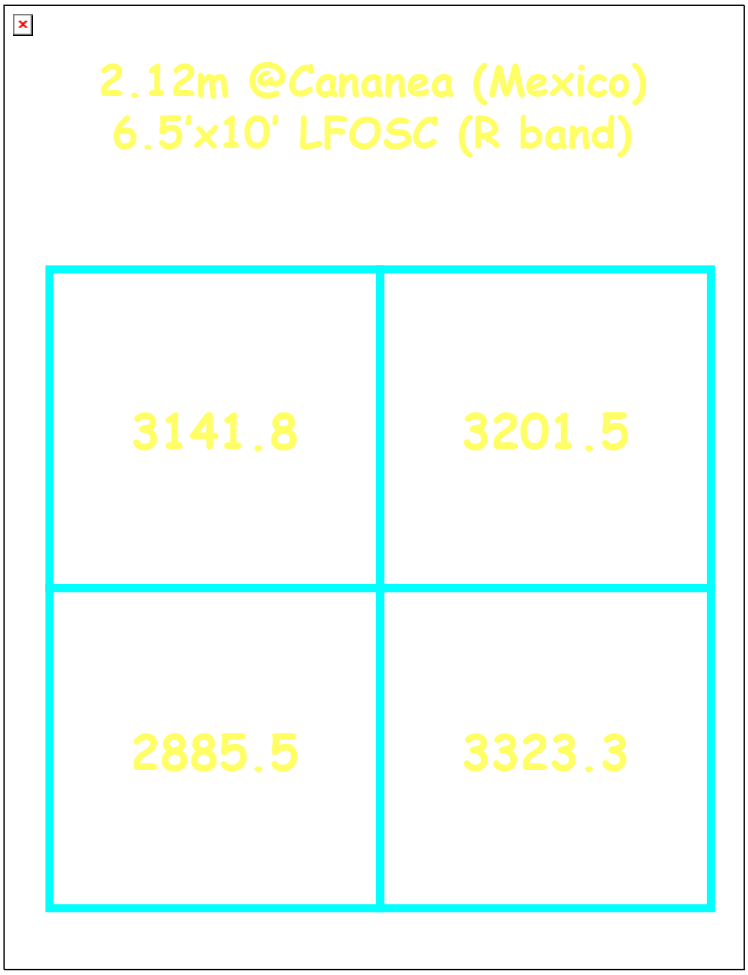

$$L_{(quad)} = 3138 \pm 184$$

M 53 (NGC 5024)

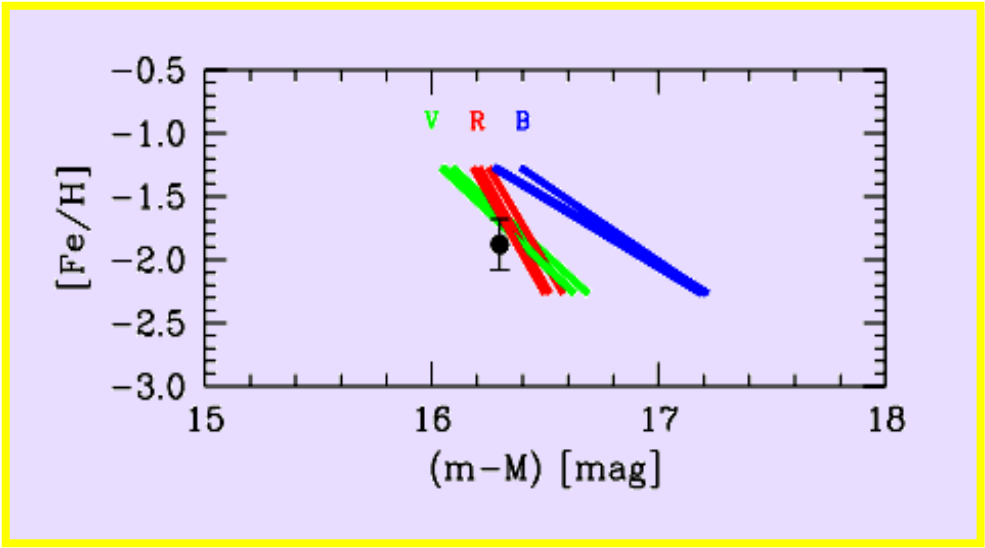

[Fe/H] = -1.88 ± 0.2 dex
(Santos & Piatti, 2004)

(m-M) = 16.3 mag
(Harris 1996)

$L_{(quad)}$ = 3138 ± 184

Luminosity Sampling and Intrinsic Color Fluctuations

$$\Delta mag = \sigma(L_{tot})/L_{tot} = 1/\sqrt{N_{eff}}$$

$$\sigma\,(B-V) = [\sigma(B)^2 \pm \sigma(V)^2\,]^{1/2} = (1/\,N_{eff}^{B} \pm 1/\,N_{eff}^{V})$$

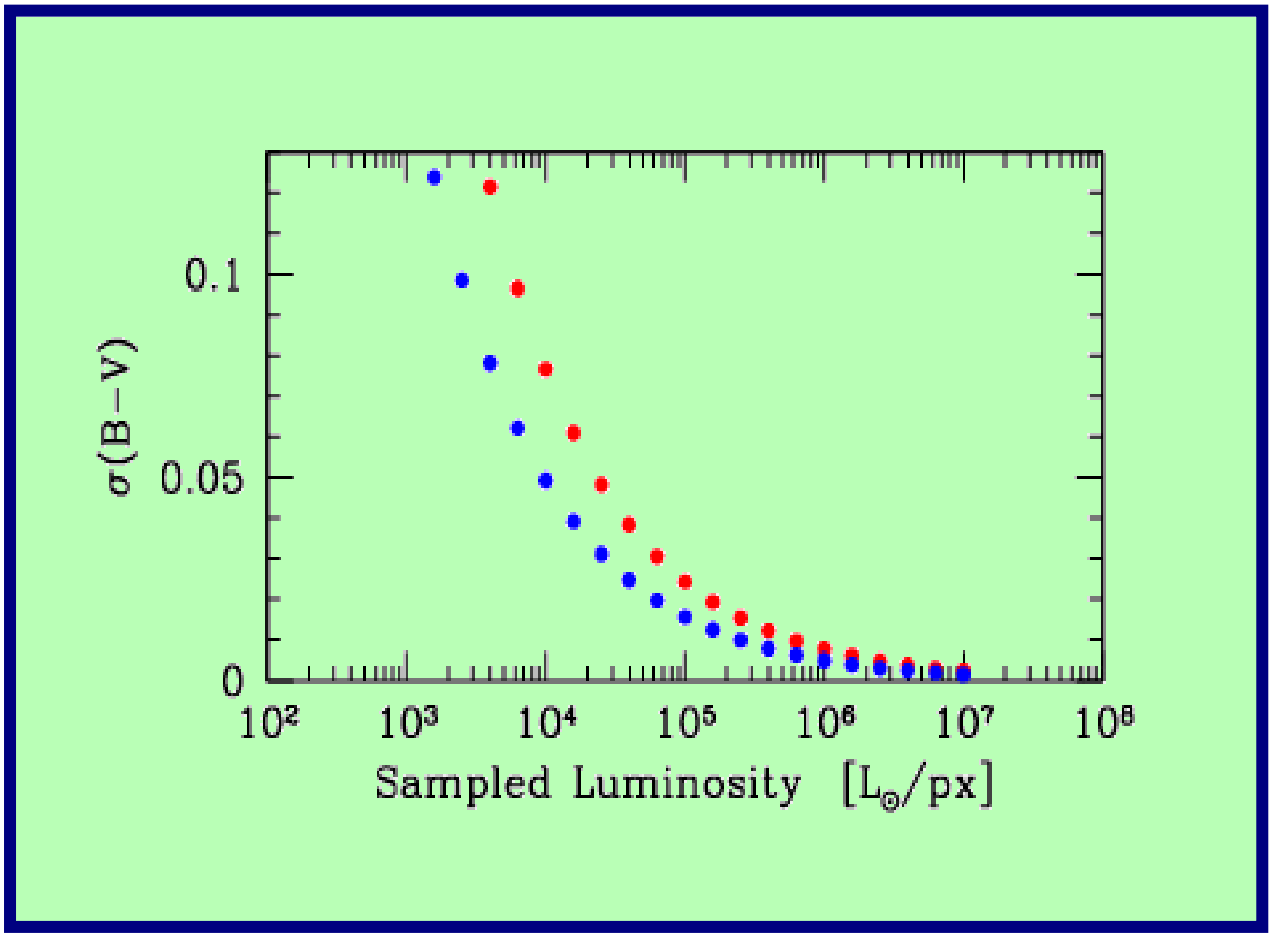

Crowding & Optical opacity

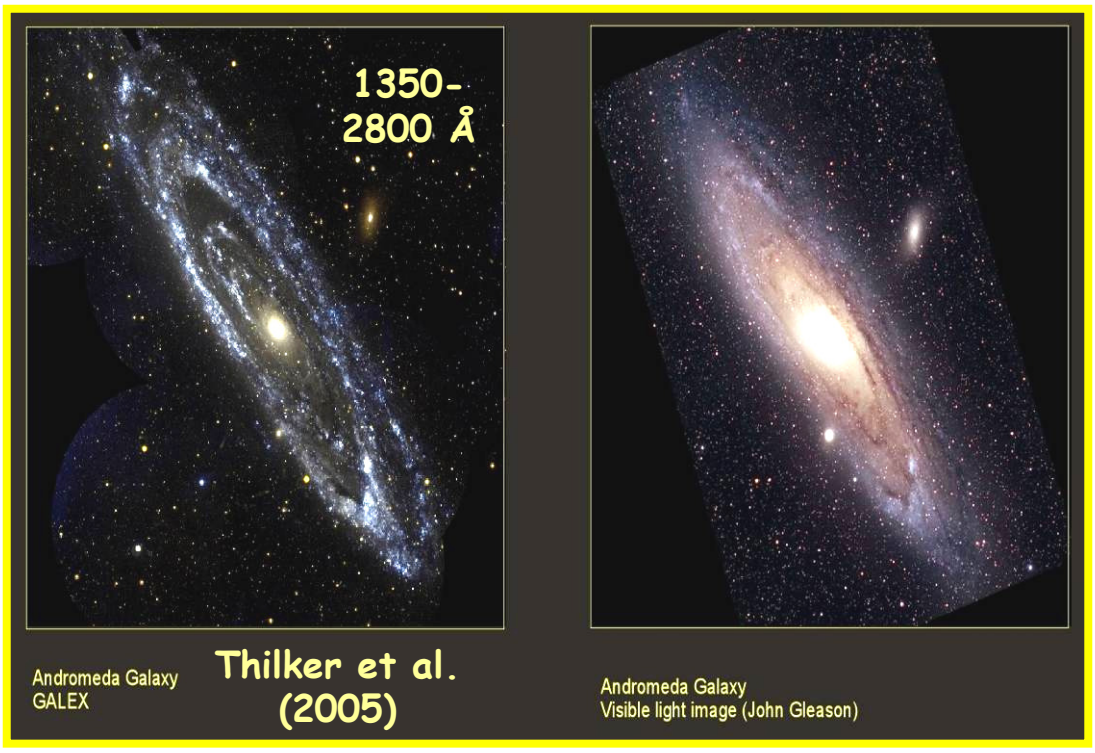

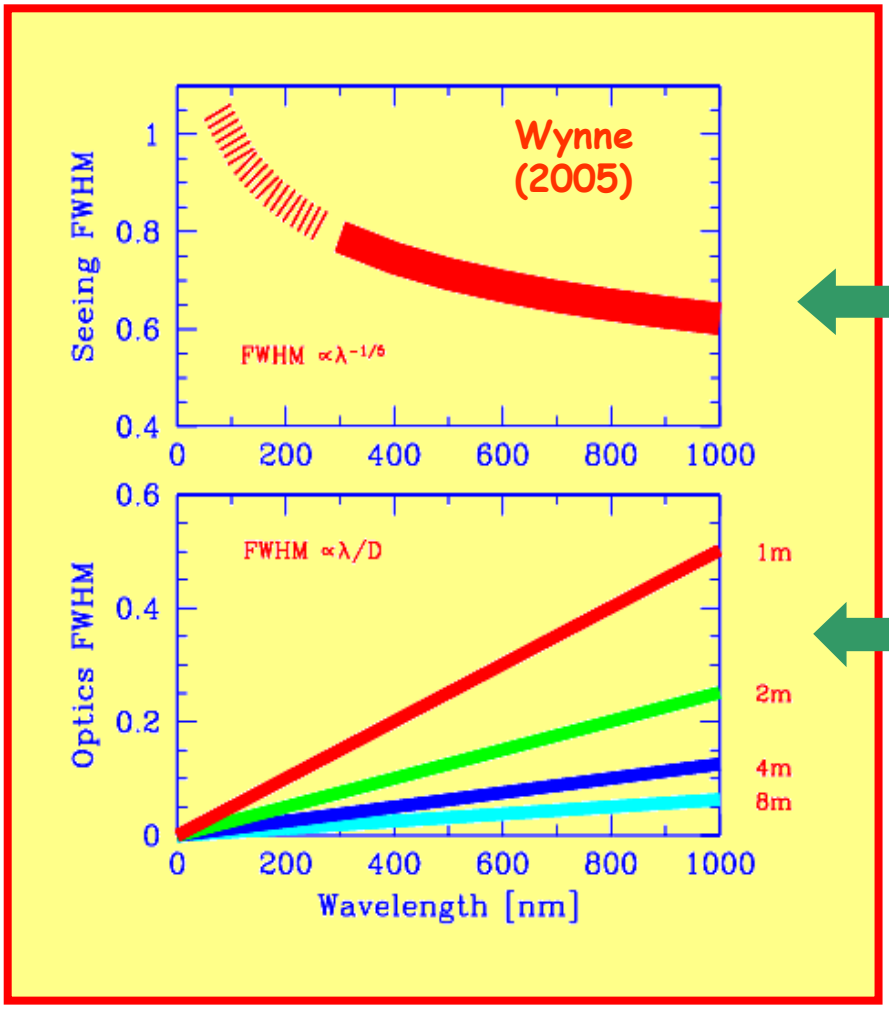

Seeing

Diffraction

Crowding & Opacity

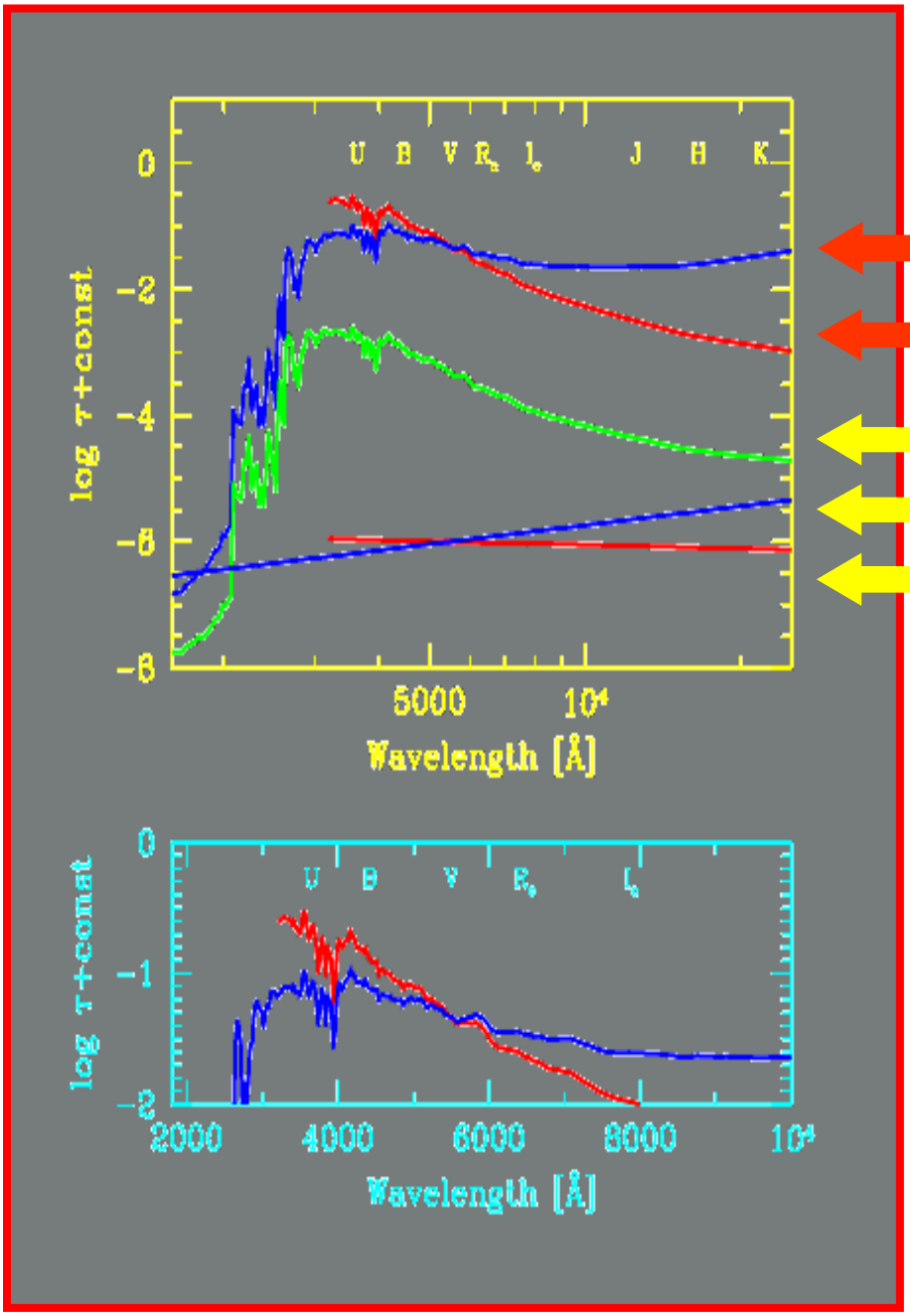

from Space

from Ground

Entropy (N_{eff})

Diffraction

Seeing

Oligarchy vs. Democracy

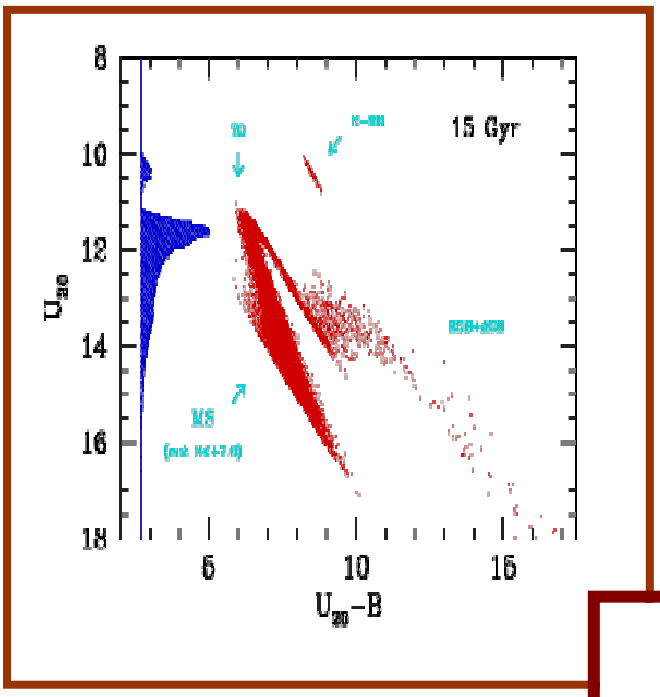

2000 Angstroms

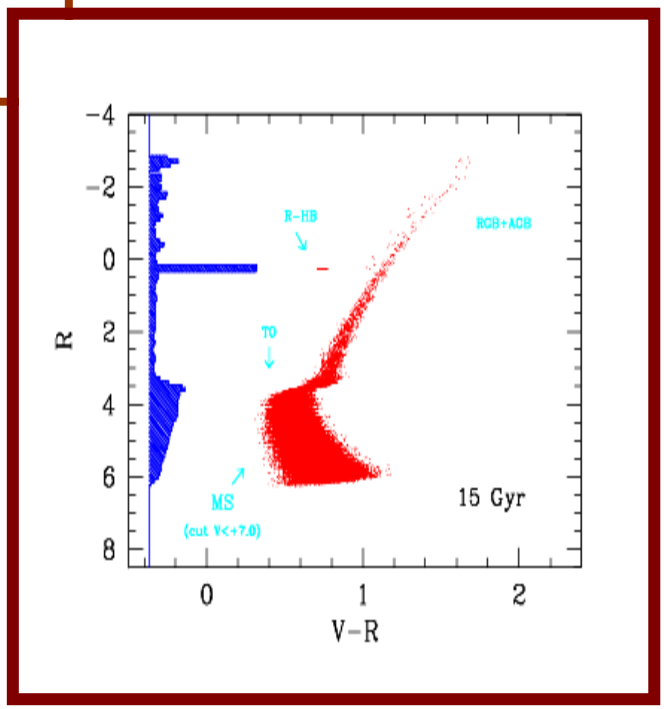

7000 Angstroms

Probing stellar populations through high-resolution synthesis

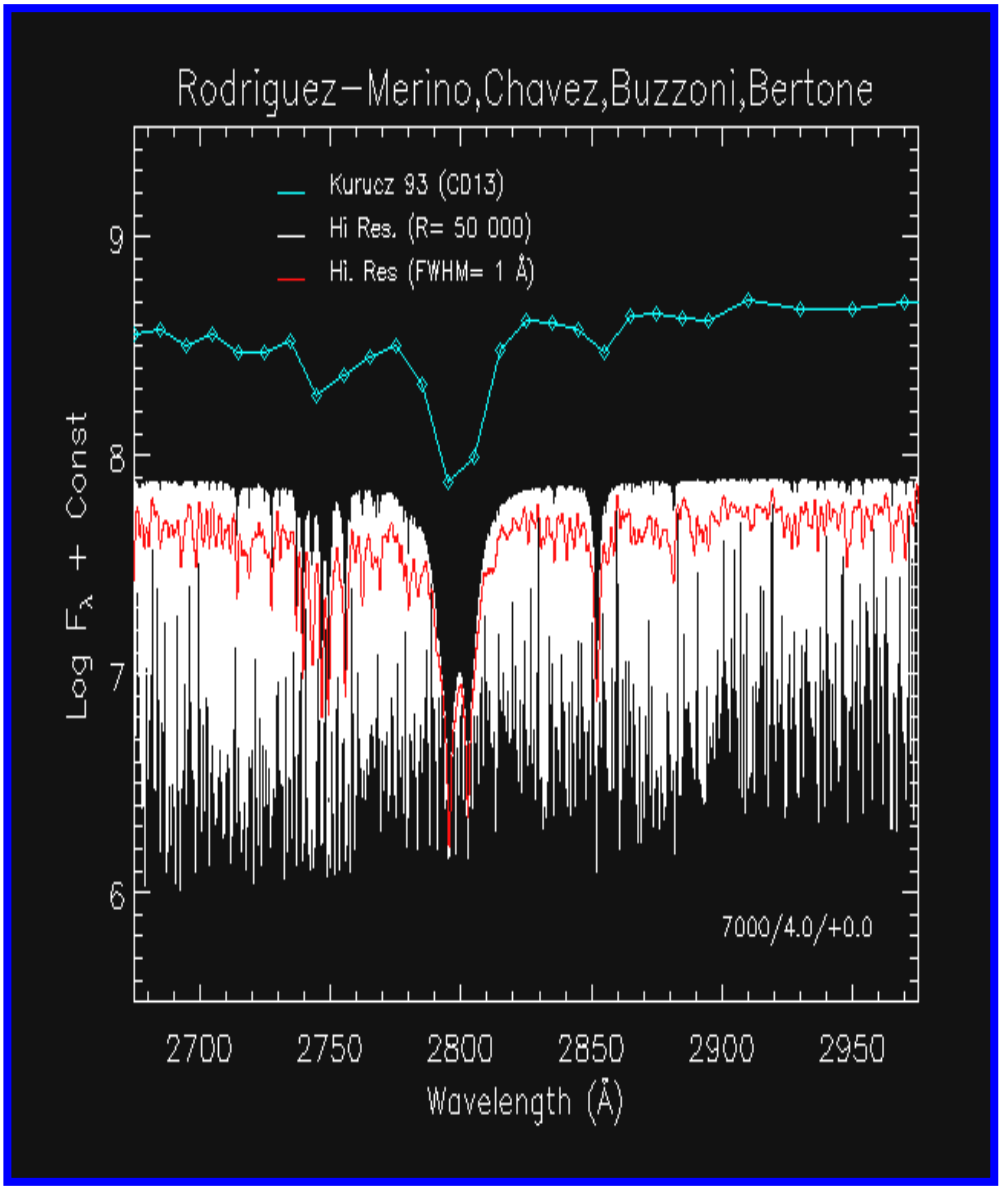

Rodriguez-Merino et al. (2005)

Recovering the Age-Metallicity degeneracy

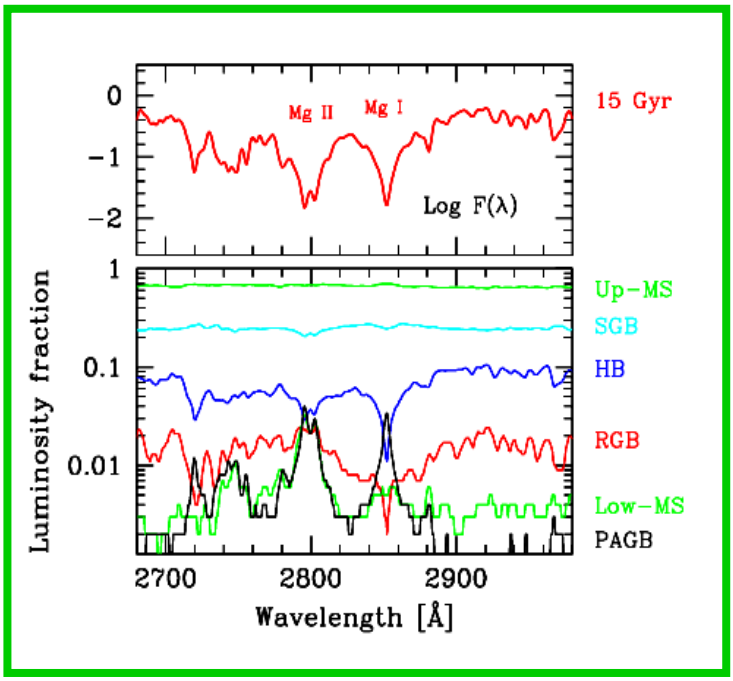

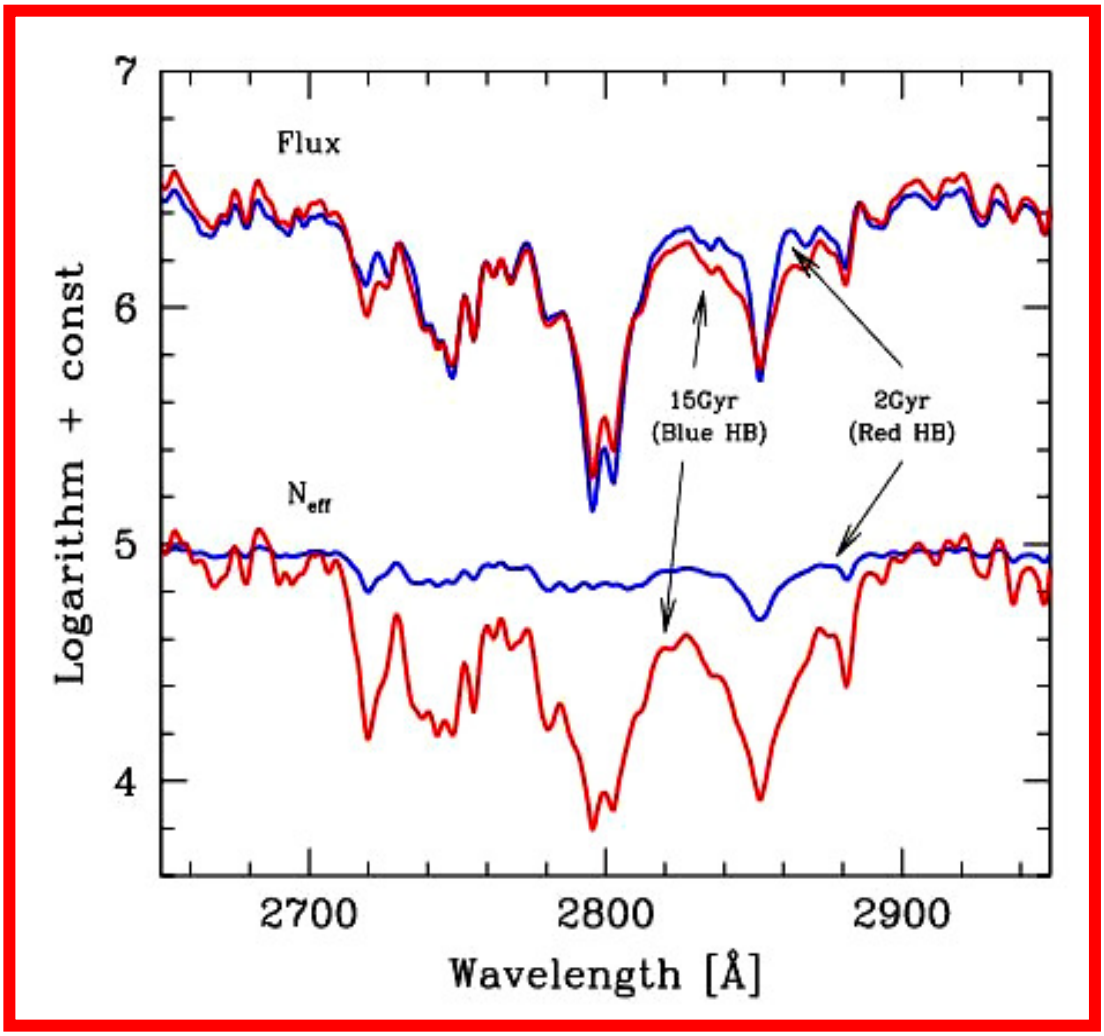

I principi della spettroscopia (Diffrazione & Interferenza)

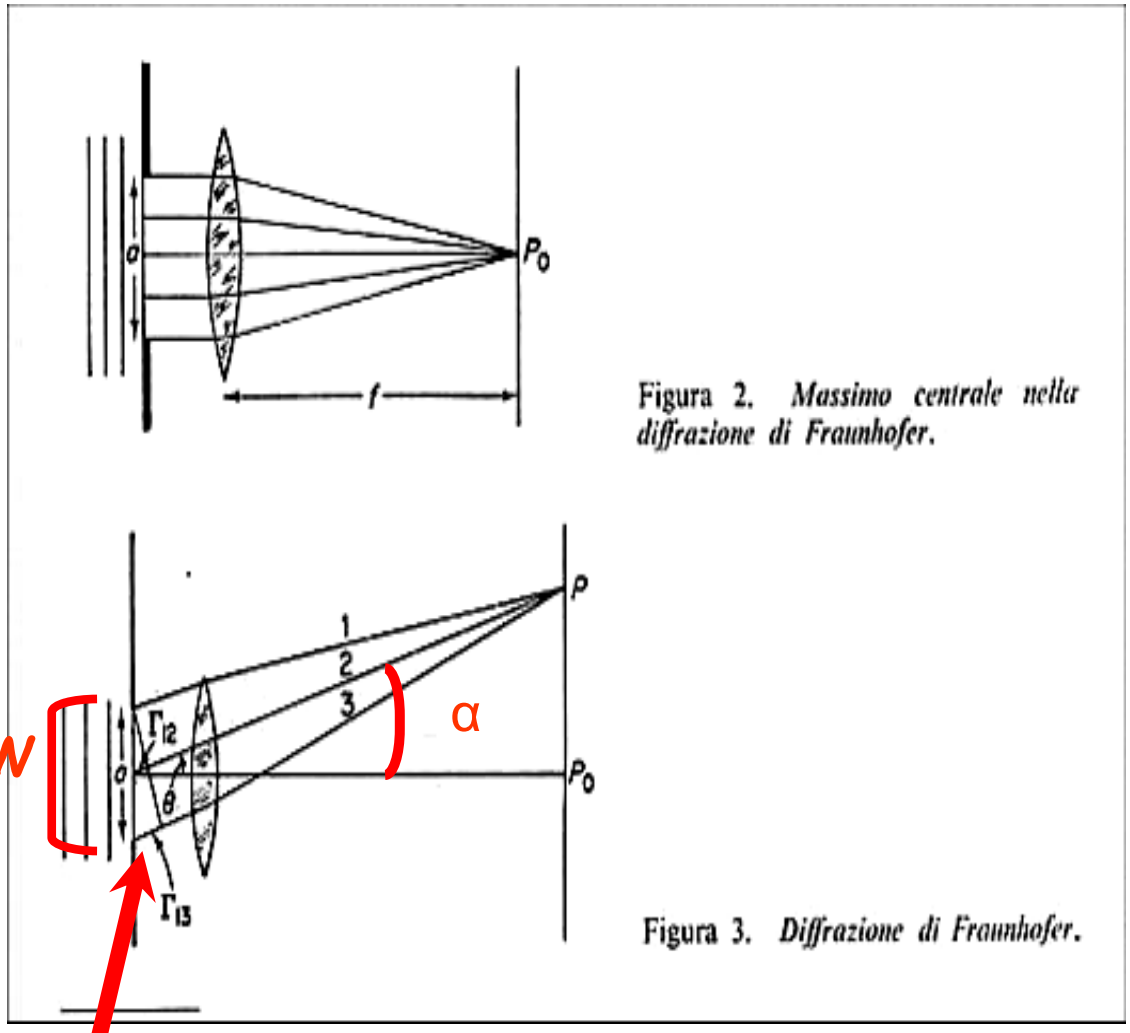

Figura 2. *Massimo centrale nella diffrazione di Fraunhofer.*

Figura 3. *Diffrazione di Fraunhofer.*

$$\frac{W}{2}\sin\alpha = \frac{m}{2}\lambda \quad \Rightarrow \quad \alpha \cong m\frac{\lambda}{W}$$

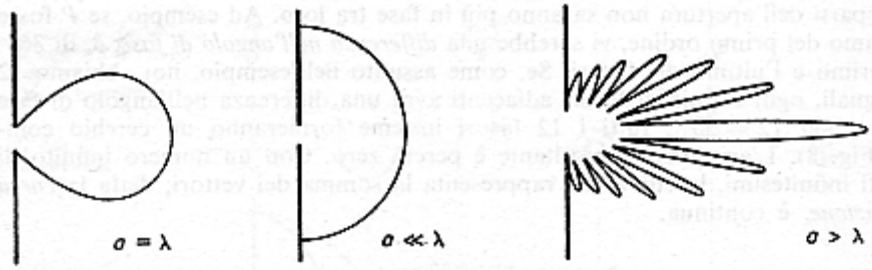

Figura 5. *Distribuzioni d'intensità dietro un'apertura di larghezza* a = λ *(a sinistra), dietro un'apertura estremamente piccola (al centro), e dietro un'apertura più larga (a destra).*

Risoluzione vs. Dispersione

$$\alpha_{\min} \cong m\frac{\lambda}{W}$$

Risoluzione

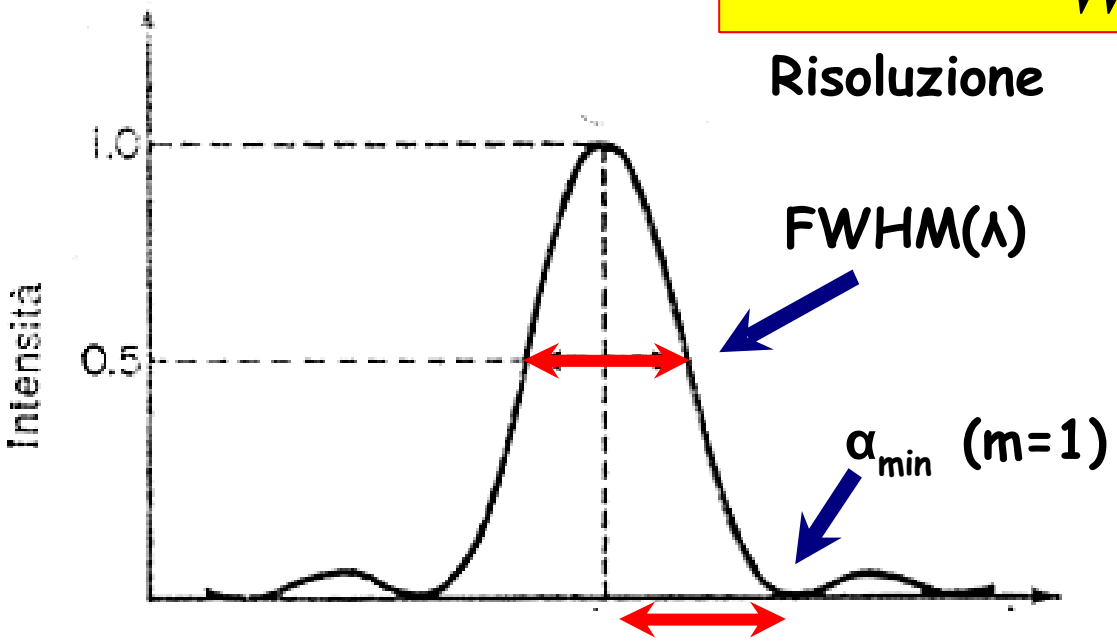

$$\alpha_{\max 1} \approx 1.5\frac{\lambda}{W}$$

$$\Delta\alpha_1 \approx \frac{1.5}{W}\Delta\lambda$$

Dispersione

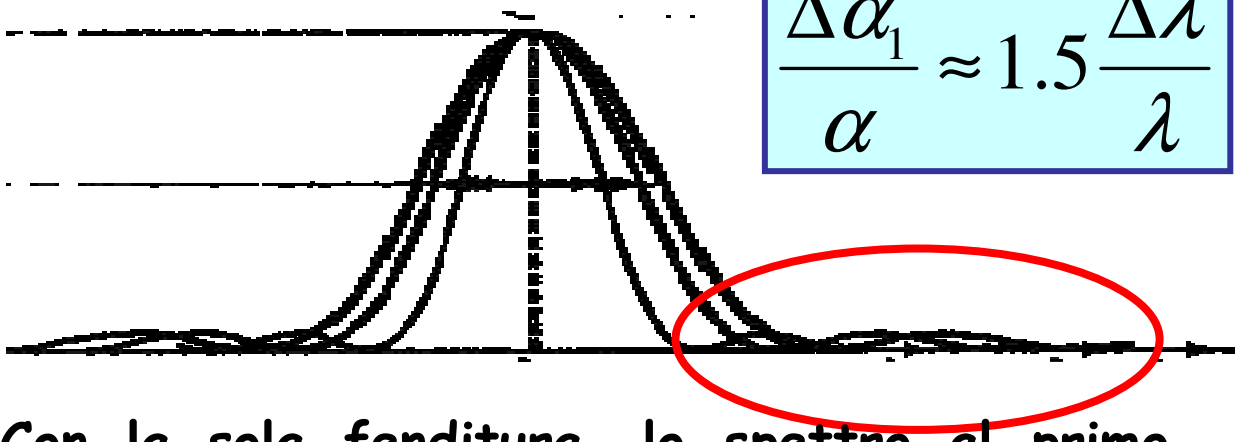

$$\frac{\Delta\alpha_1}{\alpha} \approx 1.5\frac{\Delta\lambda}{\lambda}$$

Con la sola fenditura, lo spettro al primo ordine sarebbe totalmente confuso dalla figura di diffrazione all'ordine zero, e quindi inutilizzabile

Reticoli di diffrazione

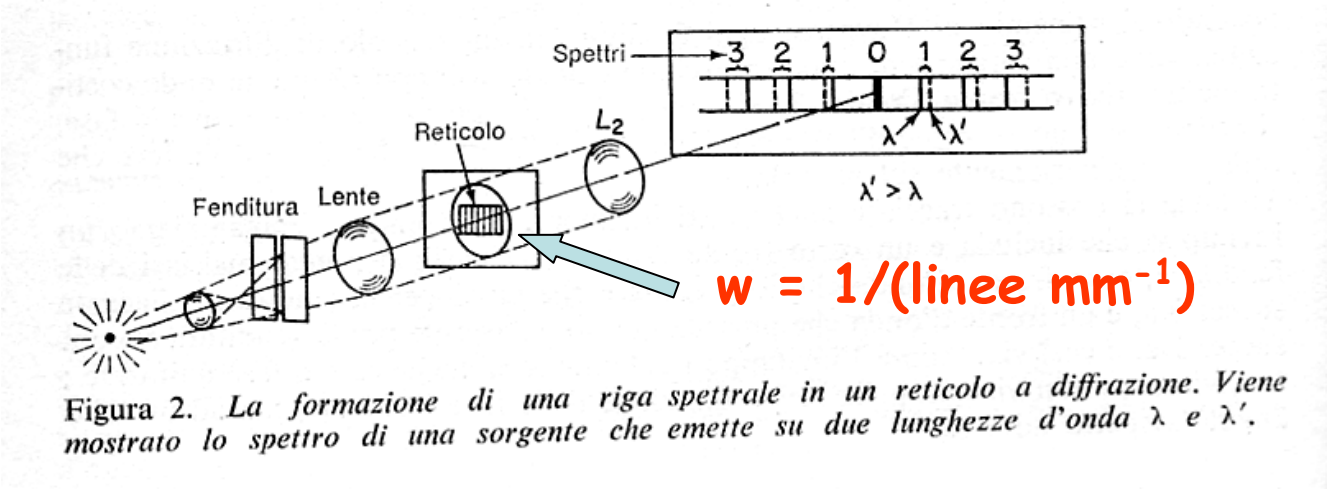

Figura 2. *La formazione di una riga spettrale in un reticolo a diffrazione. Viene mostrato lo spettro di una sorgente che emette su due lunghezze d'onda λ e λ'.*

risoluzione

$$\alpha_{\min} \cong m\frac{\lambda}{W}$$

dispersione

$$\Delta\alpha_1 \approx \frac{1.5}{w}\Delta\lambda$$

"Grism"
(per rifrazione)

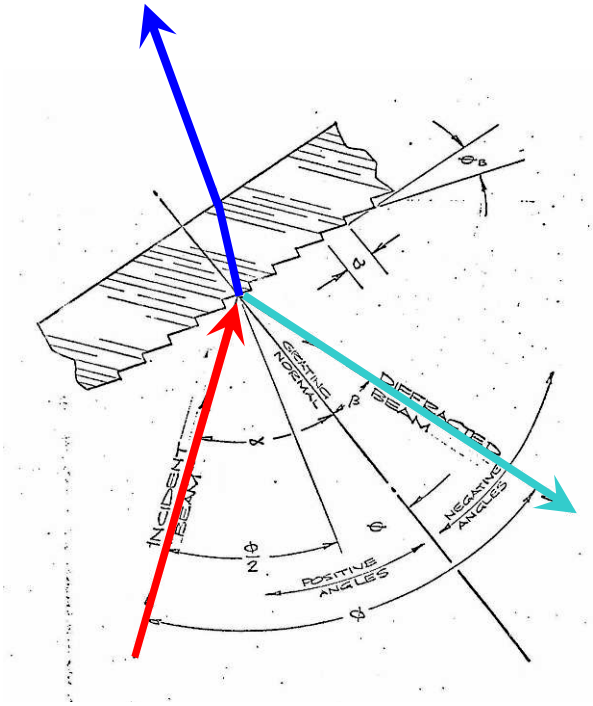

$$\frac{\Delta\alpha}{\alpha} \approx 1.5\left(\frac{W}{w}\right)\frac{\Delta\lambda}{\lambda}$$

"Grid"
(per riflessione)

Quindi:

1) l'ampiezza della fenditura determina la RISOLUZIONE

2) La frequenza di linee del grism/grid determina la DISPERSIONE

Gli spettrografi a riflessione

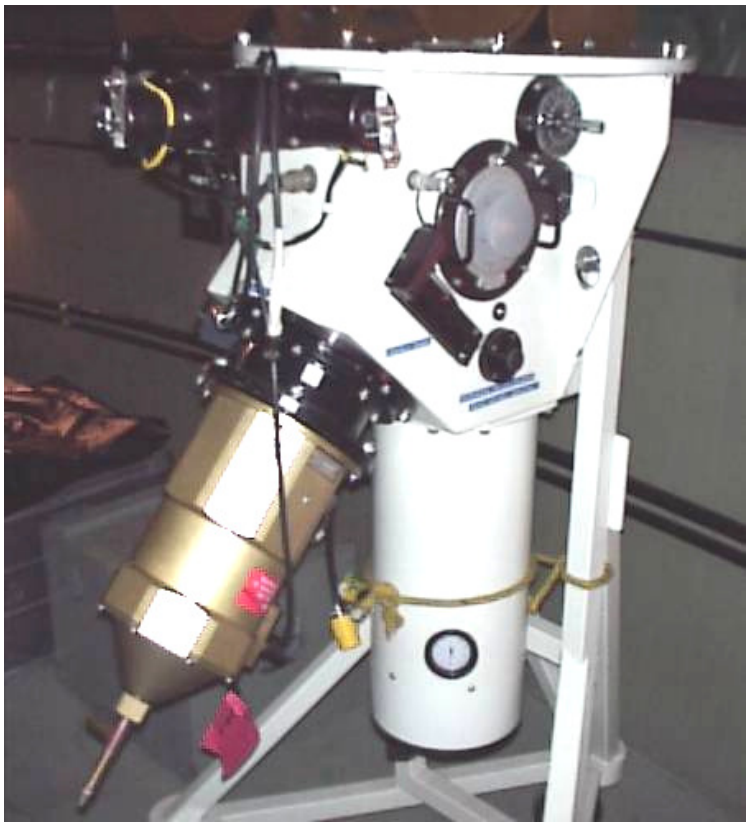

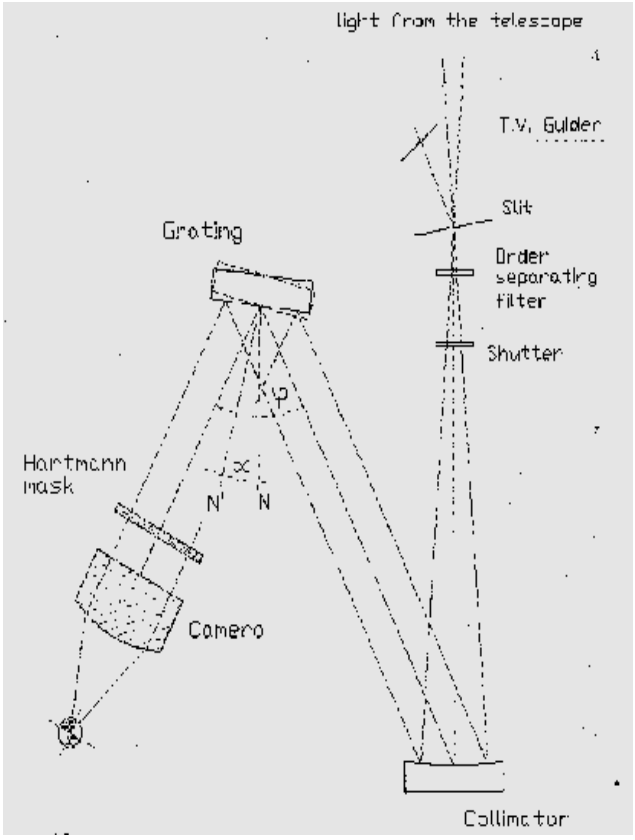

Böller & Chivens

Gli spettrografi a fibre ottiche

Hydra @KPNO (3.8m) USA

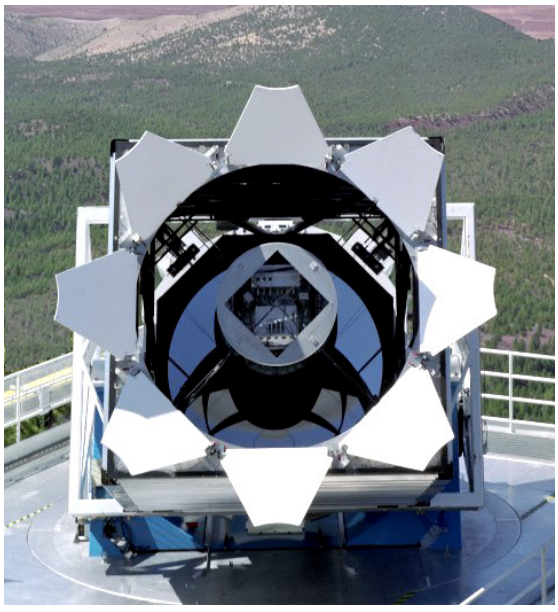

The Sloan Digital Sky Survey's 2.5-meter telescope at Apache Point Observatory, New Mexico

Spettrografi da "banco"

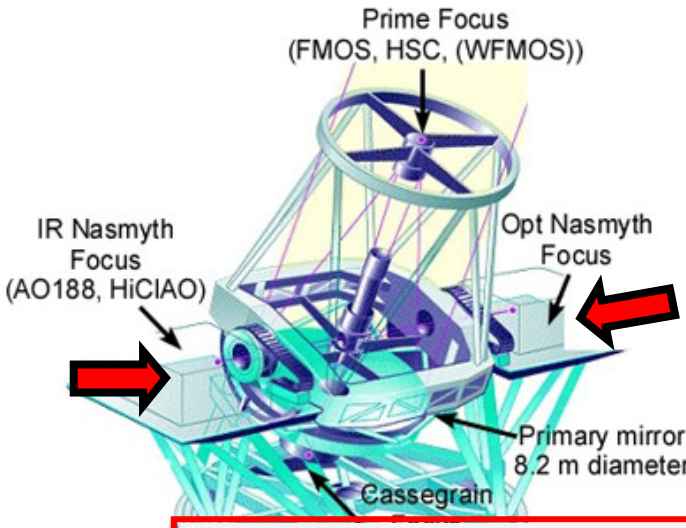

Autofib@WHT (4.2m) UK

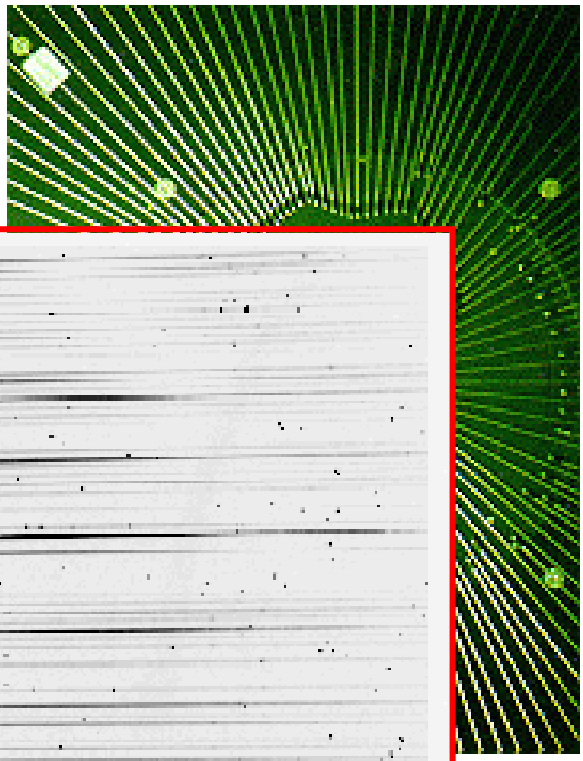

Subaru (

HECTOS
Arizona (

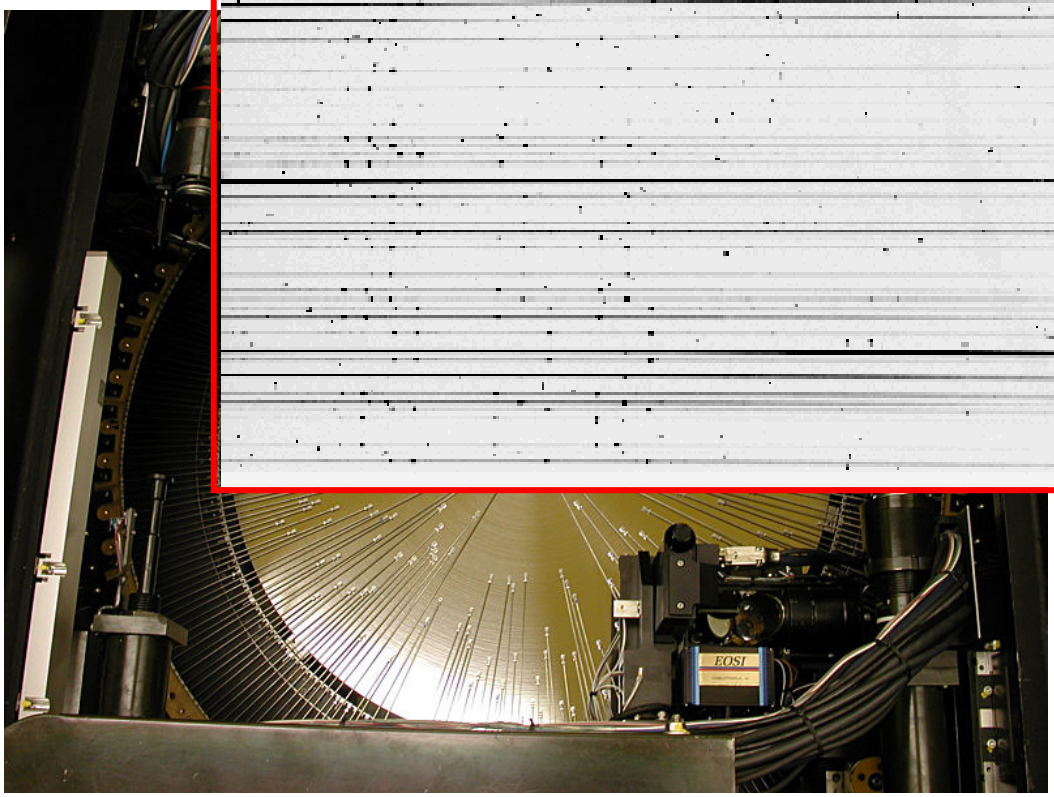

Le camere FOSC

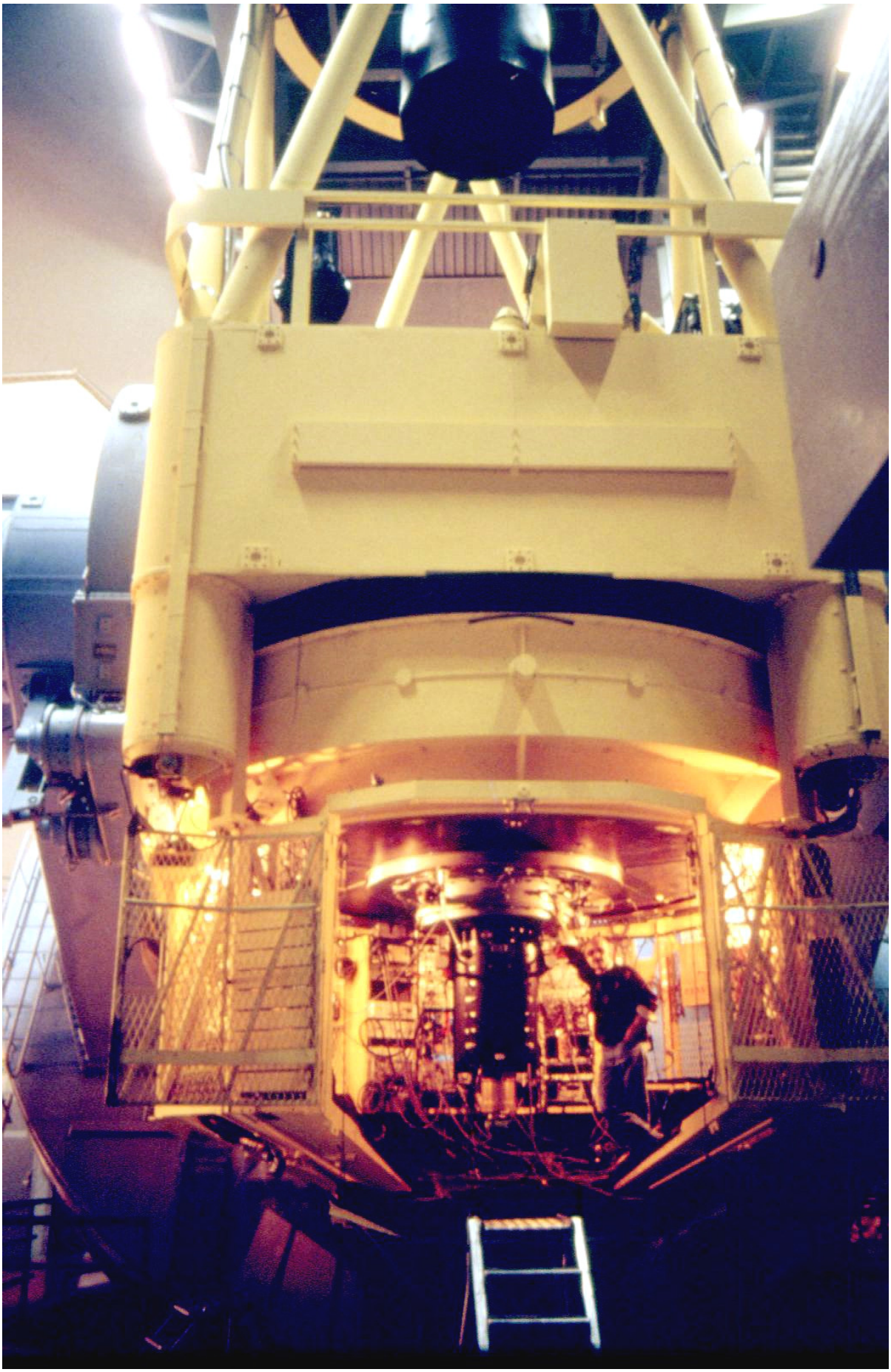

Spettroscopia "MOS" (multiobject)

Spectral resolution

FWHM ~ 2.5 ÷10Å

Resolving power

$$R = \frac{\lambda}{\Delta\lambda} = 500 \Leftrightarrow 2000$$

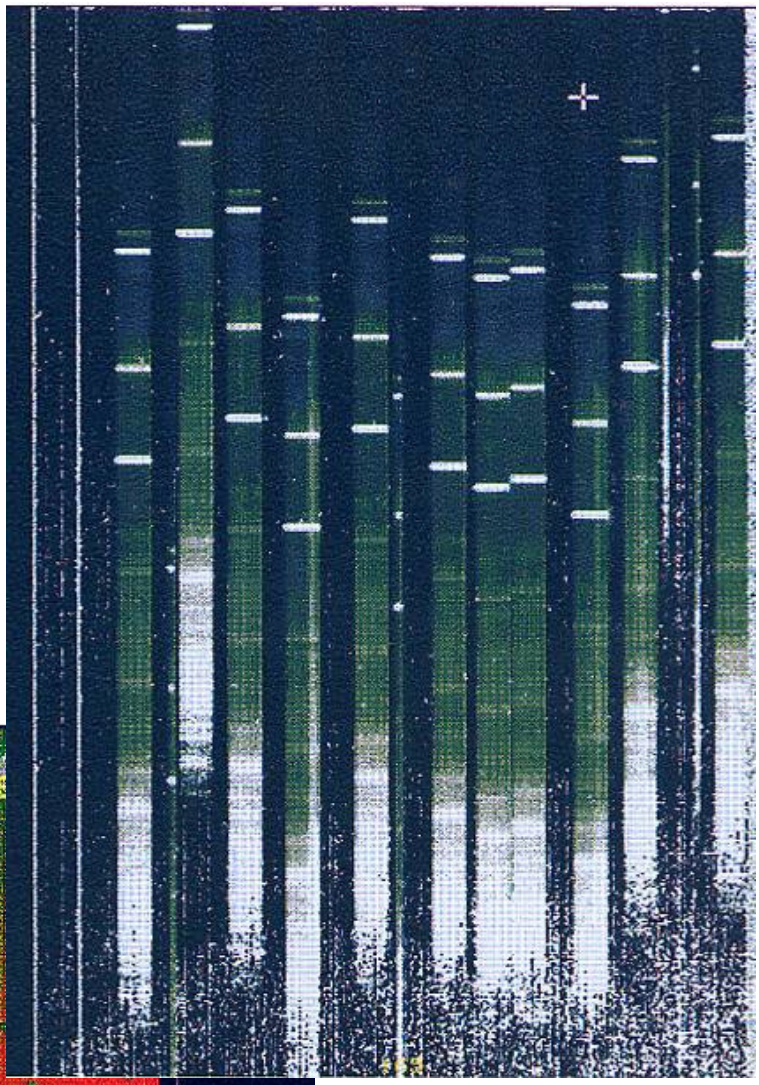

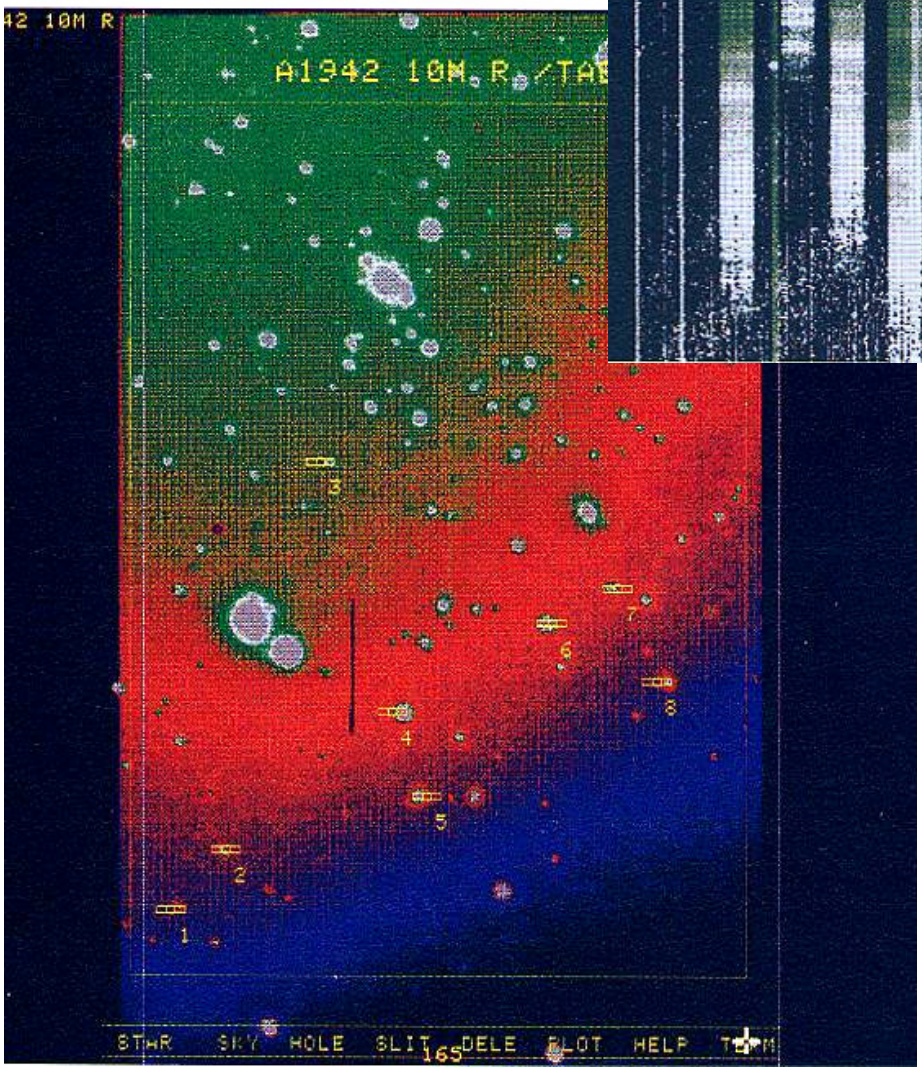

VIMOS@VLT (ESO) 8.2m, Chile

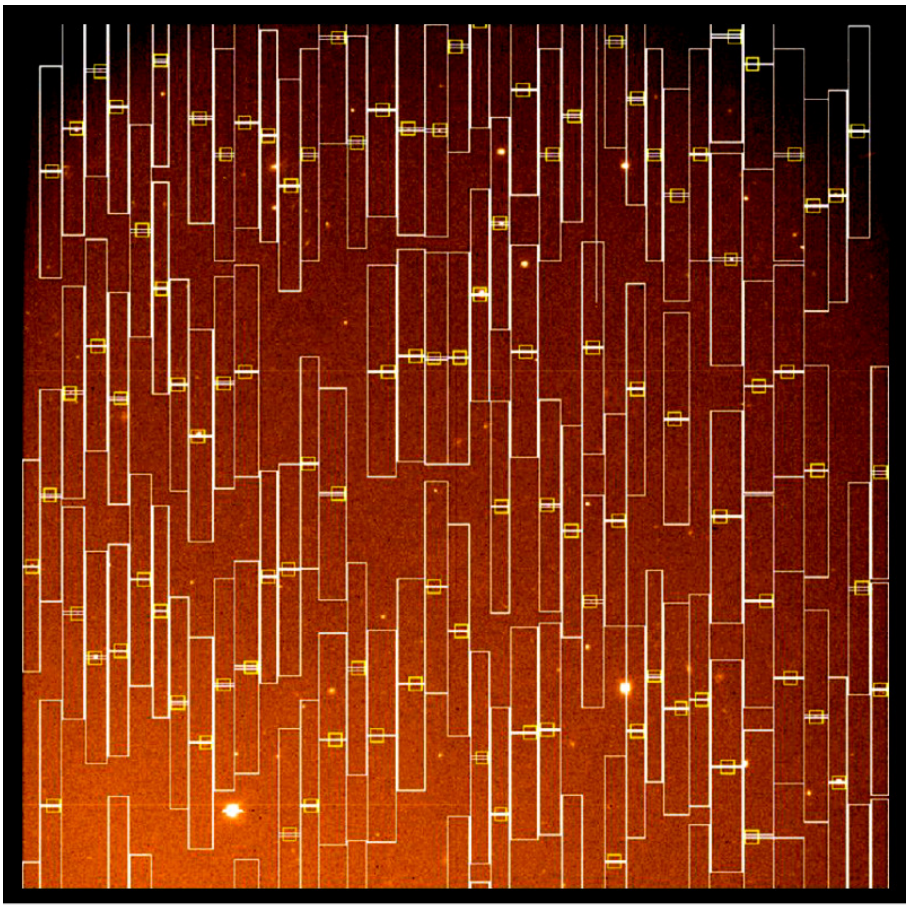

VIMOS Mask Design on Pre-Image

ESO PR Photo 09k/02 (13 March 2002)

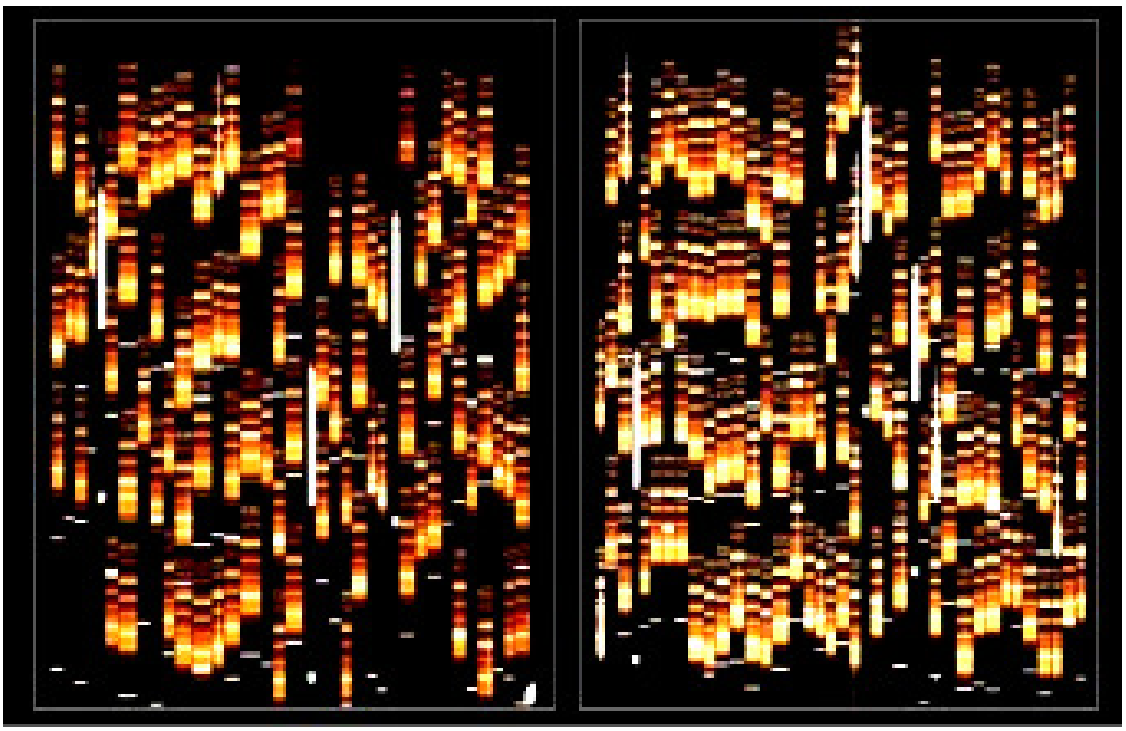

Legge di Wien : $\lambda_{\max} T \propto const$

$$\frac{\lambda_{\max}}{5500} = \frac{5780}{T_K} \longrightarrow \lambda_{\max} \approx \frac{310^7}{T_K} \ [\text{Å}]$$

T_K	λ_{max}	[eV]
100,000	300 Å	raggi γ
10,000	3000 Å	UV
6,000	5000 Å	Ottico
3,000	10,000 Å	MIR
1,000	30μm Å	FIR

Equipartizione dell'energia :

$$E \approx 3kT = 4.2\ 10^{-16} T_K \approx h\nu = \frac{hc}{\lambda}$$

$$\langle \lambda \rangle \approx \frac{hc}{kT} = \frac{6.6\ 10^{-27} \times 3\ 10^{10}}{4.2\ 10^{-16} T_K (10^{-8})} = \frac{4.7\ 10^7}{T_K} \ [\text{Å}]$$

$$T_K \approx 2400\ E_{eV}$$

Il potenziale di ionizzazione dell'H e' di 13.6eV. Quindi sono necessarie temperature superiori a circa 35,000 K

Gruppo	1	2	13	14	15	16	17	18
Periodo								
1	H 13.59844							He 24.58741
2	Li 5.39172	Be 9.32263	B 8.29803	C 11.26030	N 14.53414	O 13.61806	F 17.42282	Ne 21.56454
3	Na 5.13908	Mg 7.64624	Al 5.98577	Si 8.15169	P 10.48669	S 10.36001	Cl 12.96764	Ar 15.759
4	K 4.34066	Ca 6.11316	Ga 5.99930	Ge 7.899	As 9.8152	Se 9.75238	Br 11.81381	Kr 13.99961
5	Rb 4.17713	Sr 5.69484	In 5.78636	Sn 7.34381	Sb 8.64	Te 9.0096	I 10.45126	Xe 12.12987
6	Cs 3.89390	Ba 5.21170	Tl 6.10829	Pb 7.4167	Bi 7.2855	Po 8.41671	At 9.2	Rn 10.74850
7	Fr 4.0712	Ra 5.27892						

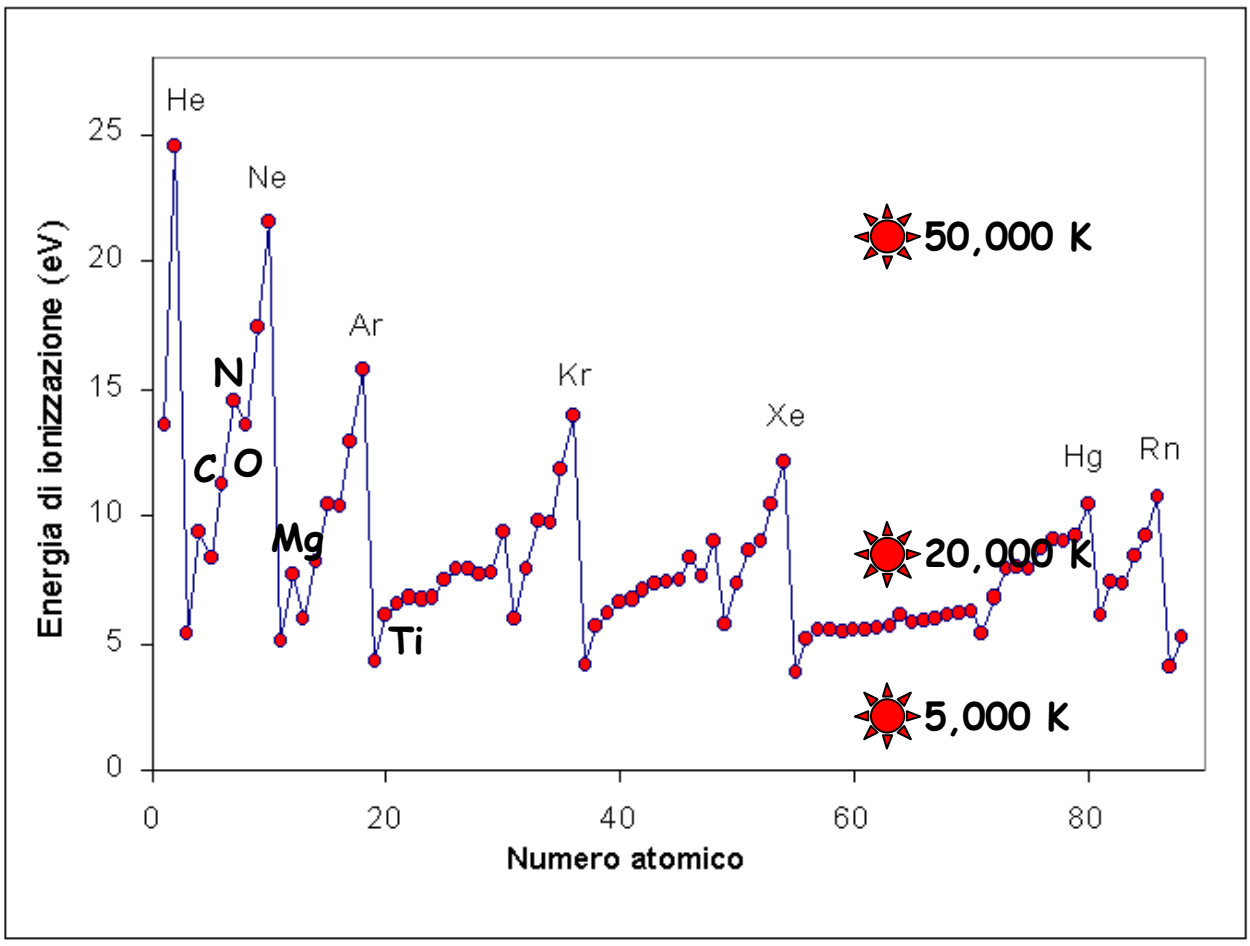

Popolazioni ionizzate

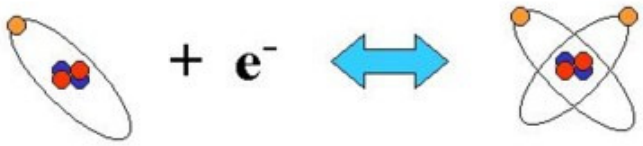

$$\log\frac{n_{r+1}P_e}{n_r} = -E_I\,\frac{5040}{T} + 2.5\log(T) - 6.48 + \log\frac{2u_{r+1}}{u_r}$$

where:

$$u_r = g_0 + \sum_i g_i \cdot e^{-\frac{E_{ii}}{KT}}$$

Equazione di Saha

E_i in eV
P_e in atm

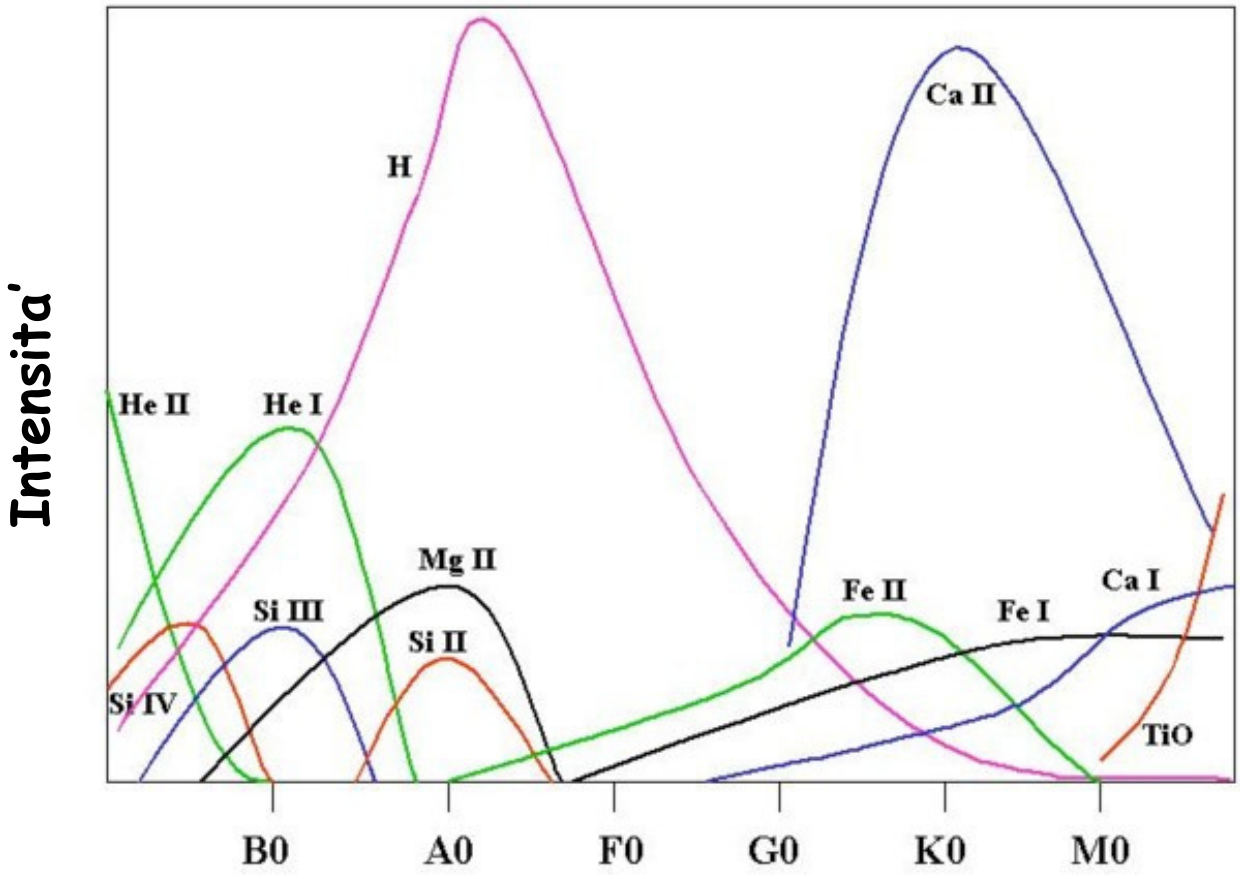

Le molecole

Aspetti generali

- La meccanica quantistica è generalmente in grado di prevedere le proprietà delle molecole (configurazione d'equilibrio, energia di legame, spettri)
- I calcoli per fare queste previsioni sono molto complicati ("quantum chemistry")
- Le regole di selezione sono meno (= più transizioni consentite) che negli atomi
- Gli spettri risultanti sono generalmente più complicati che quelli degli atomi
- Si distinguono spettroscopie vibrazionali/rotovibrazionali (IR e Raman) ed elettroniche (assorbimento visibile/UV e fluorescenza)

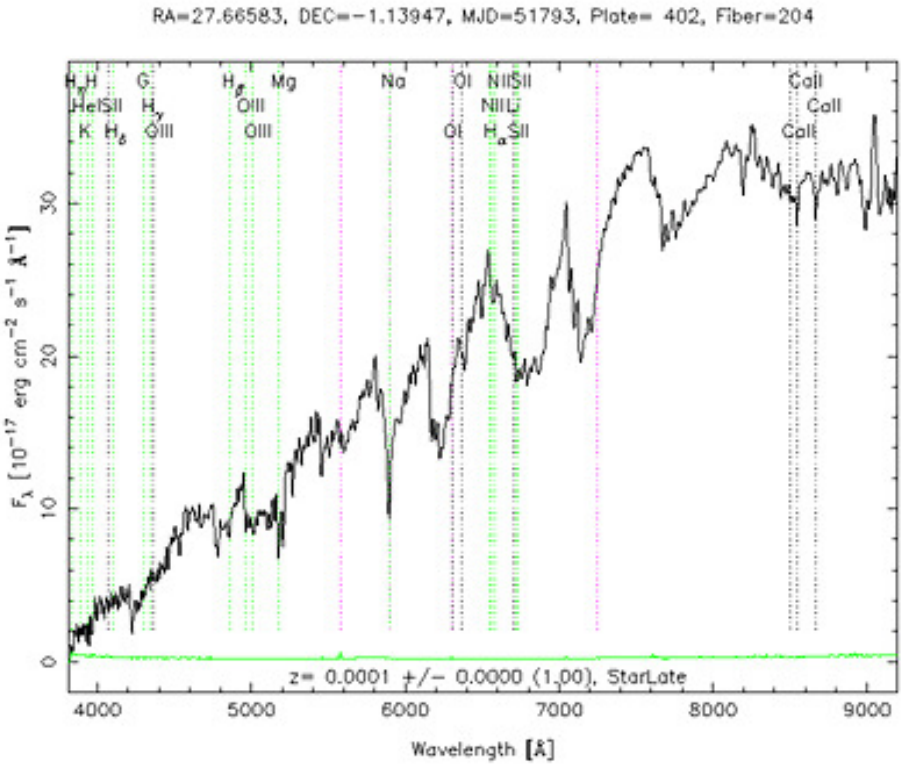

Tipi di vibrazione

- Legami chimici differenti hanno energie di legame e frequenze di vibrazione differenti e abbastanza caratteristiche
- vibrazioni di **stretching** (stiramento): i legami interatomici si allungano e si accorciano
- vibrazioni di **bending** (piegamento): i legami interatomici si piegano gli uni verso gli altri
- Assorbimento di radiazione IR per determinata frequenza (eccitazione risonante dei livelli vibrazionali molecola)
- Nelle transizioni di solito sono coinvolte contemporaneamente vibrazioni e rotazioni della molecola

Spettroscopia IR

Le radiazioni IR **non** hanno energia sufficiente per eccitare gli elettroni ma possono indurre transizioni tra i livelli **vibrazionali** e tra quelli **rotazionali** delle molecole

Spettroscopia di assorbimento: radiazioni IR inducono oscillazioni delle:

- distanze (d – stretching) e negli
- angoli di legame (α – bending)
- arrangiamento della molecola nello spazio (rotazioni)

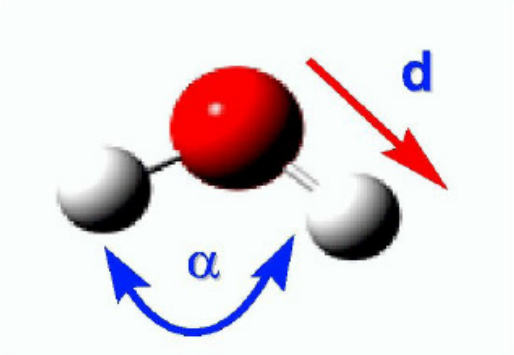

Molecole

	Molecola	I_1 (eV)
Molecole diatomiche omonucleari		
Per le molecole diatomiche omonucleari si nota che i valori delle I_1 ricordano quelle dei rispettivi atomi. Si riconosco però nelle molecole H_2 e N_2 significativi aumenti, meno marcati sono gl'aumenti per P_2 e C_2. Mentre per O_2 e per le molecole degli alogeni il valore dell'energia di ionizzazione è minore rispetto a quello dei loro atomi.	H_2	15.42593
	O_2	12.0697
	N_2	15.581
	F_2	15.697
	Cl_2	11.481
	Br_2	10.517
	I_2	9.3074
	C_2	11.4
	P_2	10.53
Idruri		
Per le molecole che per convenienza sono state qui tutte classificate come idruri, si osservano somiglianze dei valori con quelli degli atomi legati all'idrogeno, questo è vero in particolare per l'acqua e il solfuro d'idrogeno. Spiccano però i valori dell'ammoniaca e della fosfina che paiono *stranamente* bassi. Anche per gli alogenuri le energie di ionizzazione sono inferiori rispetto a quelle dei loro atomi. Vi è invece significativo aumento per il metano, il silano e notevole per il borano.	H_2O	12.621
	NH_3	10.070
	CH_4	12.61
	BH_3	12.026
	HF	16.03
	HCl	12.744
	HBr	11.68
	HI	10.386
	SiH_4	11.00
	PH_3	9.869
	H_2S	10.457

Ossidi		
Le energie di ionizzazione di CO e CO_2 sono maggiori di quelle di entrambi gli atomi che le compongono. È vero il contrario per gli ossidi dell'azoto, soprattutto per NO e NO_2 che presentano valori decisamente bassi. Per gli ossidi dello zolfo si hanno valori intermedi tra quelli degli atomi presenti nella molecola.	CO	14.014
	CO_2	13.777
	NO	9.2642
	NO_2	9.586
	N_2O	12.889
	SO_2	12.349
	SO_3	12.80

Molecole

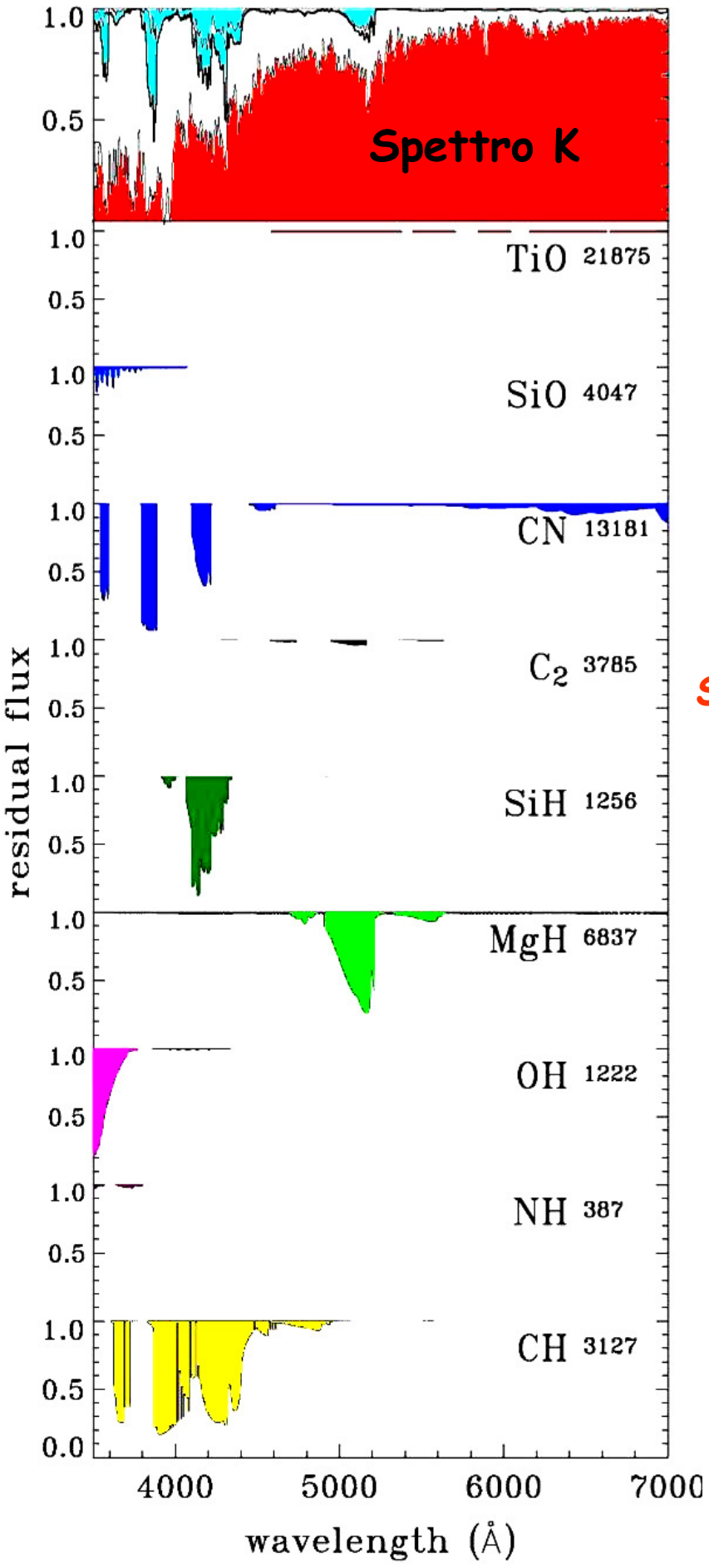

4000 > Teff > 3000 K

Diatomic molecules
(i.e. TiO, SiO,CN, SiH, MgH, OH, CH….)

3000 K > Teff

Triatomic molecules
(Water!)

La classificazione spettrale delle stelle

Classe	Temperatura (K)	Caratteristiche Spettrali
O	+28'000	He ed He+ per le piu' calde
B	28'000 - 12000	He, Balmer, Si III, O II
A	12'000 - 7'000	serie di Balmer molto intensa, deboli Mg II e Fe II
F	7'200 - 5'500	Ca II, Balmer, Fe II, Ti II, Y II, Sr II
G	6'000 - 4'500	Ca II, Balmer, metalli neutri (intensi NaI, Fe I)
K	4'700 - 3'000	Ca II, prime molecole (CN, CH), metalli neutri (Na I, Fe I, CaI)
M	< 3'300	metalli neutri (Ca I, Na I, Fe I), molecole CH, CN, TiO

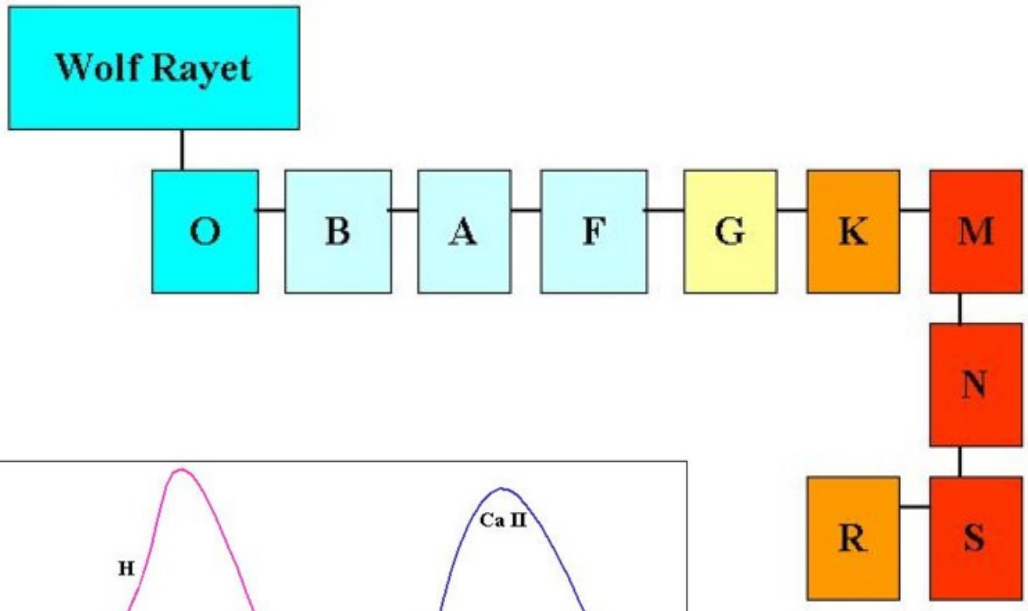

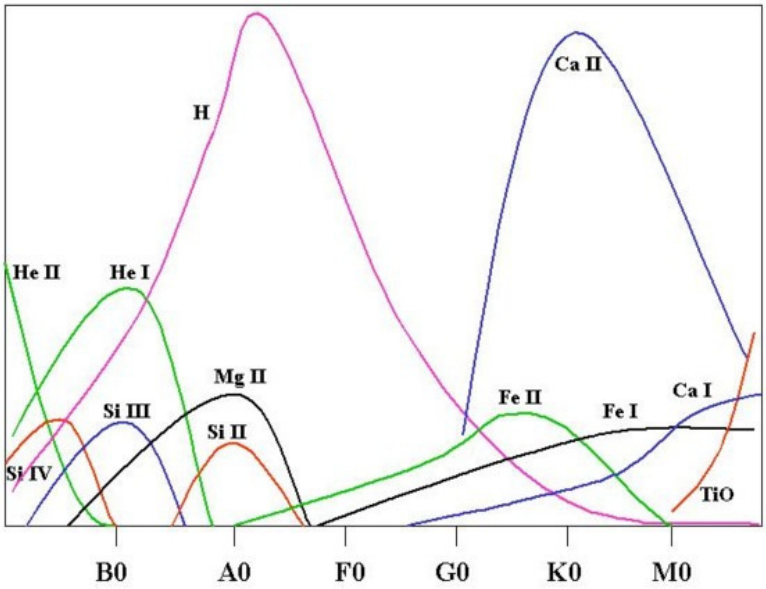

Tipo O

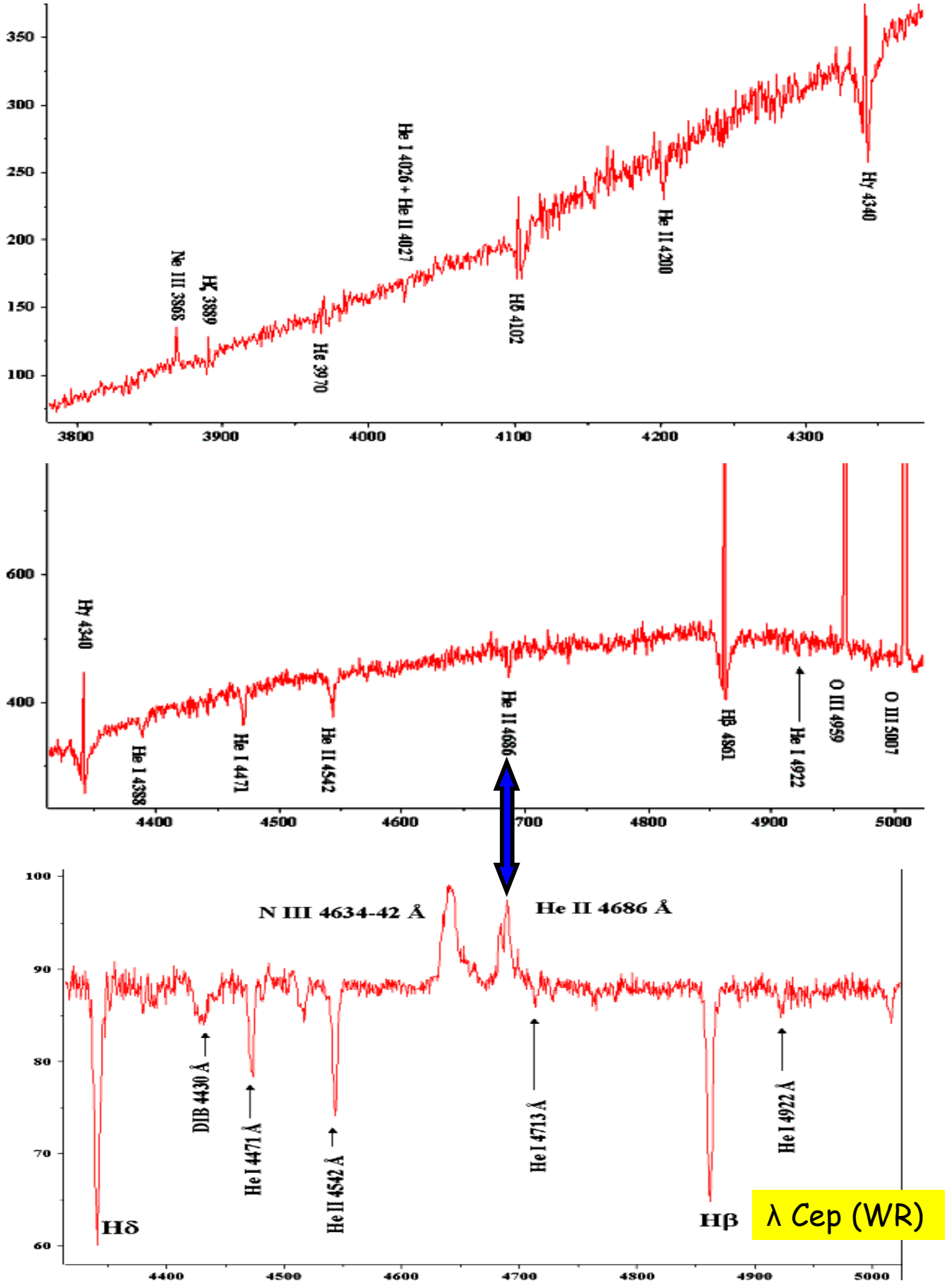
θ Ori
Ne III 3868
Hζ 3889
He 3970
He I 4026 + He II 4027
Hδ 4102
He II 4200
Hγ 4340
Hγ 4340
He I 4388
He I 4471
He II 4542
He II 4686
Hβ 4861
He I 4922
O III 4959
O III 5007
λ Cep (WR)
N III 4634-42 Å
He II 4686 Å
DIB 4430 Å
He I 4471 Å
He II 4542 Å
He I 4713 Å
He I 4922 Å
Hδ
Hβ

Emissione & Assorbimento

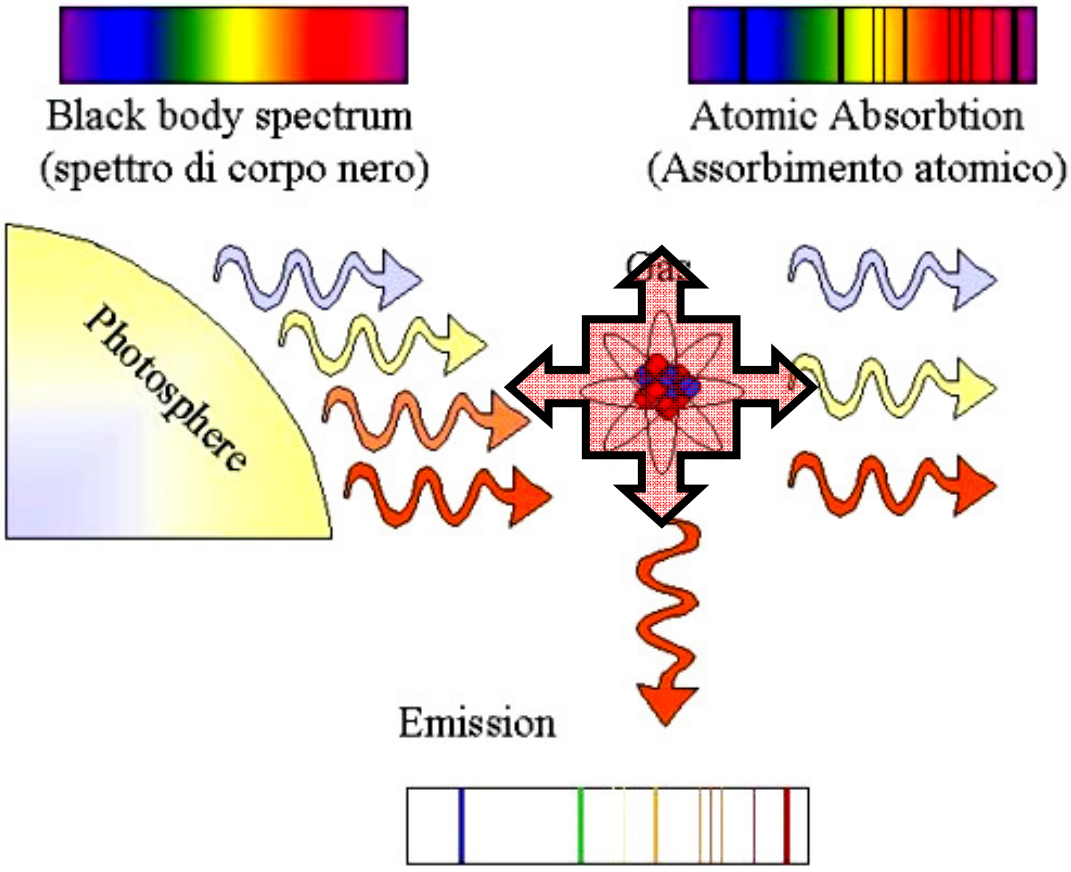

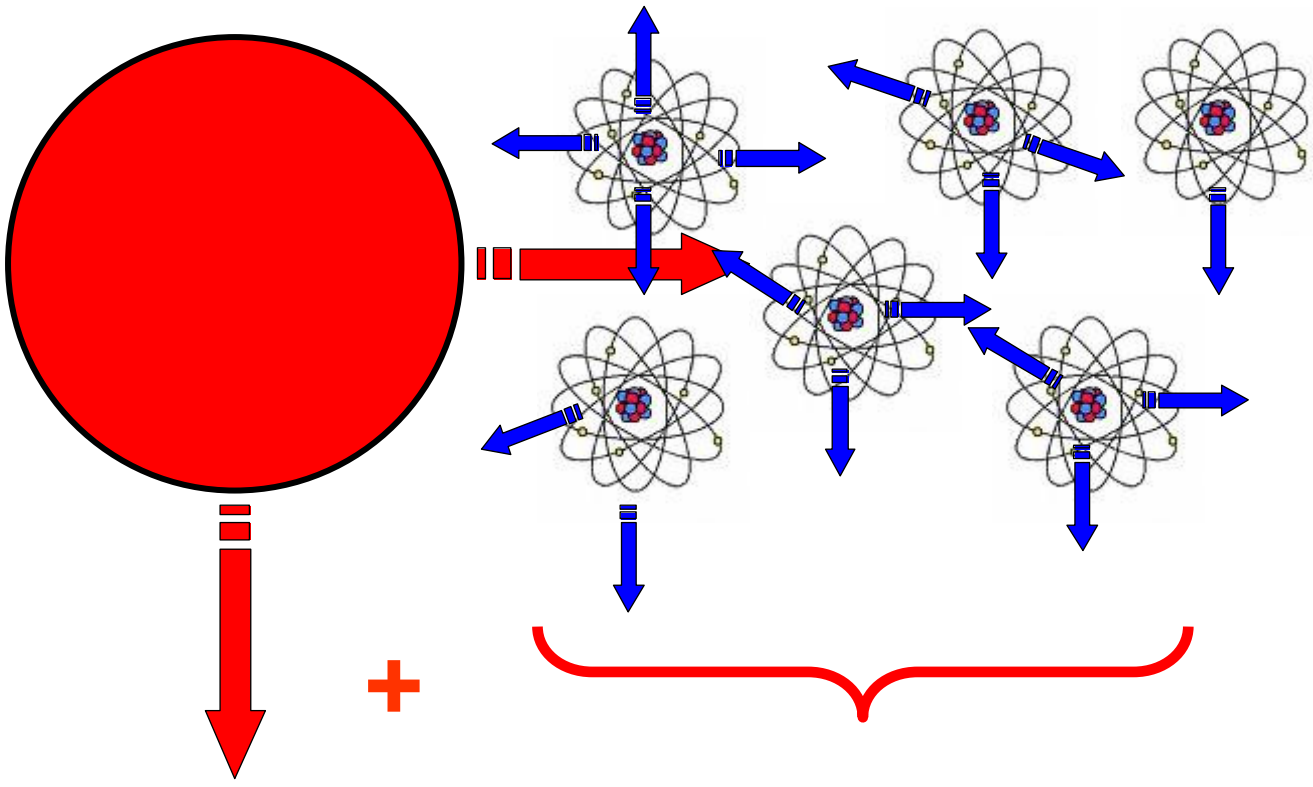

Tipo B

Bellatrix (γ Ori)

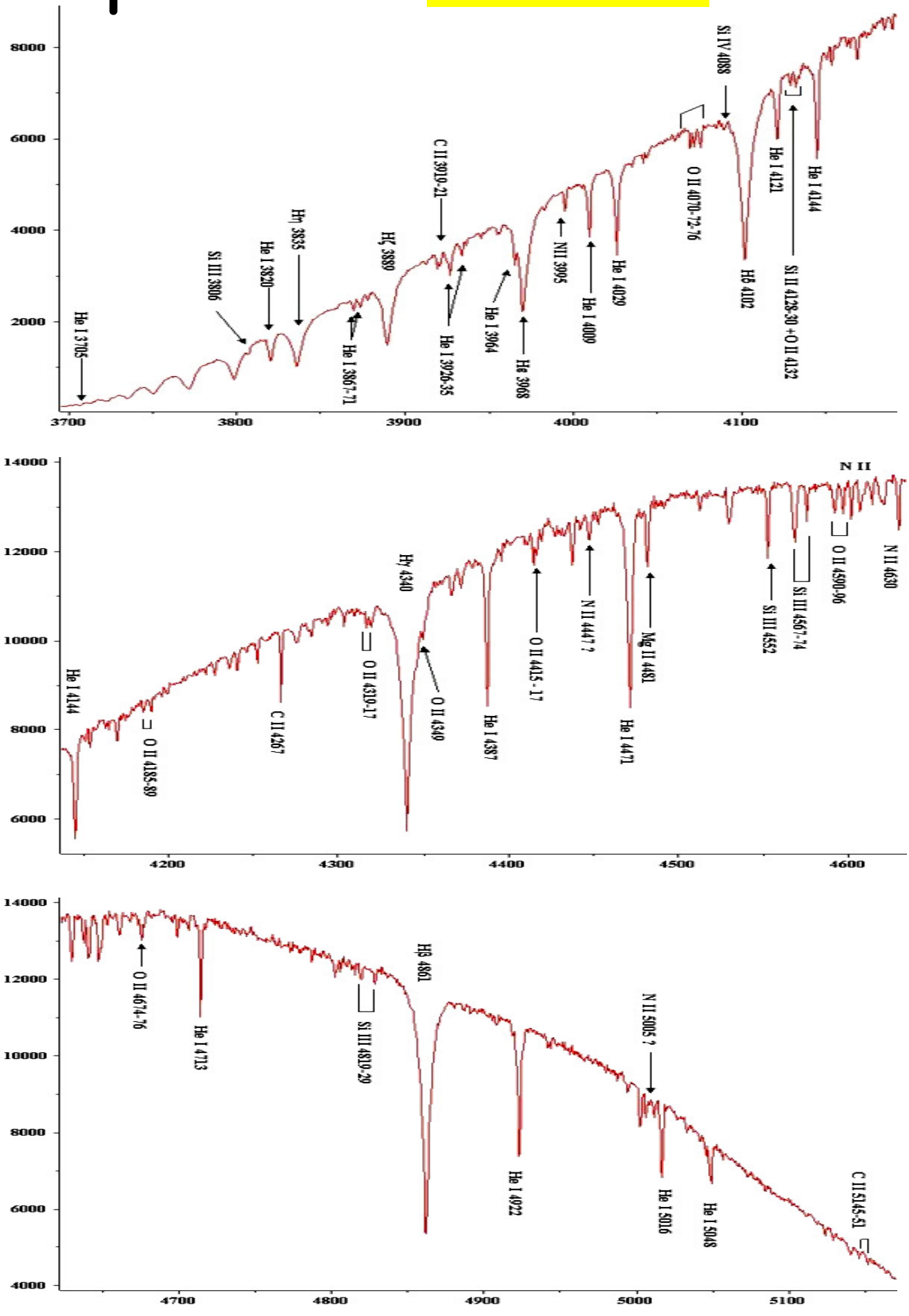

Effetti della rotazione

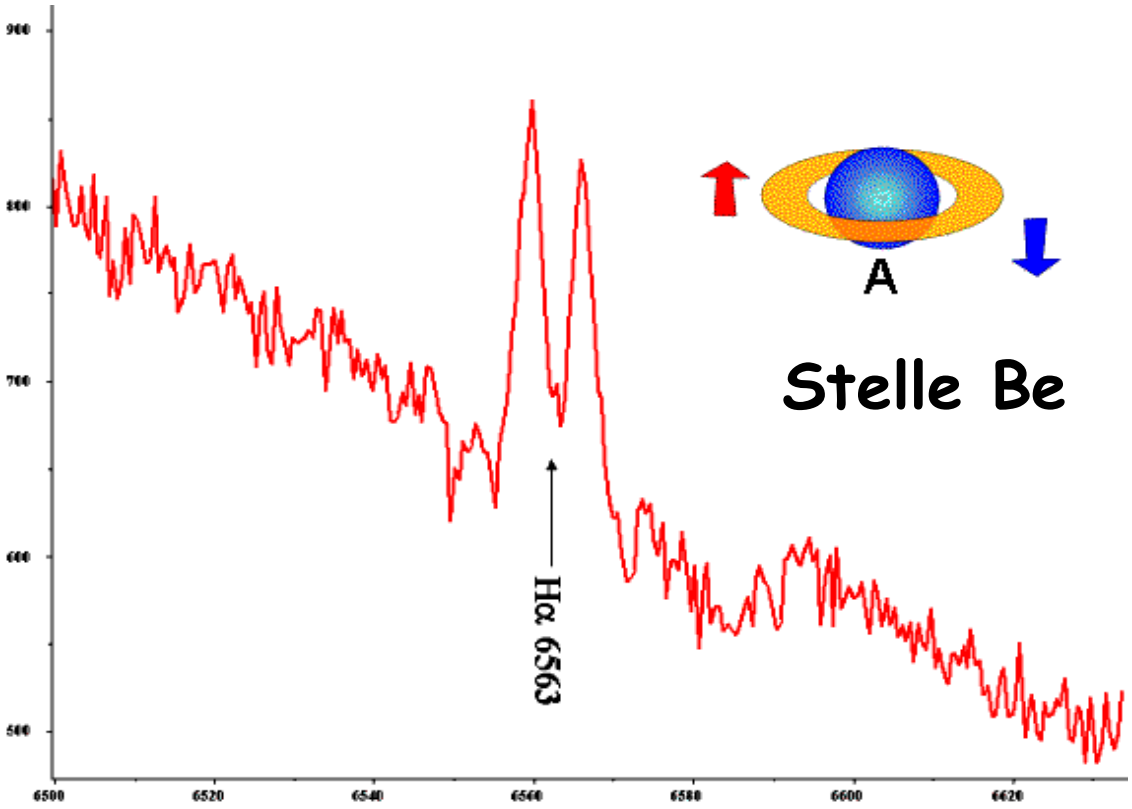

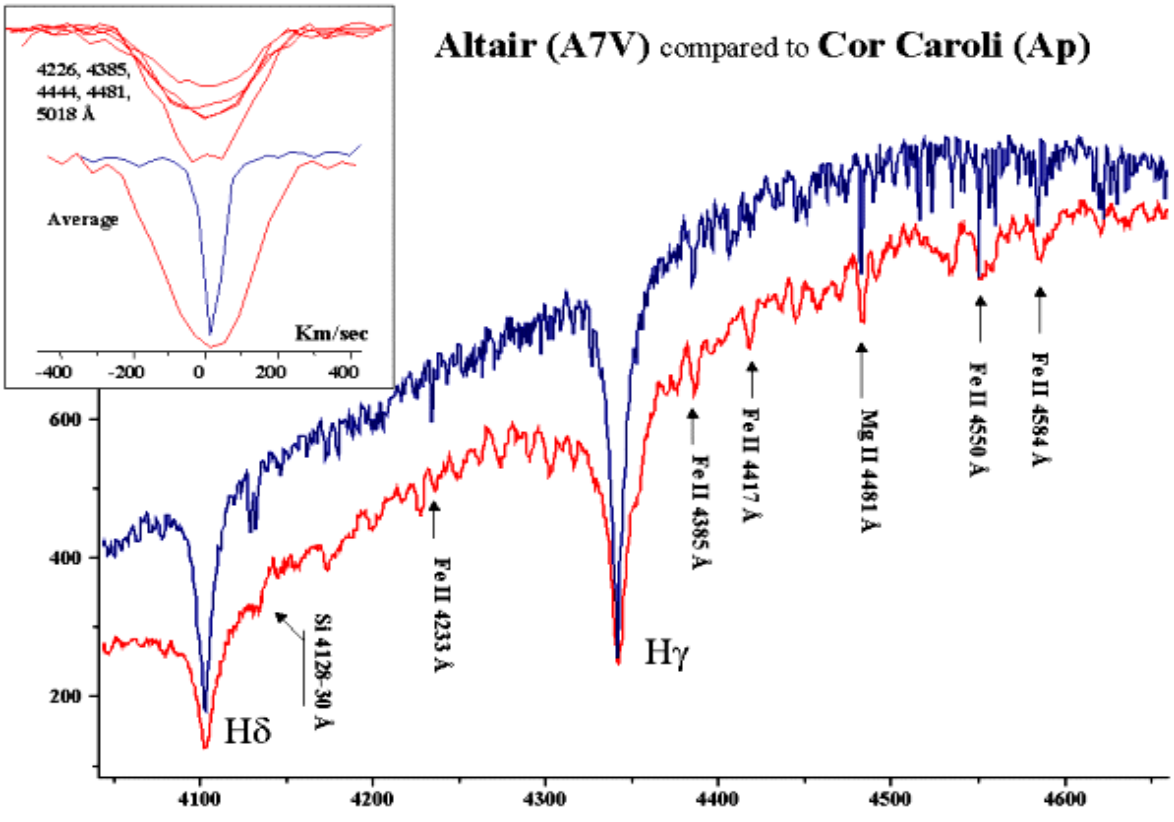

Tipo A

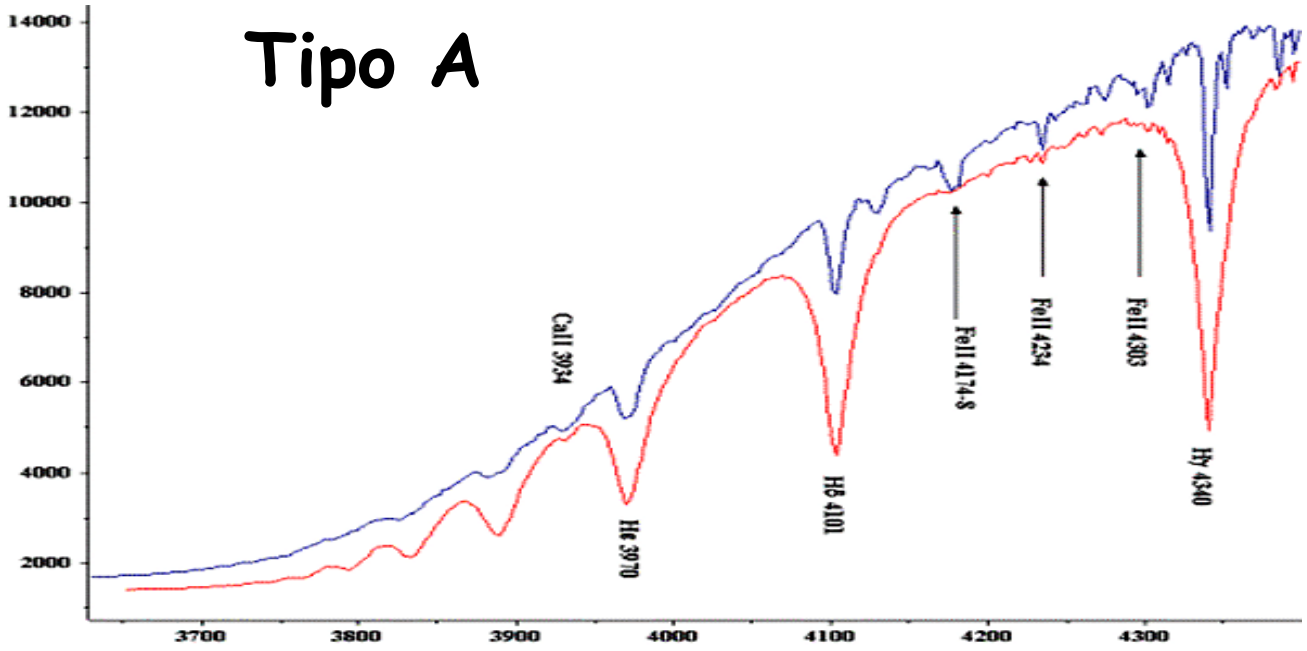

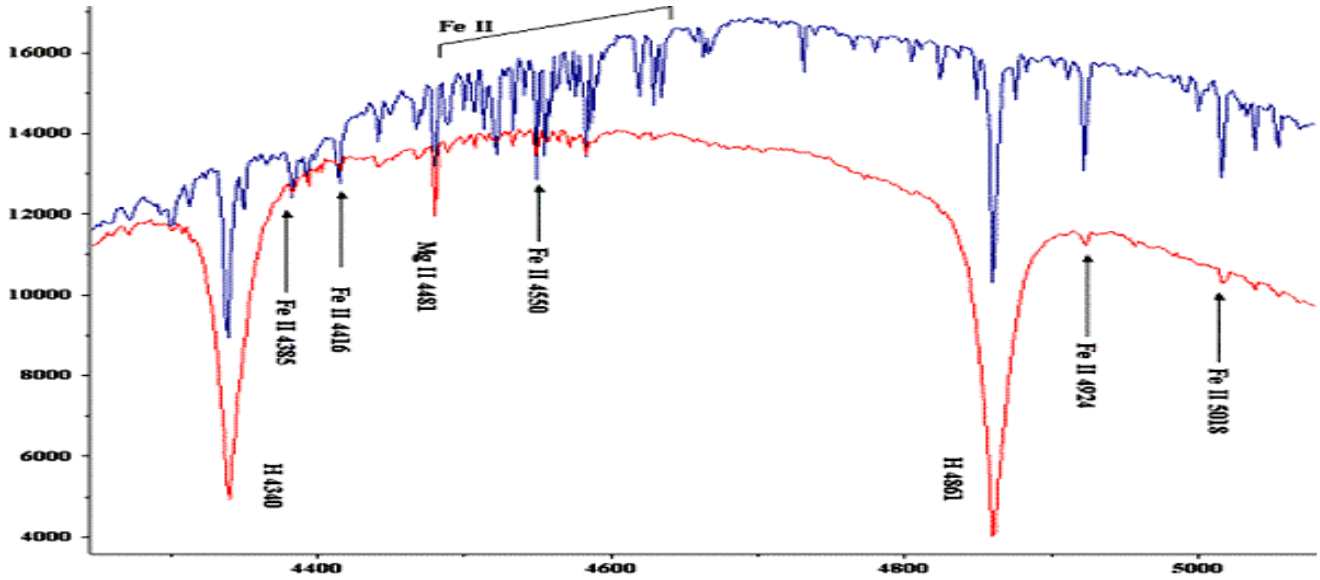

Effetto P-Cyg

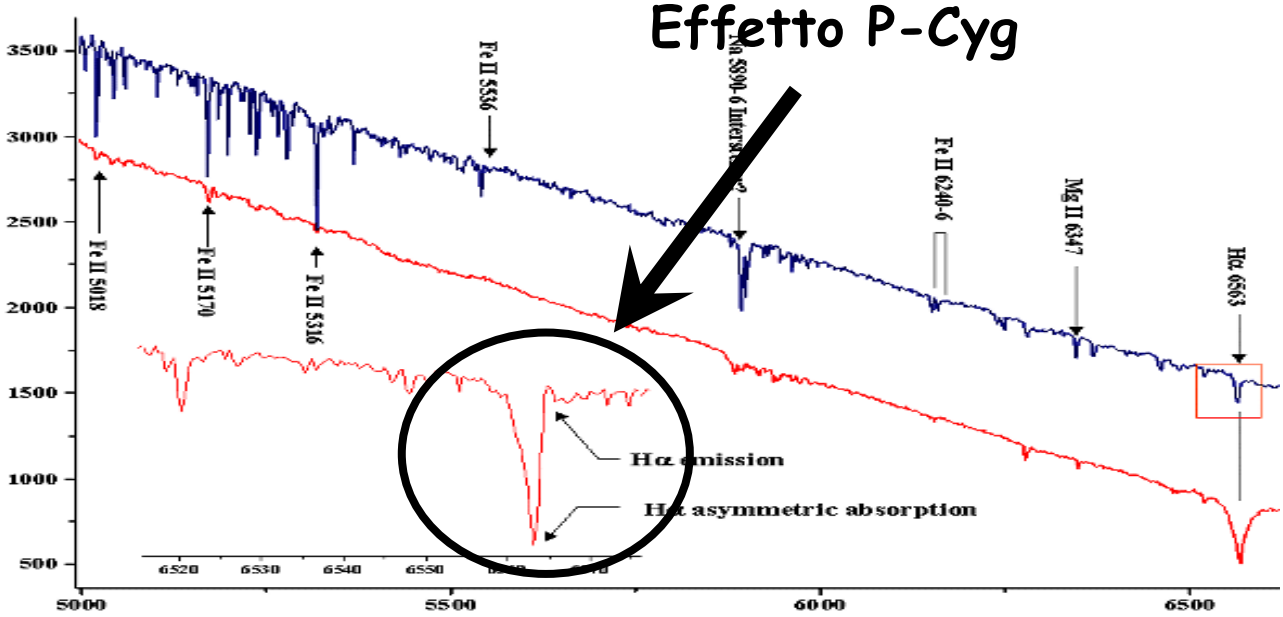

Le righe dell'Idrogeno

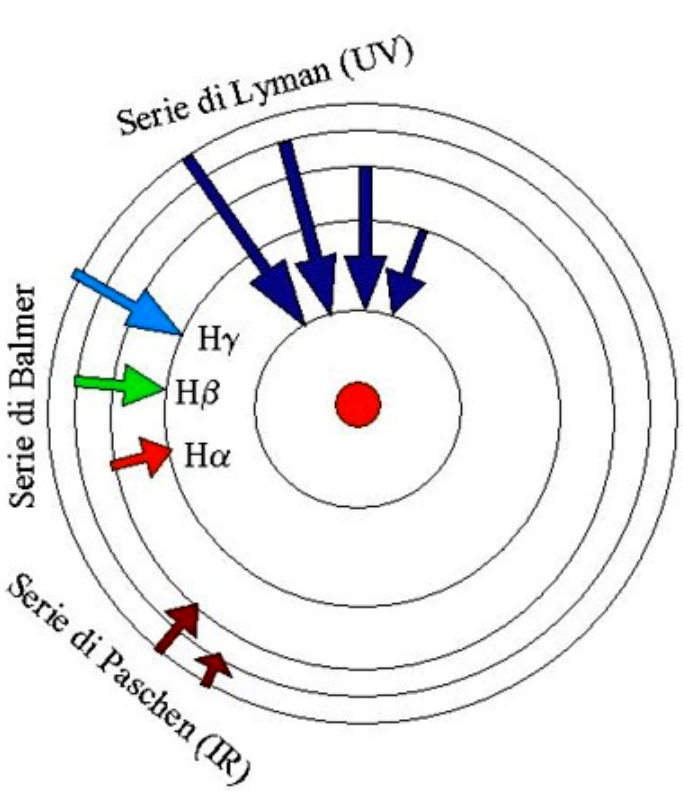

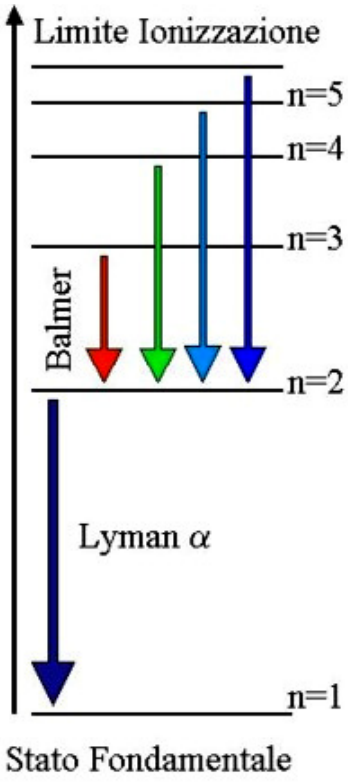

Righe emesse non solo nel visibile

$$\frac{1}{\lambda} = R\left(\frac{1}{m^2} - \frac{1}{n^2}\right) \quad m = 1,2,3,\ldots \quad n = m+1,\ldots.$$

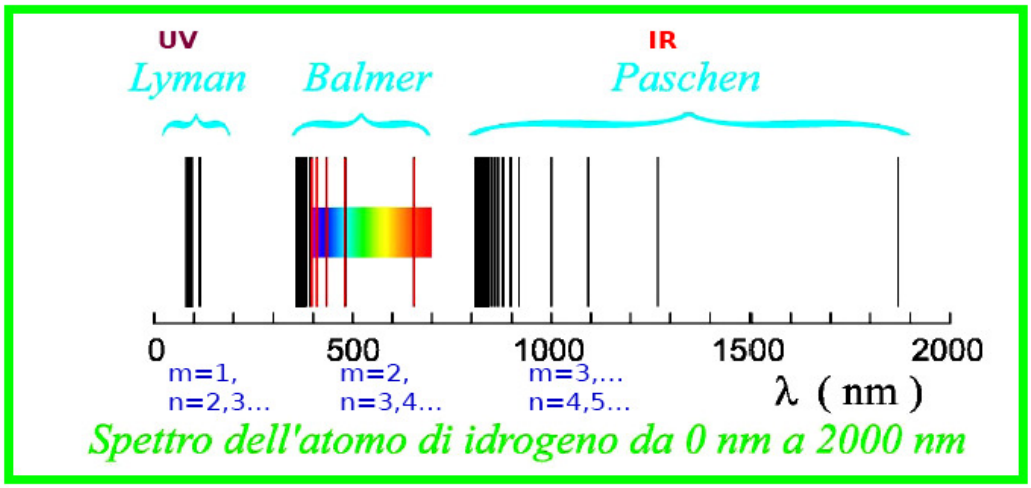

Le serie di righe

Nome della serie	Anno della scoperta	m nella formula di Rydberg	Limite della serie (nm)	λ_{max} $(n=m+1)$ (nm)	Regione spettrale
Lyman	1906-1914	1	**91.126**	**121.5**	UV lontano
Balmer	(1885)	2	**364.506**	**656.1**	Visibile-UV
Paschen	1908	3	**820.14**	**1874.6**	Infrarosso
Brackett	1922	4	**1458.03**	**4050.1**	Infrarosso
Pfund	1924	5	**2278.17**	**7455.8**	Infrarosso
Humphreys	1953	6	**3280.56**	**12365.1**	Infrarosso
Hansen-Strong	1973	7	**4465.21**	**19051.5**	Infrarosso

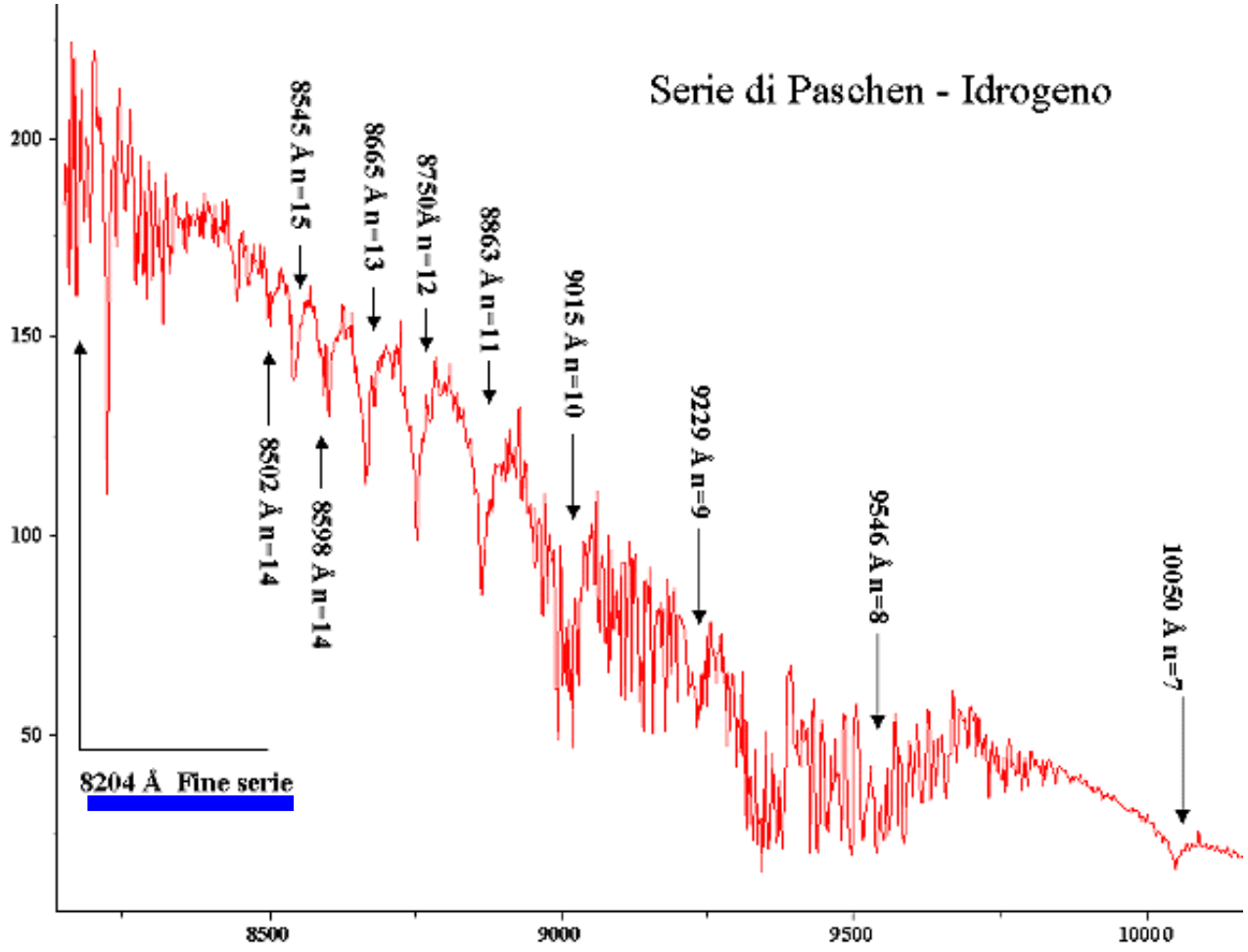

Lo spettro del Sole (tipo G)

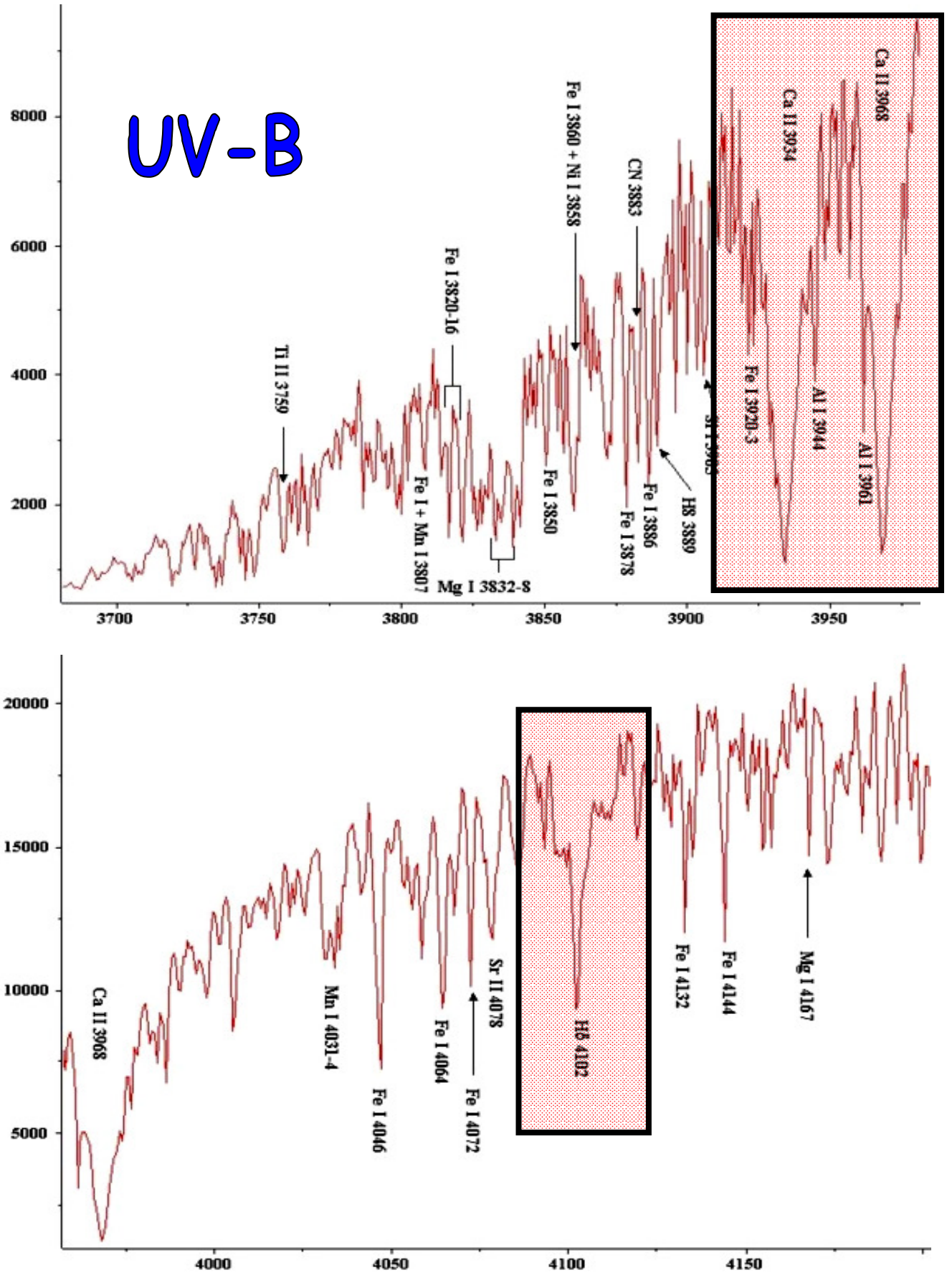

Blu (4100-4850 A)

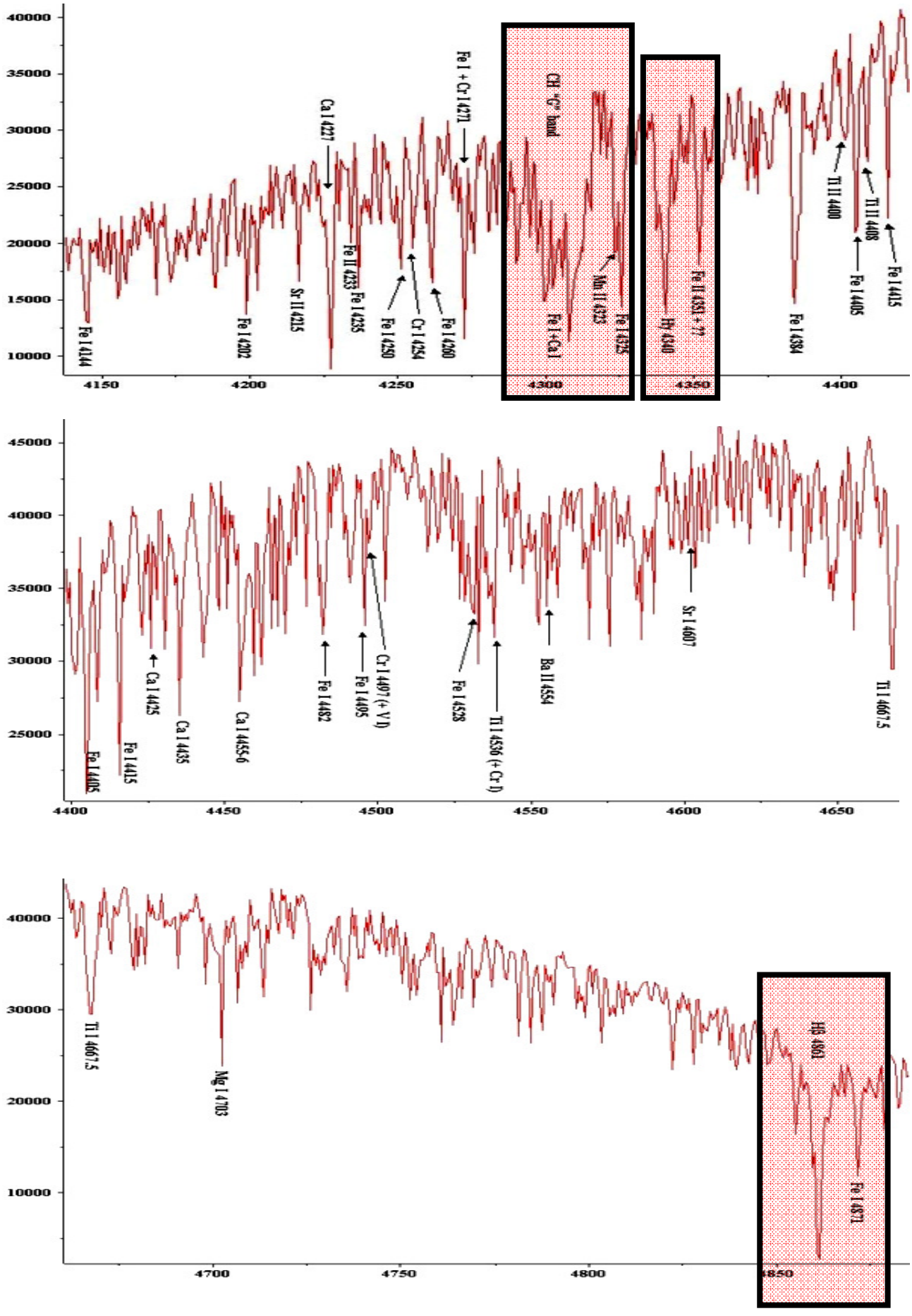

Visibile (4850-5700 A)

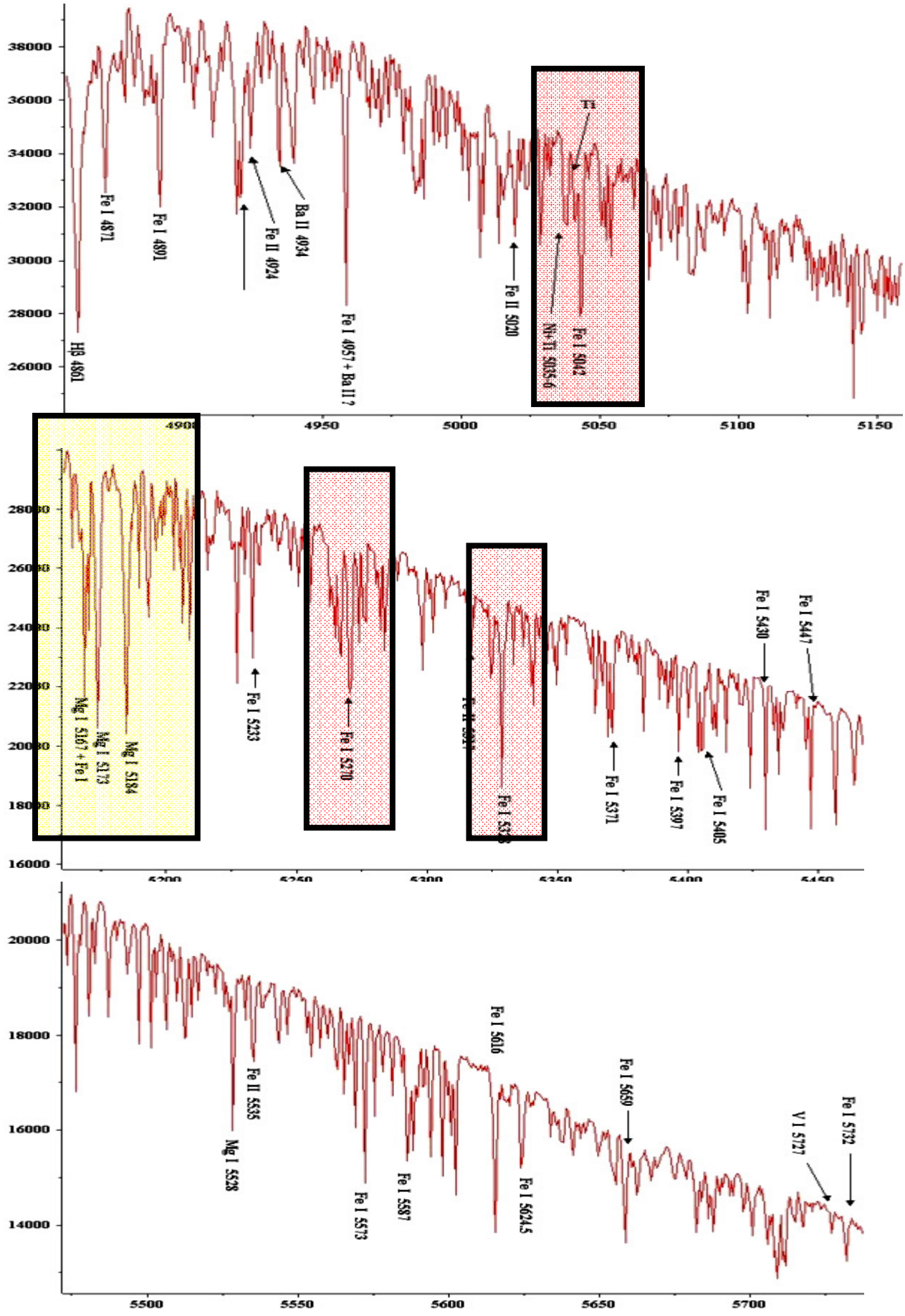

Rosso (>5800 A)

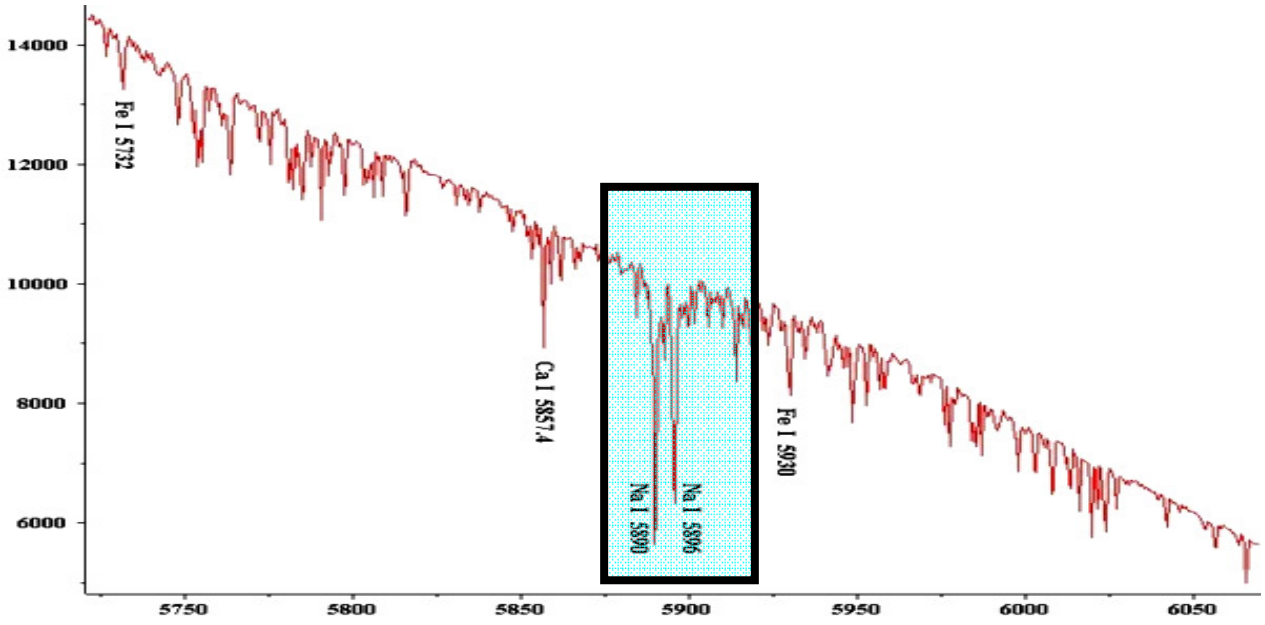

Emissione cromosferica

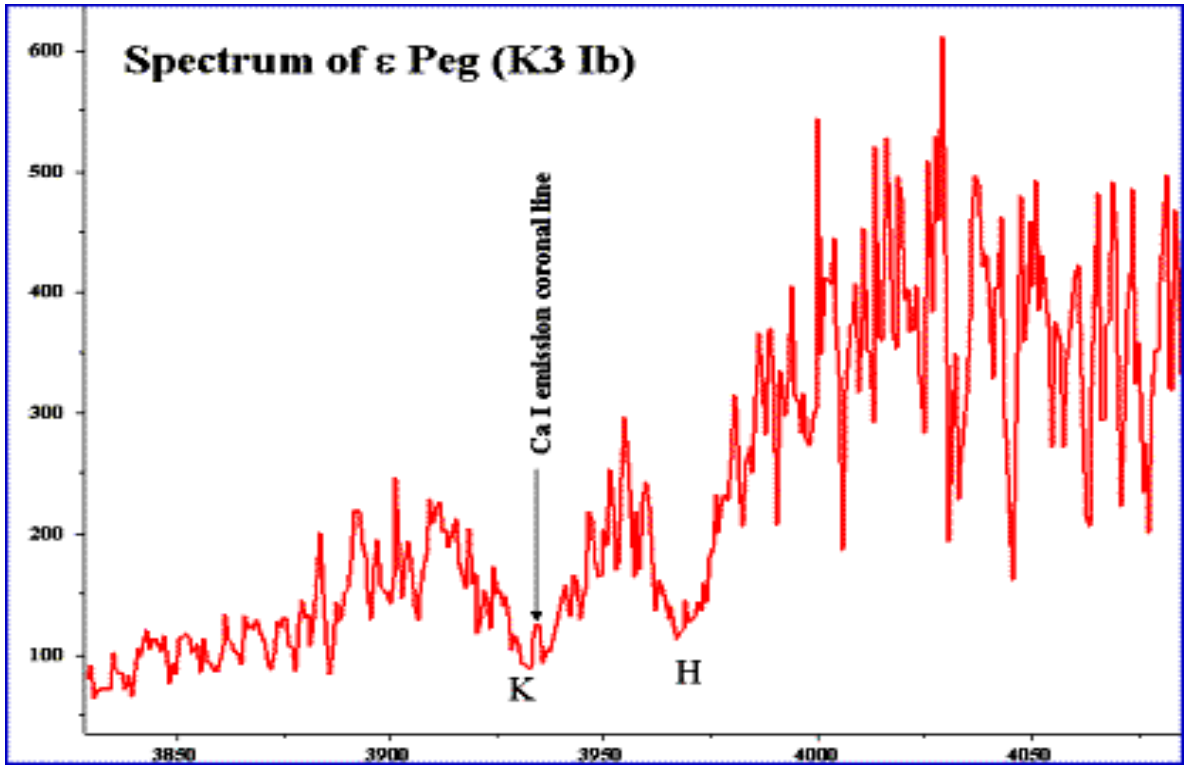

Stelle M

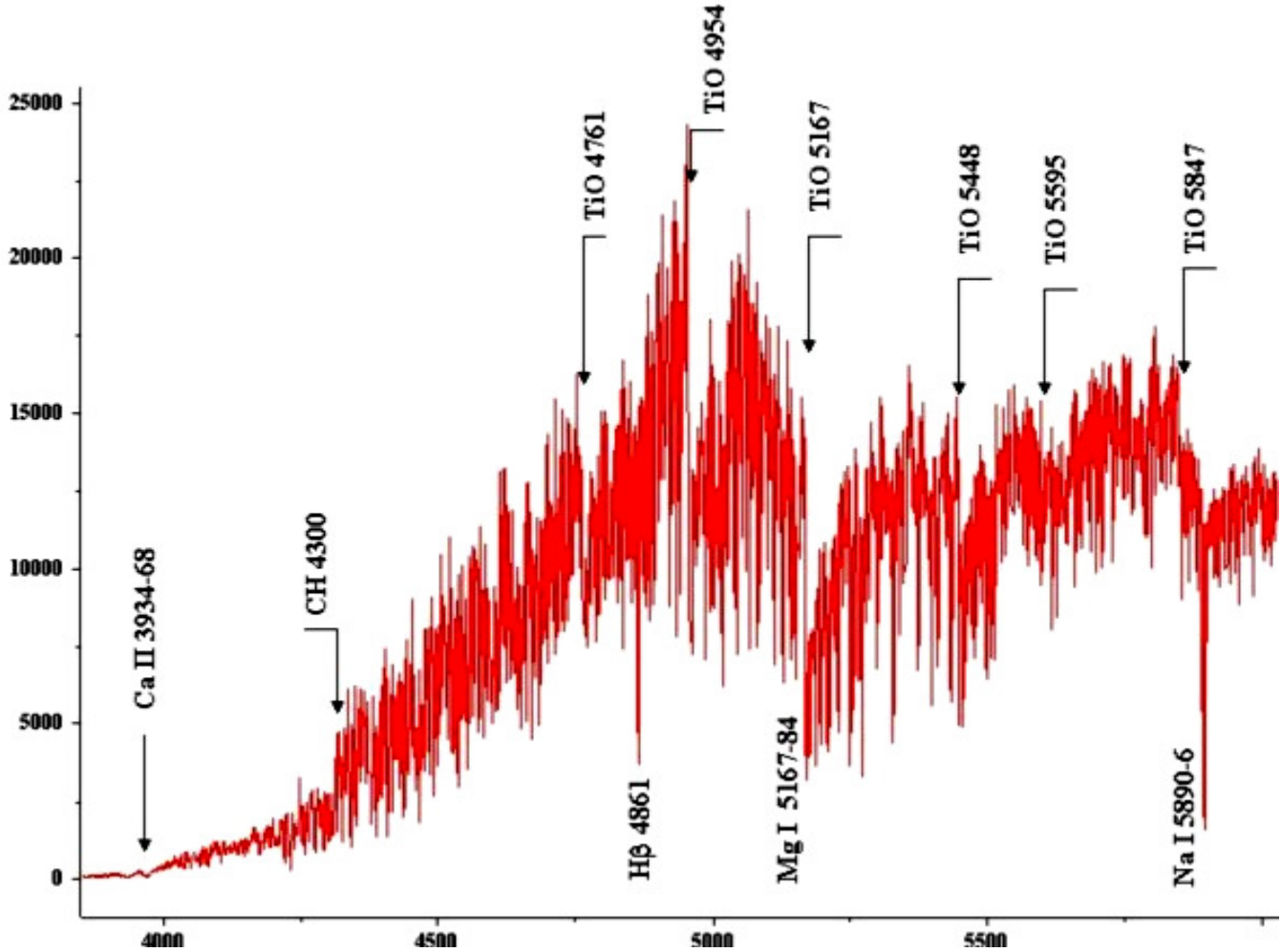
25000
20000
15000
10000
5000
0
4000
4500
5000
5500
Ca II 3934-68
CH 4300
TiO 4761
TiO 4954
TiO 5167
TiO 5448
TiO 5595
TiO 5847
Hβ 4861
Mg I 5167-84
Na I 5890-6

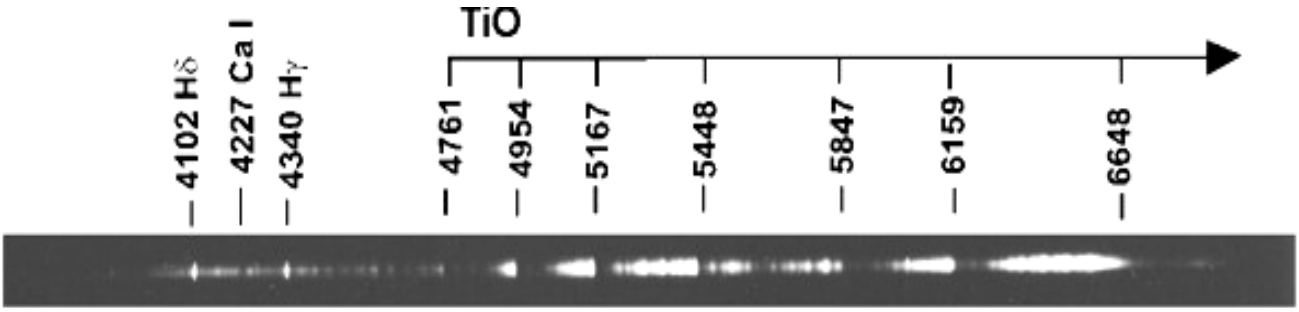
4102 Hδ
4227 Ca I
4340 Hγ
TiO
4761
4954
5167
5448
5847
6159
6648

Gli indici di Fanelli (Far-UV)
(1987)

TABLE 1

FAR-ULTRAVIOLET WAVELENGTH SEQUENCE

λ(Å)[a]	Code[b]	Comments
1240.....	L	N V (1238, 1242) resonance lines, P Cygni profile in early supergiants.
1280.....	C	
1305.....	L	Si II (1304) resonance transition; Si III multiplet no. 4 (1295–1303, six lines) O I (1302, 1304, 1306). Prominent in B2 to B9 stars.
1355.....	C	
1397.....	L	Si IV (1394, 1403) resonance lines, prominent in early B stars, maximum at B1. P Cygni profile in early supergiants.
1425.....	L/C	Feature present from O8 to B2 in dwarfs, to B5 in supergiants. Possibly blend of Fe IV, Fe V, and C III multiplets.
1450.....	L/C	Broad line feature present from O2 to B0. Probably Fe V + Fe IV blend.
1485.....	C	
1510.....	C	
1540.....	L	C IV (1548, 1551) resonance lines prominent in O and early B stars. P Cygni profile in supergiants earlier than B0 and in O3–6 dwarfs.
1550.....	L	
1560.....	L	
1590.....	C	
1620.....	L/C	Wide ($\Delta\lambda \approx 20$ Å) feature present in O to early B supergiants and O7 to B0 dwarfs. Probably blend of Fe lines. Stronger in supergiants.
1680.....	L/C	Stars later than B8 show Al II (1671).
1710.....	C	N IV (1719) may be present in early O dwarfs and supergiants to B1.
1813.....	C	
1855.....	L	Wide blend: Al II (1858, 1862), Al III (1855, 1863), Fe II, Fe III. Increase in strength from B2 to mid A.

[a] Central wavelength of bandpass. All bandpasses have a width of 20 Å.
[b] L = line, C = continuum, L/C = both, depending on spectral type.

TABLE 4

SPECTRAL INDICES[a]

Index Name and Wavelength	Sidebands
1305 Å blend	1280, 1355
Si IV 1397	1355, 1425
C IV 1550	1510, 1590
C IV abs 1540	1510, 1590
C IV ems 1560	1510, 1590
C IV P Cygni[b]	(1540/1560)
1620 Å blend	1590, 1680

Indici di (pseudo)-continuo & linea

FWHM = 6Å

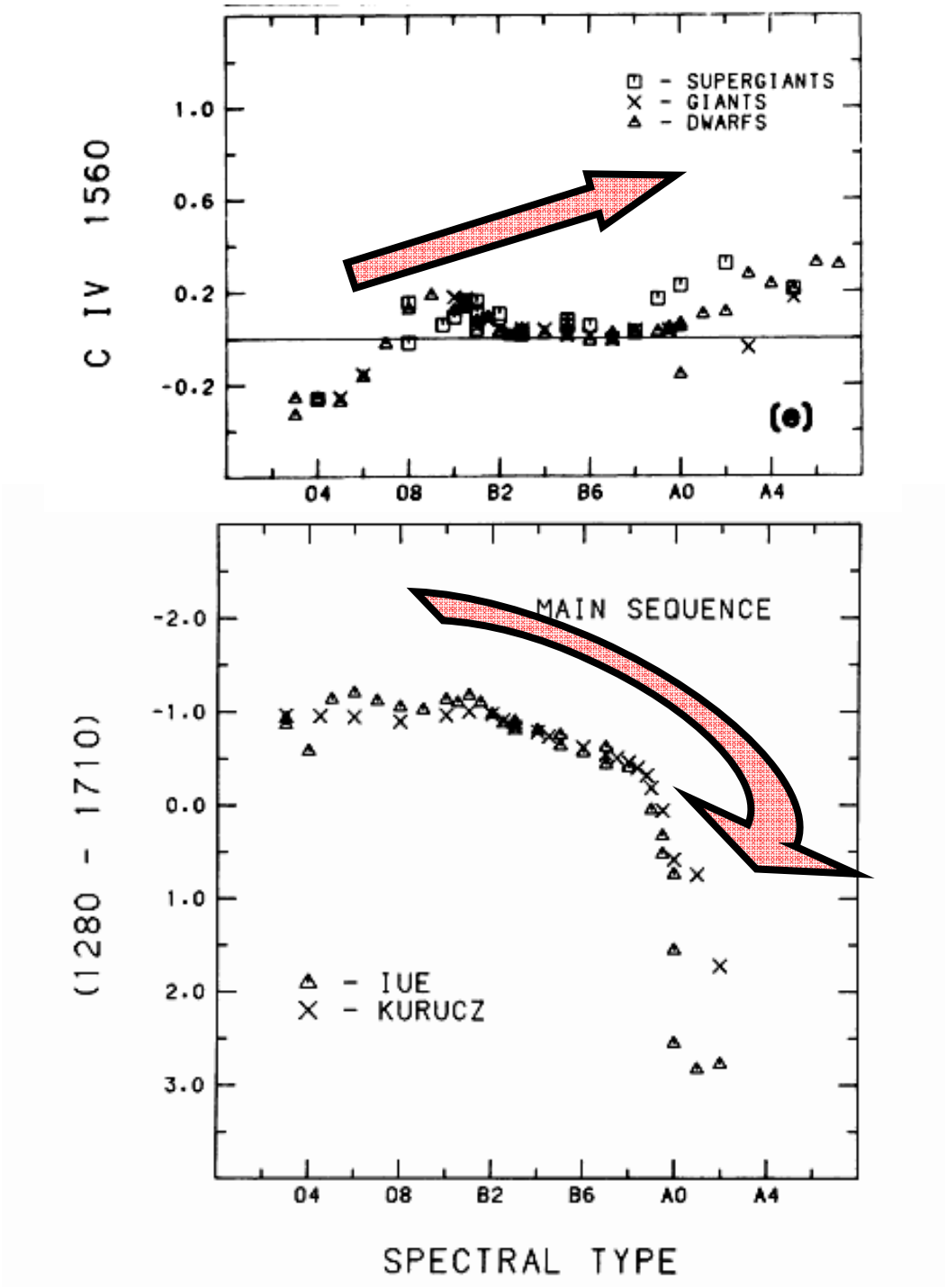

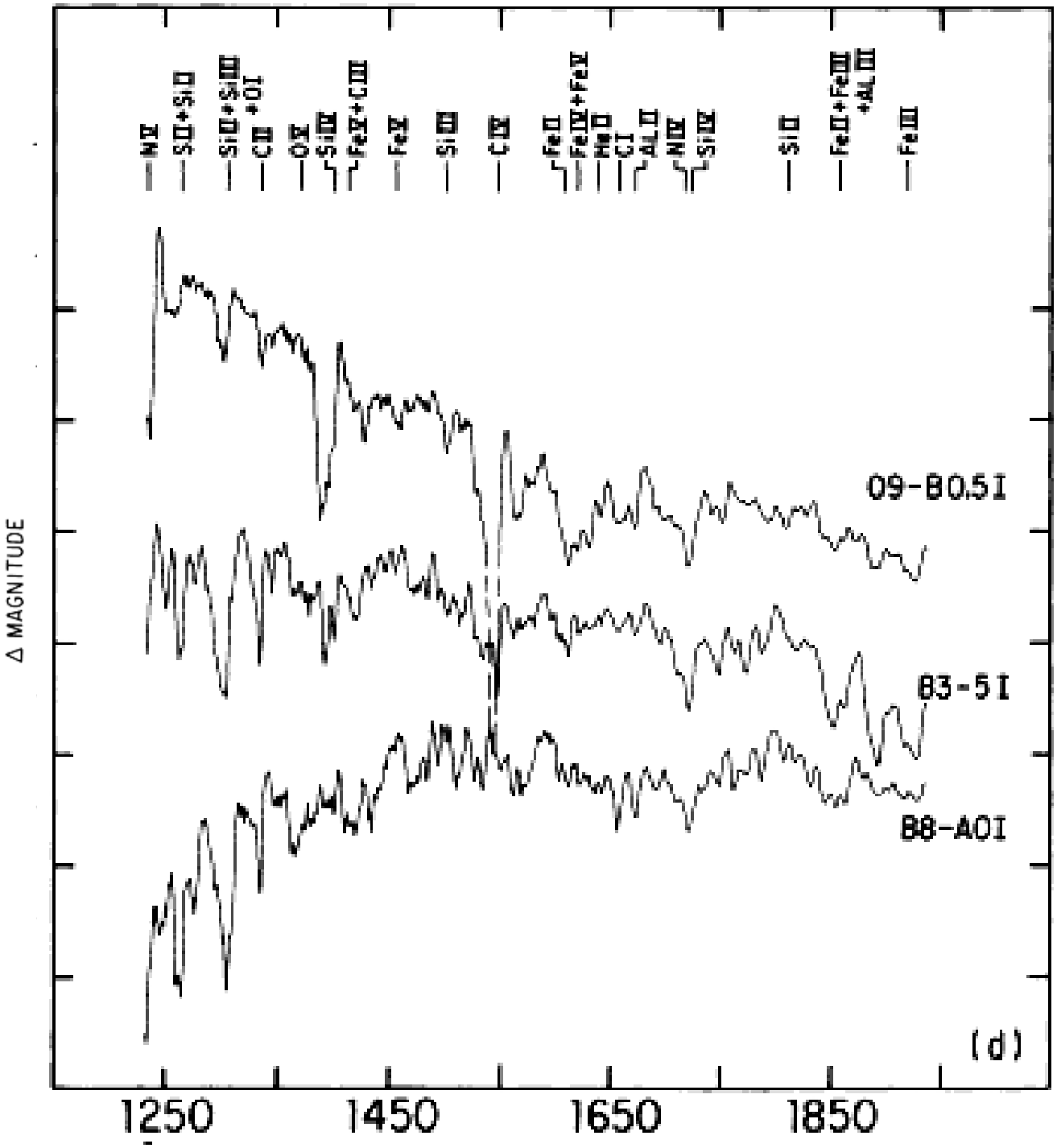
NV
SiII+SiII
SiII+SiIII
+OI
CII
OIV
SiIV
FeV+CIII
FeV
SiIII
CIV
FeII
FeIV+FeV
MgII
CI
AlII
NIV
SiIV
SiII
FeII+FeIII
+AlIII
FeIII
09-B0.5I
B3-5I
B8-A0I
(d)
Δ MAGNITUDE
1250
1450
1650
1850

UV indices & diagnostica di Star-forming galaxies

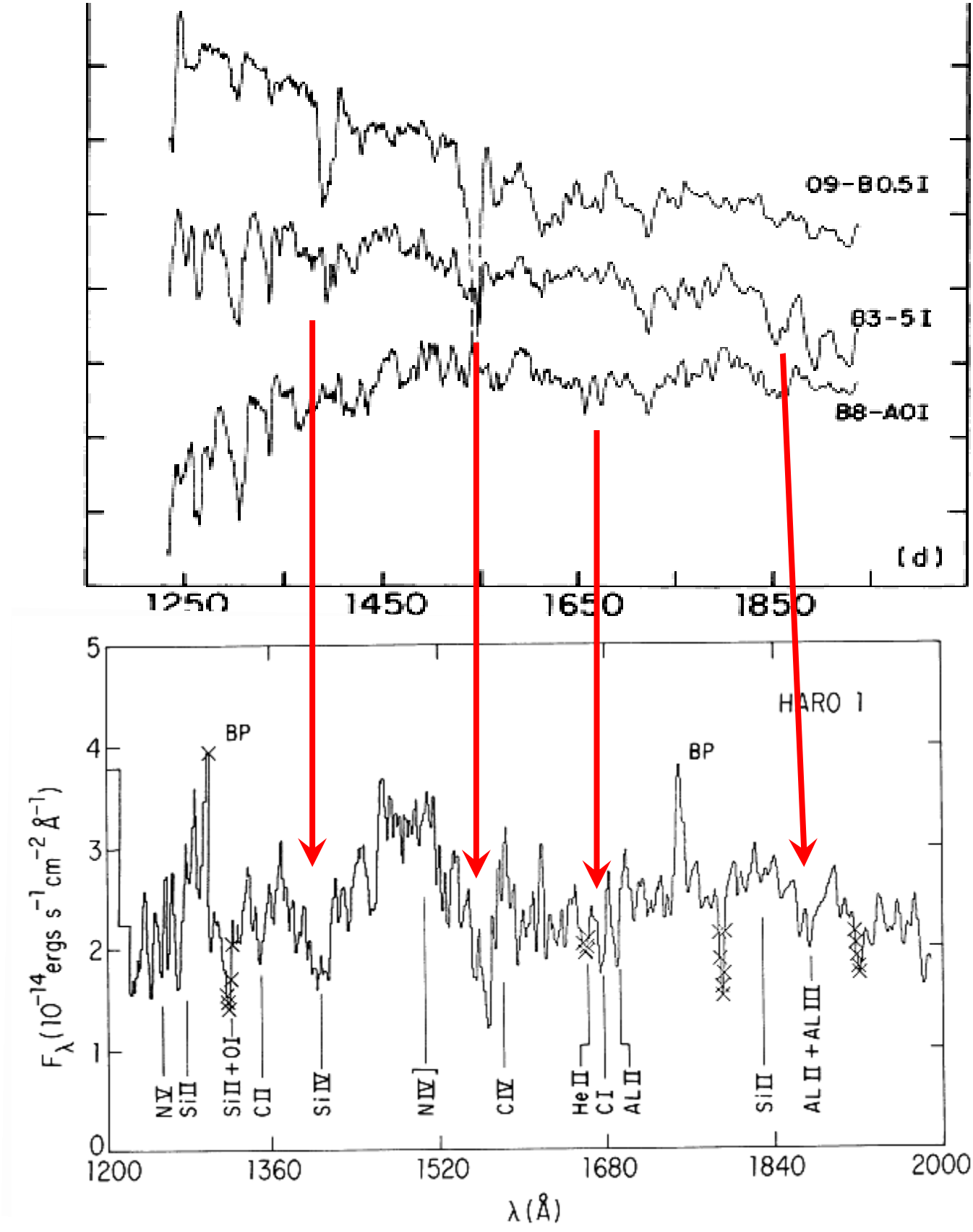

Indici di Mid-UV
(1990)

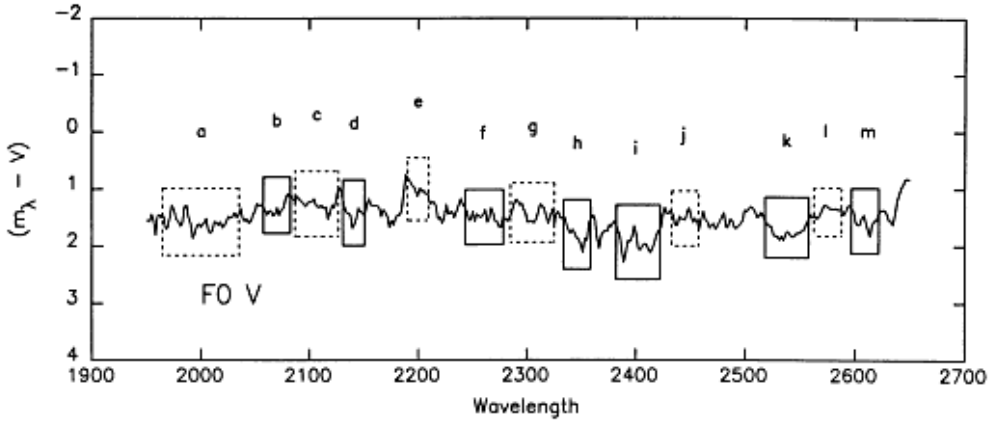

FIG. 3*a*

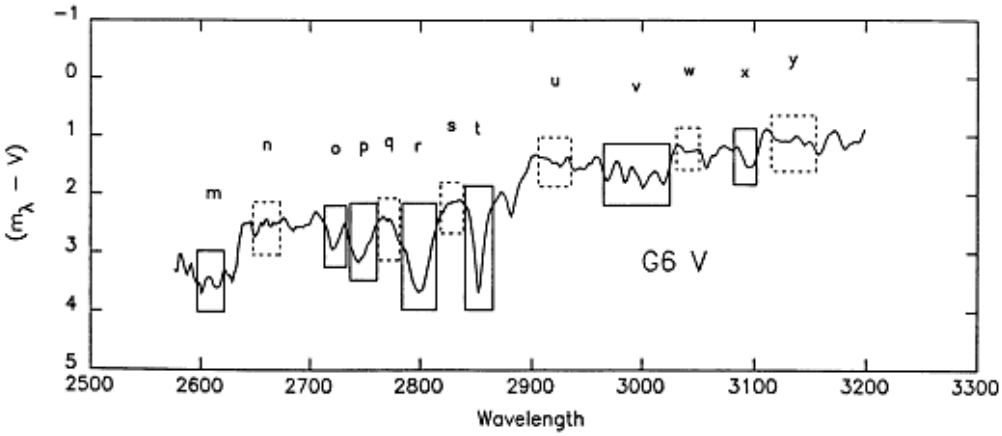

TABLE 3

MID-ULTRAVIOLET WAVELENGTH SEQUENCE

ID (1)	λ_i (2)	λ_f (3)	$\Delta\lambda$ (4)	Code* (5)	Comments (6)
a	1965	2035	70	C	
b	2057	2083	26	L	
c	2087	2127	40	C	
d	2131	2151	20	L	
e	2190	2210	20	C	
f	2243	2279	36	L	
g	2285	2325	40	C	
h	2333	2359	26	L	Fe II (3), 2338.0, 2344.3, 2343.5, 2348.3
i	2382	2422	40	L	Fe II (2), blend of ~10 lines
j	2432	2458	26	C	
k	2520	2556	36	L	Uncertain, Fe I?
l	2562	2588	26	C	
m	2596	2622	26	L	Fe II (1), blend of ~10 lines
n	2647	2673	26	C	
o	2713	2733	20	L	
p	2736	2762	26	L	Fe I, 2744.1, Fe II 2747.0, 2746.5, Cr I 2748.3
q	2762	2782	20	C	
r	2784	2814	30	L	Mg II (1) 2795.5, 2802.7
s	2818	2838	20	C	
t	2839	2865	26	L	Mg I (1) 2852.1
u	2906	2936	30	C	
v	2965	3025	60	L	Fe I 2967.0, 2973.3, 2994.4, 3020.6
w	3031	3051	20	C	
x	3086	3106	20	L	Al I 3092.7, Fe I 3091.6, Ni I?
y	3115	3155	40	C	

* C = continuum; L = line.

Il Magnesio (MgII & MgI)

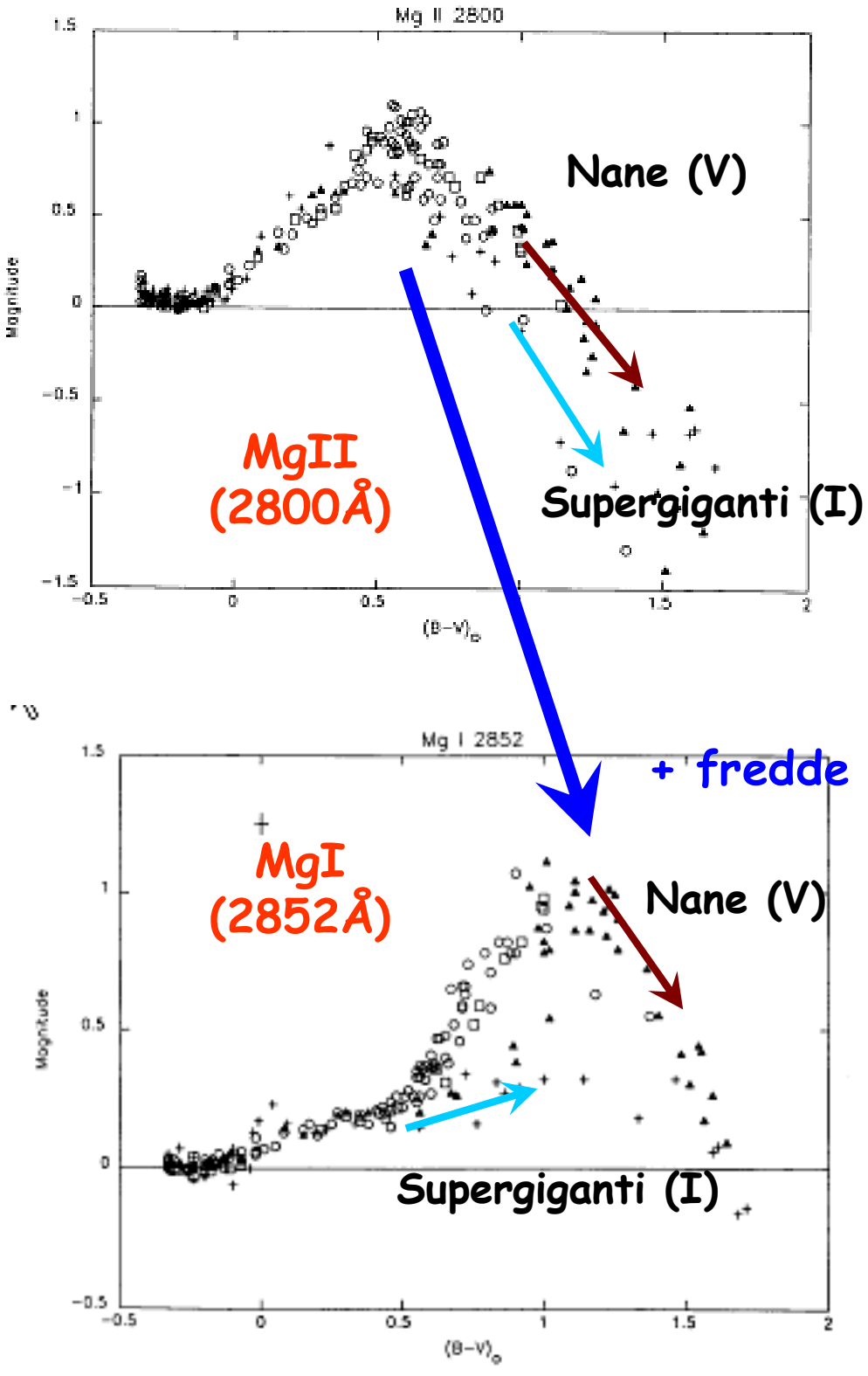

FIG. 5d

La griglia di indici

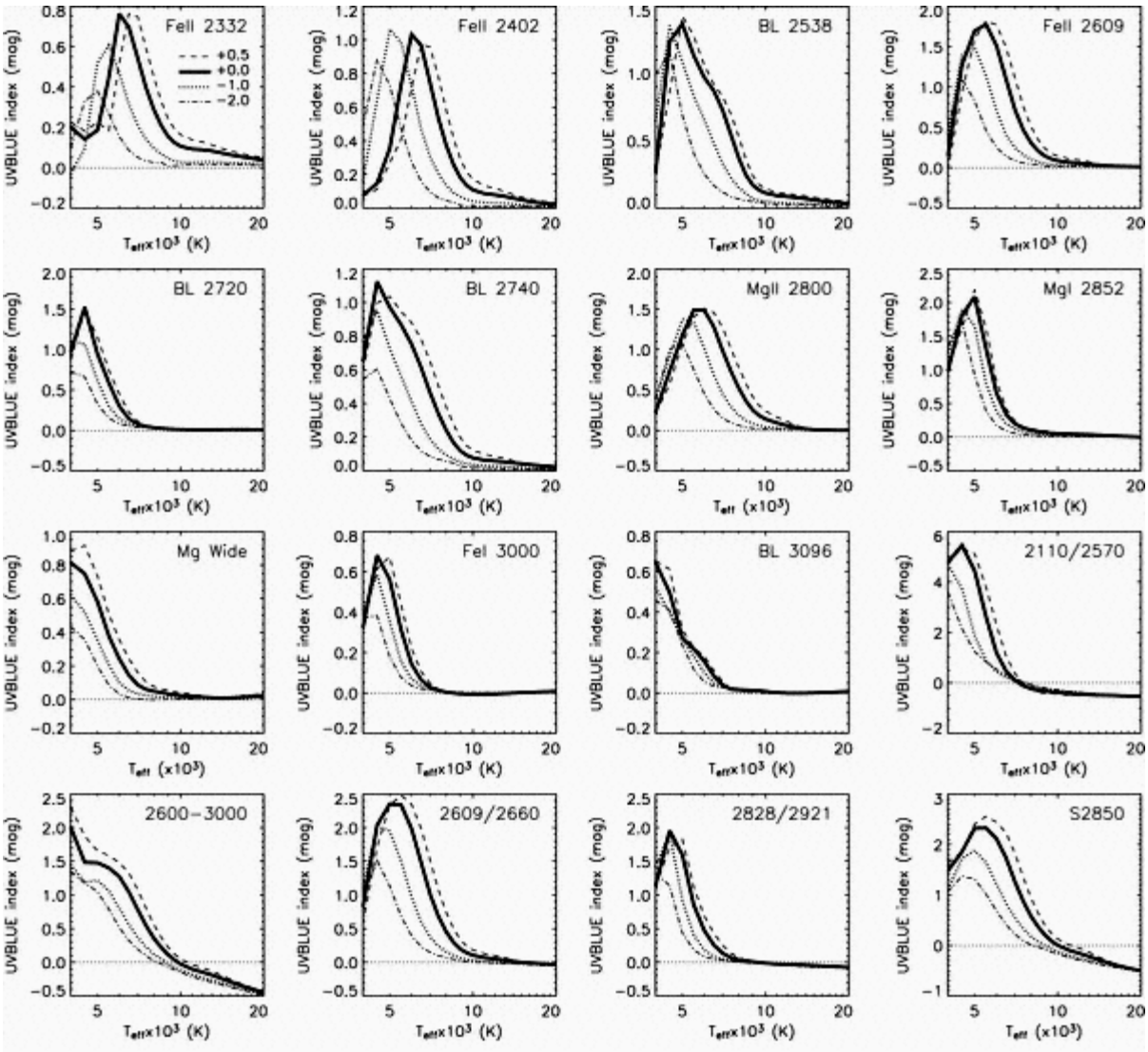

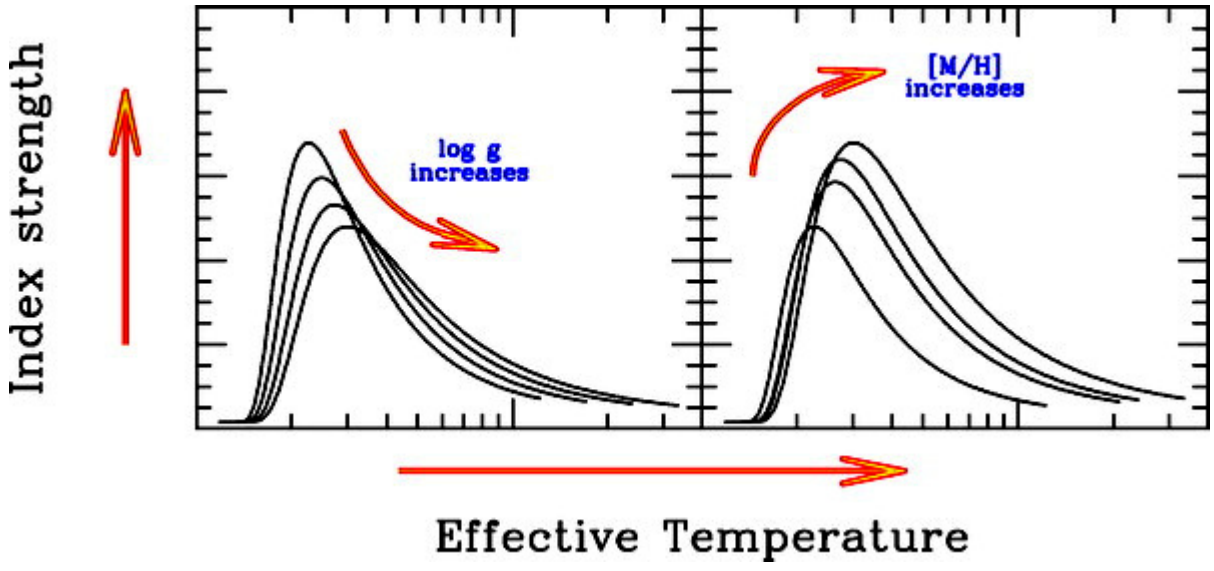

Il sistema di Lick

TABLE 1

INDEX DEFINITIONS

	Name	Index Bandpass	Pseudocontinua	Units	Measures	Error[1]	Notes
01	CN_1	4143.375-4178.375	4081.375-4118.875 4245.375-4285.375	mag	CN, Fe I	0.021	
02	CN_2	4143.375-4178.375	4085.125-4097.625 4245.375-4285.375	mag	CN, Fe I	0.023	2
03	Ca4227	4223.500-4236.000	4212.250-4221.000 4242.250-4252.250	Å	Ca I, Fe I, Fe II	0.27	2
04	G4300	4282.625-4317.625	4267.625-4283.875 4320.125-4336.375	Å	CH, Fe I	0.39	
05	Fe4383	4370.375-4421.625	4360.375-4371.625 4444.125-4456.625	Å	Fe I, Ti II	0.53	2
06	Ca4455	4453.375-4475.875	4447.125-4455.875 4478.375-4493.375	Å	Ca I, Fe I, Ni I, Ti II, Mn I, V I	0.25	2
07	Fe4531	4515.500-4560.500	4505.500-4515.500 4561.750-4580.500	Å	Fe I, Ti I, Fe II, Ti II	0.42	2
08	Fe4668	4635.250-4721.500	4612.750-4631.500 4744.000-4757.750	Å	Fe I, Ti I, Cr I, Mg I, Ni I, C_2	0.64	2
09	Hβ	4847.875-4876.625	4827.875-4847.875 4876.625-4891.625	Å	Hβ, Fe I	0.22	3
10	Fe5015	4977.750-5054.000	4946.500-4977.750 5054.000-5065.250	Å	Fe I, Ni I, Ti I	0.46	2,3
11	Mg_1	5069.125-5134.125	4895.125-4957.625 5301.125-5366.125	mag	MgH, Fe I, Ni I	0.007	3
12	Mg_2	5154.125-5196.625	4895.125-4957.625 5301.125-5366.125	mag	MgH, Mg *b*, Fe I	0.008	3
13	Mg *b*	5160.125-5192.625	5142.625-5161.375 5191.375-5206.375	Å	Mg *b*	0.23	3
14	Fe5270	5245.650-5285.650	5233.150-5248.150 5285.650-5318.150	Å	Fe I, Ca I	0.28	3
15	Fe5335	5312.125-5352.125	5304.625-5315.875 5353.375-5363.375	Å	Fe I	0.26	3
16	Fe5406	5387.500-5415.000	5376.250-5387.500 5415.000-5425.000	Å	Fe I, Cr I	0.20	2,3
17	Fe5709	5698.375-5722.125	5674.625-5698.375 5724.625-5738.375	Å	Fe I, Ni I, Mg I Cr I, V I	0.18	2
18	Fe5782	5778.375-5798.375	5767.125-5777.125 5799.625-5813.375	Å	Fe I, Cr I Cu I, Mg I	0.20	2
19	Na D	5878.625-5911.125	5862.375-5877.375 5923.875-5949.875	Å	Na I	0.24	
20	TiO_1	5938.375-5995.875	5818.375-5850.875 6040.375-6105.375	mag	TiO	0.007	
21	TiO_2	6191.375-6273.875	6068.375-6143.375 6374.375-6416.875	mag	TiO	0.006	

FWHM = 8.5Å

Worthey et al. (1994)

+ Trager et al. (1998)

Indici Blu-Vis

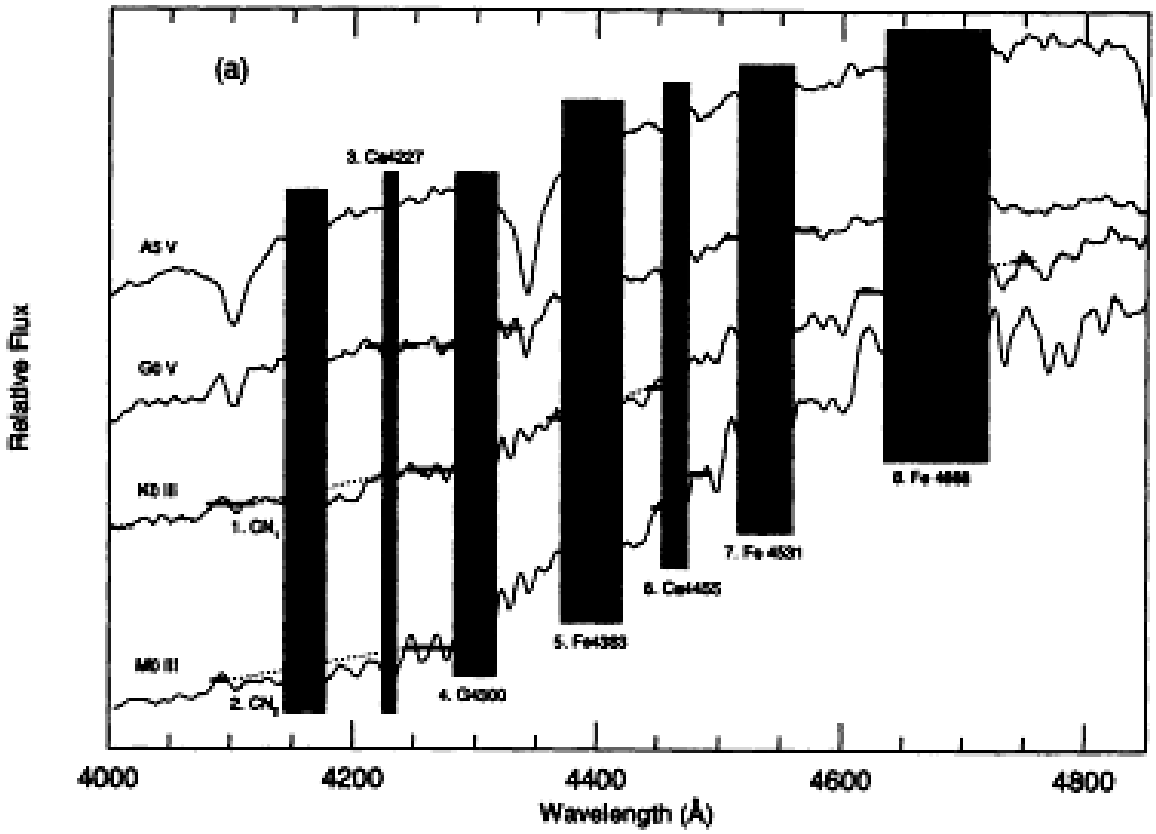

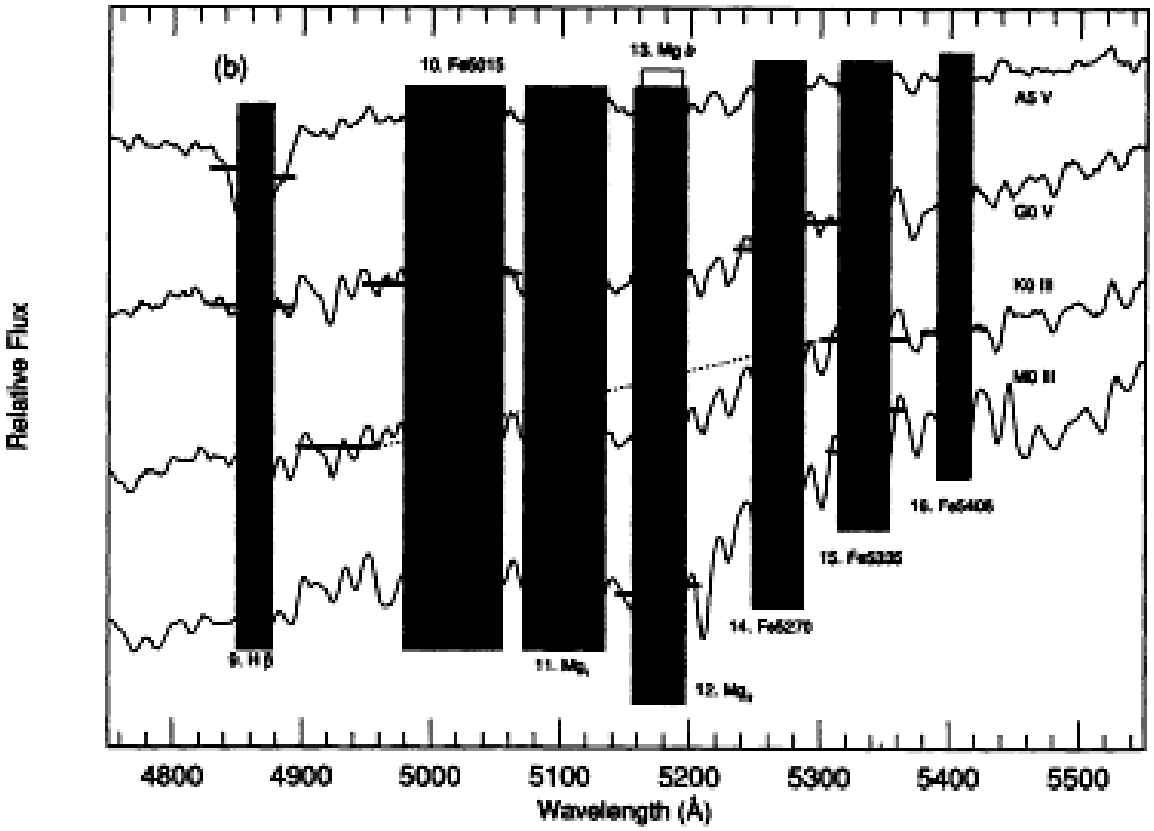

Indici Rossi

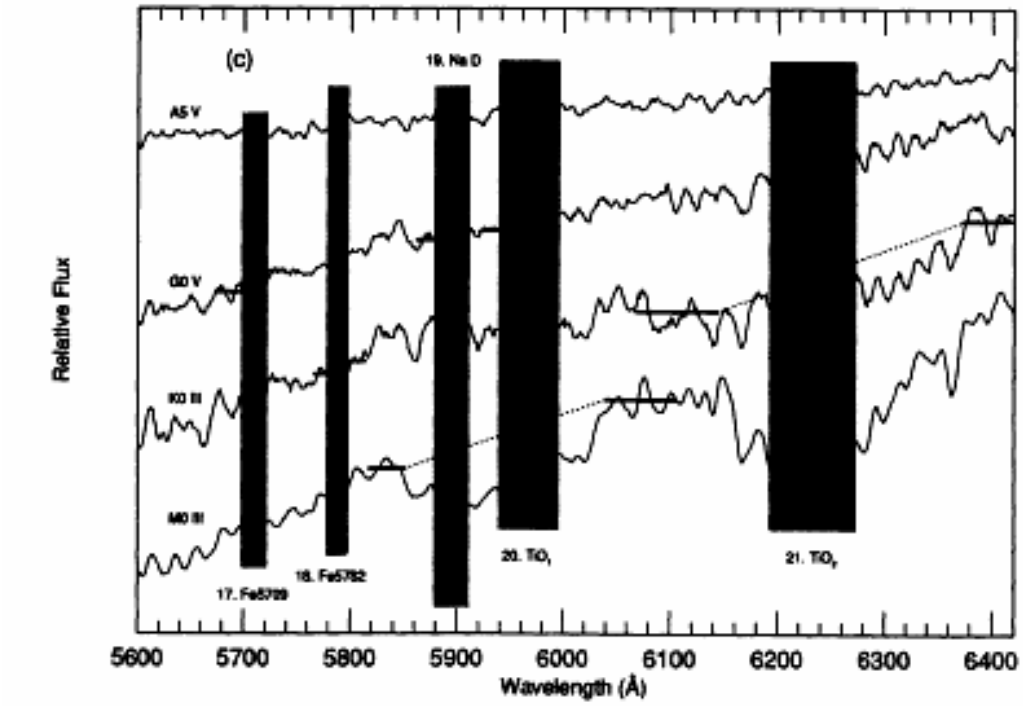

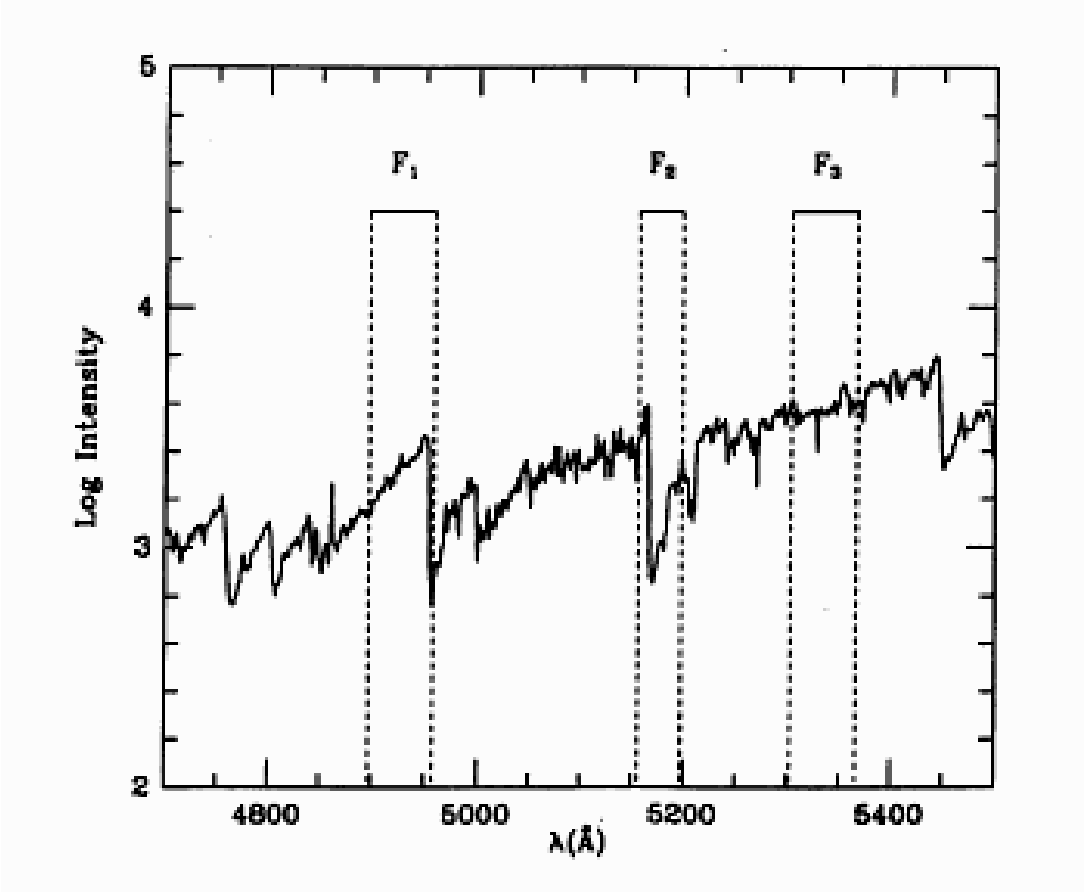

Forza di indice e Ampiezza equivalente

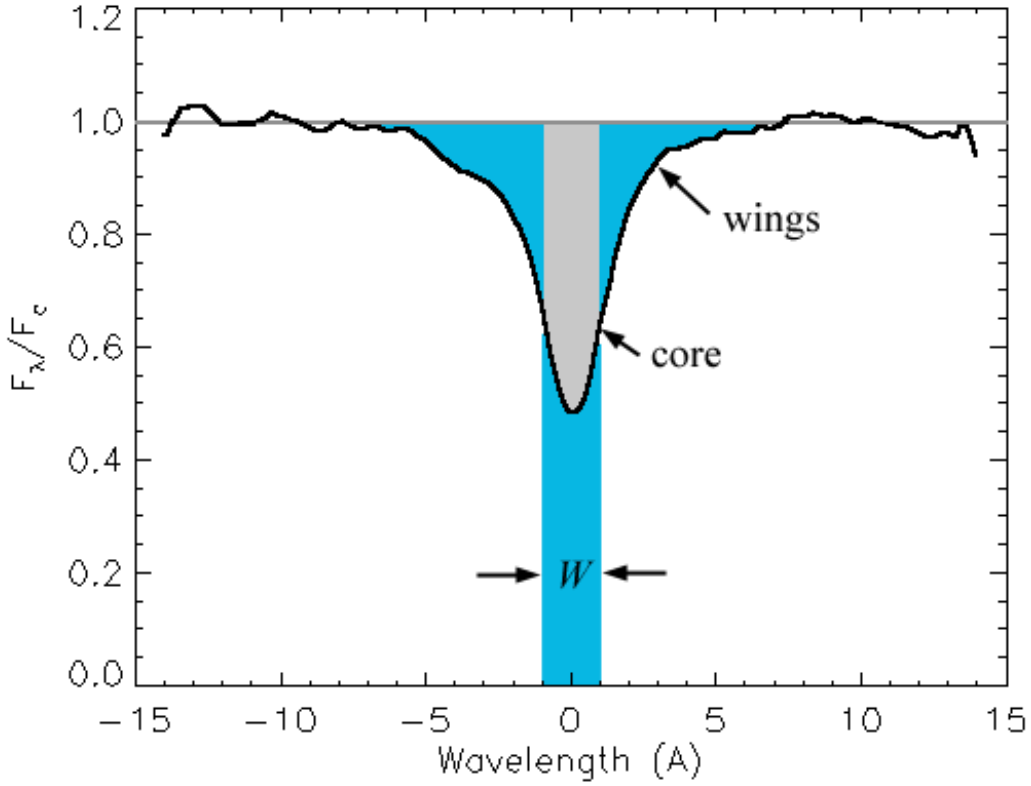

$$EW = \int \frac{f_c - f_f}{f_c} d\lambda$$

a T_{eff} fissato!!

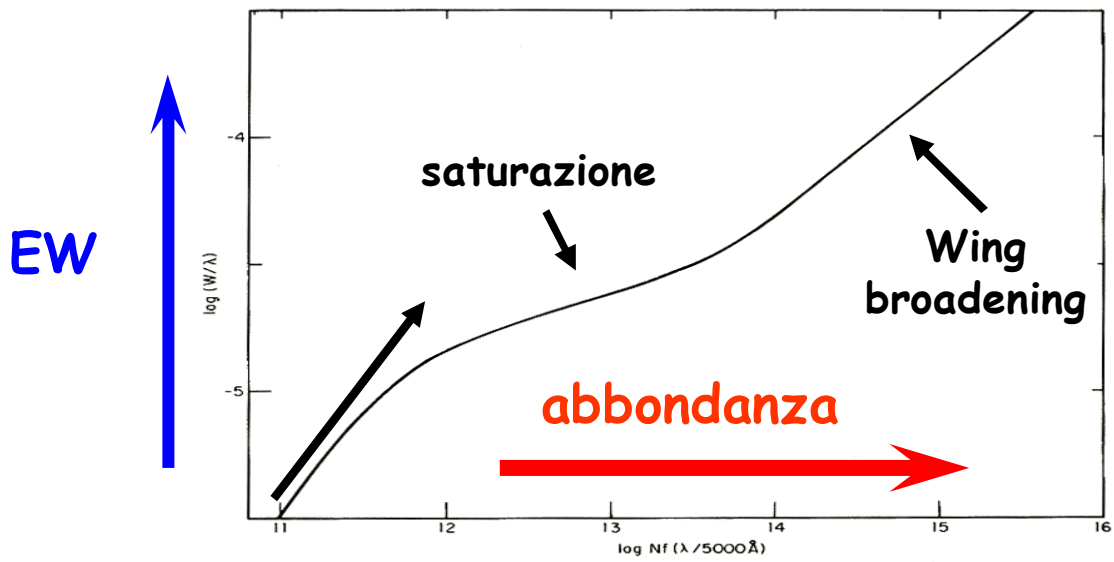

Indici in EW e in magnitudini

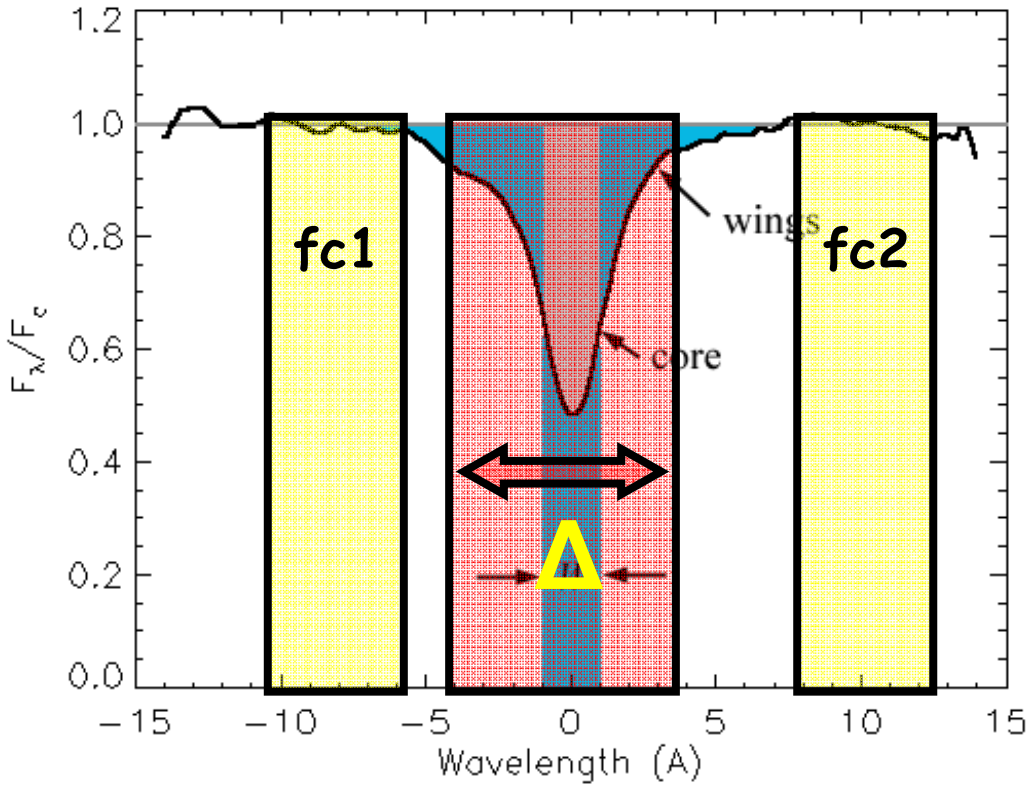

Tipicamente,

- se la riga e' atomica, l'indice si misura in EW
- se la banda e' molecolare si misura in mag

$$I_A = \Delta \frac{(f_c - f_f)}{f_c}$$

$$I_{mag} = -2.5 \log \left[1 - \left(\frac{I_A}{\Delta} \right) \right]$$

$$I_{mag} = -2.5 \log \left(\frac{f_f}{f_c} \right)$$

$$I_A = \Delta \left[1 - 10^{-0.4 I_{mag}} \right]$$

Indici e analisi "tomografica" delle pop stellari

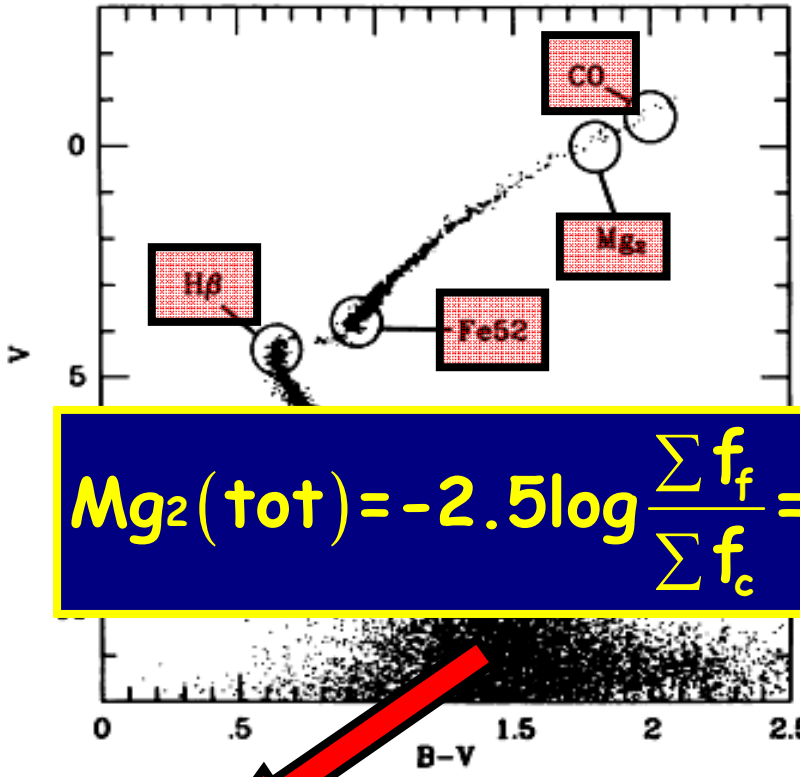

$$Mg_2(tot) = -2.5 \log \frac{\sum f_f}{\sum f_c} =$$

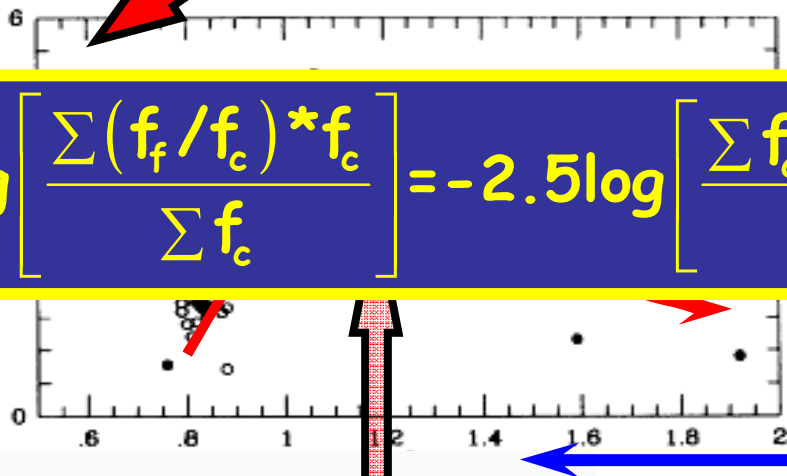

$$I_{tot} = -2.5 \log \left[\frac{\sum (f_f / f_c) * f_c}{\sum f_c} \right] = -2.5 \log \left[\frac{\sum f_c 10^{-0.4I}}{\sum f_c} \right]$$

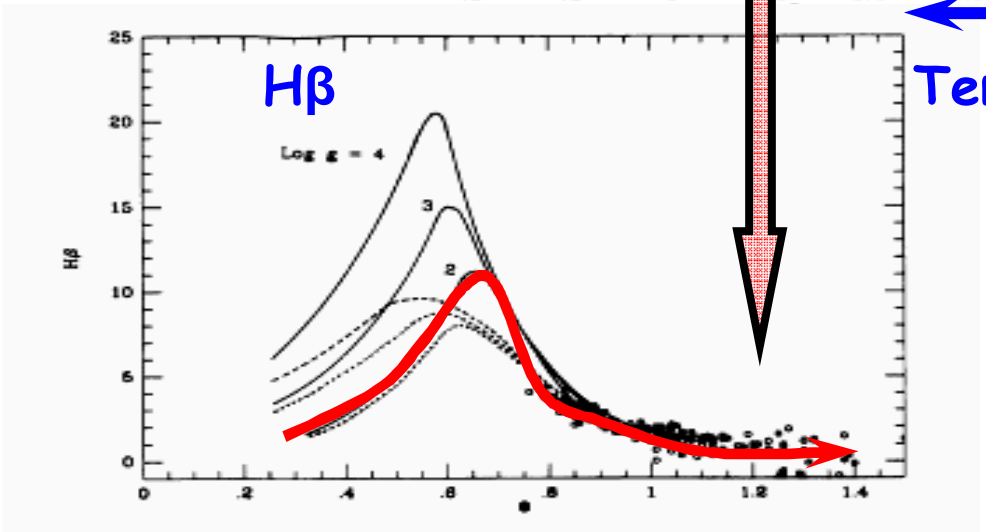

Temperatura

Narrow-band indices & SSP tomography

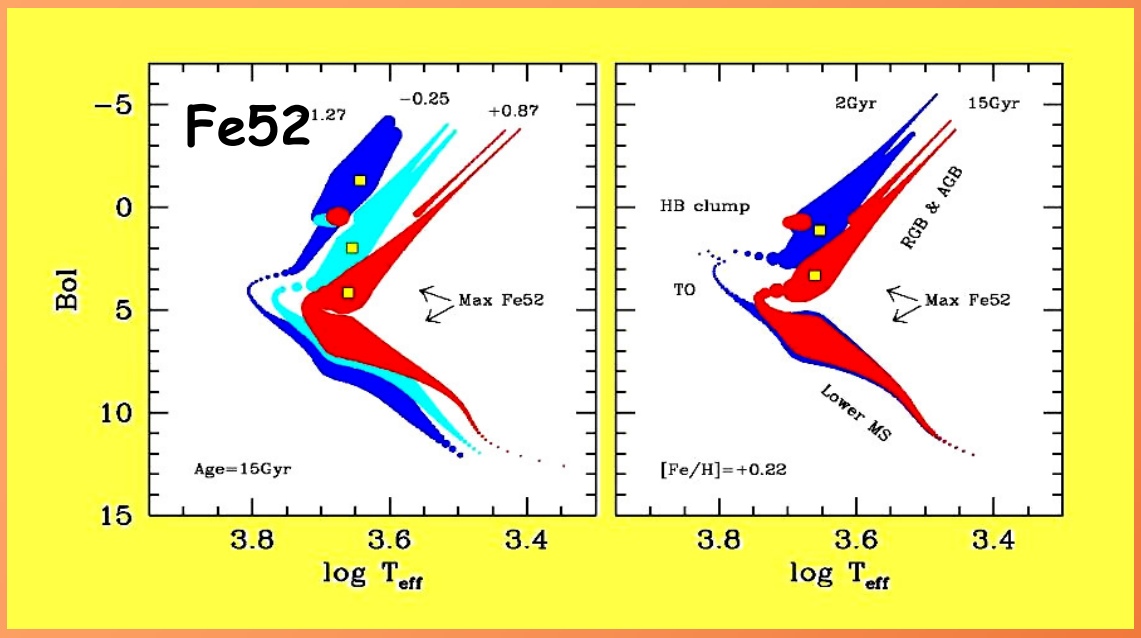

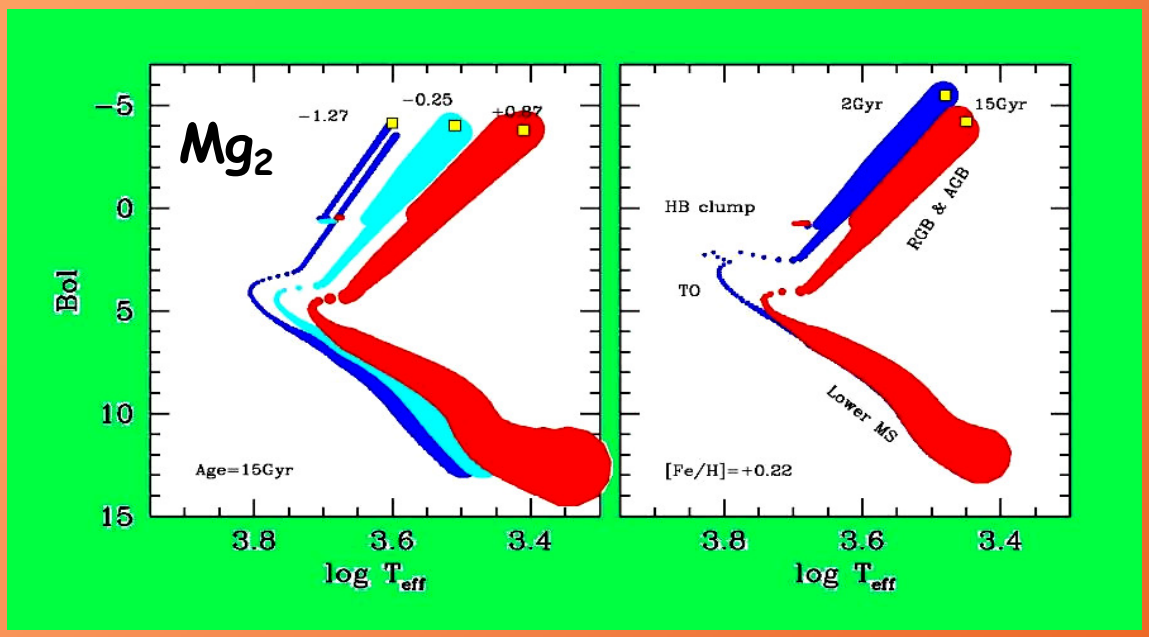

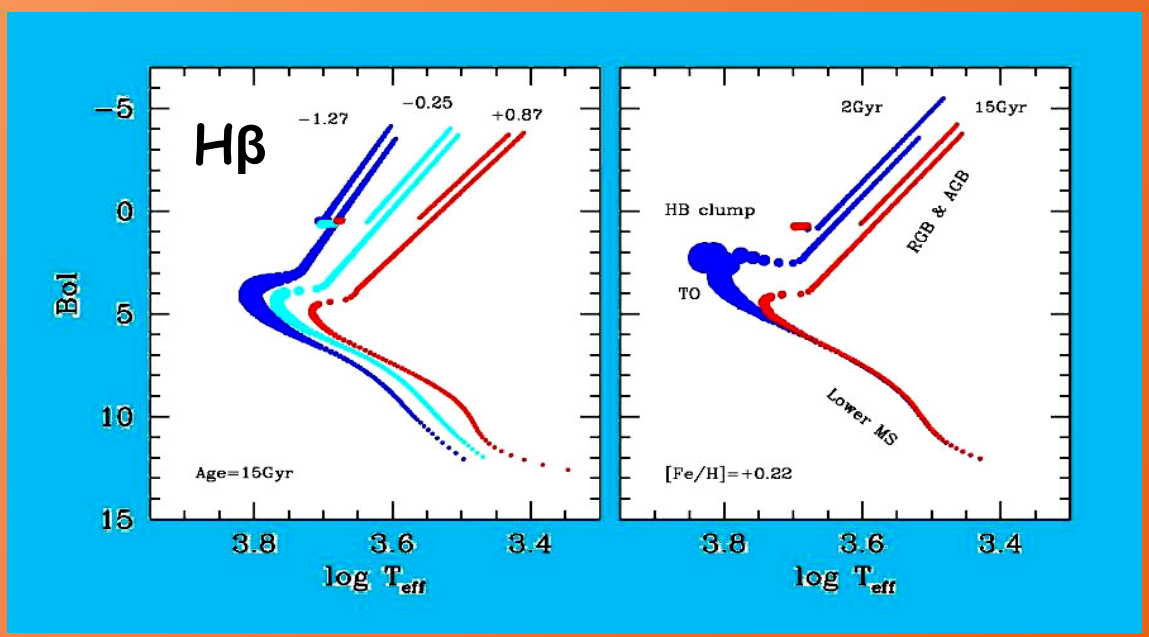

Gradienti radiali nelle ellittiche

NGC 4472

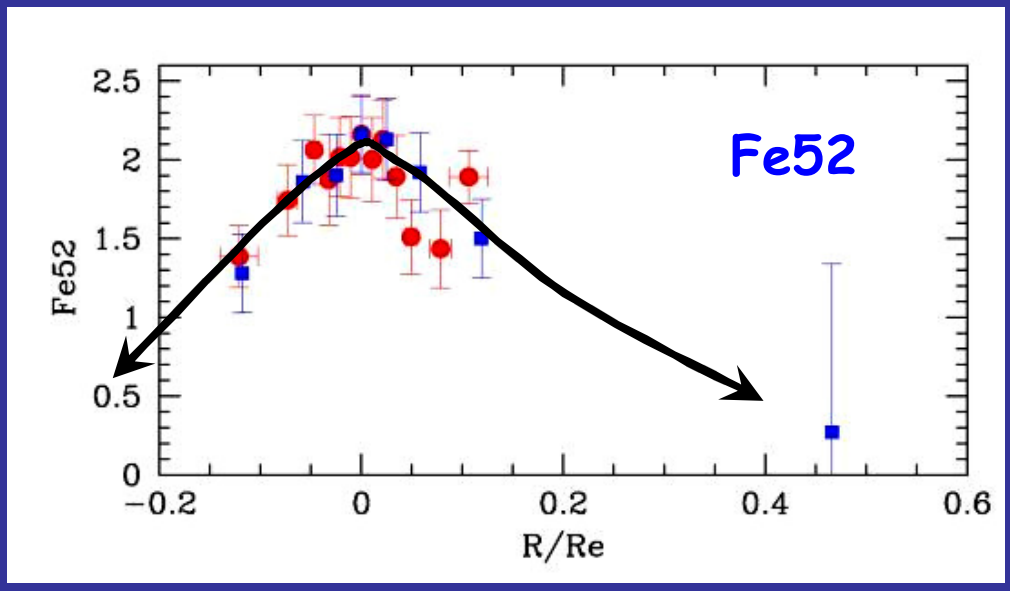

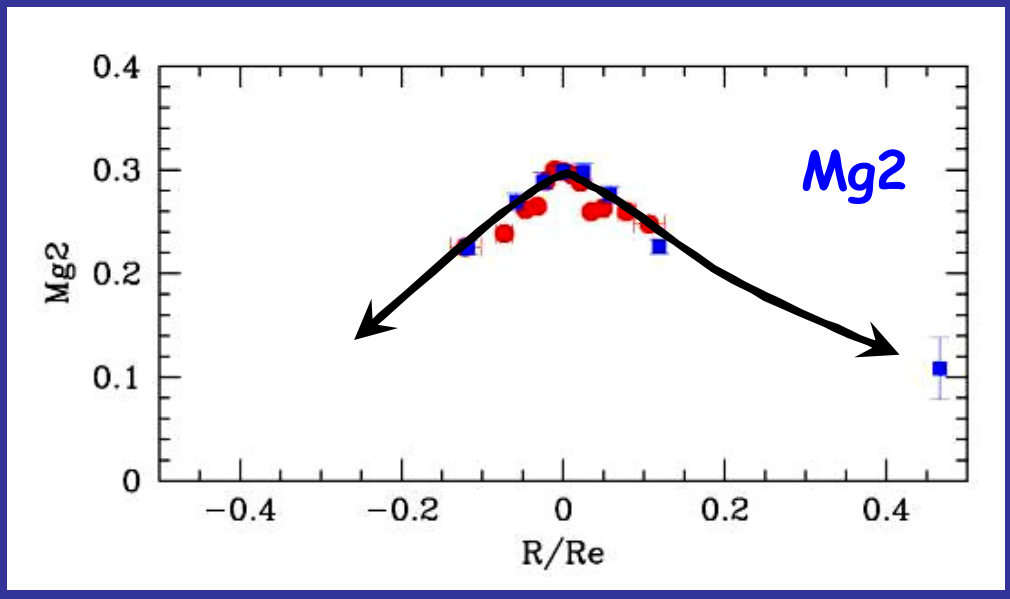

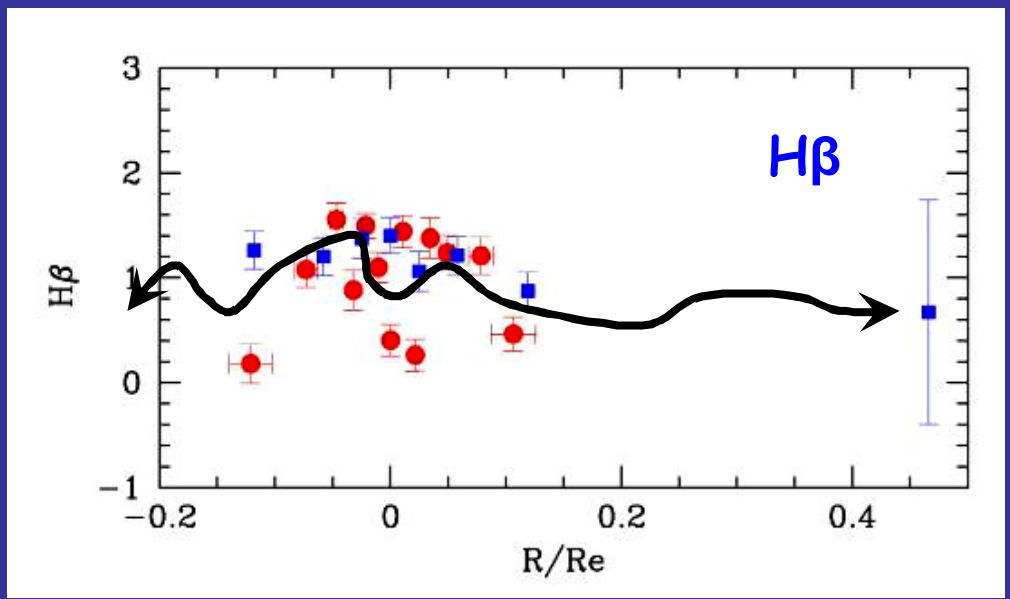

Fe vs. Mg_2 = **RGB temperature location**

Within { Fe ↓ , Mg_2 ↓ }

Among { Fe ↔ , Mg_2 ↓ }

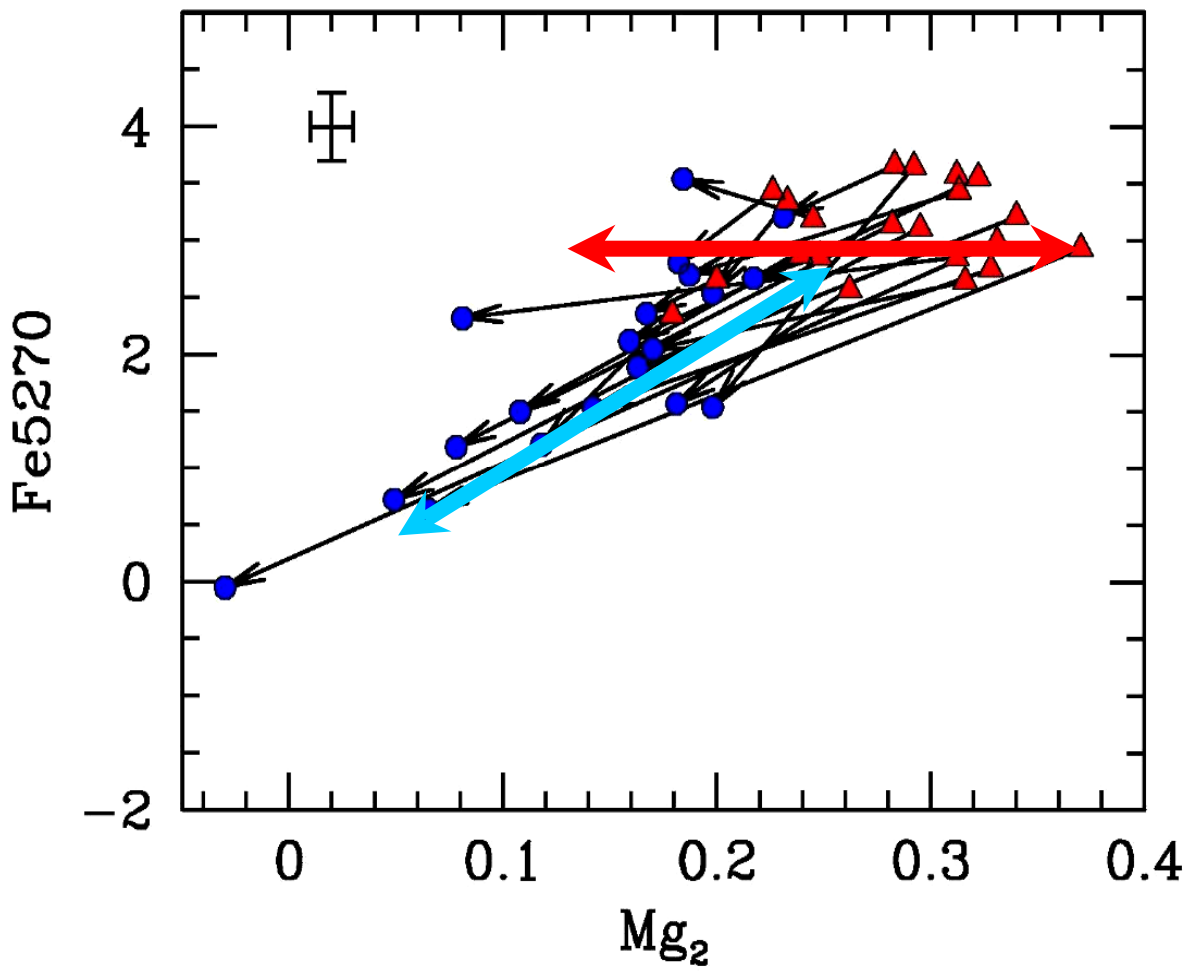

Hβ vs. Mg_2 = Turn Off vs. RGB

Within { Hβ, Mg_2 } ↔ ↓

Among { Hβ, Mg_2 } ↑ ↓

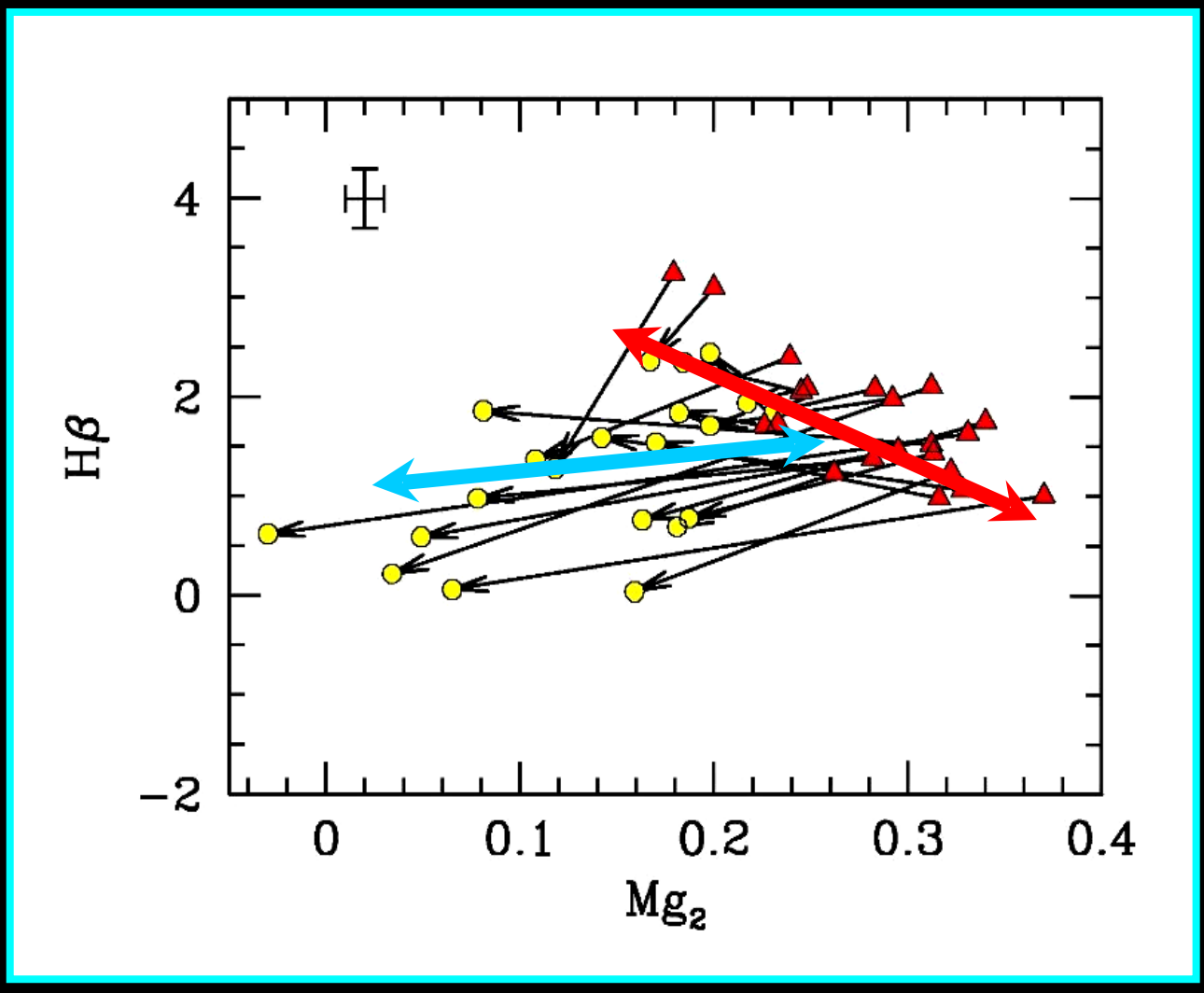

Spettri & masse delle galassie

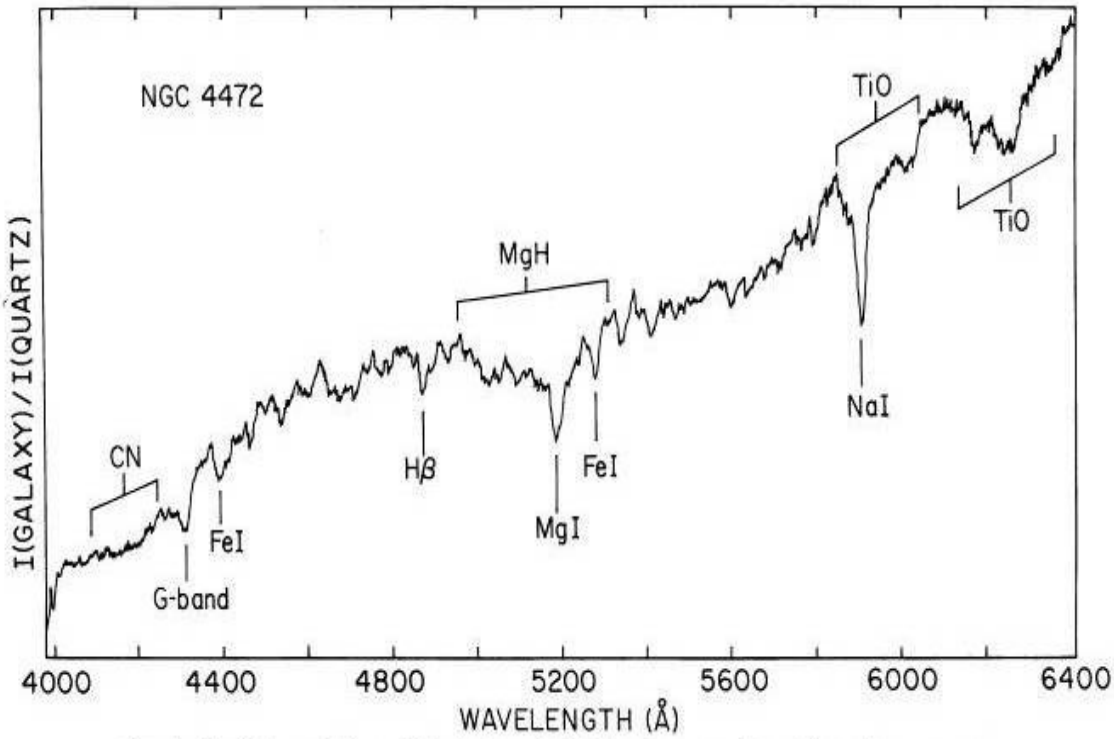

FIG. 1.—Typical scan of giant elliptical galaxy, divided by the tungsten lamp (denoted by "quartz")

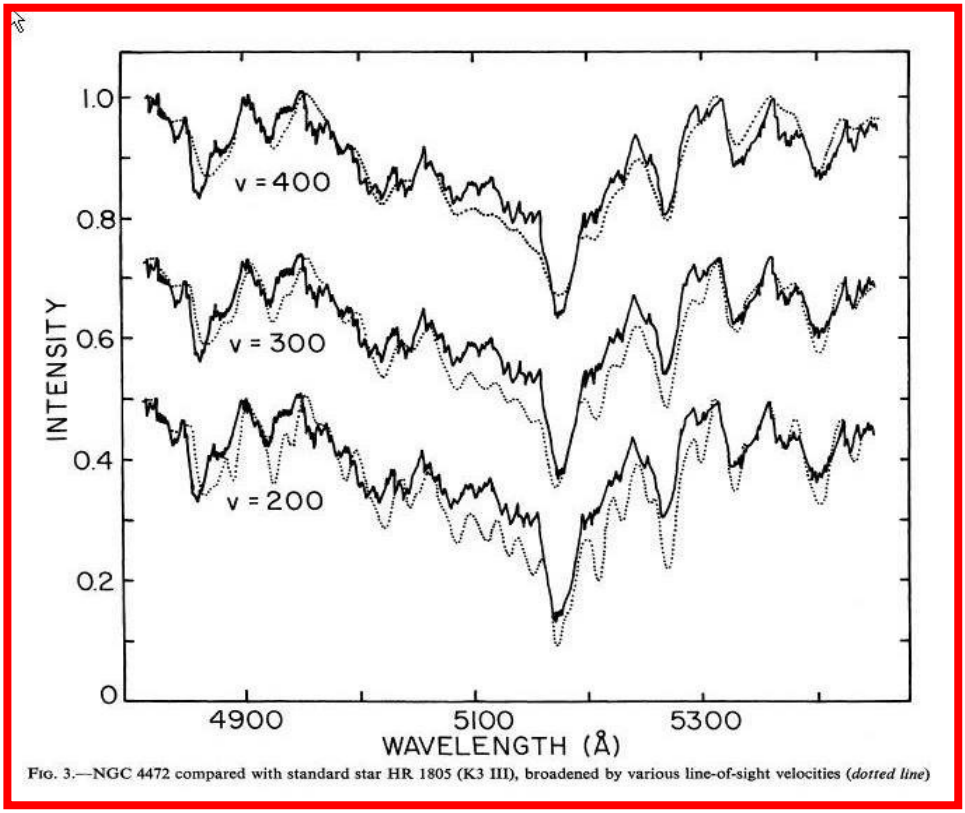

FIG. 3.—NGC 4472 compared with standard star HR 1805 (K3 III), broadened by various line-of-sight velocities (*dotted line*)

La legge di Faber-Jackson (1976)

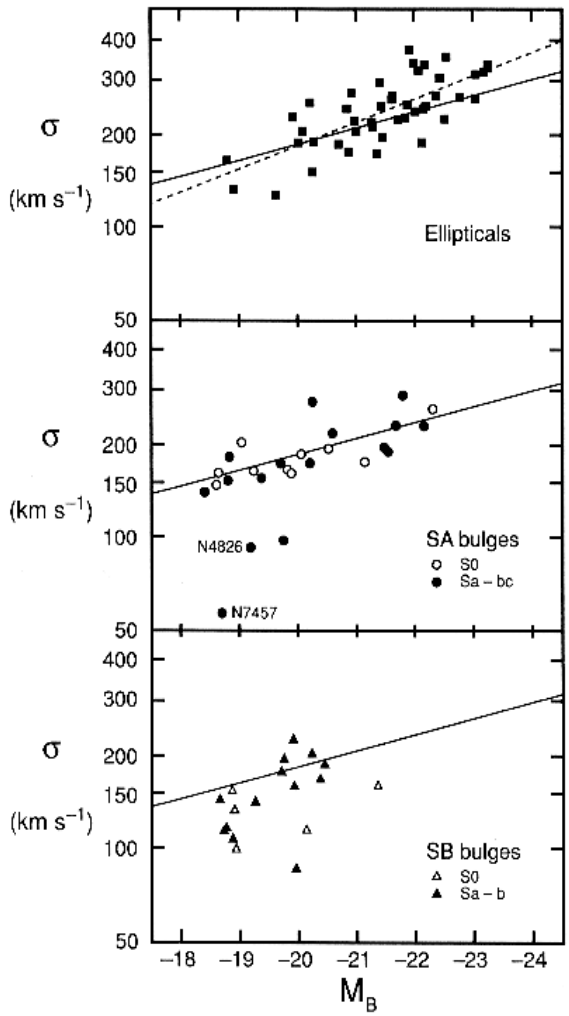

Fig. 6. Correlation between central velocity dispersion σ and absolute magnitude M_B for elliptical galaxies and for bulges of unbarred (SA) and barred (SB) disk galaxies. The solid line is a fit to the galaxies in the middle panel; the dashed line is a fit to the ellipticals. Except for the NGC 4826 point, this figure is from Kormendy and Illingworth (1983).

$$\begin{cases} v^2 \approx \dfrac{GM}{R} \\ \mu = \dfrac{L}{\pi R^2} \approx \text{const} \\ \left(\dfrac{M}{L}\right) = \text{const} \end{cases}$$

Se il moto e' caotico, allora $v^2 \equiv \sigma^2$

$$\sigma^4 \propto \mu L$$

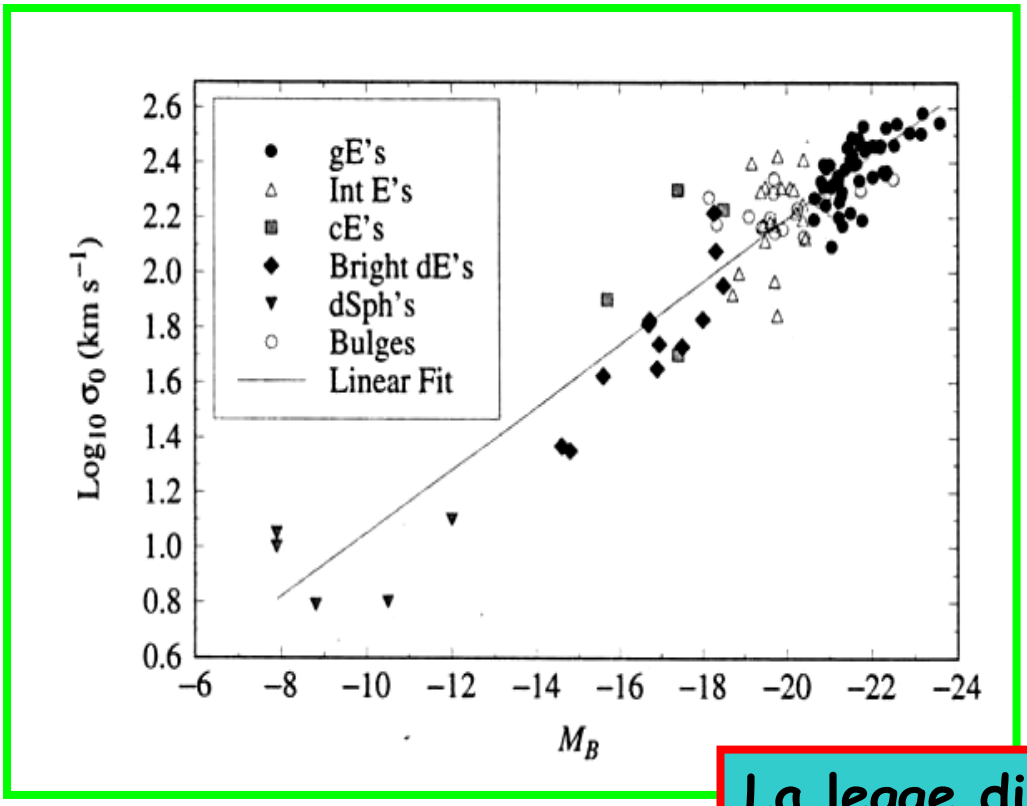

La legge di F&J vale in differenti contesti galattici

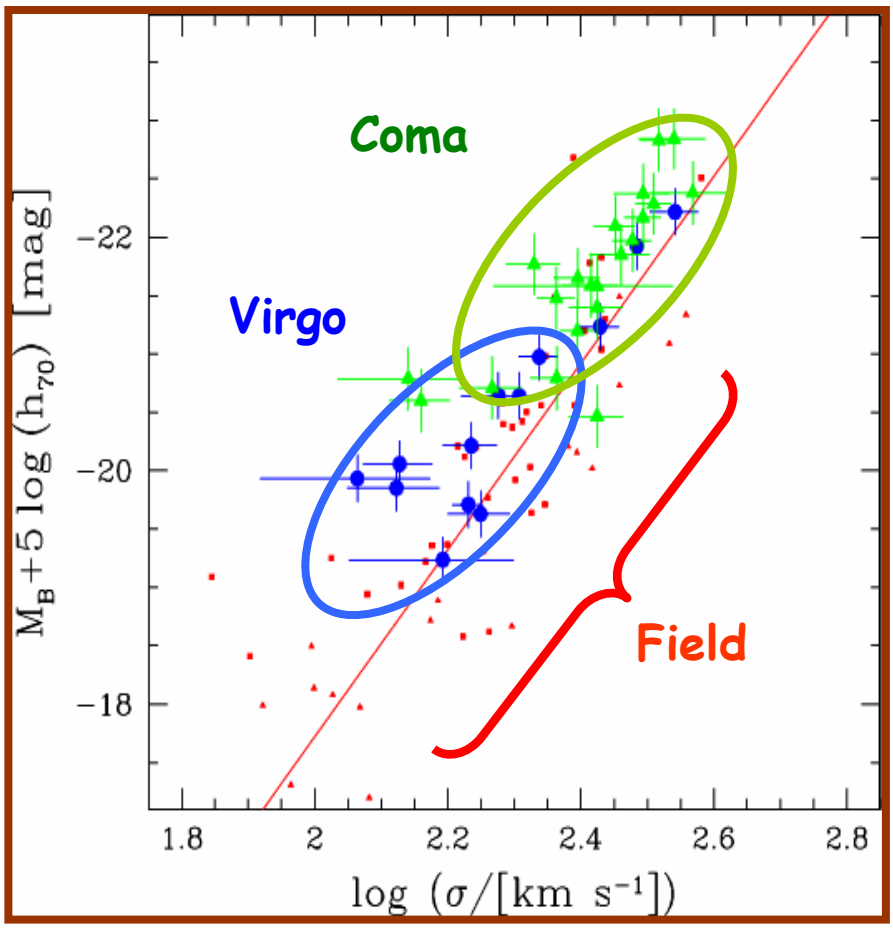

Spettri & Massa delle Spirali

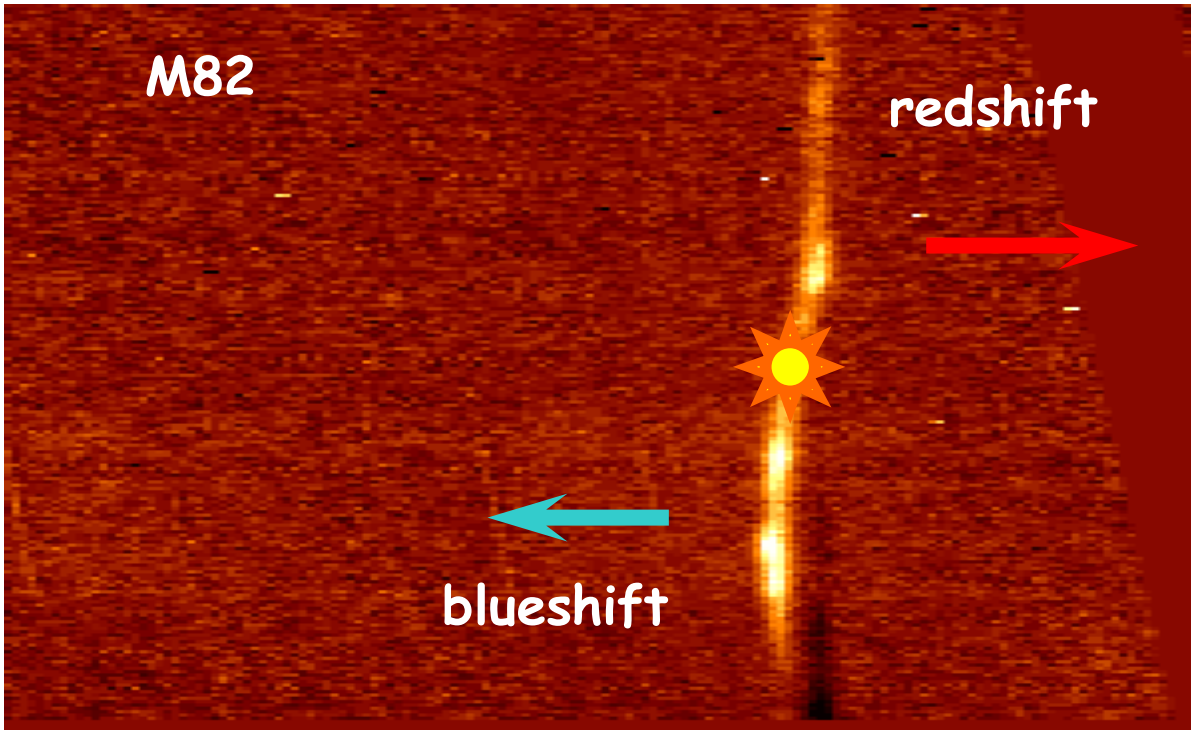

@SUBARU (Japan)

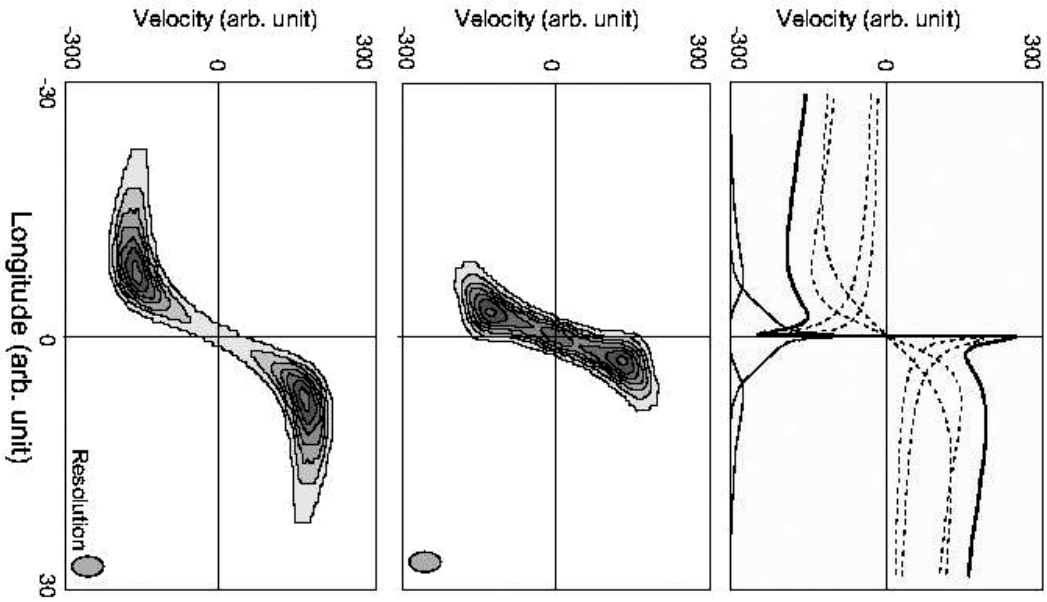

La massa "oscura"

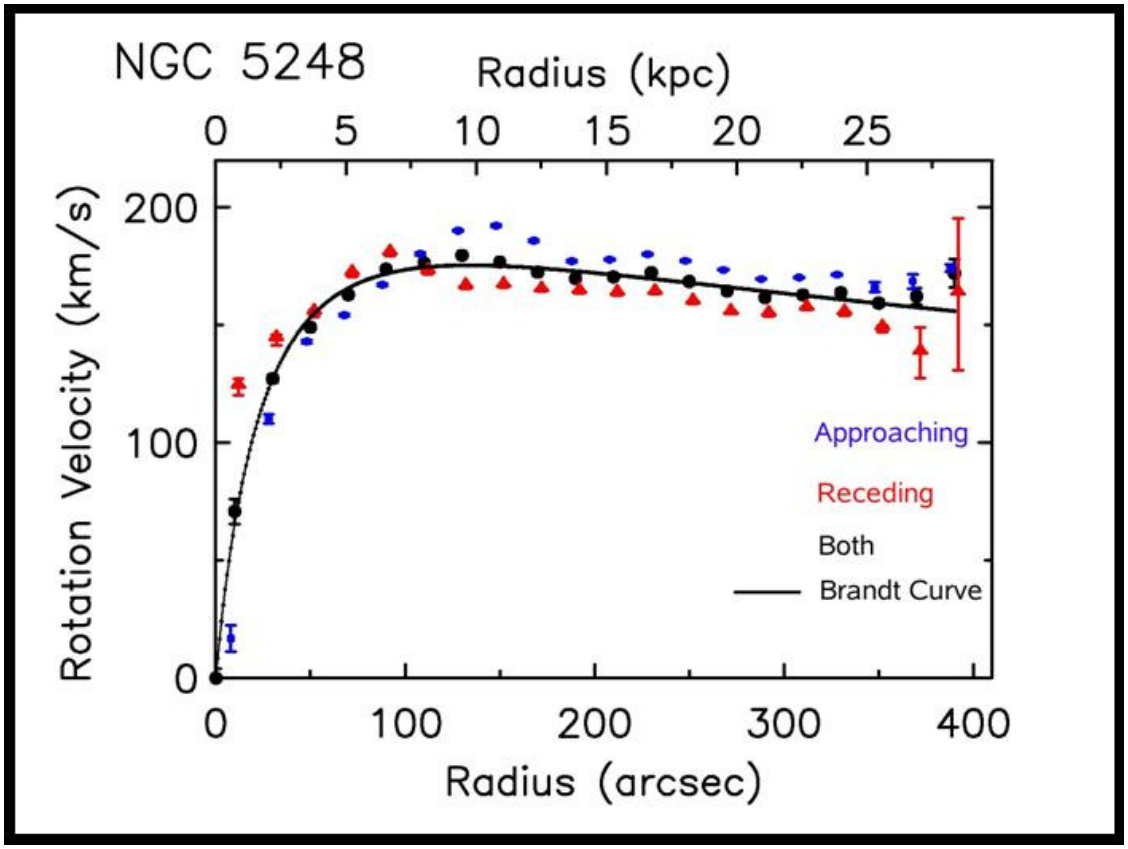

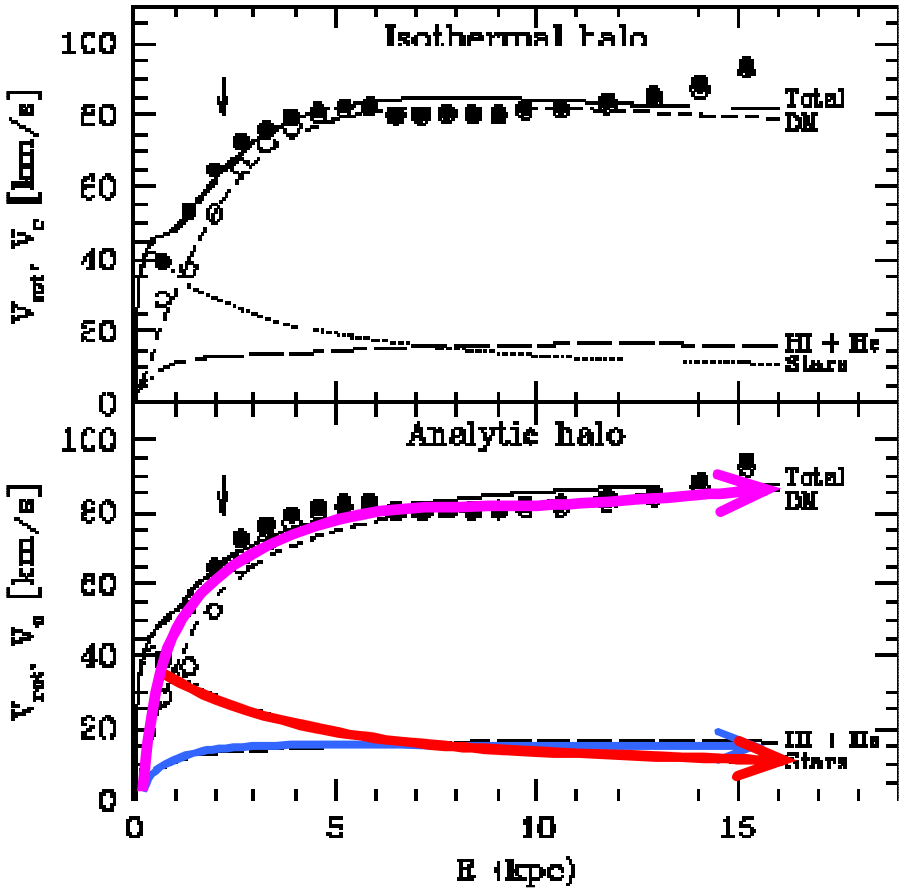

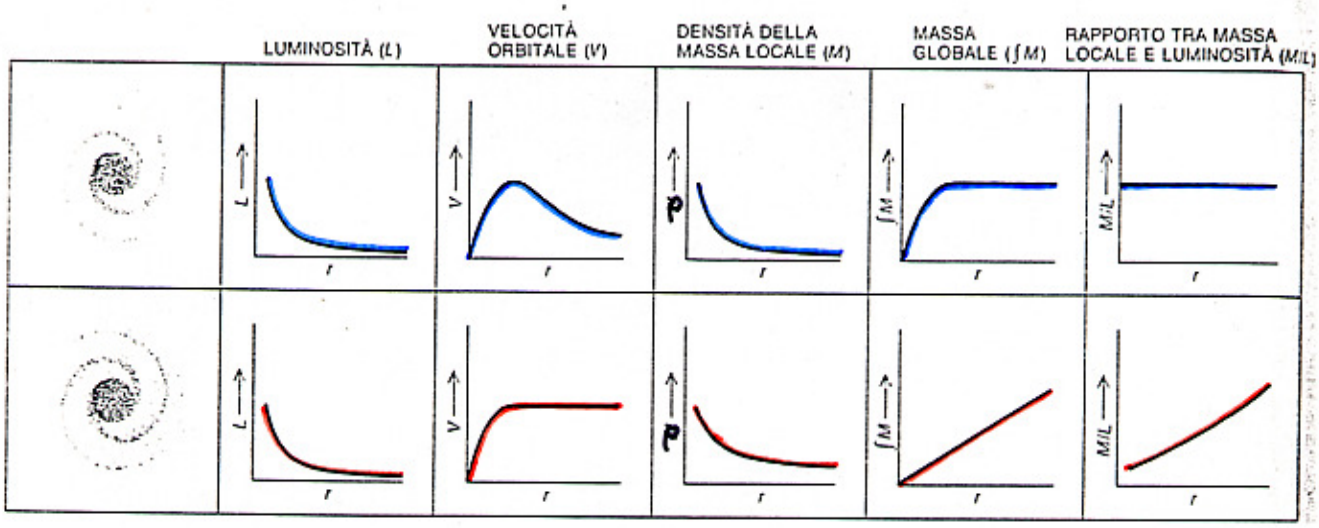

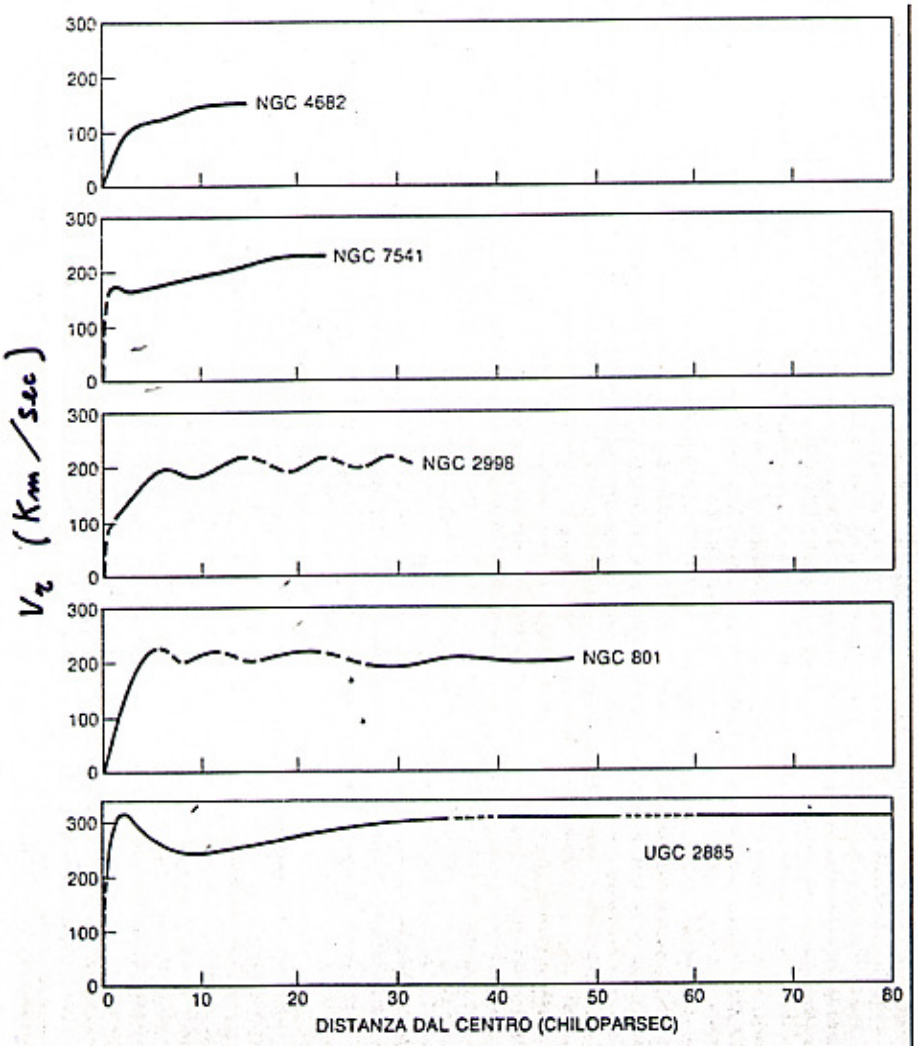

Queste curve di rotazione indicano la variazione delle velocità orbitali al crescere della distanza dal centro in nove galassie Sc di luminosità crescente dall'alto verso il basso. Via via che la luminosità aumenta, le galassie diventano sempre più grandi e così pure le velocità orbitali, mentre i gradienti di velocità in prossimità del centro galattico si fanno progressivamente più rapidi.

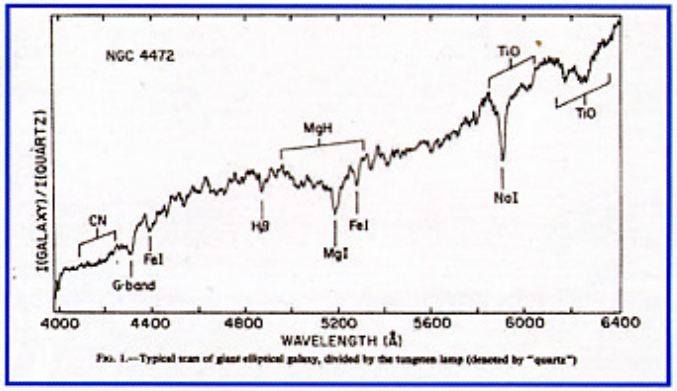

FIG. 1.—Typical scan of giant elliptical galaxy, divided by the tungsten lamp (denoted by "quartz")

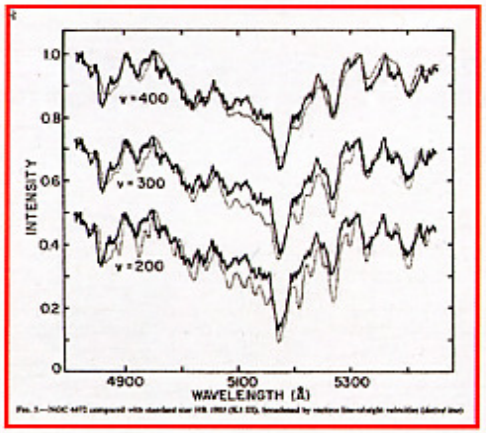

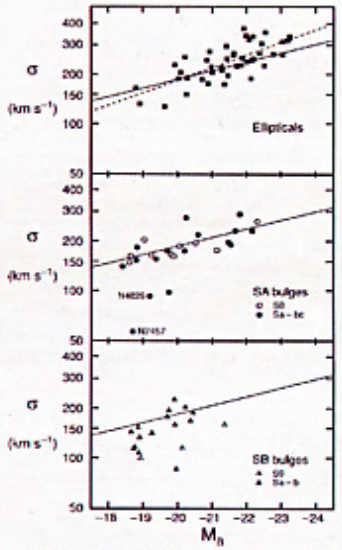

Fig. 6. Correlation between central velocity dispersion σ and absolute magnitude M_B for elliptical galaxies and for bulges of unbarred (SA) and barred (SB) disk galaxies. The solid line is a fit to the galaxies in the middle panel; the dashed line is a fit to the ellipticals. Except for the NGC 4826 point, this figure is from Kormendy and Illingworth (1983).

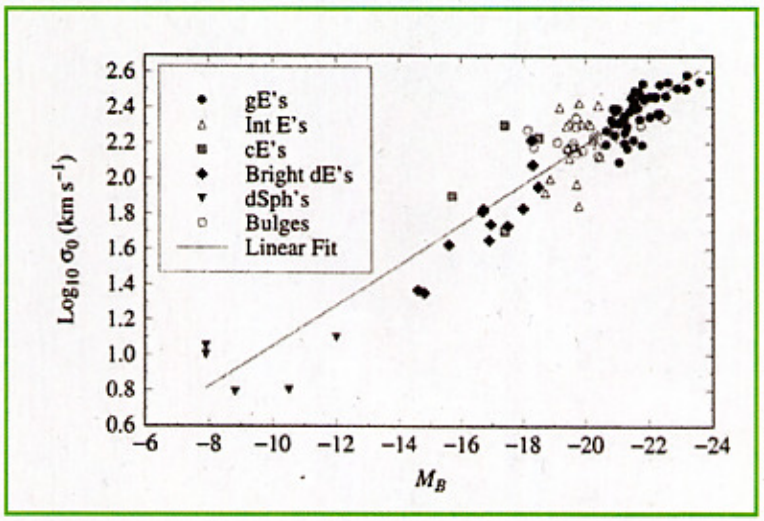

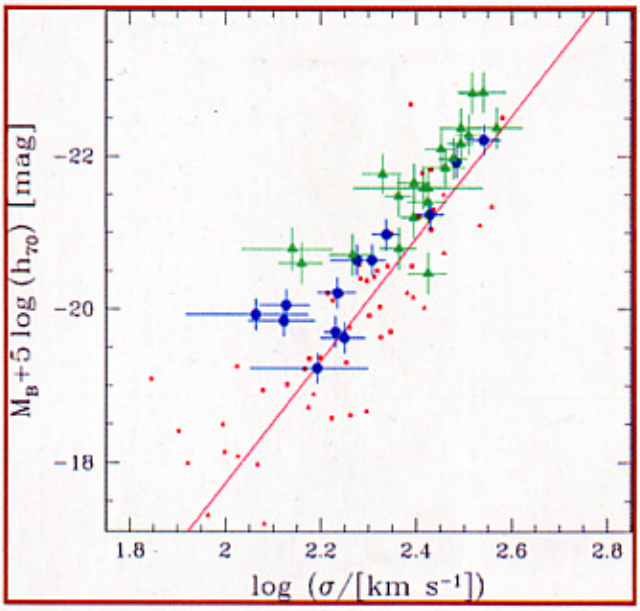

- LOCAL GALX (+ VIRGO ▲ + COMA ■)
- ▲ CLUSTERS
- ■ FIELD

THEORY OF CSPs

Definition:

$$[CSP] = \int [SSP] \otimes SFR$$

A relevant case: SFR = const

$$\mathcal{L}_{CSP} = \int_0^T L_{SSP}\, dt$$

$L_{SSP} \downarrow t^{-\alpha}$ $\quad (\alpha < 1)$

$$\mathcal{L}_{CSP}\Big|_T = \frac{T^{1-\alpha}}{1-\alpha}$$

$$\mathcal{L}_{CSP} \propto t^{0.15}$$

Conclusion: Total luminosity in a CSP is an INCREASING function of time

Color evolution:

SSP	CSP
$L_B \propto t^{-\alpha_B}$	$\mathcal{L}_B \propto t^{1-\alpha_B}$
$L_V \propto t^{-\alpha_V}$	$\mathcal{L}_V \propto t^{1-\alpha_V}$

SAME LAW!

$$\frac{L_B}{L_V} \propto t^{-(\alpha_B - \alpha_V)}$$

LUMINOSITY EVOLUTION

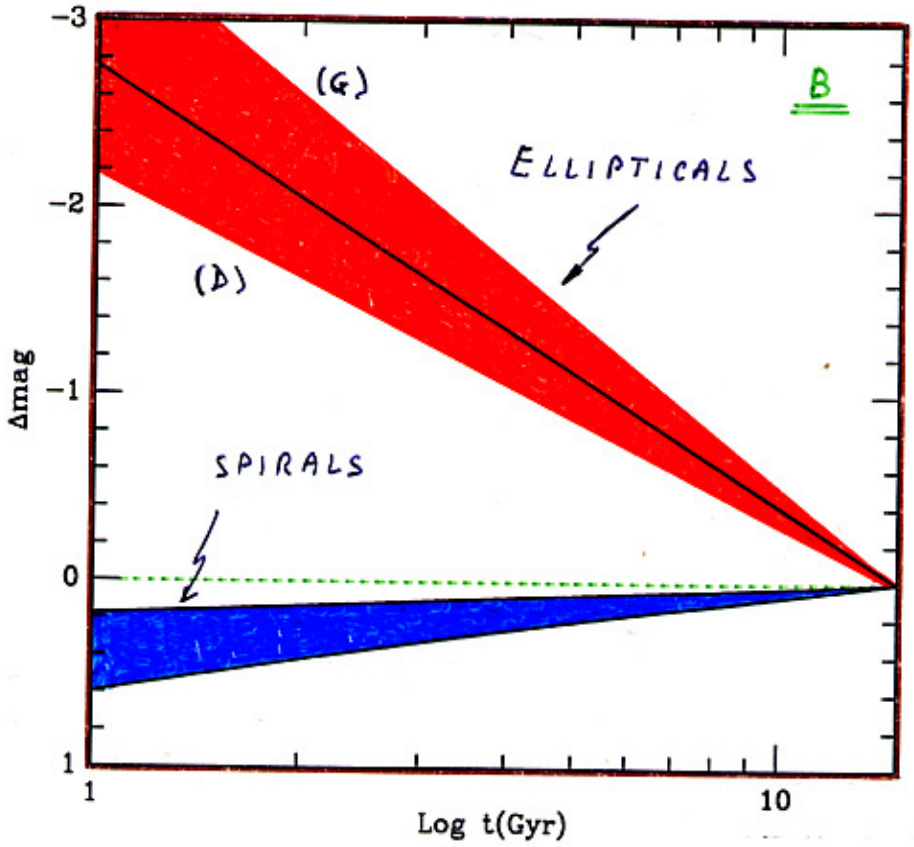

Ellipticals $L_t \propto t^{-\alpha} \sim t^{-0.8}$

Spirals (disk) $L_t \propto t^{1-\alpha} \sim t^{+0.2}$

$M_{UB} \in [5, \infty]$

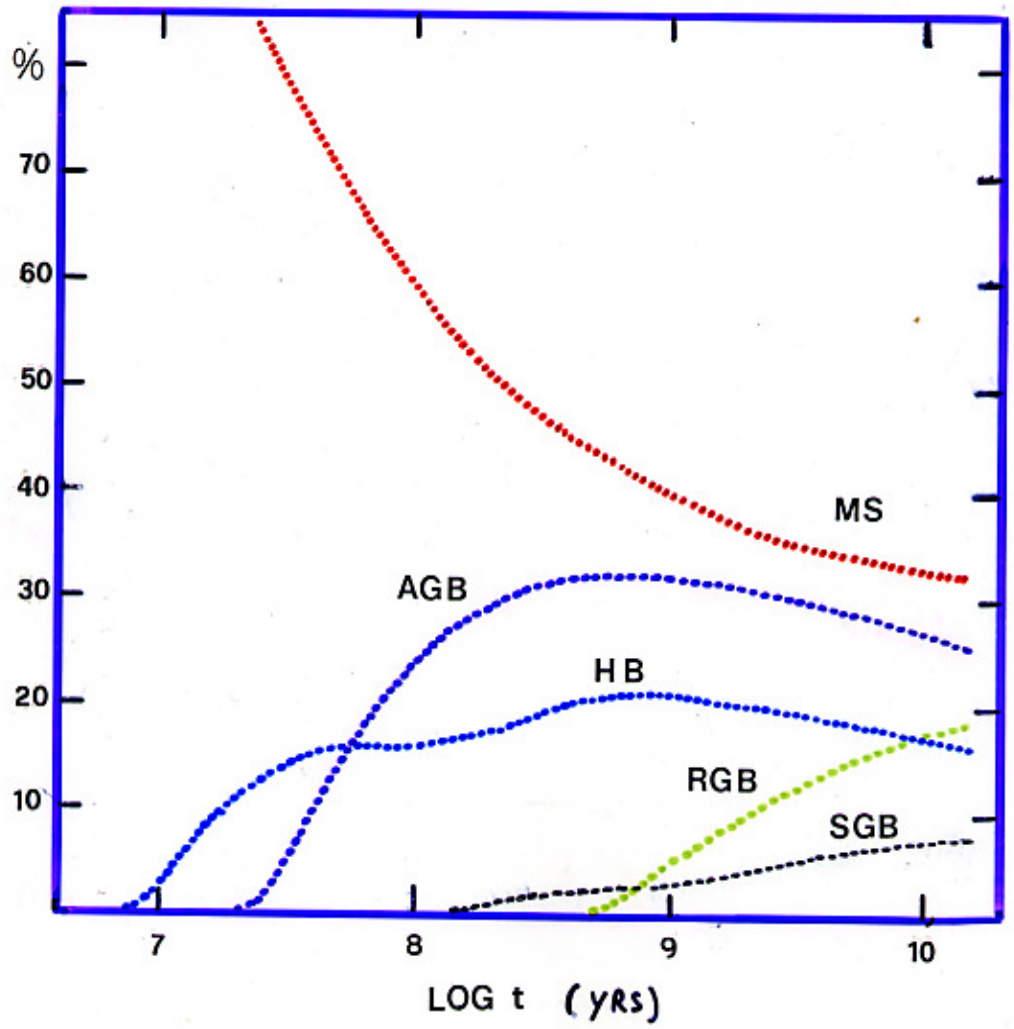
%
70
60
50
40
30
20
10
MS
AGB
HB
RGB
SGB
7
8
9
10
LOG t (yRs)

STAR FORMATION RATE

$$SFR = -\frac{d f_{gas}}{d t}$$

$$PDMF_{(M,t)} = \int_0^{\tau \leq T} SFR \times IMF_{(M)}\, dt$$

$\Downarrow$

OBSERVED $\quad 0 \leq \tau \leq T$

ASSUMED $\quad SFR \propto f_{gas}^{n} \quad n = 2 \quad$ SCHMIDT LAW

$n = 1 \quad SFR = k f = -\dot{f} \quad SFR = k e^{-kt}$

$n = 2 \quad SFR = k f^2 = -\dot{f} \quad SFR = \frac{k}{(1-kt)^2}$

$k = \frac{1}{\tau}$ (star formation timescale)

$\lim k \to \infty \quad \tau \to 0 \Rightarrow$ SSP

$SFR \to \delta(0)$

ROBERTS & HAYNES (1994)

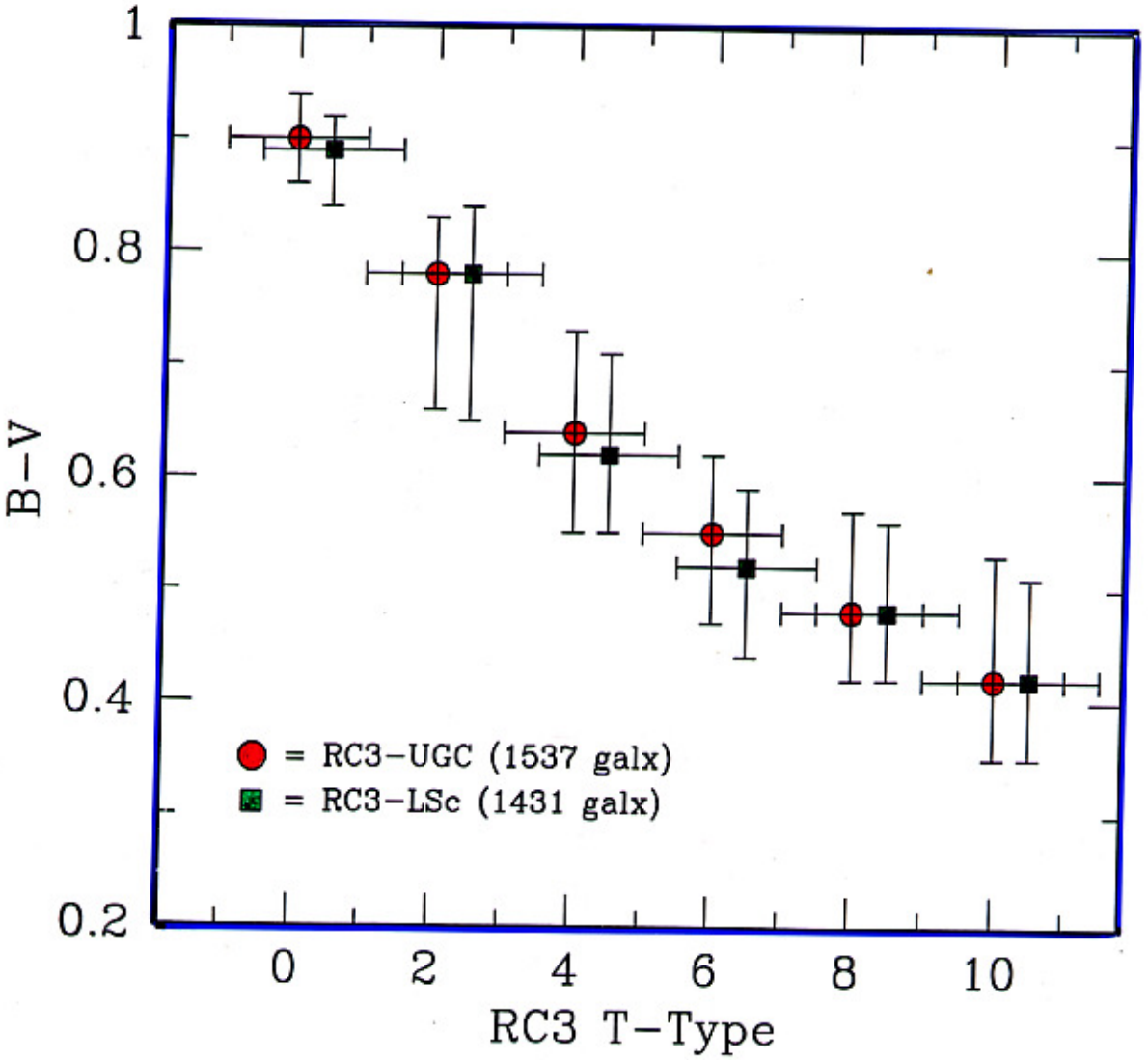

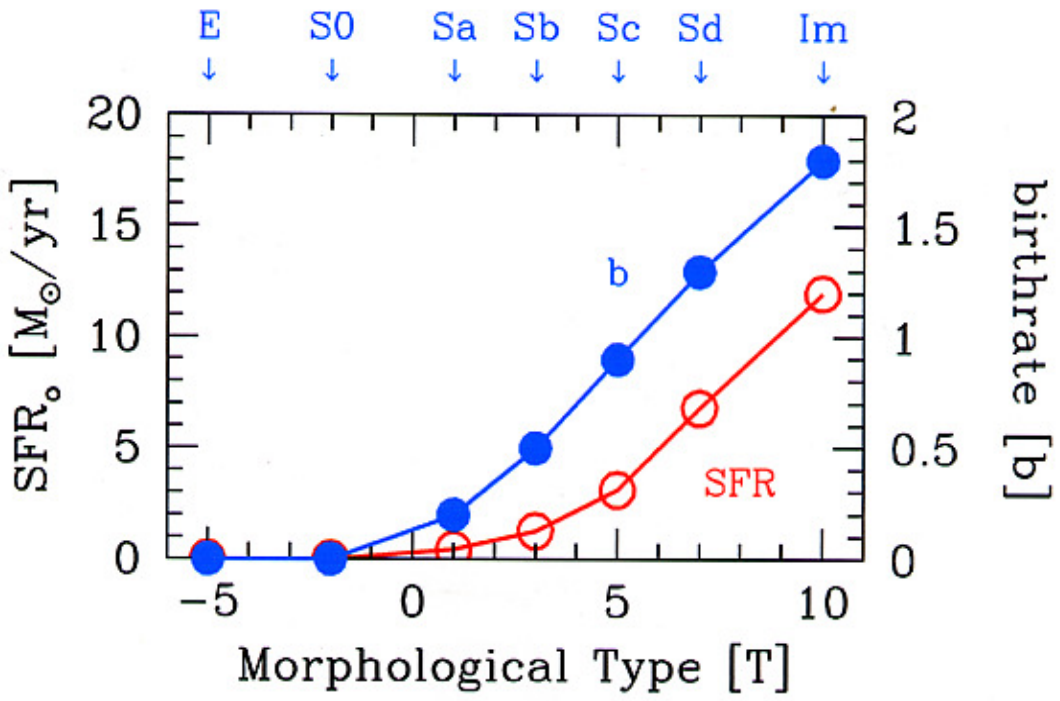

(Buzzoni 2002)

FREE-FALL TIME

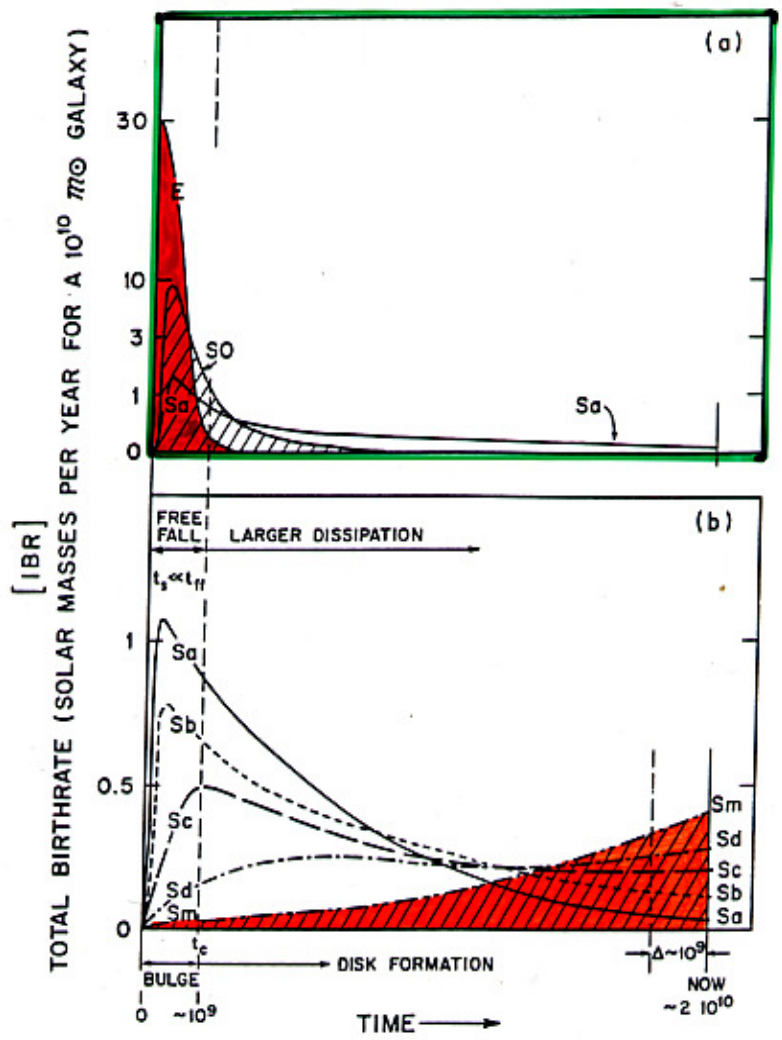

Fig. 10. Same as Fig. 9 with later Hubble types shown in the lower panel. The integral under the Sm curve is shaded for illustration. The curves are only schematic showing the trends that have been established by Gallagher et al. (1984)

SANDAGE (1986)

METAL ABUNDANCE

$$X + Y + Z = 1$$

HYDROGEN HELIUM "OTHERS"

$$\left[\frac{Fe}{H}\right] = \log\frac{Fe}{Fe_\odot} - \log\frac{H}{H_\odot}$$

IF $Fe \propto Z$

$$\left[\frac{Fe}{H}\right] = \log\frac{Z}{0.017} - \log\frac{1-Z-Y}{0.71} \approx \lg Z + 1.8$$

$$(X, Y, Z)_\odot = (0.70, 0.28, 0.017)$$

$1\,gr\ H \rightarrow 1\,gr\ Z$ ENERGETICS

$6.6\ 10^{18}$ ergs

IN A GALAXY: $M_Z \sim 2\ 10^9\ M_\odot \sim 4\ 10^{42}\ gr$

$$M_Z = \frac{\int L \times t}{6.6\ 10^{18}} \sim \frac{\langle L\rangle\ 10^{10}\ yr}{6.6\ 10^{18}\ ergs}$$

$\langle L\rangle \sim 2.2\ 10^{10}\ L_\odot$ $\frac{M}{L} \leq 5$ in primordial galx

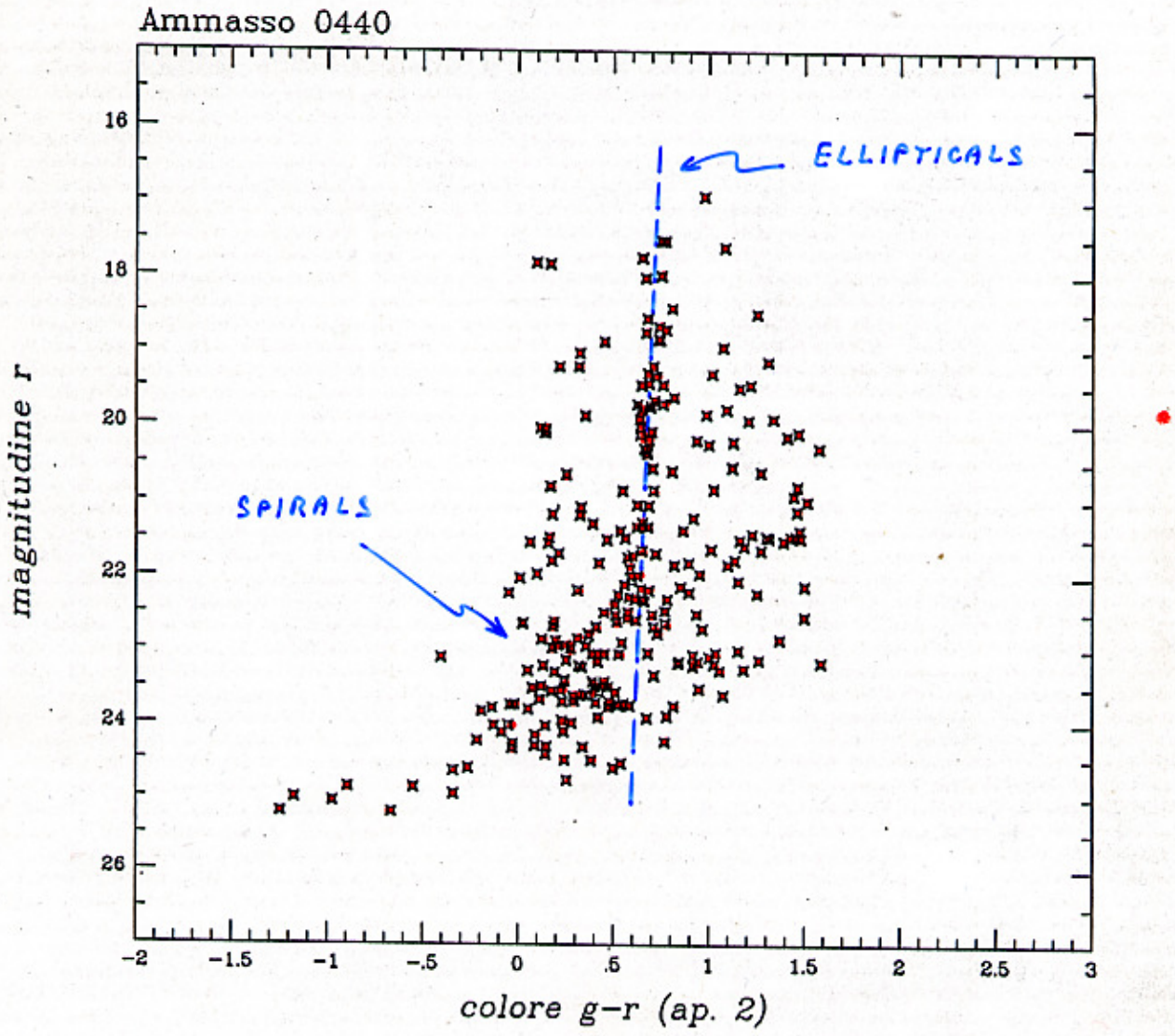

$$r = 61\,(g-z) + C_{(H_0;\,q_0,\,z)}$$

11/88 CB

PARDI & FERRINI (1994)

SFR

$[M_\odot/pc^2/yr]$

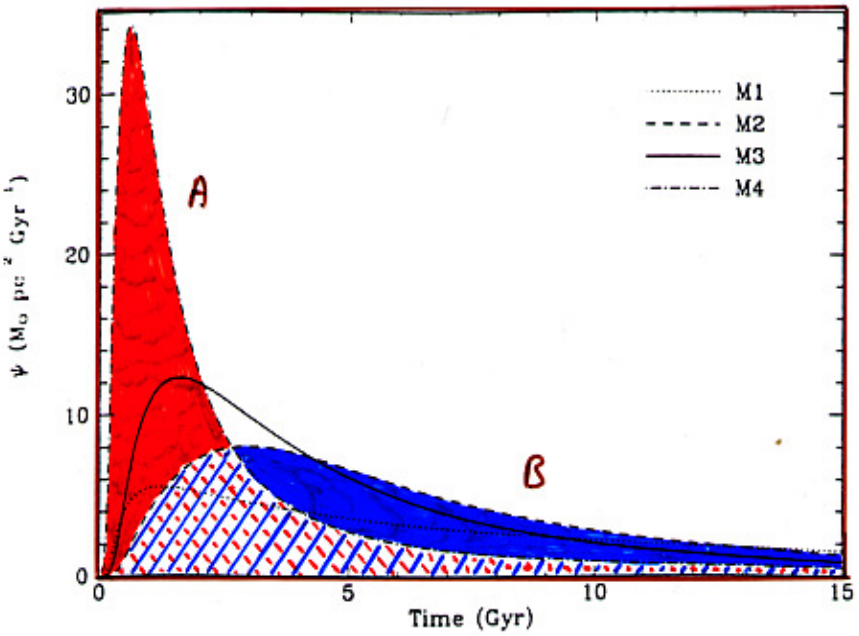

FIG. 3.—SF rate vs. time (M1–M4)

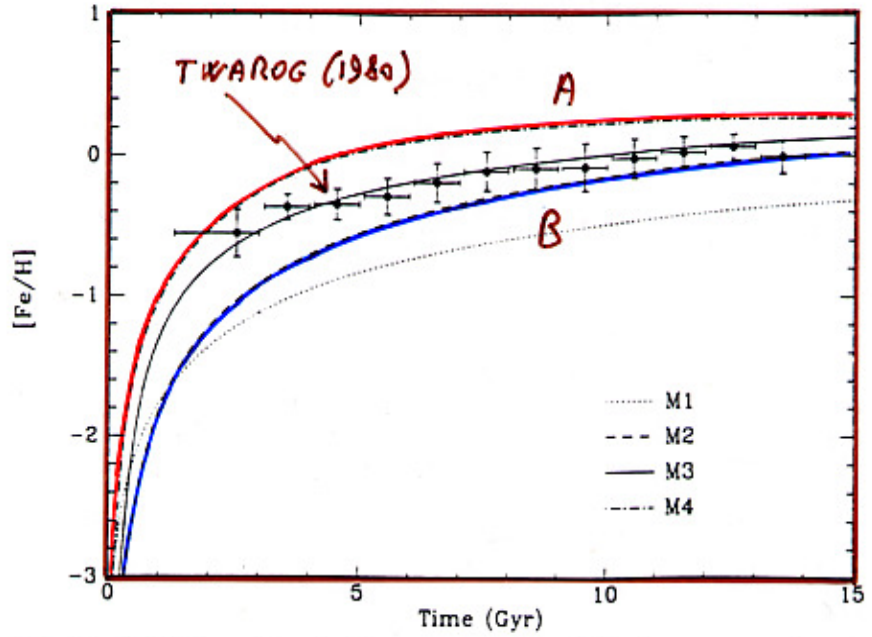

FIG. 4.—[Fe/H] vs. time for the same models of Fig. 3, superposed on data of Twarog (1980).

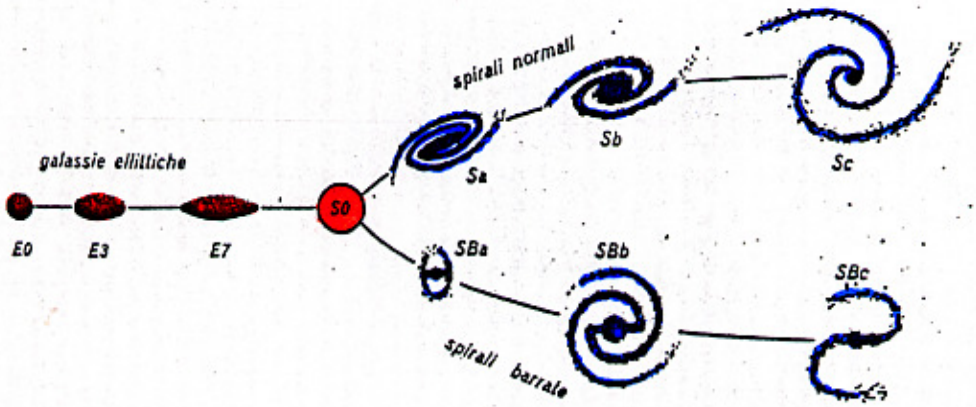
galassie ellittiche
E0
E3
E7
S0
spirali normali
Sa
Sb
Sc
SBa
SBb
SBc
spirali barrate

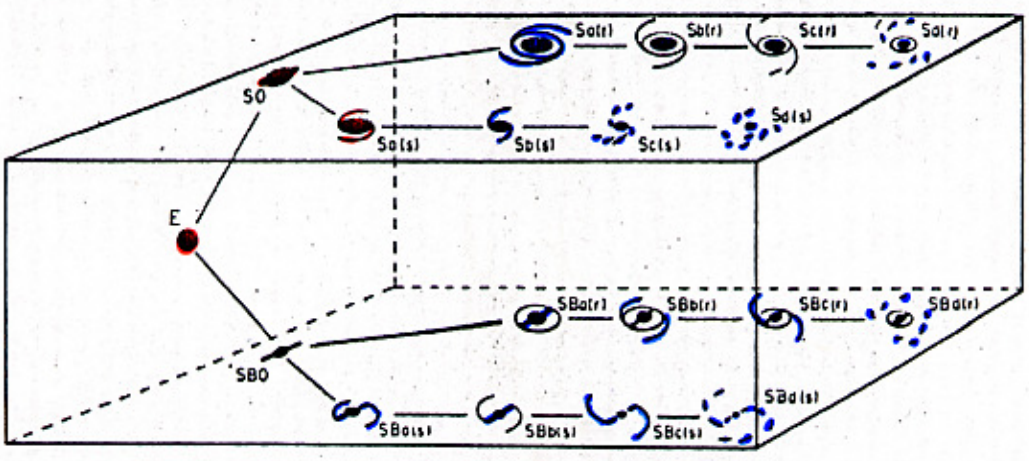
S0
E
SBO
Sa(r)
Sb(r)
Sc(r)
Sd(r)
Sa(s)
Sb(s)
Sc(s)
Sd(s)
SBa(r)
SBb(r)
SBc(r)
SBd(r)
SBa(s)
SBb(s)
SBc(s)
SBd(s)

SURFACE BRIGHTNESS Σ_B

SURFACE DENSITY σ_T

GAS (HI)

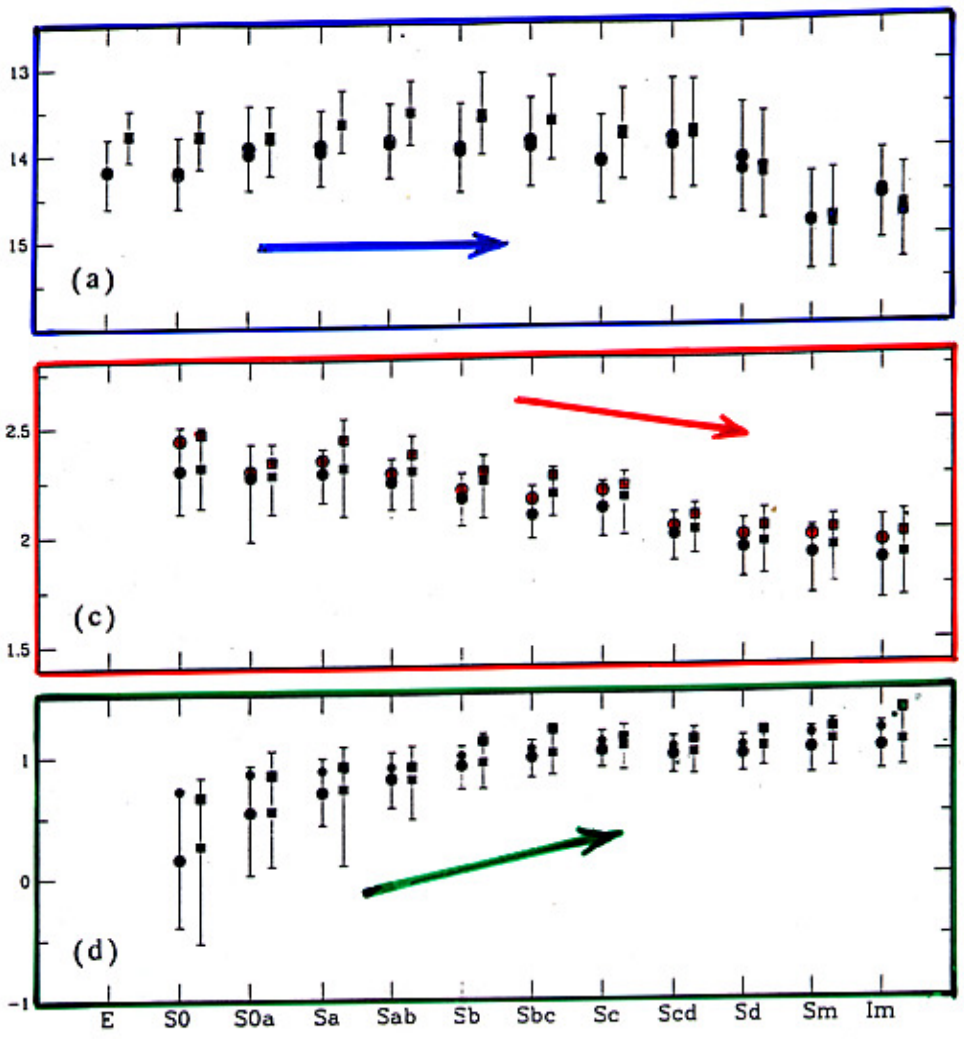

E SØ Sa Sb Sc Sd I

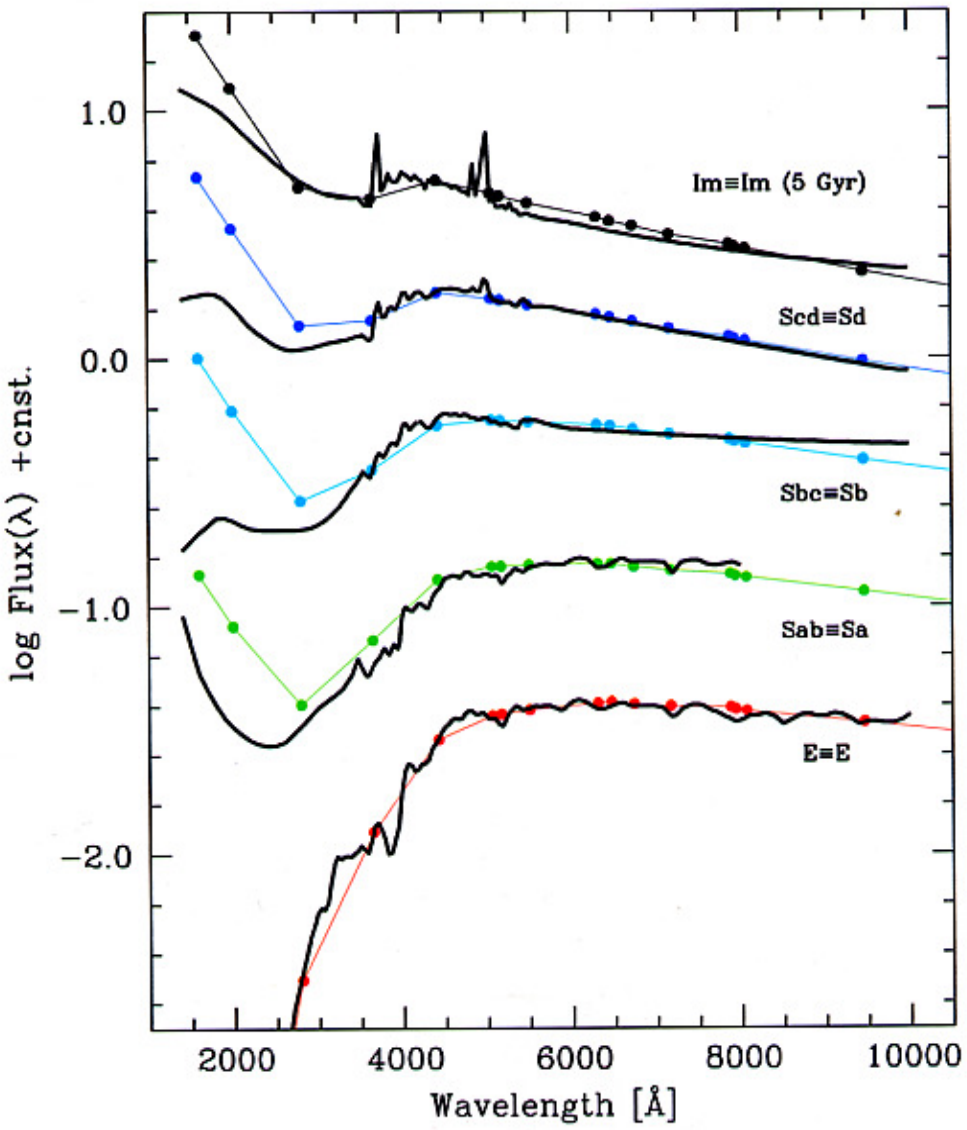

(Buzzoni 2003)

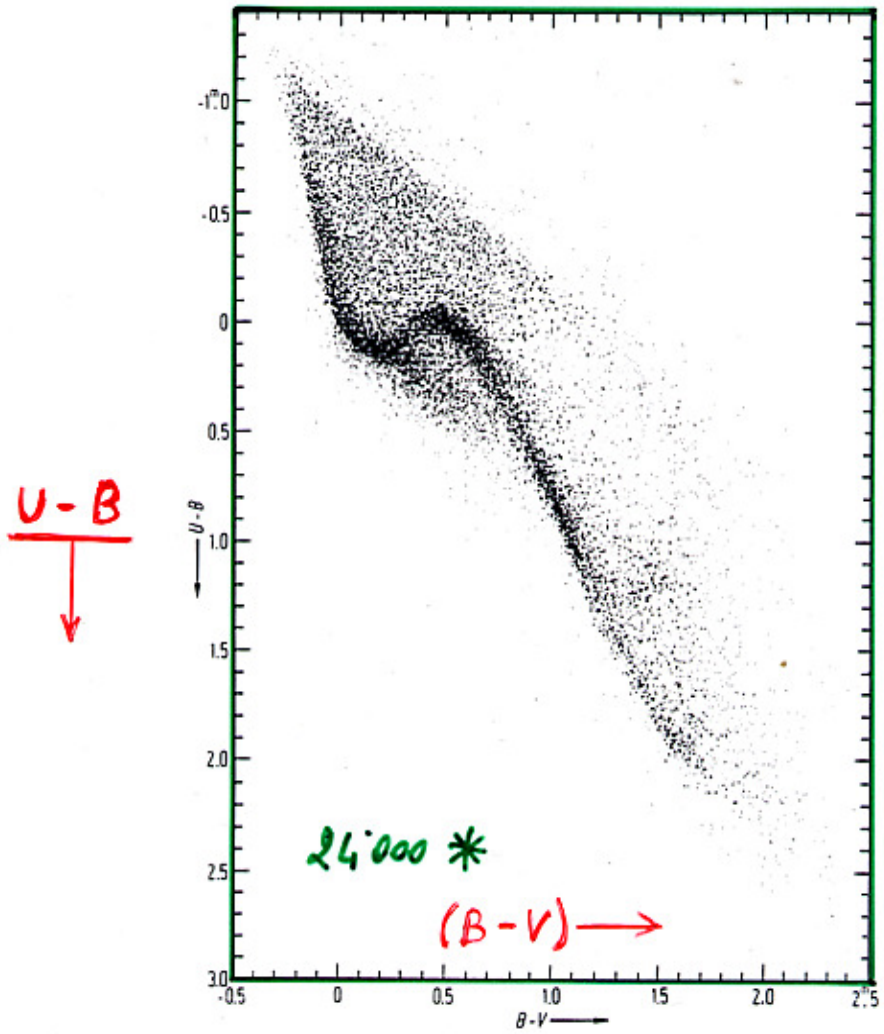

Fig. 1. *UBV* color-color diagram of 24000 stars [5].

FLOWER (1977)

$$\frac{df}{f} = -\rho K \, dD \quad \rightarrow \quad f = f_0 \, e^{-\rho K D}$$

$$\Delta mag_\lambda = 1.086 \, \bar{\rho} \, K_\lambda \, D = 1.086 \times$$

→ OPACITÁ (K)

→ DENSITÁ DI COLONNA (ρD)

$$\frac{A_\lambda}{A_B - A_V} = \frac{A_\lambda}{E(B-V)} = \frac{K_\lambda}{K_B - K_V}$$

CURVA DI SEATON

$\frac{A_\lambda}{A_V}$

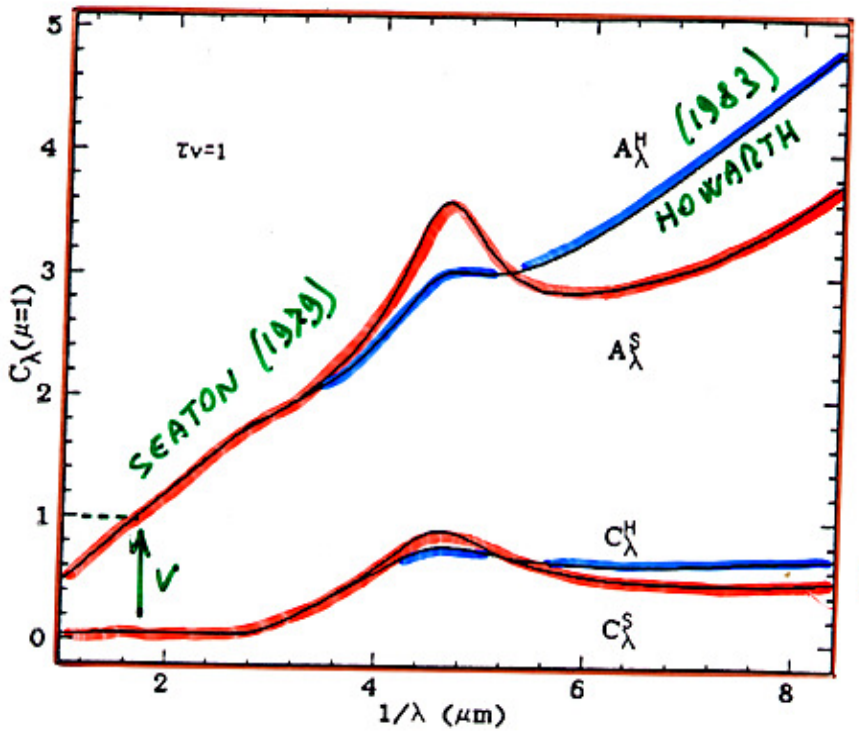

LMC

MILKY WAY

(face-on)

BRUZUAL et al. 1988

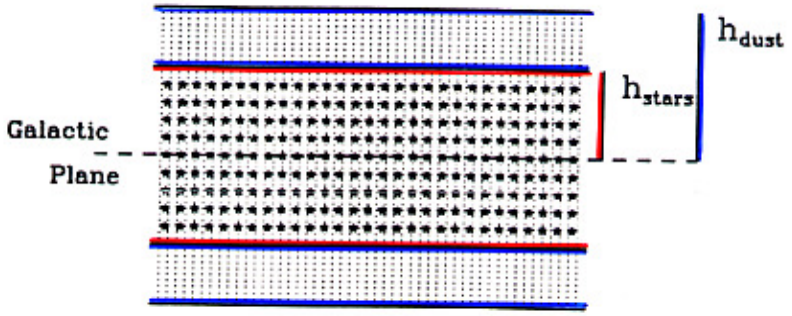

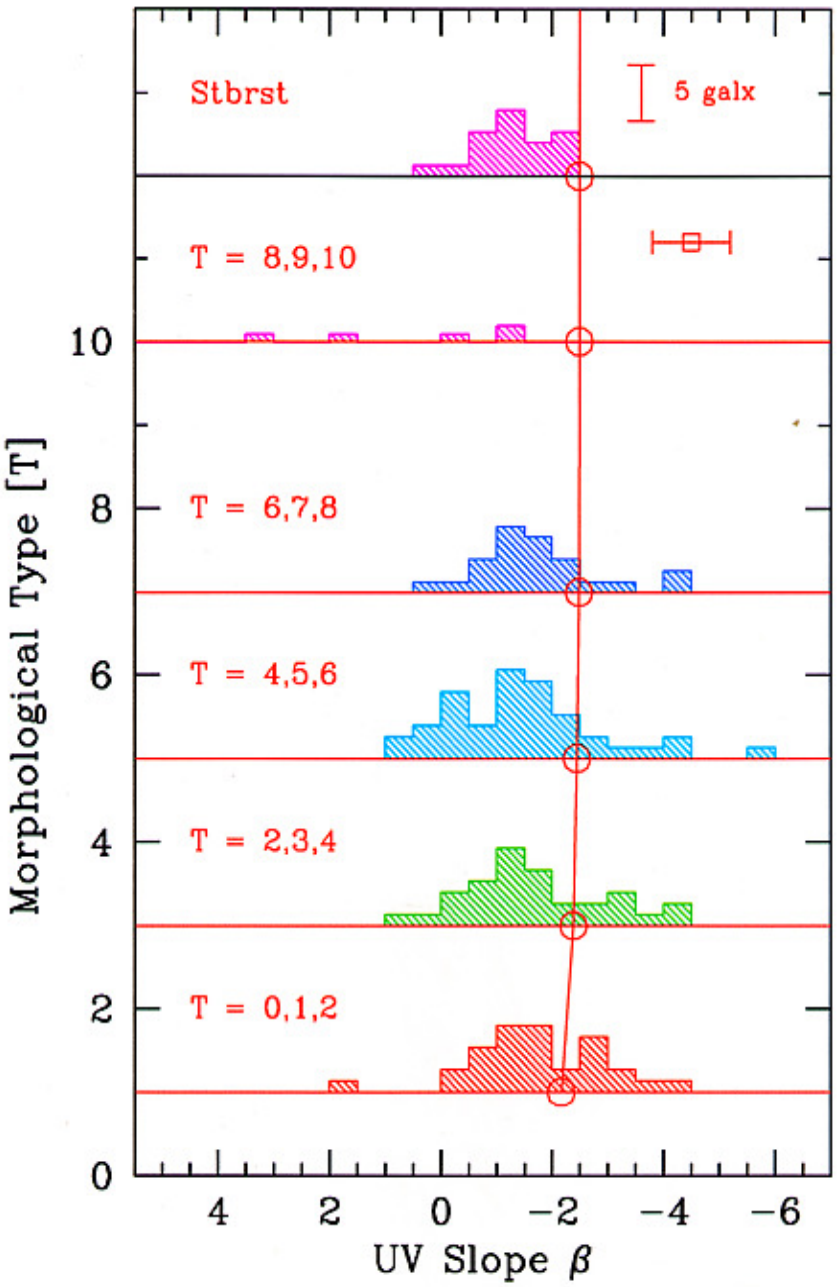

(Buzzoni 2002)

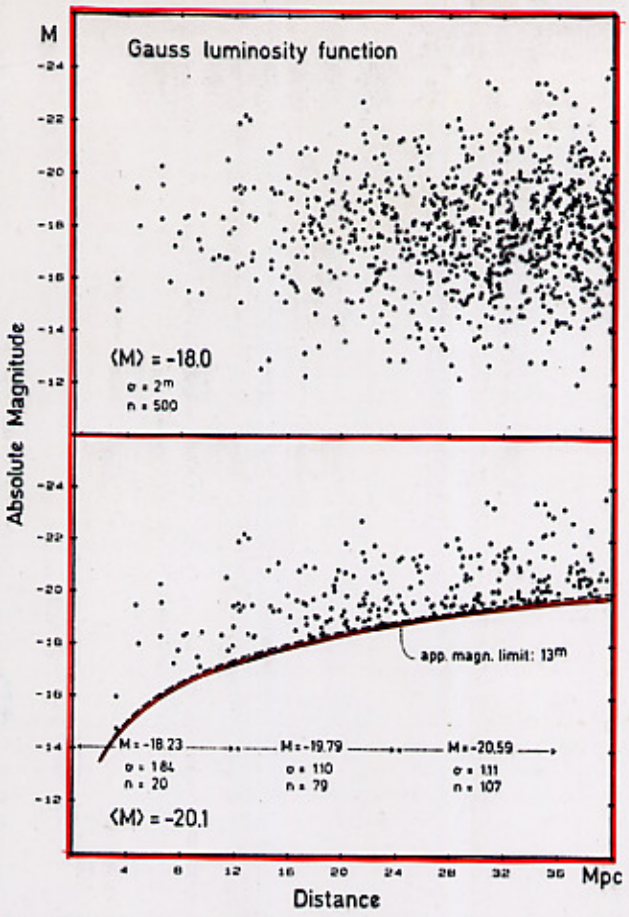

Fig. 1. Upper panel: Monte Carlo distribution in distance and absolute magnitude of 500 galaxies within 38 Mpc. Constant space density and a mean absolute magnitude of $< M > = -18^m$ with a Gauss standard deviation of $\sigma_M = 2^m$ are assumed. Lower pannel: The same sample cut by an apparent-magnitude limit of $m = 13^m.0$. Note the increase of the galaxian luminosities with increasing distance and the small effective (observable) scatter σ_M within individual distance intervals.

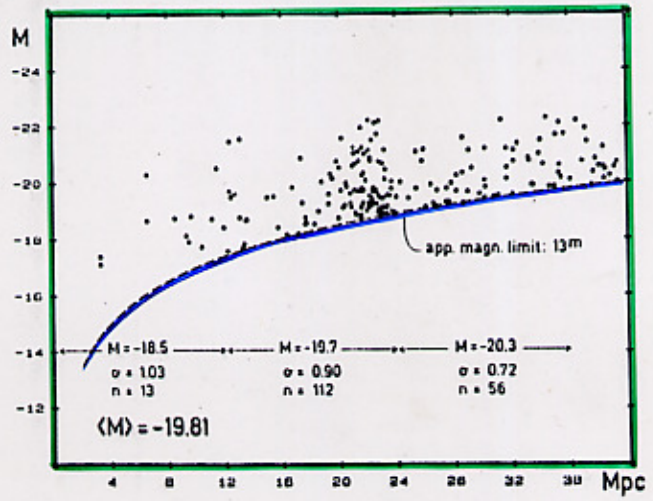

Fig. 2. Same as Fig. 1, but for 500 galaxies with $M < -17^m$ following a Schechter luminosity function typical for E to Im galaxies (Kraan-Korteweg 1981). A density fluctuation (cluster) of 150 galaxies is added at r = 22 Mpc. The true mean absolute magnitude of this sample is $< M > = -18.56$. Here only the subsample is shown which would appear in a catalog complete for $m < 13^m$. Note the increase of luminosity with distance, the small effective scatter σ_M, and the additional effect of the density fluctuation.

(Buzzoni 1998)

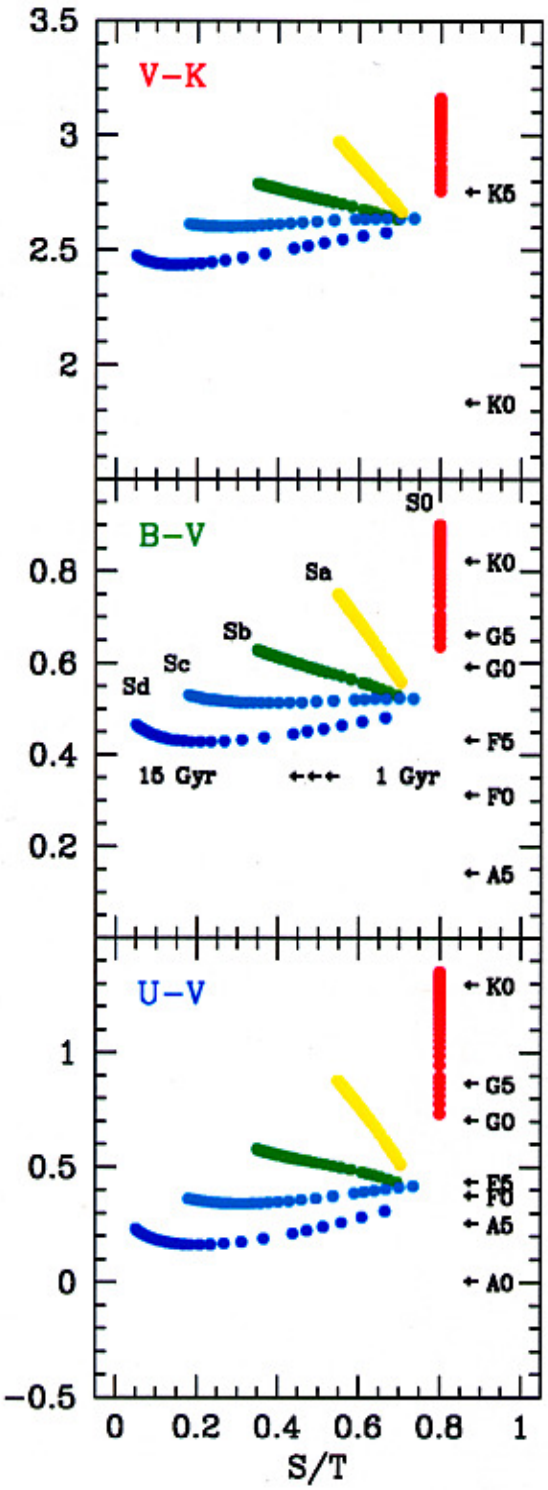

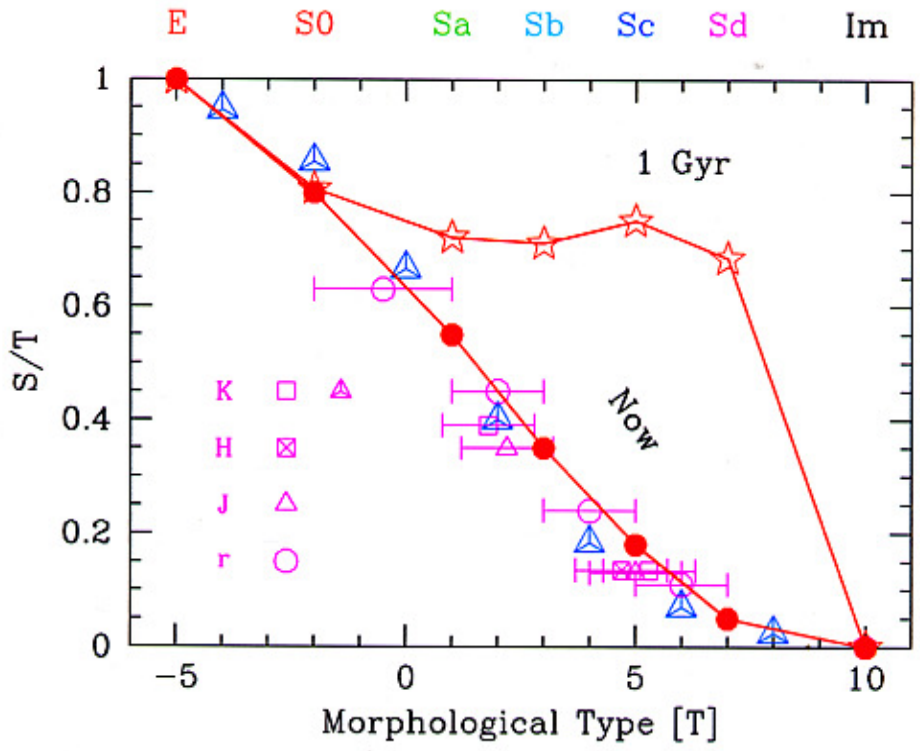
E
S0
Sa
Sb
Sc
Sd
Im
1
0.8
0.6
0.4
0.2
0
S/T
1 Gyr
Now
K
H
J
r
−5
0
5
10
Morphological Type [T]

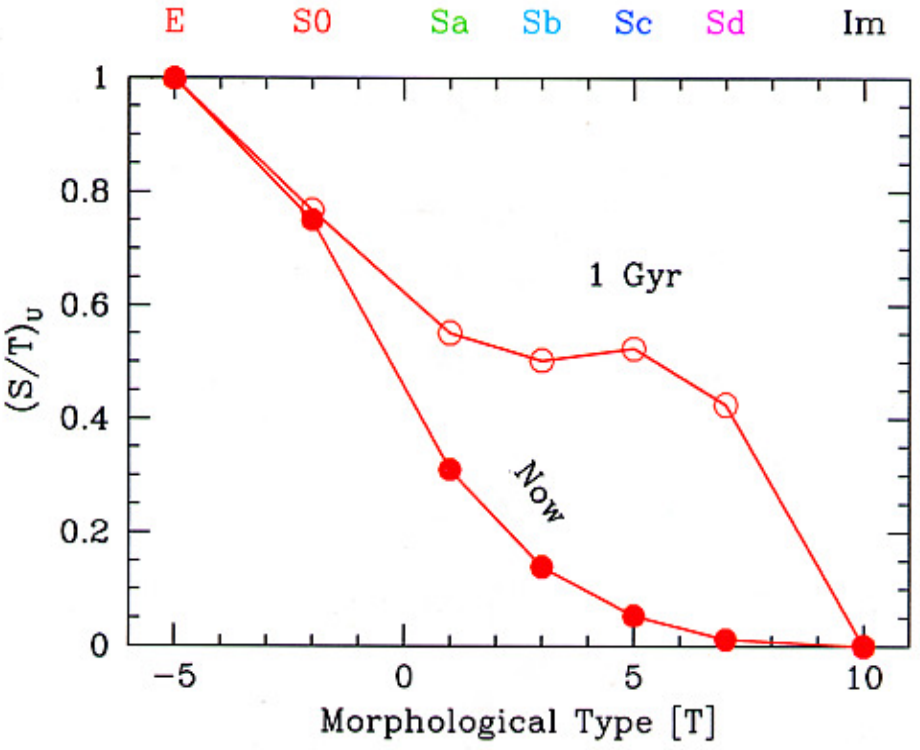
E
S0
Sa
Sb
Sc
Sd
Im
1
0.8
0.6
0.4
0.2
0
(S/T)u
1 Gyr
Now
−5
0
5
10
Morphological Type [T]

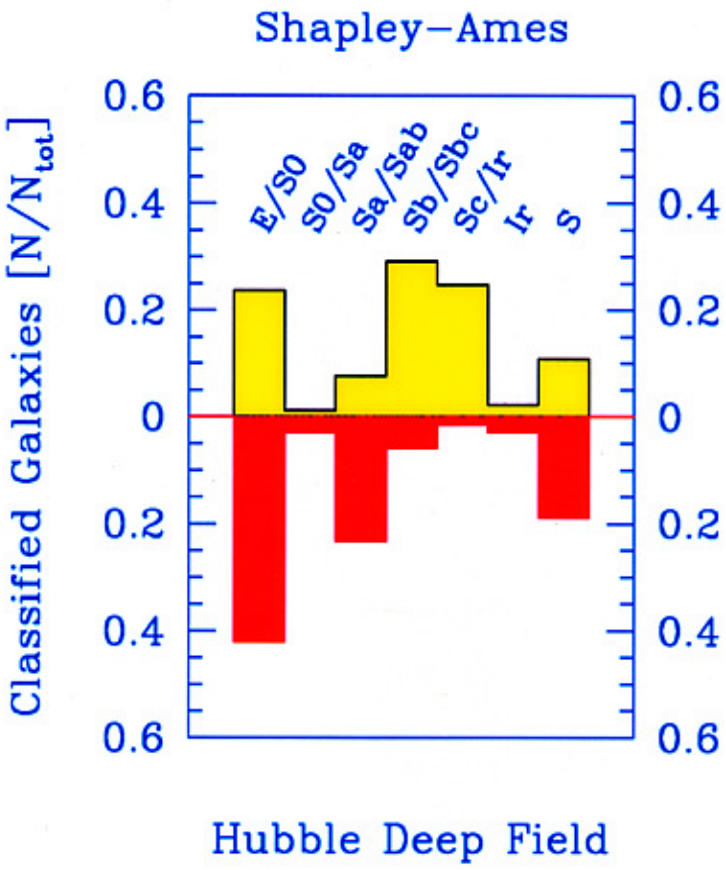

(VAN DEN BERGH et al. 1996)

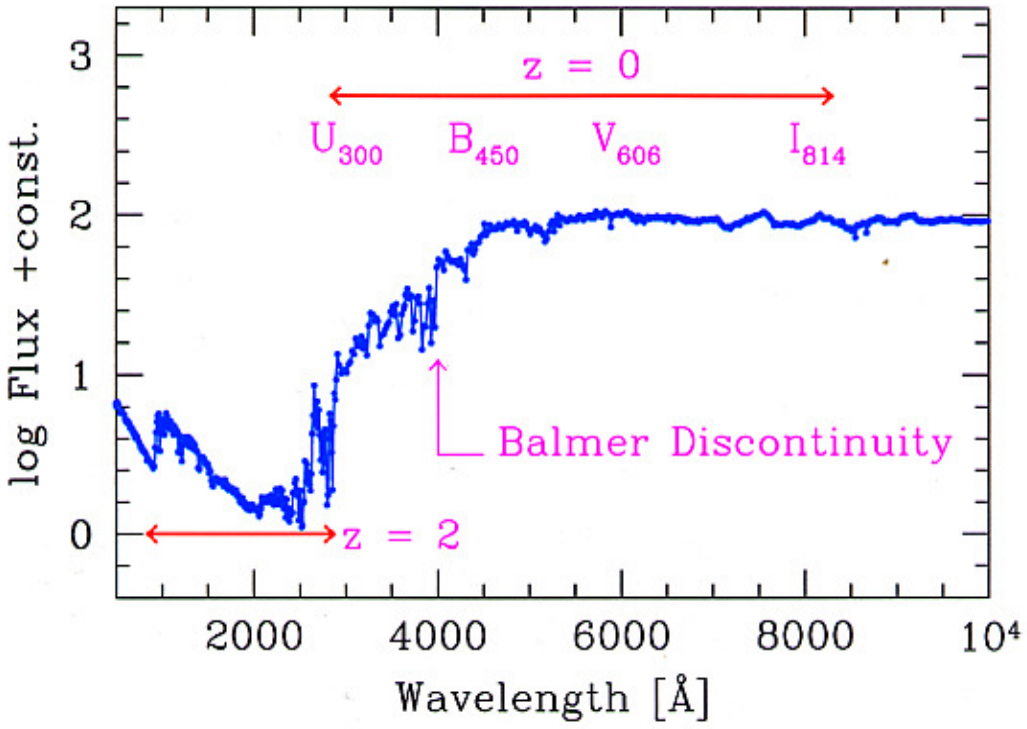

(MASSAROTTI et al. 2001)

$$M - M_0 = 5 \log \frac{\ell}{\ell_0} + K(z) + e(z)$$

$$K(z) = 2.5 \log(1+z) - 2.5 \log \int F_{(\lambda/1+z)} R_\lambda \, d\lambda \Big/ \int F_\lambda R_\lambda \, d\lambda$$

$$e(z) = -2.5 \log \int F_{(\lambda/1+z;\, t_z)} R_\lambda \, d\lambda \Big/ \int F_{(\lambda/1+z;\, 0)} R_\lambda \, d\lambda$$

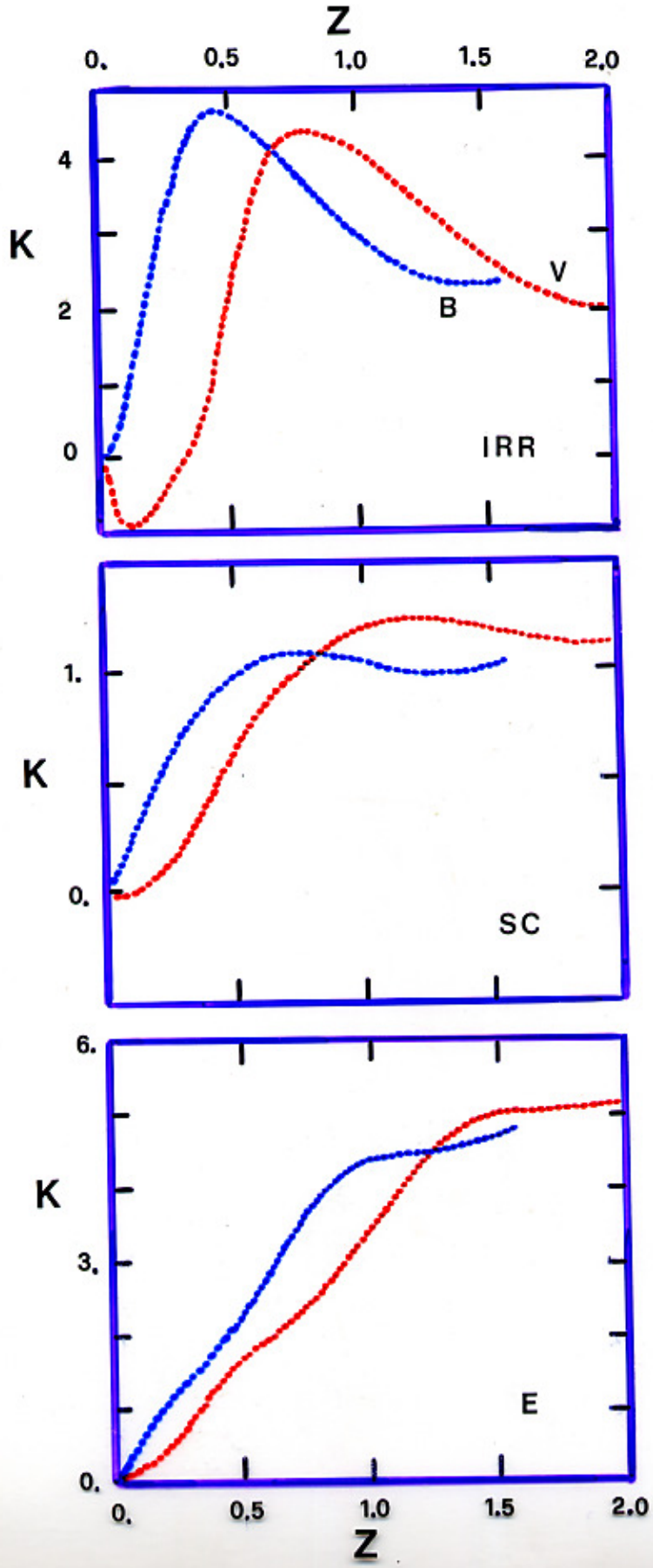

WITHOUT EVOLUTION

WITH [redacted]

$H_0 = 50 \quad q_0 = 0.$

$k(g)$

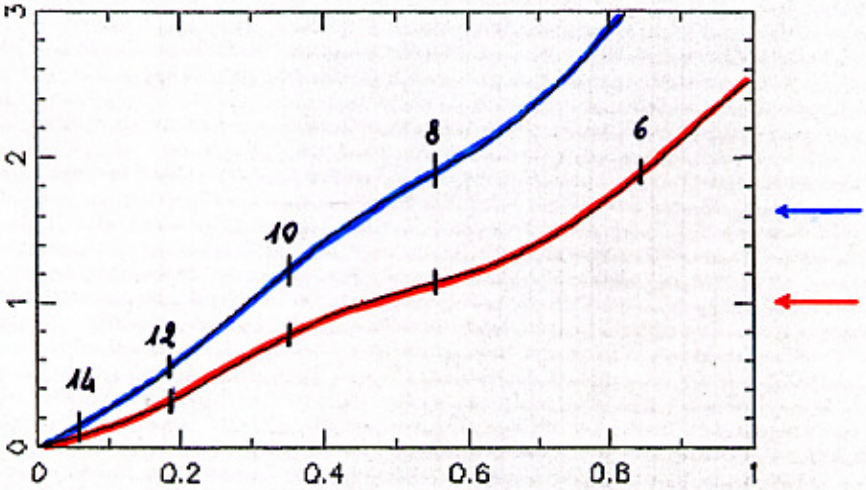

$k(r)$

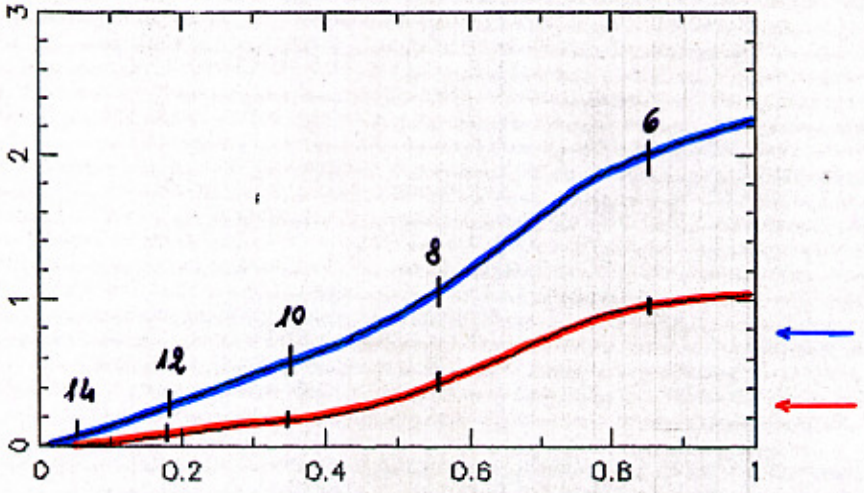

$k(i)$

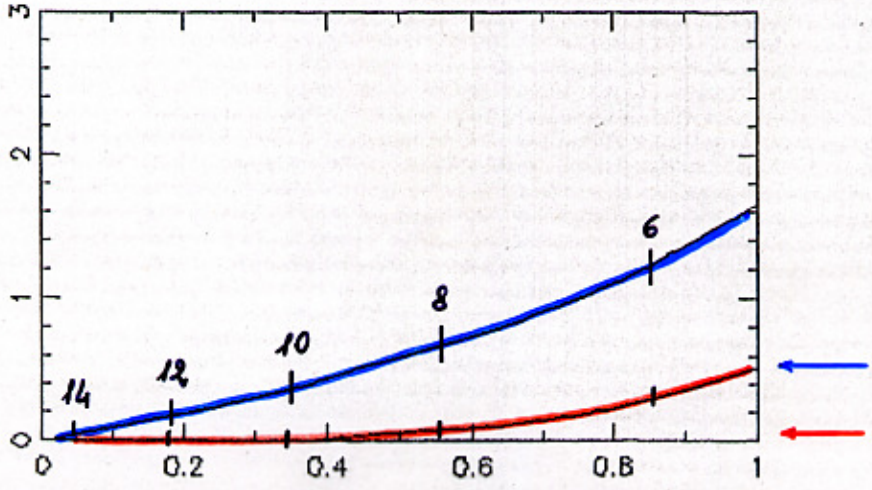

REDSHIFT (z)

Apparent Color vs. Redshift

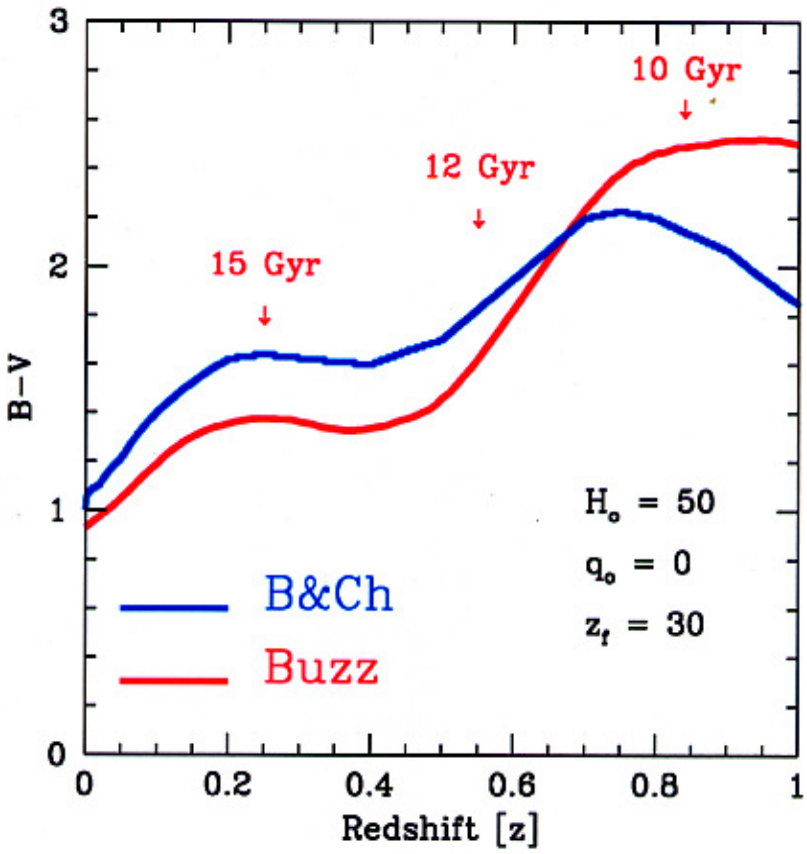

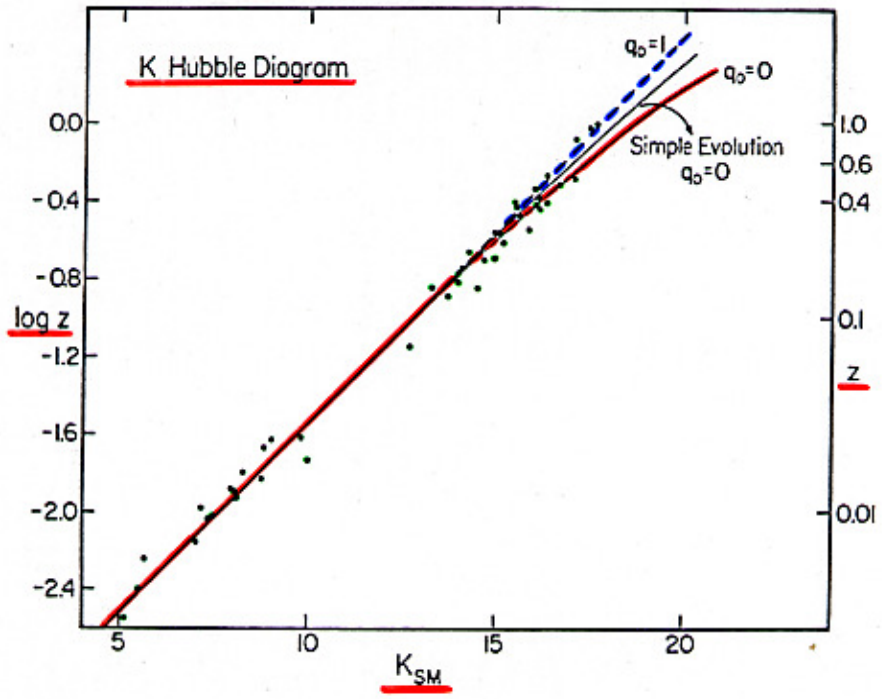
K Hubble Diagram
$q_0=1$
$q_0=0$
Simple Evolution
$q_0=0$
0.0
-0.4
-0.8
log z
-1.2
-1.6
-2.0
-2.4
1.0
0.6
0.4
0.1
z
0.01
5
10
15
20
K_{SM}

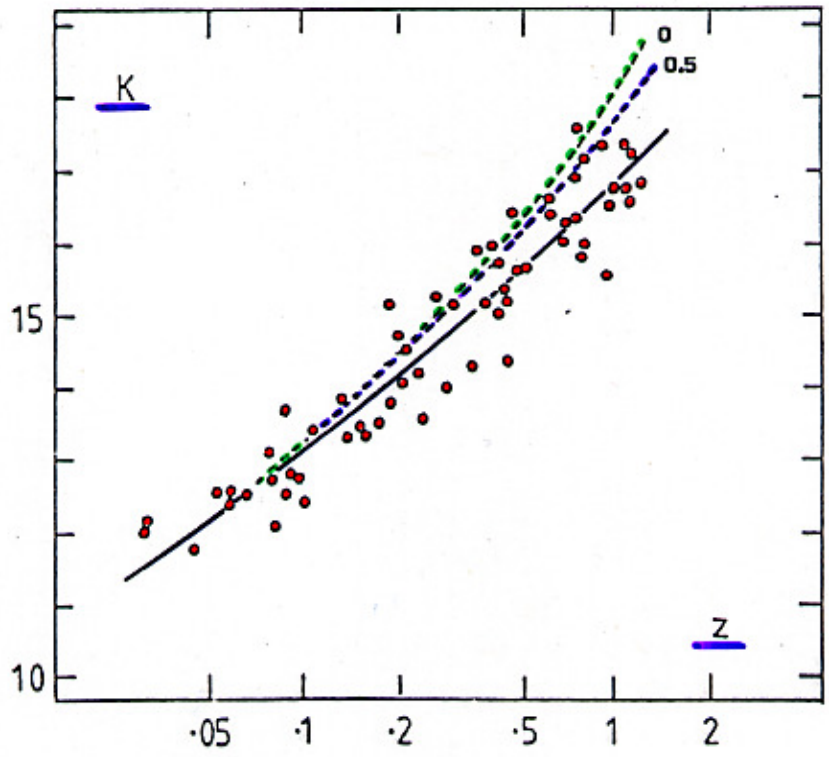
K
0
0.5
15
10
z
·05
·1
·2
·5
1
2

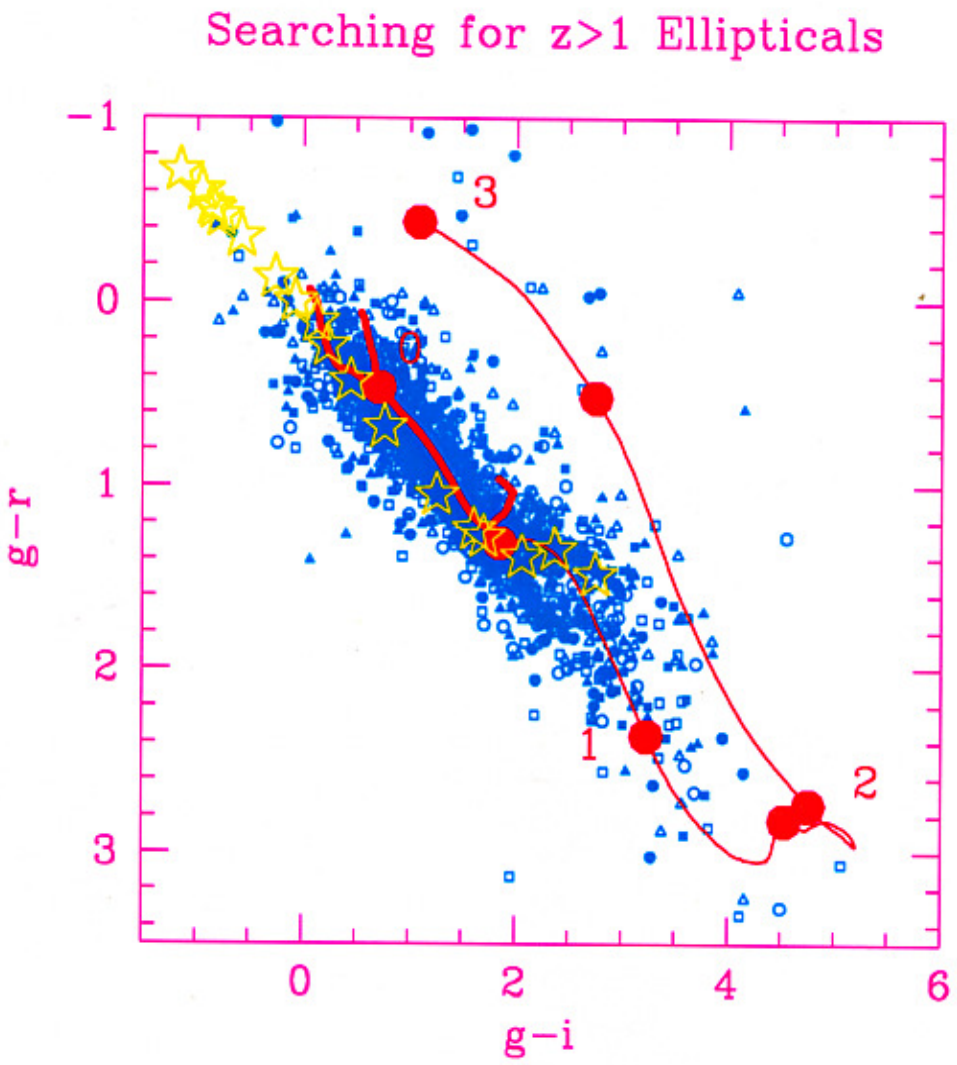
Searching for z>1 Ellipticals
−1
0
1
2
3
g−r
0
2
4
6
g−i
3
0
1
2

APPARENT COLOR DIAGNOSTICS

23 < g < 24

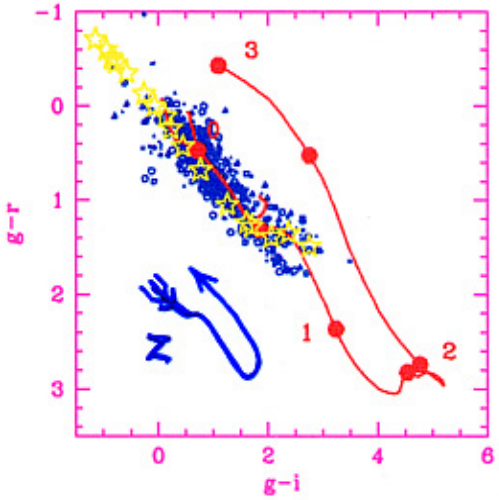

24 < g < 25

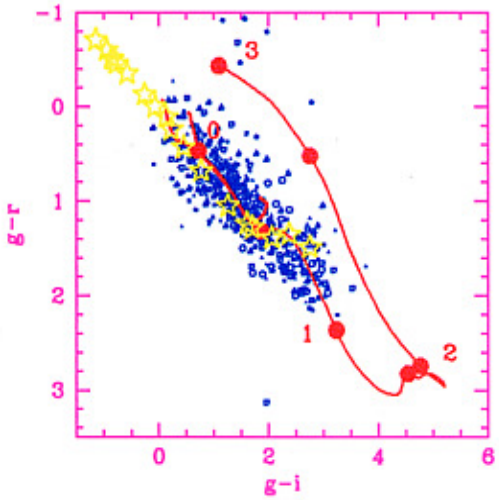

26 < g < 27

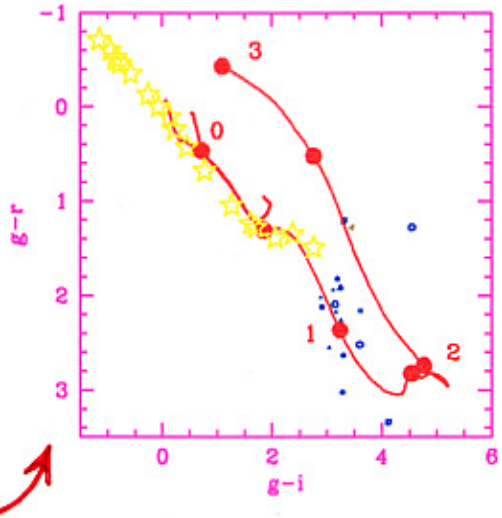

25 < g < 26

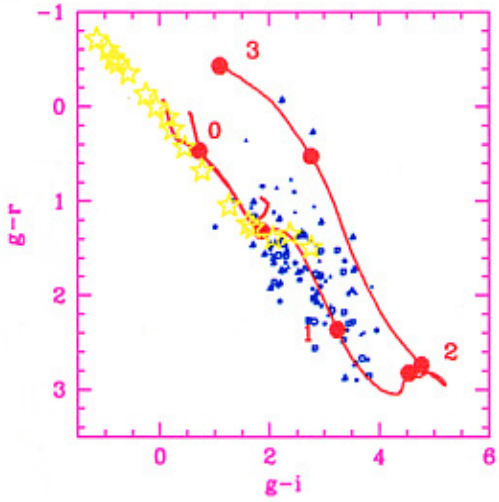

PHOTOMETRIC REDSHIFT

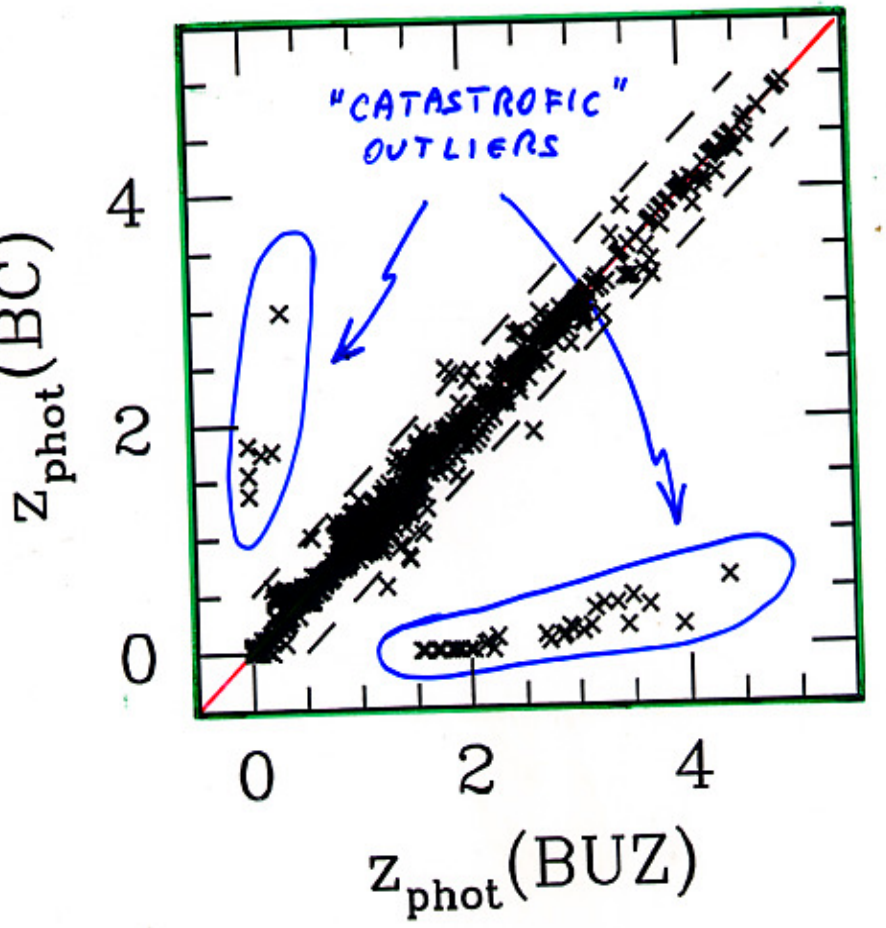

HDFN - 1041 galx

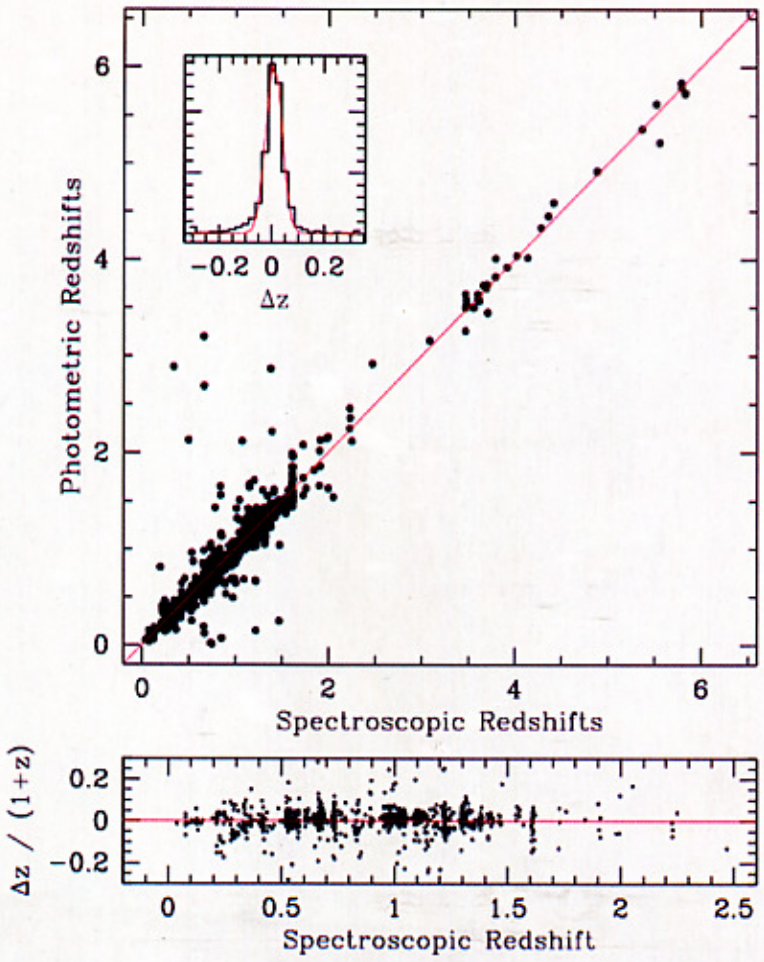
Photometric Redshifts
Spectroscopic Redshifts
Δz
−0.2 0 0.2
0
2
4
6
Δz / (1+z)
0.2
0
−0.2
0
0.5
1
1.5
2
2.5
Spectroscopic Redshift

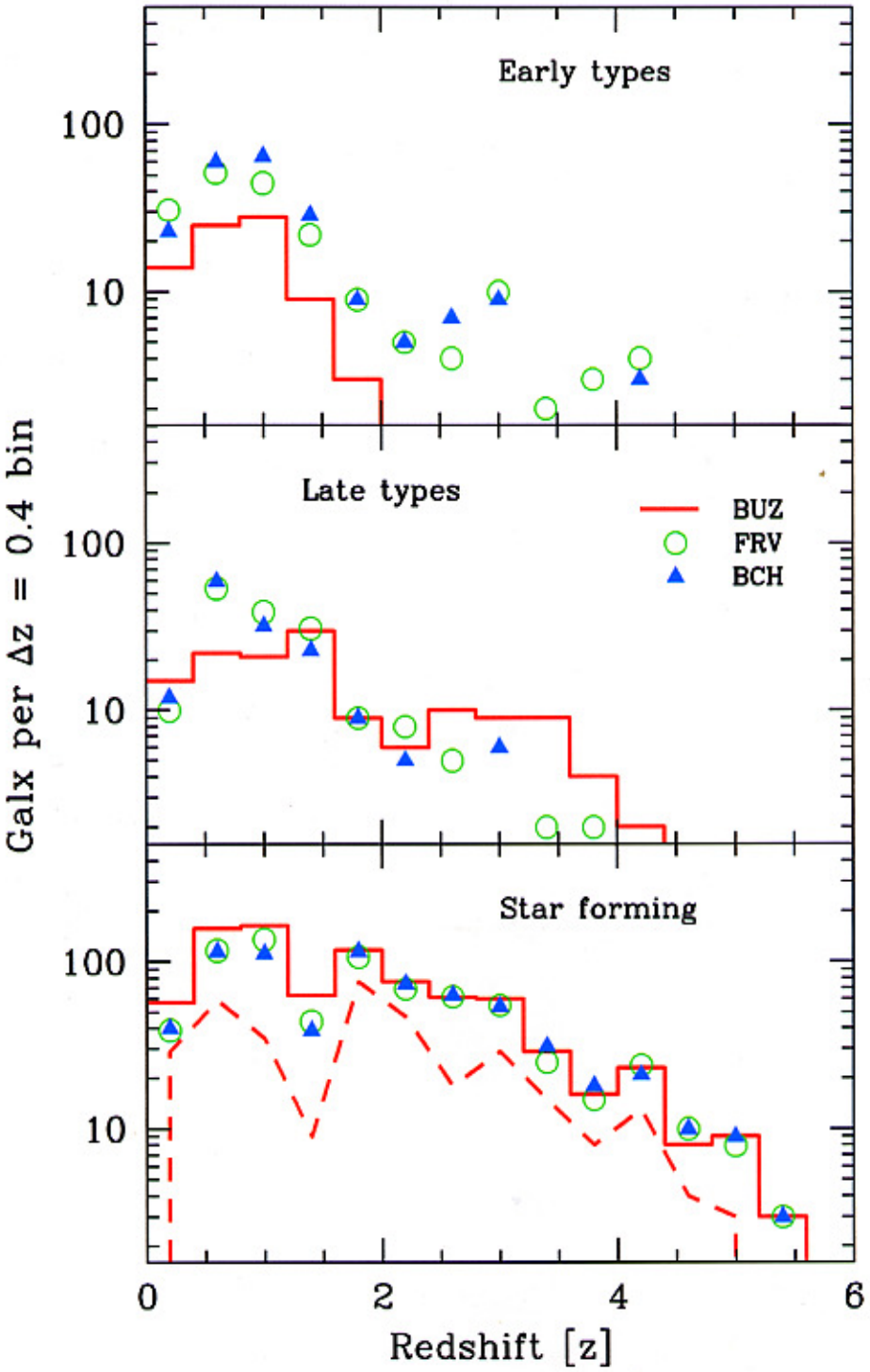

(Buzzoni et al. 2003)

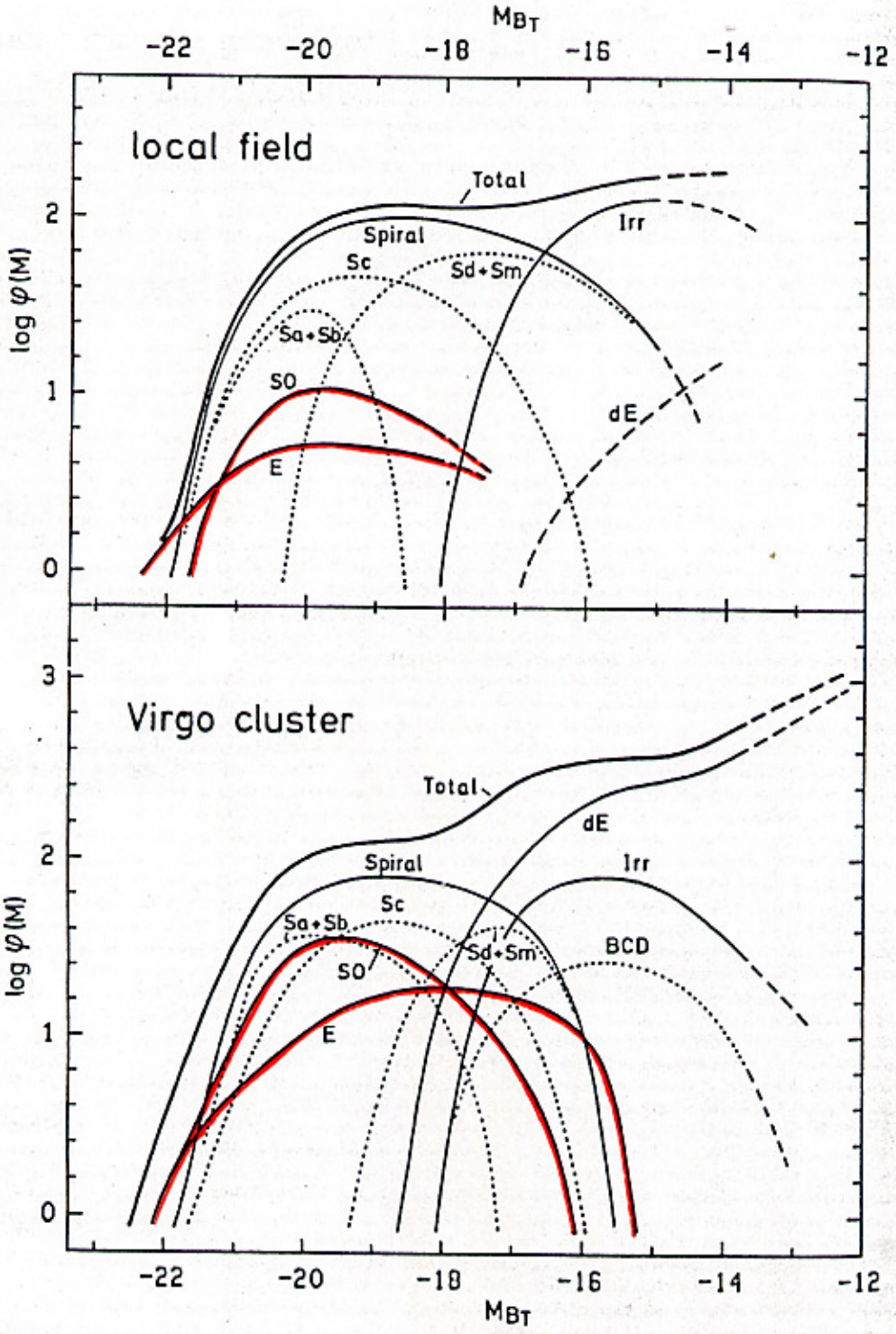

Figure 1 The LF of field galaxies (top) and Virgo cluster members (bottom). The zero point of $\log \varphi(M)$ is arbitrary. The LFs for individual galaxy types are shown. Extrapolations are marked by dashed lines. In addition to the LF of all spirals, the LFs of the subtypes Sa + Sb, Sc, and Sd + Sm are also shown as dotted curves. The LF of Irr galaxies comprises the Im and BCD galaxies; in the case of the Virgo cluster, the BCDs are also shown separately. The classes dS0 and "dE or Im" are not illustrated. They are, however, included in the total LF over all types (heavy line).

IL GRUPPO LOCALE

WITHIN 1.5 Mpc

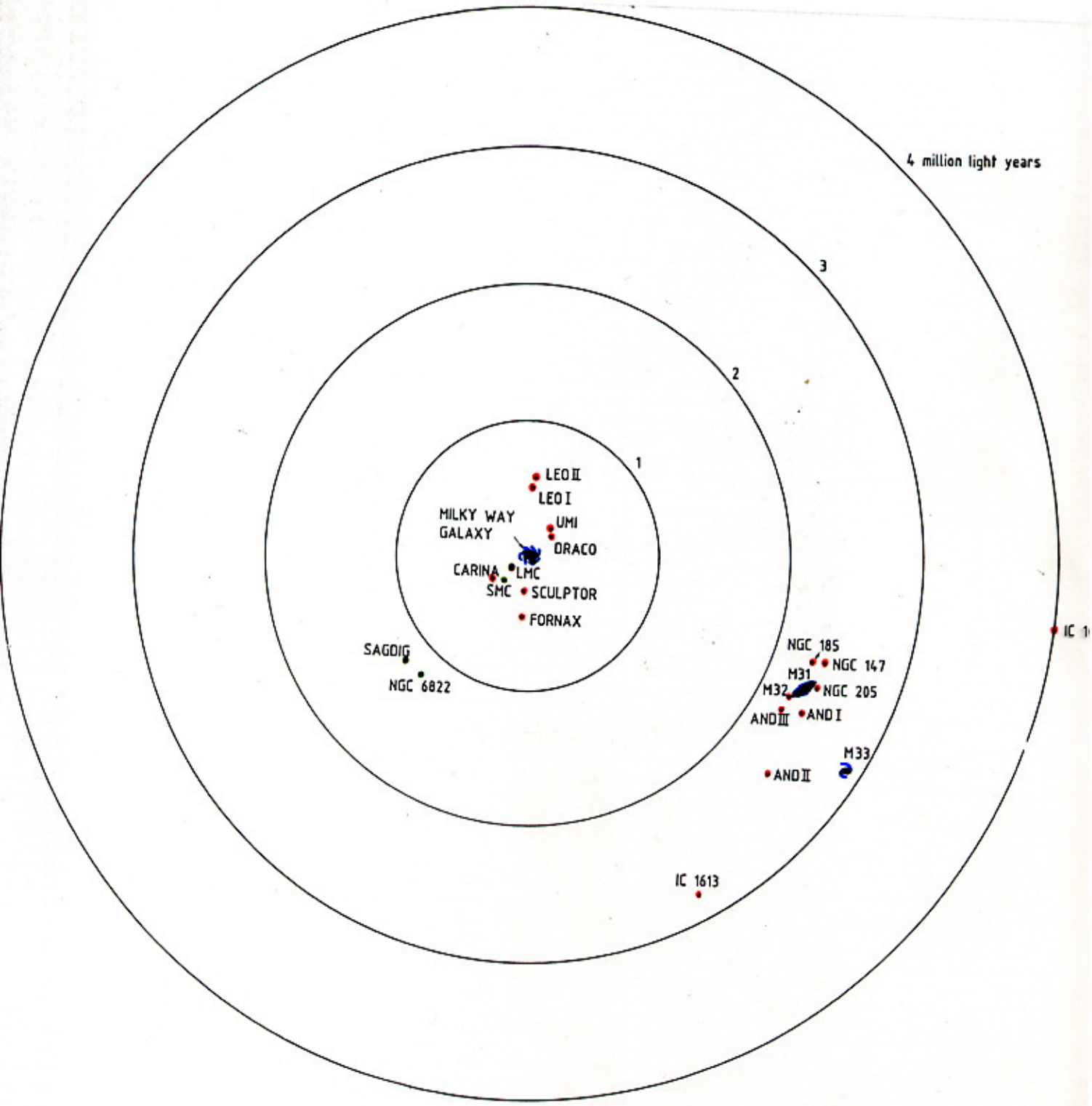

$\log \rho = \log \Gamma_{(\gamma+\alpha)} + \log L^* + \log Q^*$

Log (LUMINOSITY FUNC)

E. S. P.

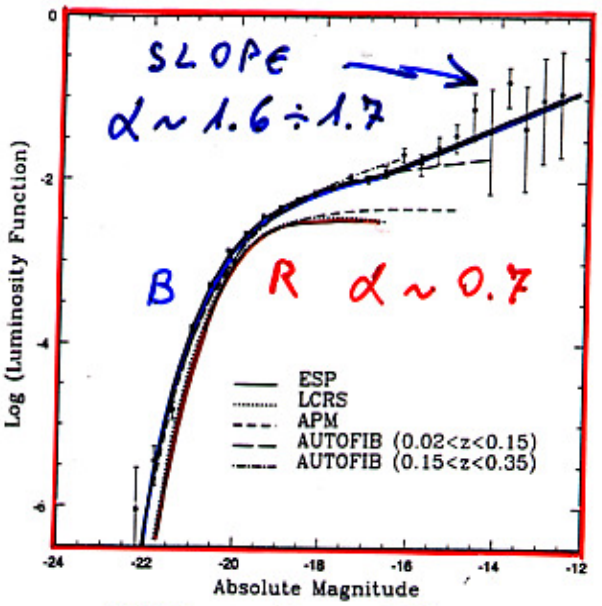

ABSOLUTE MAG

(Zucca et al. 1997)

Differential Correction for Incompleteness

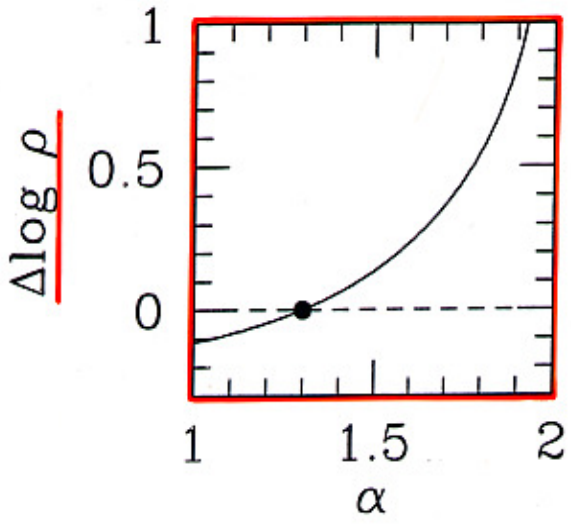

Schechter's Power-law Index

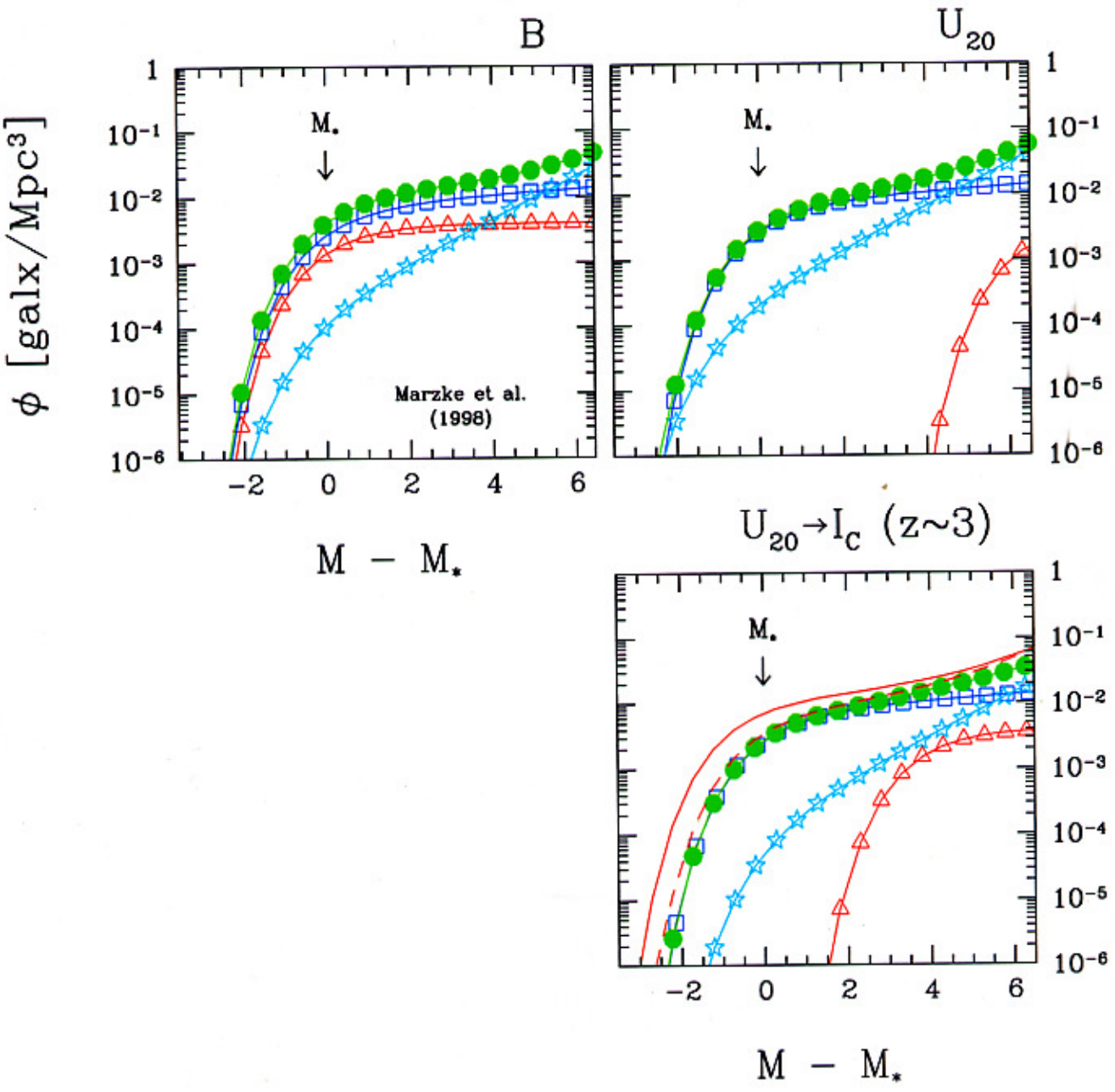
B
U_{20}
$U_{20} \rightarrow I_C$ (z~3)
ϕ [galx/Mpc^3]
M*
Marzke et al. (1998)
M − M*

(Madau 1997)

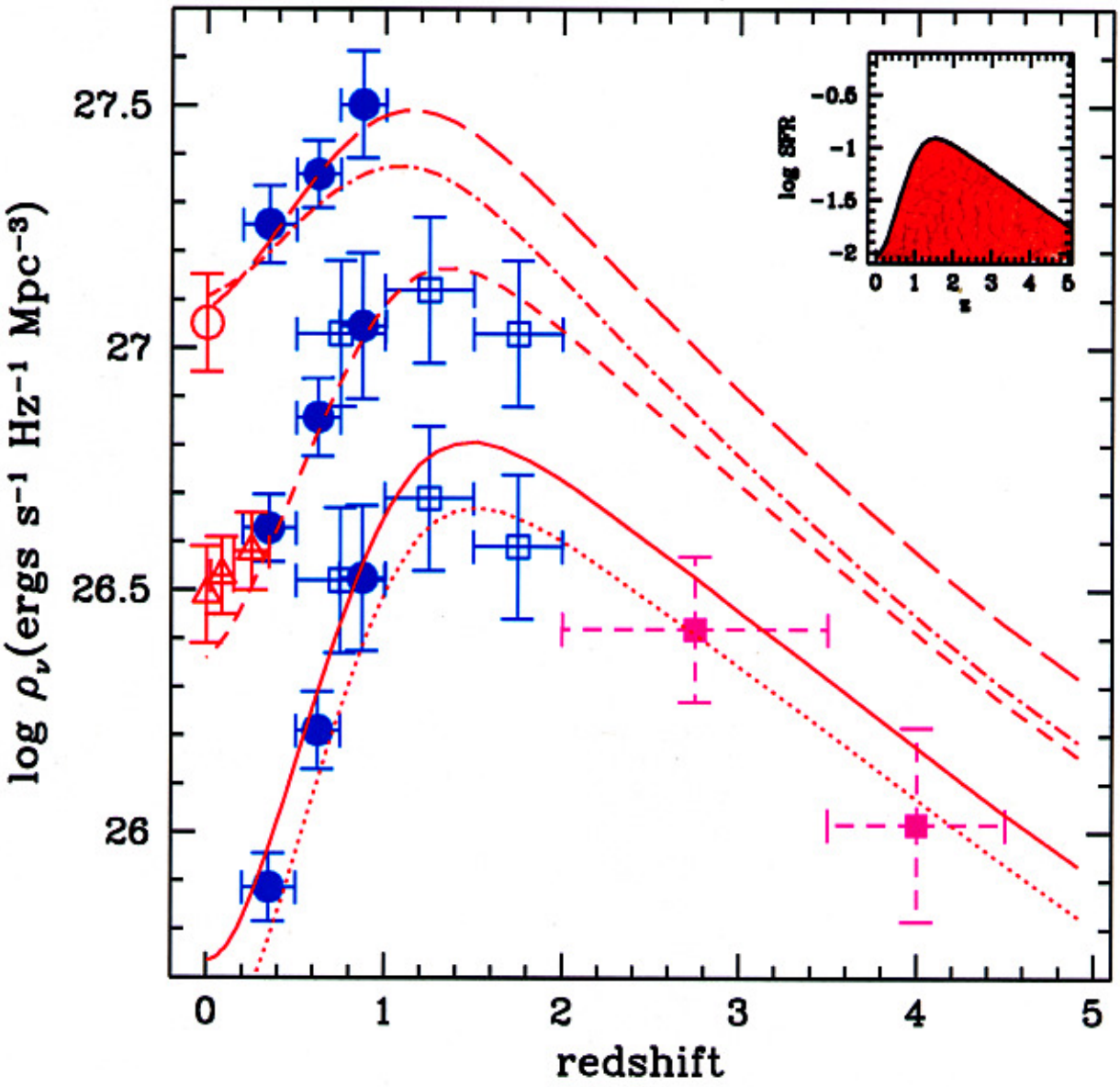
log ρ_ν(ergs s^{-1} Hz^{-1} Mpc^{-3})
27.5
27
26.5
26
0
1
2
3
4
5
redshift
log SFR
-0.5
-1
-1.5
-2
0
1
2
3
4
5
z

STEIDEL et al. (1998)

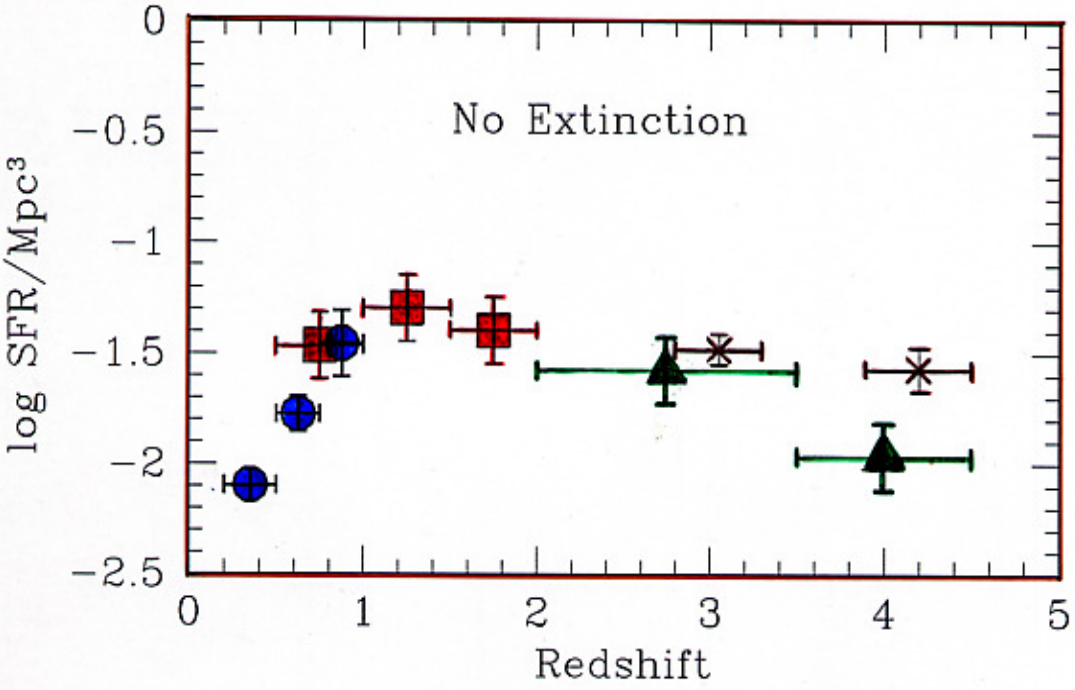

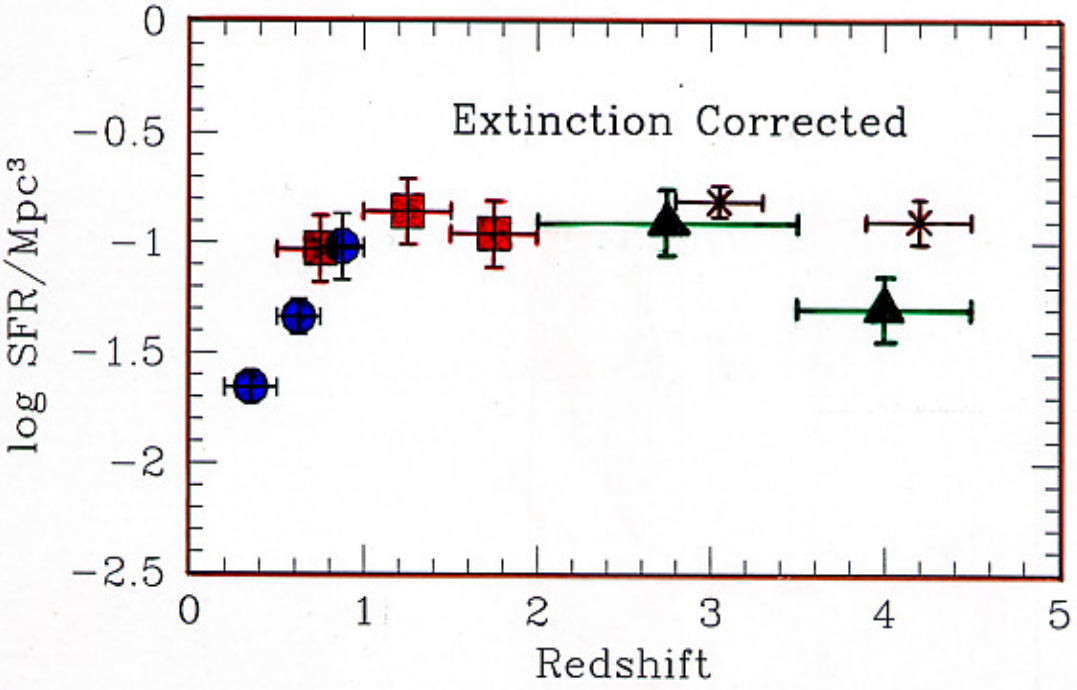

● = LILLY et al. (1996)

■ = CONNOLLY et al. (1997)

▲ = MADAU et al. (1997)

X = STEIDEL et al. (1999)

$(H_0, q_0) = (50, \frac{1}{2})$